AD-A257 054

ARO 29180·1-PH-CF

FERROELECTRICS

The international journal devoted to the theoretical, experimental, and applied aspects of ferroelectrics and related materials.

PROCEEDINGS OF

THE THIRD INTERNATIONAL CONFERENCE ON FERROELECTRIC LIQUID CRYSTALS

Part I of II Parts

June 23–28, 1991
Boulder, Colorado, USA

DTIC
ELECTE
OCT 2 6 1992
S A D

Guest Editors:

Noel A. Clark
David M. Walba
Mark A. Handschy
Garret Moddel

FERROELECTRICS
and related materials

GENERAL INFORMATION

Aims and Scope *Ferroelectrics* is designed to provide a forum for people working in ferroelectrics and related materials such as ferroelastics, ferroelectric-ferromagnetics, electrooptics, piezoelectrics, pyroelectrics, nonlinear dielectrics, and liquid crystals. *Ferroelectrics* publishes experimental and theoretical papers aimed at the understanding of ferroelectricity and associated phenomena and applied papers dealing with the utilization of these materials in devices and systems. An important aspect of *Ferroelectrics* is to provide a vehicle for the publication of interdisciplinary papers involving ferroelectricity.

The editor invites original papers and short communications on the theory, fabrication, properties, and applications of ferroelectrics and related materials. In addition to research papers, *Ferroelectrics* publishes appropriate and timely review articles. There are no charges to authors or to institutions.

Notes for contributors can be found at the back of the journal.

Please see inside back cover for information on subscription rates and ordering information.

SEPTEMBER 1991

PROCEEDINGS OF

THE THIRD INTERNATIONAL CONFERENCE
ON FERROELECTRIC LIQUID CRYSTALS

June 23–28, 1991
Boulder, Colorado, USA

Guest Editors:

Noel A. Clark
David M. Walba
Mark A. Handschy
Garret Moddel

DTIC QUALITY INSPECTED 1

92-27547

CONTENTS—PART I

Note on Pagination, Author Index and Table of Contents

The Proceedings of the Third International Conference on Ferroelectric Liquid Crystals are being published in two volumes of FERROELECTRICS (Volumes 121 and 122). Volume 121, Part 1 includes Sections A–D. Volume 122 begins with Section E and runs through Section L. To facilitate indexing and referring to these Proceedings, the page numbers of Volume 122 will run continuously from the end of Volume 121. The Table of Contents and Author Index will be repeated in full in both Volumes.

The alpha-numeric code e.g., [O-24], [P-78], given at the end of each paper in the Table of Contents, indicates the position of that paper in the Program Book of Abstracts. Papers that were not received in time to be printed in the special editions of Ferroelectrics dedicated to the 1991 Conference will appear in regular issues of Ferroelectrics with a footnote tying them into the Conference.

Section A: Dynamics

Section C: New Materials

CONTENTS—PART II

Note on Pagination, Author Index and Table of Contents

The Proceedings of the Third International Conference on Ferroelectric Liquid Crystals are being published in two volumes of FERROELECTRICS (Volumes 121 and 122). Volume 121, Part I includes Sections A–D. Volume 122 begins with Section E and runs through Section L. To facilitate indexing and referring to these Proceedings, the page numbers of Volume 122 will run continuously from the end of Volume 121. The Table of Contents and Author Index will be repeated in full in both Volumes.

The alpha-numeric code e.g., [O-24], [P-78], given at the end of each paper in the Table of Contents, indicates the position of that paper in the Program Book of Abstracts. Papers that were not received in time to be printed in the special editions of Ferroelectrics dedicated to the 1991 Conference will appear in regular issues of Ferroelectrics with a footnote tying them into the Conference.

Section E: Device Technology

Section H: Antiferroelectrics

Section I: Optics

Section J: Interfaces

PROCEEDINGS OF THE THIRD INTERNATIONAL CONFERENCE ON FERROELECTRIC LIQUID CRYSTALS

June 23–28, 1991
Boulder, Colorado, USA

SPONSORS

The Organizing Committee gratefully acknowledges the following Organizations for their support of the Third International Conference on Ferroelectric Liquid Crystals:

Canon, Inc.
Chisso Corporation
Department of the Army, U.S. Army Research Office
F. Hoffmann-La Roche Ltd.
Ferroelectrics
Fujitsu Labs.
GEC Research
Gordon and Breach Science Publishers S.A.
Hoechst AG
IBM Corporation
Material Science and Technology
Merck, EM Industries
Monsanto
Polaroid Corporation
San Nopco Limited
Sharp Corporation
3M Information and Imaging
Toshiba
U.S. Air Force Rome Laboratory at Hanscom AFB, MA
Varitronix Limited

ORGANIZING AND
SCIENTIFIC COMMITTEE

Noel A. Clark, Chairman

David Walba	Mark Handschy
Garret Moddel	Sven Lagerwall
Kristina Johnson	Christian Destrade

INTERNATIONAL ADVISORY BOARD

L. Bata (Hungary)	G. Heppke (Germany)
R. Blinc (Yugoslavia)	C. C. Huang (USA)
L. M. Blinov (Russia)	T. Inukai (Japan)
D. Demus (Germany)	V. Janovec (Czechoslovakia)
G. Durand (France)	J. Kanbe (Japan)
C. Escher (Germany)	S. Matsumoto (Japan)
A. Fukuda (Japan)	J. Prost (France)
T. Geelhaar (Germany)	M. Schadt (Switzerland)
J. W. Goodby (UK)	

LIST OF PARTICIPANTS

BELGIUM
DE MEYERE, A.

CZECHOSLOVAKIA
GLOGORAVA, M.
LUBOR, L.
PAVEL, J.

FRANCE
BRUNET, M.
DESBAT, B.
DESTRADE, C.
DURAND, G.
KELLER, P.
LEGRAND, C.
MACLENNAN, J.
MALTHETE, J.
PARNEIX, J. P.

GERMANY
BARH, C.
BERESHEV, L.
ESCHER, C.
GEELHAAR, T.
GRUENEBERG, K.
GRULER, H.
HENTSCHEL, D.
JOACHIMI, D.
JUNGE, M.
KITZEROW, H.
KREMER, F.
KRESSE, H.
LOTZ, A.
MICHALSKI, B.
PFEIFFER, M.
PLEINER, H.
POLOSSAT, E.
REINHART, K.-F.
SCHEROWSKI, G.
SCHILLER, P.
SCHLOSSER, H.
SEIMENSMEYER, K.
TSCHIERSKE, C.
WAHL, J.
ZENTEL, R.

HUNGARY
BATA, L.
ÉBER, N.

INDIA
BAWA, S. S.
CHANDRASEKHAR, B. S.
KRISHNA PRASAD, S.
RAJA, V. N.

ISRAEL
COHEN, G.

ITALY
MALTESE, P.

JAPAN
HAGIWARA, T.
HIRAOKA, K.
HIYAMA, T.
ISOZAKI, T.
KANETSUGU, T.
KAZUTOSHI, M.
KIMURA, M.
KODEN, M.
KONDO, H.
KONDO, K.
MARUYAMA, M.
MITSURI, K.
MOCHIZUKI, A.
NAGAYA, T.
NAKAGAWA, M.
NAOYA, I.
NOHIRA, H.
ONNAGAWA, H.
ORIHARA, H.
OZAKI, M.
SAKAGUCHI, K.
SAKAIGAWA, A.
SEKINE, H.
SHIROH, I.
SUMITAKA, T.
SUZUKI, Y.-I.
TAKAHASHI, K.
TAKANISHI, Y.

TAKEZOE, H.
TORIUMI, H.
TSURO, S.
YAMMOTO, S.
YANG, Y. B.
YOKOYAMA, A.
YUASA, K.

NETHERLANDS
HARTMANN, W.
VERHULST, T.

PORTUGAL
FIGEUIRINHAS, J.

SPAIN
ETXEBARRIA, J.
OLARTE, F.
OMENAT, A.
ROS, B.
SANCHEZ-PEÑA, J.
SERRANO, J.
ZUBIA, J.

SWEDEN
DAHL, I.
GOUDA, F.
KOMETOV, L.
LAGERWALL, T.
MATSZCZYK, M.
MATSZCZYK, T.
SKARP, K.

SWITZERLAND
BUCHECKER, R.

UK
BONE, M. F.
COLES, H. J.
DAVEY, A.
DUNMAR, D.
JONES, C.
NICHOLAᴕ, B.
TOWLER, M.

USA
AIHARA, Y.

ARMITAGE, D.
BRANDOW, S.
CLARK, N. A.
DOROGKI, D.
FAIR, D.
FREIDMAN, L.
FUNG, B. M.
HANDSCHY, M.
JAKLI, T.
KUDO, Y.
LIEN, S.-C.
LIU, J.-Y.
MACIRI, J.
MAHMOOD, R.
MERY, S.
MEDDEL, G.
NAKAUCHI, J.
NEUBERT, M.
OUCHI, Y.
PANG, J.
PARK, C. S.
PFEIFFER, S.
PARMAR, D.
RAPPAPORT, A.
RUTH, J.
SABOL-KEAST, S.
SHAO, R.
SUBRAMANIAM, G.
THURMES, W.
VOHRA, R.
WALBA, D.
WAND, M.
WILLIS, P. C.
YANG, K. H.
ZOU, Z.

USSR
CHIGRNOV, V.
CHILAYA, G.
GERASIMOV, A.
LOSEVAS, M.
PITKIN, S. A.
PODNEKS, V.
POZHIDAEV, E.

YUGOSLAVIA
BLINC, R.
ZEKS, B.

PREFACE

The present volumes form the proceedings of the Third International Conference on Ferroelectric Liquid Crystals, held in Boulder, Colorado, USA June 23–28, 1991. These volumes continue the publication of this conference series, the proceedings of the first conference (1987) held at Bordeaux/Arcachon appearing in Volumes 84 and 85, and the proceedings of the second conference (1989) held at Göteborg appearing in Volumes 113 and 114.

As for the two preceding conferences, FLC-91 provided a broad forum for the exchange of information on FLCs, with most of the groups working in the field well represented. Exciting developments were reported in all FLC areas. The world-wide effort at developing new FLC materials continues apace, with the report of an FLC material possessing a spontaneous polarization nearly equal to the sum of all transverse molecular dipoles, and new thrusts in polymer FLCs and FLCs for electronic nonlinear optical applications. The conference saw many new developments in FLC basic and device physics, including the use of dielectric spectroscopy as a tool for studying the molecular origins of the polarization in FLCs. Particularly exciting were the FLC device developments with the emergence of sophisticated FLC devices for opto-electronic computing, display, and other light control applications, including a demonstration of a flexible polymer FLC display!

Due to the intense interest in FLCs in Japan and the large number of Japanese FLC workers, the Fourth International Conference on Ferroelectric Liquid Crystals will be held in Japan in the summer of 1993, organized by Professor A. Fukuda of Tokyo Institute of Technology.

In preparing this proceedings it was the express intention of the Guest Editors to be as timely as possible in publishing the papers of those who submitted and/or revised manuscripts describing their most recent work in time to meet the necessarily tight deadline for 1991 publication. These volumes should thus provide a view of the state of FLC science as of the summer of 1991. It should be noted that some papers submitted for the proceedings for one reason or another could not be made ready in time for inclusion in these volumes. Such papers will be published in future issues of *Ferroelectrics* either as type-set full papers or as letters, with a footnote indicating that they are part of the proceedings of FLC-91.

The Guest Editors would like to thank the sponsors, administrative assistants, and especially all of the scientists who made the meeting such a great success.

Boulder, Colorado, USA, September 1991

Noel A. Clark
David M. Walba

SECTION A
DYNAMICS

BROADBAND DIELECTRIC RELAXATION STUDY
IN A FERROELECTRIC LIQUID CRYSTAL
BY TIME DOMAIN REFLECTOMETRY

RYUSUKE NOZAKI AND TAPAN K. BOSE
Groupe de Recherche sur les Dielectriques, Departement
de Physique, Universite du Quebec a Trois-Rivieres,
Trois-Rivieres, Quebec, Canada

JAN THOEN
Laboratorium voor Akoestiek en Warmtegeleiding,
Departement Natuurkunde, Katholieke Universiteit
Leuven, B-3001 Leuven, Belgium

Abstract Complex permittivity of a ferroelectric liquid
crystal, 4-[(S,S)-2,3-epoxyhexyloxy]-phenyl 4-
(decyloxy)-benzoate, has been measured in the frequency
range between 10MHz and 4GHz, at temperatures from 112°C
down to 53°C by using a time domain reflectometry.
Spectral decomposition of the experimental data showed
that two types of relaxation are involved. The faster
relaxations are active in the ferroelectric phase
whereas the slower ones are very much hindered. It can
be concluded that this hindered relaxation may
correspond to the slowing down of the molecular motion
around the long axis, which has been considered as
leading to a resultant macroscopic polarization.

INTRODUCTION

It is well known that a liquid crystal shows non-isotropic
phases, nematic and smectic phases, in which the average
direction of the long axis of the molecule is not random but
possesses some orientational order. It has been found that,
in non-isotropic phases, the complex permittivity gives rise
to multiple relaxations, which are due to molecular
rotations around their short and long axes, respectively.
These relaxations corresponding to the above rotations can
be observed using special configurations.

When the direction of the applied electric field is
parallel to the molecular long axis, one can measure the

parallel component of the complex permittivity, $\epsilon_{//}$, in which generally low frequency relaxations are dominant. On the other hand, for the perpendicular configuration the complex permittivity, $\epsilon_\perp$, higher frequency relaxations are generally present.[1,2]

According to the conventional understanding[3,4], the ferroelectricity appears as a result of slowing down of the molecular rotation around the long axis of the molecule in the ferroelectric phase. Therefore, it is quite important to follow the high frequency perpendicular relaxations in the temperature range starting before the ferroelectric phase until the beginning of the solid phase.

In this work, complex permittivity measurements on a ferroelectric liquid crystal, 4-[(S,S)-2,3-epoxyhexyloxy]-phenyl 4-(decyloxy)-benzoate, which shows ferroelectricity in the chiral smectic C phase (SmC*), have been performed by using a time domain reflectometry (TDR), for both perpendicular and parallel configurations, at frequencies between 10MHz and 4GHz, in the temperature range from 112°C, 15°C above the nematic-isotropic phase transition point, down to 53°C, well in the crystalline solid phase.

A quick look at the experimental result shows that mean frequency of the relaxation which is about 1GHz in the isotropic phase shows a small positive temperature dependence. Apart from a decrease of 20% in the mean relaxation frequency at the isotropic-nematic transition, the temperature dependence of the perpendicular component in the liquid crystalline phases is similar to the isotropic phase. Somewhat similar behavior has also been observed by Vallerien et al.[5] for a sample of [4-(3)-(S)-methyl-2-(S)-chloropentanoyloxy]-4'-octyloxy-biphenyl. They suggest[6] that the theory, in which slowing down of the molecular rotation around the long axis is considered to be responsible for the ferroelectricity of liquid crystal, may have to be modified because the observed relaxation showed no retardation in the ferroelectric phase.

However, a careful frequency decomposition of the data shows that, in the frequency range used here, multiple relaxation processes are involved both in the isotropic and the liquid crystalline phases. These relaxations fall into two categories: high frequency relaxations with small activation energy are active in the nematic, smectic A and ferroelectric phases and the other already very much hindered in the nematic phase and possibly attaining a very low frequency in the ferroelectric phase. As the frequency limit for our measurement is about 10MHz, we cannot reach a definite conclusion on the presence of the hindered low frequency relaxation in the ferroelectric phase.

EXPERIMENTAL

For the complex permittivity measurements in the frequency range from 10MHz to 4GHz, a time domain reflectometry method (TDR) is used. Detailed description of the system has already been reported elsewhere.[7] In the present case, in order to obtain the complex permittivity, a bilinear coefficient method is employed. Using the Fourier transform of the reflected signal from the dielectric cell with the sample placed at the end of a coaxial line, $V_x(\omega)$, and $V_o(\omega)$ for the empty cell, the complex permittivity of the sample, $\epsilon^*(\omega)$, is given in a bilinear form by

$$\epsilon^* = (1-A^*)\Omega \ /(1+B^*\Omega) \tag{1}$$

and

$$\Omega = (c/j\omega d) \ (V_o-V_x)/(V_o+V_x) \tag{2}$$

where c is the speed of light, ω is an angular frequency and d is the effective electrical length of the cell. The complex coefficients A^* and B^* are determined by measuring standard samples with known permittivity. Acetonitrile, acetone and chlorobenzene were used in this work.

In order to align the molecular long axis, a permanent magnet was used. The diameter of the flat surface of the tapered pole is 6cm and the gap between the two poles is

15mm. The magnetic flux density at the center where the brass made dielectric cell is located is about 1.4T.

In the case of perpendicular configuration, a parallel plate capacitor with d=2.7mm is used where the orienting magnetic field is parallel to the electrode disks. On the other hand, a coaxial cell with d=14.9mm is used to obtain the half-parallel and half-perpendicular component, ϵ_{hp-hp}, and the parallel component, $\epsilon_{//}$, is calculated from the relation

$$\epsilon_{hp-hp} = (\epsilon_{//} + \epsilon_\perp) / 2. \tag{3}$$

The ferroelectric liquid sample, 4-[(S,S)-2,3-epoxyhexyloxy]-phenyl 4-(decyloxy)-benzoate, 98%, was purchased from Aldrich Chemical Company (Cat. No. 32,853-7). Chemical structure of the sample and its phase transition temperatures are shown in Fig. 1. The cell temperature is

Crys. ← Sm3 ← SmC* ← SmA ← N ← I
     60   64   80   81 97 [°C]
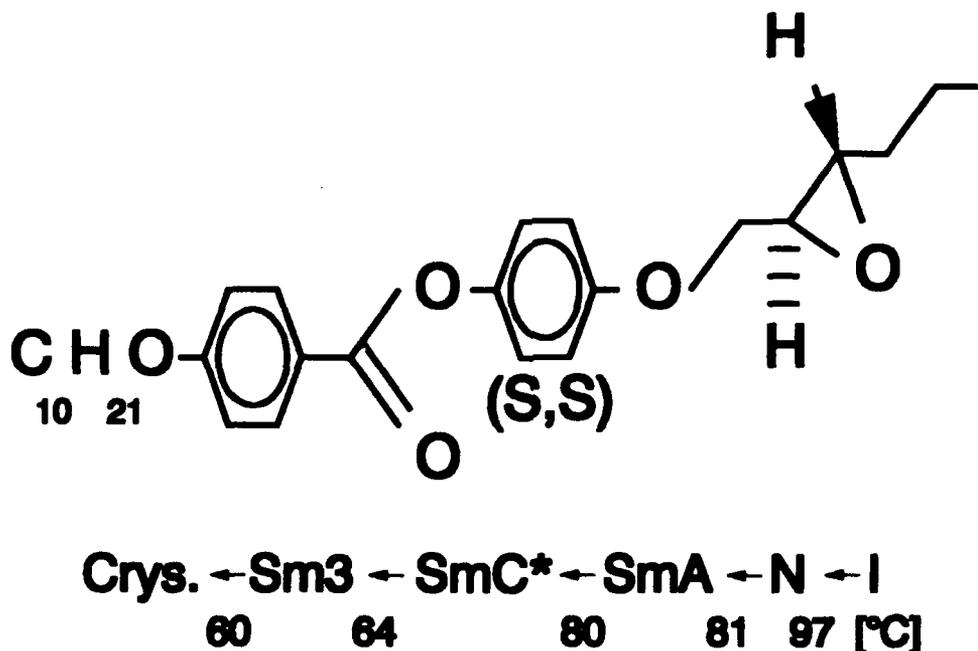
FIGURE 1.   Chemical structure and the phase transition temperatures of the sample.

stabilized by use of a liquid flow jacket with circulating polyethylene glycol controlled by a refrigerated bath unit (NESLAB model RTE-210). In order to change the temperature, the setpoint for the bath is controlled by a 16bit personal computer through 12bit D/A convertor. Complex permittivity measurements were performed using cooling rate of 2.7°C/hour.

RESULTS AND DISCUSSION

In figure 2, the temperature dependence of the permittivity at 10MHz for both perpendicular and parallel components are shown. In the case of perpendicular component, the value of
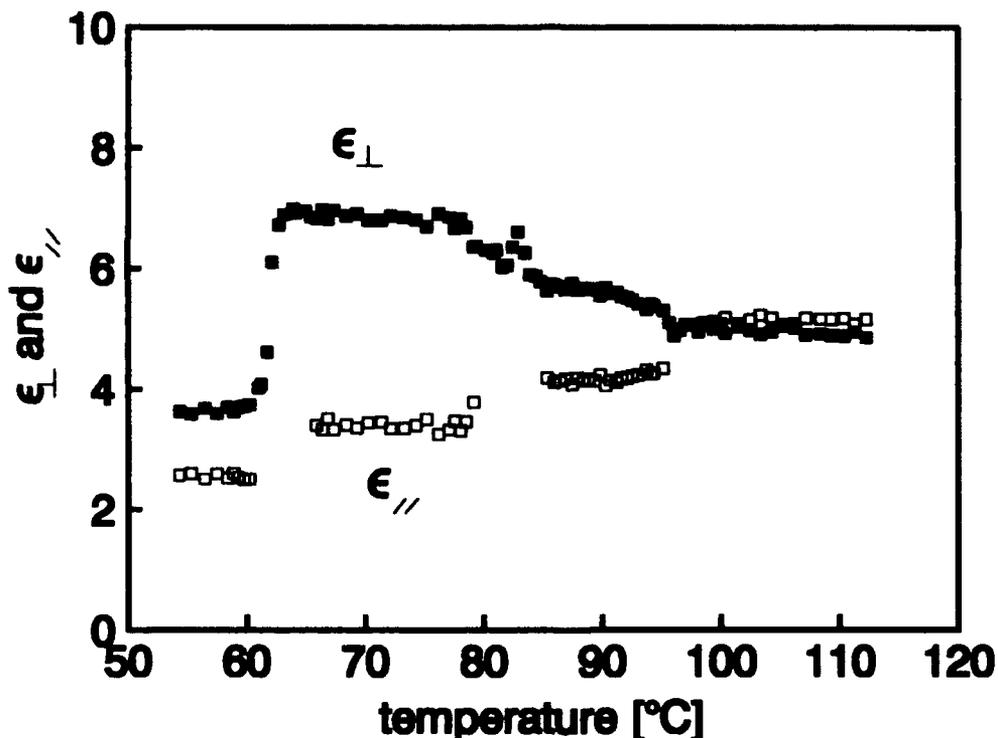
FIGURE 2.   Permittivity at 10MHz for the perpendicular (■) and the parallel (□) components.

the permittivity increases somewhat monotonously as temperature decreases from the isotropic to the ferroelectric phase, and then drops sharply at the end of the ferroelectric phase. These are essentially the same

behavior as those given by Vallerien et al.[5] for the sample
of [4-(3)-(S)-methyl-2-(S)-chloropentanoyloxy]-4'-octyloxy-
biphenyl. On the other hand, for the parallel component,
the value of the permittivity at 10MHz in the nematic phase
and lower temperature phases is very small compared to that
for the perpendicular component, but still larger than that
in the solid phase. The temperature dependence of the
permittivity of the parallel component is positive contrary
to that of the perpendicular component.

In figure 3, frequency dependence of the complex
permittivity at 87.19°C, in the nematic phase, is shown for
parallel, perpendicular and half-parallel and half-
perpendicular configurations. It is clear from figure 3
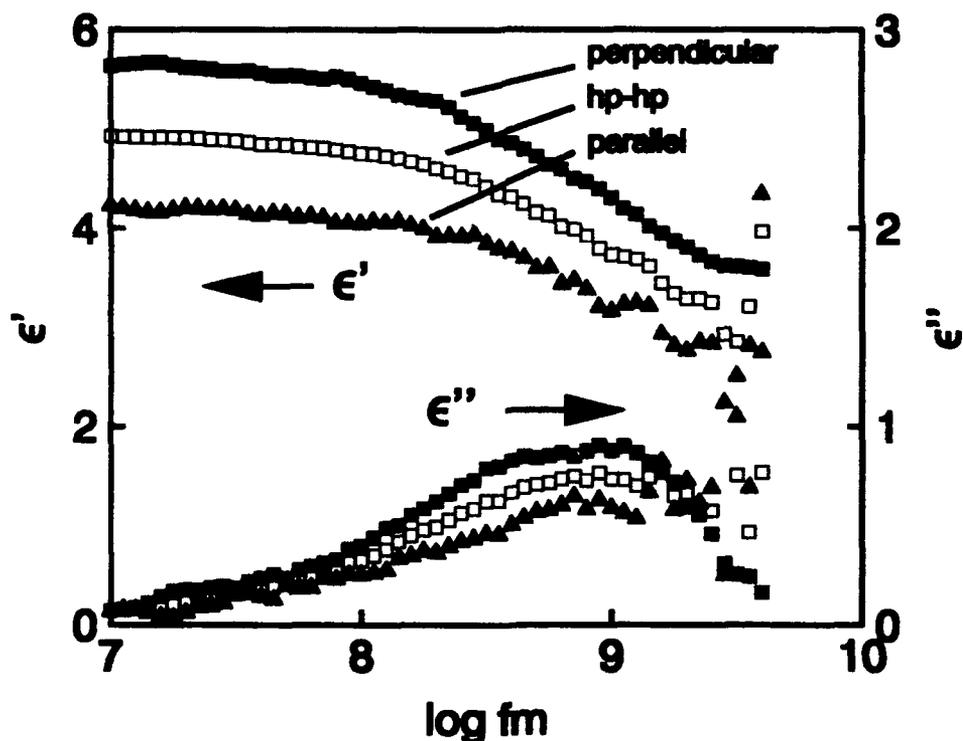
FIGURE 3. ϵ' and ϵ'' against frequency at 87.19°C.

that all relaxation curves are somewhat broad and thus
indicating the presence of more than one relaxation
mechanisms. Since multiple relaxations seem to be involved
but are not clearly separated, it is natural to consider an

analysis with multiple Debye relaxations. The following equation is used to describe the experimental data:

$$\epsilon^{*}_{measured} = \sum_{k}^{m} \Delta\epsilon_{k}/(1+j\omega\tau_{k}) + \epsilon_{\infty} \qquad (4)$$

where $\epsilon^{*}_{measured}$ is the measured complex permittivity, ω is the angular frequency, $\Delta\epsilon_{k}$ and τ_{k} are dielectric relaxation strength and time for the kth process, and ϵ_{∞} is the permittivity at limiting high frequency. The number of Debye relaxations m involved in the data at each temperature was estimated by using a least square fitting procedure.[8]

Figure 4 shows the relaxation map, log f_{m} vs 1/T, for the perpendicular component. It is indicated that four relaxation processes (A, B, C and D) can be assumed for entire temperature range. The temperature dependence of the relaxation strength for each process is shown in figure 5 where the value of ϵ_{∞} is also given.

The relaxation map for the parallel component is shown in figure 6 and the corresponding dielectric strength and ϵ_{∞} against temperature are given in figure 7. In the case of parallel component, also four relaxation processes (E, F, G and H) can be assumed. The isotropic phase relaxation values obtained from the two measuring configurations are identical within the experimental error.

Because of very high relaxation frequencies for the processes C and D, one can assume them to be due to internal molecular motions. In fact, the processes G and H in the parallel component, shown in figure 6, are very similar to C and D in the perpendicular component (figure 4) and thus cannot be attributed to the rotational motion of the molecule.

On the other hand, the process B has an activation energy of 31kJ/mol in the isotropic phase and it increases to 300kJ/mol in the nematic phase. In the smectic A phase, this process goes out of the measured frequency range. The
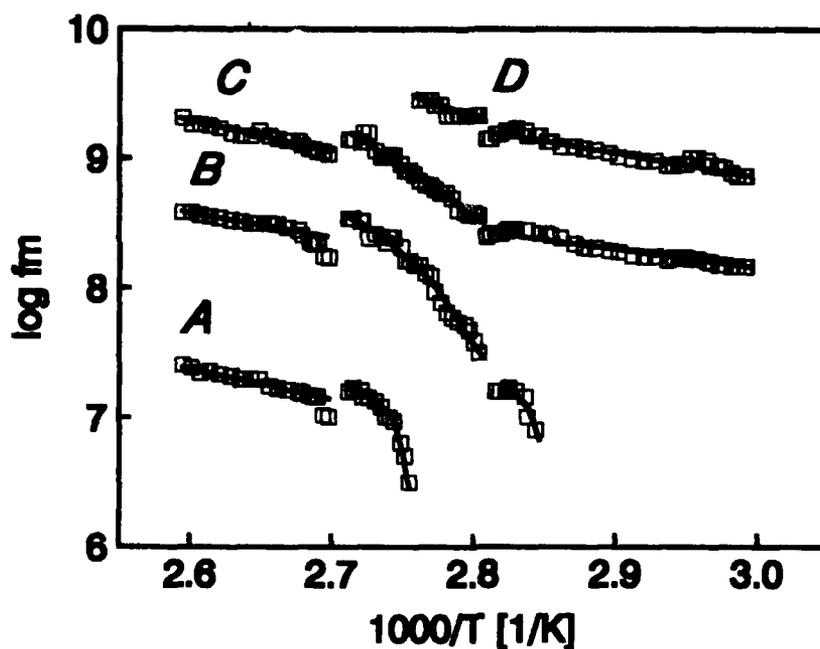
FIGURE 4.   log f_m against 1/T for the perpendicular components.
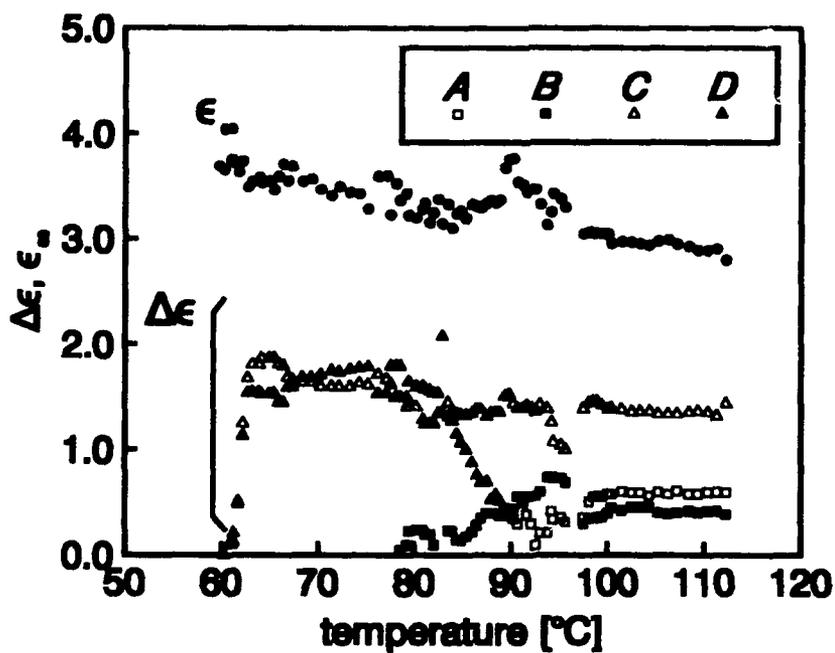
FIGURE 5. $\Delta\epsilon$ and ϵ_∞ against temperature for the perpendicular component.
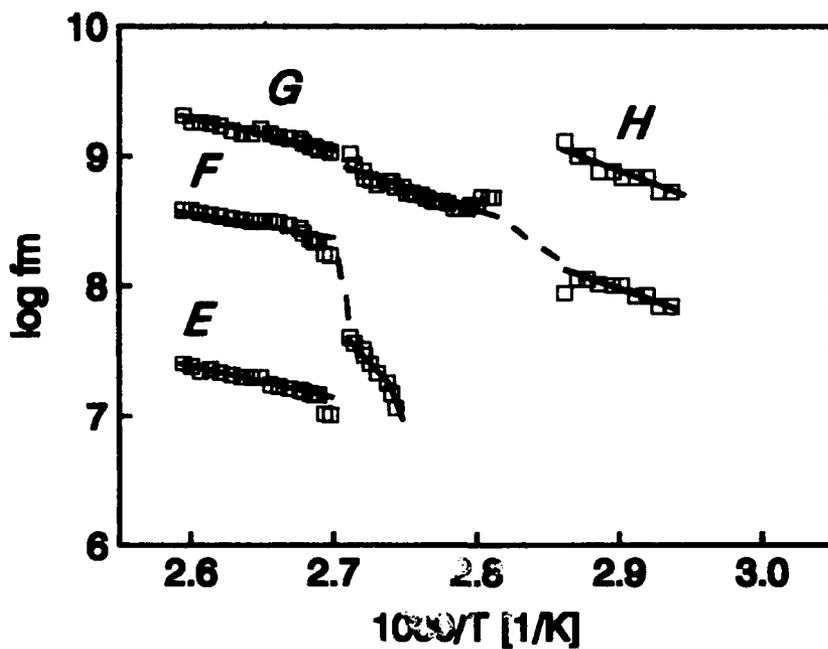
FIGURE 6.   log f_m against 1/T for the parallel
component.
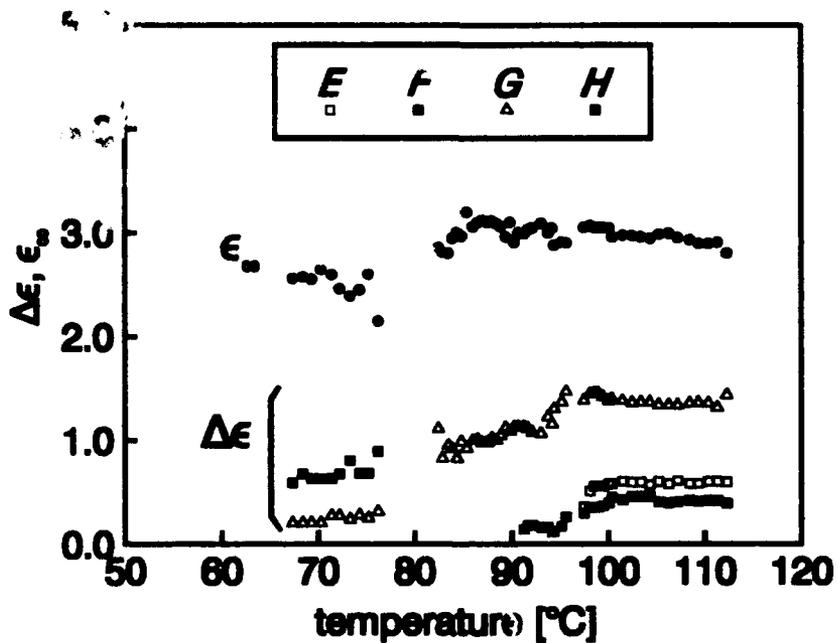
FIGURE 7. $\Delta\epsilon$ and ϵ_∞ against temperature for the
parallel component.

dielectric strength $\Delta\epsilon$ of this process decreases with decreasing f_m in the nematic and smectic A phases. The behavior for the process A is essentially the same as that for the process B within the measured frequency range

Based on the above observations, it may be assumed that the processes A and B are due to the molecular rotation around the long axis. Actually, these are very much retarded in the nematic and the smectic A phases. It can therefore be easily concluded that such a rotational motion is also strongly hindered in the ferroelectric phase. It is important to note that the different relaxation mechanisms obtained from the experimental data of the perpendicular component are also corroborated by the data obtained independently in the half-parallel and the half-perpendicular configuration.

It is important to point out for phenomenological interpretation of present dielectric data that most of the contributions to the permittivity even at 10MHz for the perpendicular component, shown in Figure 2, are due to the high frequency processes C and D as shown in Figure 5. The contribution of the others (A and B) are very small compared to those of C and D.

It should also be pointed out that the process D is seen to appear in the nematic phase with decreasing temperature and attains a constant value in the ferroelectric phase. Although the process D is near the high frequency limit, the value of ϵ_∞ indicates that there is no more relaxation at higher frequencies. As shown in Figure 5, the amplitude of highest frequency relaxation (process D) grows substantially from the nematic to the ferroelectric phase with the lowering of temperature. Since this process is absent in the isotropic phase, this relaxation mechanism may be an internal mode associated with some kind of aligned structure.

REFERENCES

1. T. K. Bose, R. Chahine, M. Merabet, and J. Thoen, J. Phys. (Paris), 45, 1329 (1984).
2. T. K. Bose, B. Campbell, S. Yagihara, and J. Thoen, Phys. Rev. A, 36, 5767 (1987).
3. R. B. Meyer, L. Liebert, L. Strzelecki, and P. Keller, J. Phys. (Paris) Lett., 36, L69 (1975).
4. J. R. Lolanne, J. Buchert, C. Destrade, H. T. Nguyen, and J. P. Marcerou, Phys. Rev. Lett., 62, 3046 (1989).
5. S. U. Vallerien, F. Kremer, T. Geelhaar, and A. E. Wächtler, Phys. Rev. A, 42, 2482 (1990).
6. F. Kremer, S. U. Vallerien, K. Kapitza, R. Zentel, and E. W. Fischer, Phys. Rev. A, 42, 3667 (1990).
7. R. Nozaki and T. K. Bose, IEEE Trans. Instrum. Meas., 39, 945 (1990).
8. T. K. Bose, G. Delbos, and M. Merabet, J. Phys. Chem., 93, 867 (1989).

THE MOLECULAR ORIGIN OF FERROELECTRICITY IN FLC: A CHALLENGE FOR DIELECTRIC SPECTROSCOPY AT MICRO-WAVE FREQUENCIES

F. KREMER, A. SCHÖNFELD, S.U. VALLERIEN, A. HOFMANN, N. SCHWENK

Max–Planck–Institut für Polymerforschung, Postfach 31 48,

W–6500 Mainz, FRG

Abstract Broadband dielectric spectroscopy delivers in the frequency regime from 10 Hz to 10 GHz two collective relaxation processes (soft- and Goldstone–mode) and one molecular relaxation (β–relaxation). The latter does <u>not</u> split or broaden at the phase transition SmA*/SmC*. Its dielectric strength does not decline — in pronounced contrast to the (generalized) Landau theory of the phase transition SmA*/SmC* in FLC. Our experimental findings contradict the common explanation of the spontaneous polarization which is based on the existence of a free rotation inside the SmA* phase and its strong hindrance in the ferro-electric SmC* phase.

INTRODUCTION

The molecular origin of ferroelectricity in FLC is usually attributed to a "free" rotation of the mesogenes around their long molecular axis in the (non–ferroelectric) SmA–phase and its strong hindrance in the (ferroelectric) SmC*–phase[1,2]. The Landau theory[3] also in its generalized form[4] predicts in the SmA*–phase <u>one</u> high– frequency polarization mode, <u>which splits in frequency</u> at the phase transition SmA*/SmC* and declines strongly in its dielectric strength in the SmC*–phase.

EXPERIMENTAL

To cover the entire frequency regime from 10 Hz to 20 GHz three different measurement systems were employed (i) an automatic AC–bridge (HP 4192A), (ii) a coaxial line reflectometer (HP 4191A) and a network analyser (HP 8510 E). Rubbed, polyimid coated metal electrodes ($\emptyset$: 3 mm, spacing: 20 μm) were developed and could be used in the <u>entire frequency</u> range from 10 Hz to 20 GHz. Furthermore in the identical sample capacitor arrangement the spontaneous polarization was measured. Similar values as for semitransparent FLC–cells were found ($\approx$ 300 nC/cm²) thus proving the existence of a bookshelf geometry.

A pure liquid–crystalline sample ([4–(3)–(S)–methyl–2–(S)–chloro–pentanoyloxy]–4′–octyloxy–binphenyl) having two chiral centers was used (sample 1)

$$CH_3\text{--}(CH_2)_7\text{--}O\text{--}\hexagon\text{--}\hexagon\text{--}O\text{--}\overset{\overset{\textstyle O}{\|}}{C}\text{--}\overset{*}{\underset{\underset{\textstyle Cl}{|}}{CH}}\text{--}\overset{*}{\underset{\underset{\textstyle CH_3}{|}}{CH}}\text{--}C_2H_5$$

$$\text{cryst.} \xrightarrow{305\ K} \text{SmX*} \xrightarrow{322\ K} \text{SmC*} \xrightarrow{327\ K} \text{SmA*} \xrightarrow{338\ K} I$$
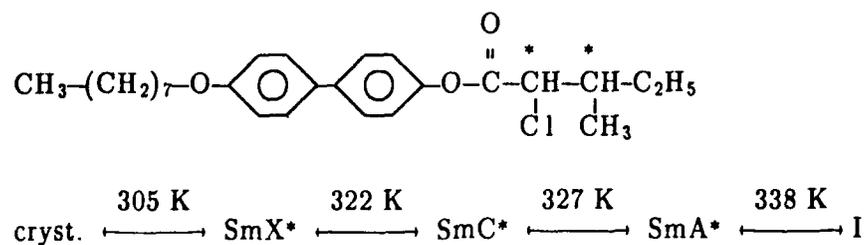
(Here, I represents isotropic.) Its synthesis and characterization by differential–scanning–calorimetry (DSC) and X–ray structure analysis is described elsewhere[5,6].
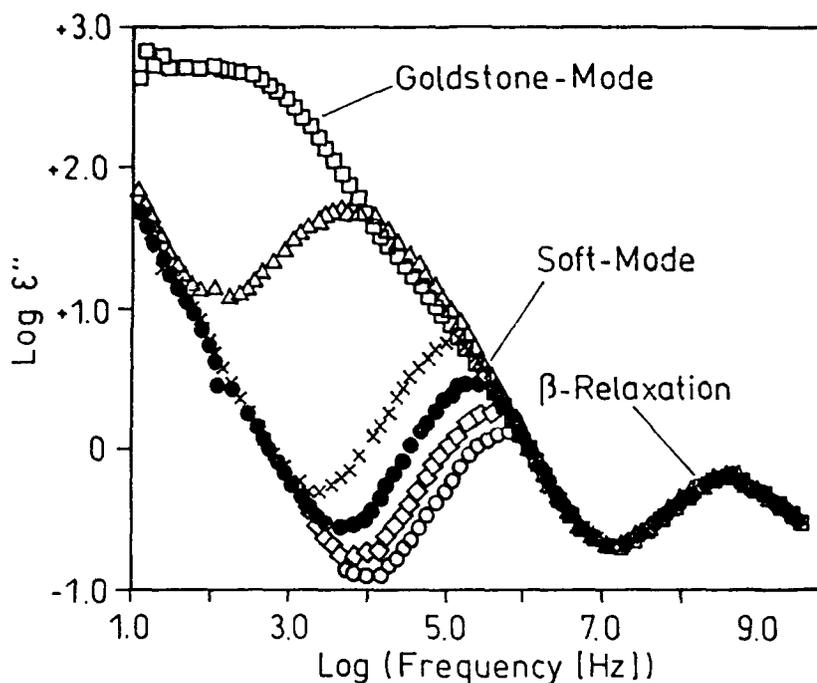
FIGURE 1 Goldstone—, soft—mode and β—relaxation at the phase transition SmA/SmC* (□): 331.3 K, (○): 330.4 K, (●): 329.4 K, (x): 328.5 K, (△): 327.5 K, (●): 326.5 K. The phase transition SmA*/SmC* is at 327.0 K. The sample was oriented in the bookshelf geometry.

RESULTS AND DISCUSSION

Below 10^6 Hz the ferroelectric modes, soft— and Goldstone—mode are observed as expected (Fig. 1). In the microwave regime (10^6–10^{10} Hz) only one relaxation process is found. At the phase transition SmA*/SmC* this process does not split or broaden (Fig. 2). Its dielectric strength does not decrease (Fig. 3). The molecular assignment of the β—relaxation is a hindered rotation of the mesogenes around their long molecular axis.
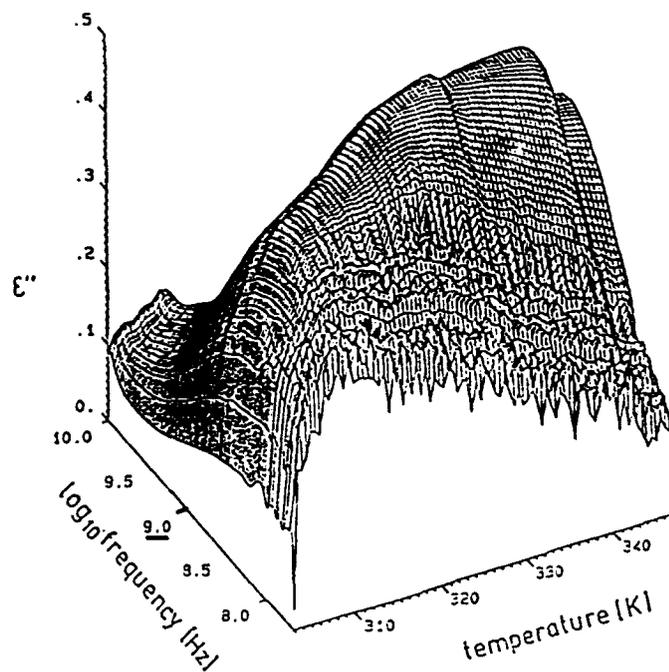
FIGURE 2   Frequency and temperature dependence of the dielectric loss
ϵ''. The sample was aligned in the bookshelf geometry.

For a quantitative analysis the data were fitted with the generalized relaxation
function of Havriliak and Negami[7]

$$\hat{\epsilon}(\omega) = \epsilon_{\infty} + \frac{\Delta \epsilon}{\left(1 + (i \, \omega \tau)^{\alpha}\right)^{\gamma}}$$

where ϵ_{∞} describe the real part of the dielectric function for $\omega \gg 1/\tau$, with τ
being the relaxation time. $\Delta \epsilon$ is the dielectric strength. The constants α resp.
γ determine the symmetric resp. asymmetric broadening of the relaxation
function. The temperature dependence of the relaxation rate $1/\tau$ is Arrhenius–
like and shows no decline (Fig. 3) at the phase transition SmA*/SmC*. The
dielectric strength of the β–relaxation does not decrease at the phase

transition. Instead it increases slightly (Fig. 3). This is caused by the change of the aspect angle of the lateral dipole moments with respect to the outer electrical field at the phase transition. A racemic mixture corresponding to sample 1 showed a similar β–relaxation, with an Arrhenius type activation energy. Its slope is slightly different in the different mesophases.
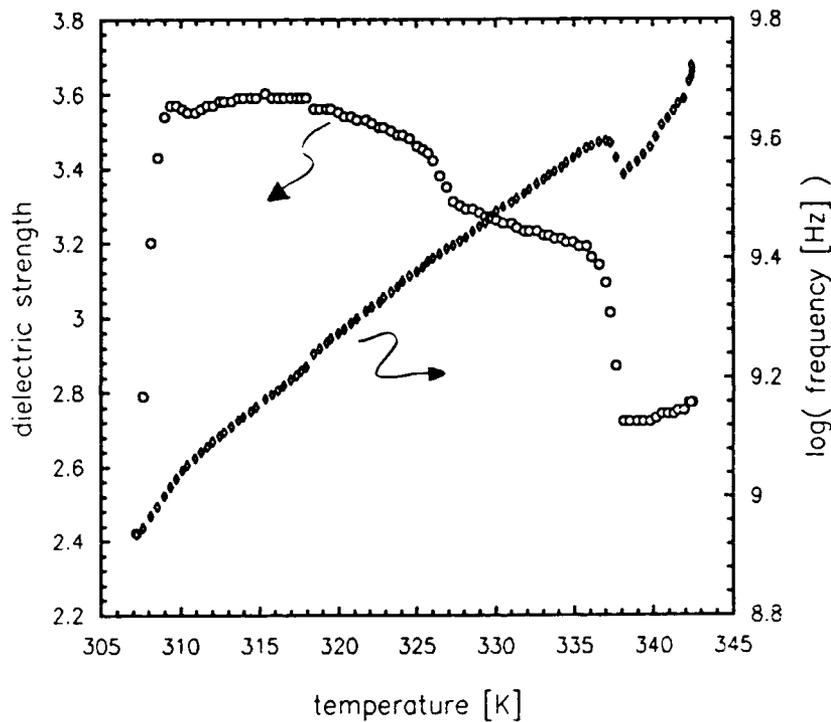
FIGURE 3   Temperature dependence of the relaxation rate $\frac{1}{\tau}$ and the dielectric strength $\Delta \epsilon$ of the β–relaxation. Otherwise as Fig. 2.

CONCLUSION

To summarize the experimental findings: The β–relaxation in FLC does not show a splitting or broadening at the phase transition SmA*/SmC*. Its dielectric strength does not decrease, instead it increases slightly at the phase

transition SmA*/SmC* − in pronounced contrast to the (generalized) Landau theory of the phase transition SmA*/SmC*[3,4].

This discrepancy between theory and experiment can be traced back to a redundant dynamic variable − according to Brand and Pleiner[8]: In the (generalized) Landau theory[3,4] four dynamic variables are introduced, two components of the primary order parameter, the tilt vector $\vec{\xi}$ and two components of the secondary−order parameter, the in−plane polarization $\vec{P}$. Undoubtedly, the two components of the tiltvector are dynamic variables, but rotations of the macroscopic polarization are already described by the rotation of the tilt angle. Thus only a third free variable is needed, the absolute value of the polarization $|\vec{P}|$. It reflects the average over the molecular dipoles, the excursion of their hindered rotation, the different interactions between the mesogenes, etc.

Our results which are also in agreement with NMR−measurements[9] demonstrate that the β−relaxation is not at all a "free" rotation, which becomes strongly hindered in the SmC*−phase. If this "picture" would be correct one would have to expect a strong discontinuity of the relaxation rate $\frac{1}{\tau}$ at the phase transition SmA*/SmC* and a pronounced decrease of the dielectric strength in the SmC*−phases, in sharp contrast to the experimental findings. Instead the β−relaxation has to be comprehended as a librational motion. In the SmA*−phase all angular orientations of the lateral dipolmoments have the same probability. In the SmC*−phase, the tilt induces a pronounced anisotropy of these angular orientations, thus giving rise to the local spontaneous polarization and hence the ferroelectricity in FLC.

REFERENCES

1. L.M. Blinov, Electro–optical and Magneto–optical Properties of Liquid Crystals (Wiley, New York , 1983).
2. J.R. Lalanne et al., Phys. Rev. Lett., 62, 3046 (1989).
3. R. Blinc and B. Žekš, Phys. Rev., A 18, 740 (1978).
4. T. Carlsson, B. Žekš, C. Filipič and A. Levstik, Phys. Rev., A 42, 877 (1990).
5. S.U. Vallerien, F. Kremer, T. Geelhaar and A. Wächtler, Phys. Rev., A 42, 2482 (1990).
6. F. Kremer, S.U. Vallerien, H. Kapitza, R. Zentel and E.W. Fischer, Phys. Rev., 42, 3667 (1990).
7. S. Havriliak, S. Negami, J. Polym. Sci., C 14, 89 (1966).
8. H.R. Brand, H. Pleiner, Phys. Rev. A, in press.
9. K. Yoshino, M. Ozaki, S. Kishio, T. Sakurai, N. Mikami, R. Higuchi, M. Huoma, Mol. Cryst. Liq., 144, 87 (1987).

Electroclinic effect in the N* phase near a N* SA SC* multicritical point

C. LEGRAND+, N. ISAERT++, J. HMINE++, J.M. BUISINE++, J.P. PARNEIX*, H.T. NGUYEN**, C. DESTRADE**

+ Centre Hyperfréquences et Semiconducteurs,
  UA CNRS n° 287
++ Laboratoire de Dynamique et Structure des Matériaux
  Moléculaires, UA CNRS n° 801
  Université de Lille Flandres Artois,
  59655 Villeneuve d'Ascq Cedex - France
* ̒ ̒ Nationale Supérieure de Chimie Physique de Bordeaux
** Centre de Recherche Paul Pascal Université de Bordeaux 1,
  33405 Talence Cedex - France

Abstract

From structural, thermodynamical analysis and polarization measurements, we show that the N* S_C^* phase transition of the homologous n = 8 of a biphenyl benzoate series appears near a N* SA S_C^* multicritical point. Dielectric measurements detect a relaxation process in the N* phase. The temperature dependence of the dielectric strength and of the critical frequency are similar to these of the soft mode classically observed in the SA phase.

This relaxation process is attributed to an electroclinic effect in the N* phase near a N* S_C^* phase transition. Its large amplitude is probably connected with the proximity of the N* SA S_C^* multicritical point.

1 - Introduction

The electroclinic effect near a S_A - S_C^* phase transition is now well know [1]. A great number of data have been reported in the S_A and in the S_C^* phases from optical observation in planar thin cells [2] and from dielectric measurements [3]. Only, some results concern the cholesteric N^* phase [4 - 7]. In this phase, this effect is found to be of relatively small amplitude and is optically measured in materials with very large N^* pitch in order to obtain an unwound structure in thin cells. We present here the first dielectric evidence of an electroclinic effect in the N^* phase in the biphenyl benzoate series given in table I.

For $n \leq 9$, no S_A phase is observed whereas it appears on a small temperature range for $n \geq 10$ (< 1 °C for $n = 10$). The proximity of a N^* S_A S_C^* multicritical point may be suspected. We present a complete characterization (pitch, tilt angle, polarization, D.S.C., thermobarometric analysis and dielectric measurements) of the homologous $n = 8$. The N^* S_C^* phase transition of this compound appears near the N^* S_A S_C^* multicritical point. The amplitude of the electroclinic effect is enhanced by the hight polarization of the compound and by the proximity of the N^* S_A S_C^* multicritical point.

$$C_nH_{2n+1}O-\bigbenzene-CO_2-\bigbenzene-\bigbenzene-O_2C-\overset{*}{C}H-\overset{*}{C}H-C_2H_5$$

with Cl and CH$_3$ substituents.

n	K	$S_?$	S_C^*	S_A	N^*	BP	I
7	• 100	• (52)	• 134	–	• 166	• 166.1	•
8	• 88	–	• 138	–	• 165.5	• 166.5	•
9	• 89	–	• 142	–	• 162	• 162.1	•
10	• 88	–	• 143	• 144	• 159	• 160	•
11	• 88	–	• 146	• 149	• 157	• 157.1	•
12	• 81	–	• 145.5	• 150	• 154	• 154.5	•

Table I : Chemical formulae and phase sequences of the biphenyl benzoate series.

2 - Structural studies

Pitch, tilt angle and polarization measurements were performed. The data are reported in Figures 1 to 3.

The helical pitch (Figure 1) was measured by the Grandjean - Cano method with prismatic planar samples in the N* phase and prismatic complanar samples in the S_C^* phase [8]. The temperature dependence of the pitch is rather classical. The pitch in the N* phase is very small (it gives rise to selective reflexion of visible light). In the S_C^* phase, its value increases from 1 μm at low temperature to 1.5 μm at the N* S_C^* phase transition. The temperature variations of the tilt angle are reported (Figure 2) for two methods : from X-ray diffraction and from planar unwound sample reversed by an electric field [9]. The temperature dependence of the rotatory power has also been used. In X-ray measurements, the molecular length is the layer spacing in the S_A phase of the homologous n = 10 reduced of the C - C bonds length. The temperature dependence of the tilt angle is not classical for a N* S_C^* phase transition : the tilt angle
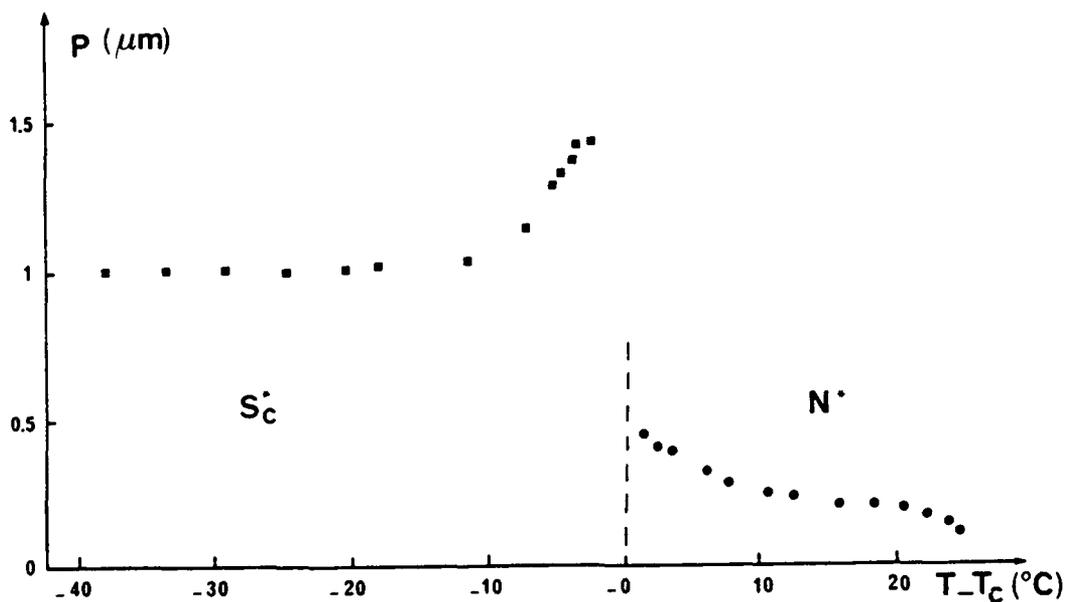
Figure 1 : Pitch temperature dependence in the N* and in the S_C^* phases.
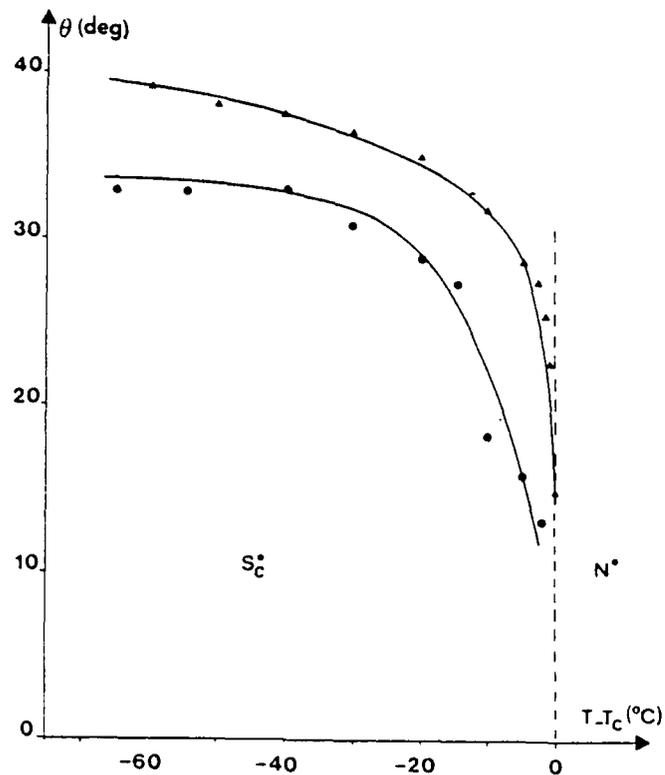
Figure 2 : Tilt angle temperature dependence (• from X-ray, ▲ from planar sample reversed by an electric field).
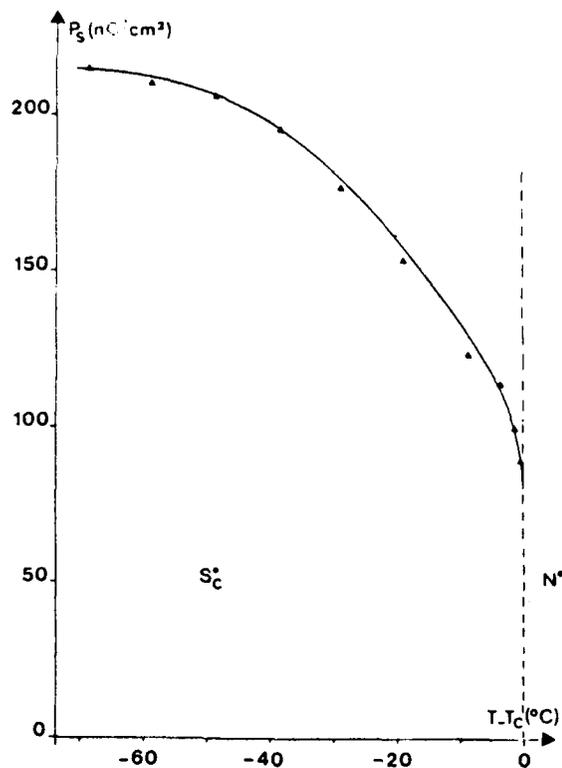
Figure 3 : Polarization temperature dependence.

value is about 35° for below T_C and decreases up to 10° at the transition. This behaviour is confirmed by the rotatory power which almost vanishes at the $\overset{\bullet}{S_C}$ N* transition. As usual, higher values of the tilt angle are found by the method using an electric field ; the general behaviour is similar. The polarization is measured with the same set-up as the tilt angle in planar unwound samples with a triangle wave of high enough amplitude to reverse the polarization. The anomaly of the tilt angle at the transition is also observed for the polarization (Figure 3). The polarization is relatively high and decreases from 210 nC/cm^2 to 70 nC/cm^2 at the transition.

3 - Thermodynamical studies

Differential scanning calorimetry (DSC 7 Perkin Elmer) and isochoric thermobarometric analysis (metabolemeter MAB 02 - MTM Leader) was performed [10]. D.S.C. shows that the N* $\overset{\bullet}{S_C}$ phase transition is clearly first order (250 cal/mole). On cooling, two transitions are observed with a total variation of 300 cal/mole : a monotropic S_A phase exists over a few degrees. The pressure-temperature phase diagram is given in figure 4 . The S_A phase is induced under pressure with a N*$S_A\overset{\bullet}{S_C}$ multicritical point of coordinates 144° C, 150 bars. The $\overset{\bullet}{S_C}$ S_A and S_A N* phase transitions detected at higher pressure are found second order or weakly first order.

4 - Dielectric measurements

We used a previously described experimental procedure [11]. The measurements were made in the frequency range 5 Hz - 1 MHz in the planar orientation, without and with superimposition of a D.C. bias on the measurement electric field [12] . The cell thickness was about 50 μm. The dielectric strength and the relaxation frequency of the observed relaxation process as a function of temperature are given in Figures 5 and 6.

Figure 4 : Pression-temperature phase diagram.

S$_C^*$ phase

In the S$_C^*$ phase, the results are rather classical. Without bias, a relaxation process is detected ; its dielectric strength increases far below T$_C$ (150 at T$_C$ - T = 5° C) and its relaxation frequency is temperature independent (3 kHz). This relaxation process corresponds to the classical Goldstone mode ("in phase" fluctuations of the orientations of the order parameters [13] or orientation tilt mode [14]). Under bias, the Goldstone mode disappears. An other relaxation process is detected ; its dielectric strength increases near T$_C$ whereas the relaxation frequency has the reversed behaviour. This relaxation process corresponds to the soft mode (" in phase" fluctuations of the amplitudes of the order parameters [13] or amplitude tilt mode [14]) . Usually, linear temperature dependence of the inverse dielect ic strength and of the critical frequency of this mode are found [15]. In our case, these parameters saturate as the temperature decreases (1.2 and 80 kHz). The soft mode also exists in measurements without bias. Far below T$_C$, this process

is completely masked by the Goldstone mode. Near T$_C$, the characteristic parameters of the two modes become similar and it is difficult to separate them. For this reason, it is not possible to say if the Goldstone mode dielectric strength is discontinuous or not at T$_C$ althougth the phase transition is first order.
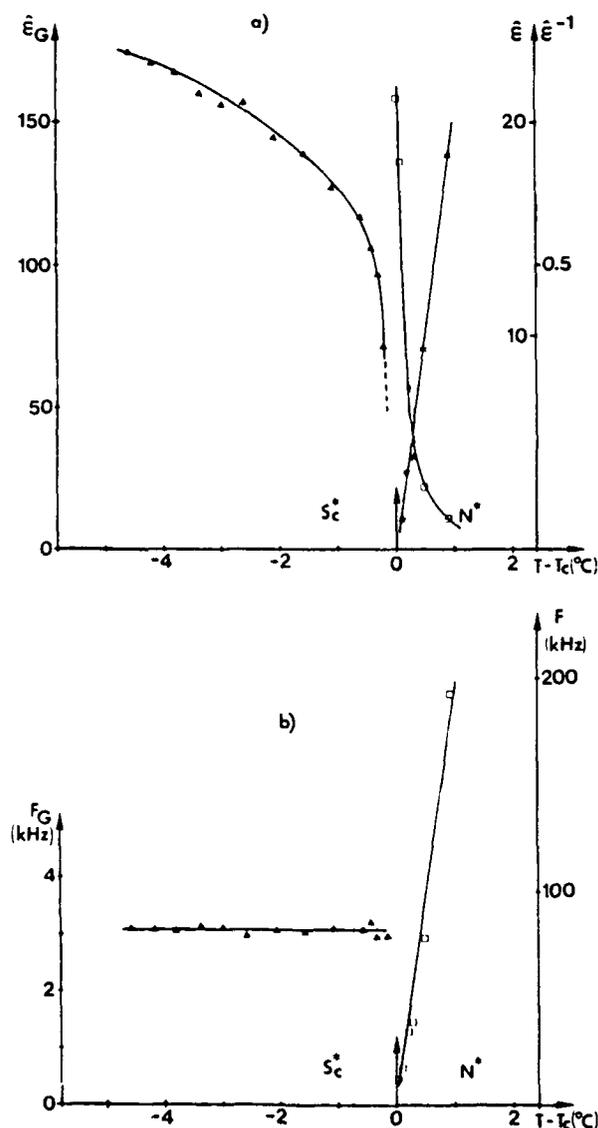
Figure 5 : Dielectric strength (a) and relaxation frequency (b) temperature dependence of the Goldstone mode (▲) and of the relaxation process observed in the N⁺ phase (□) without bias. The inverse dielectric strength is also reported (∗).
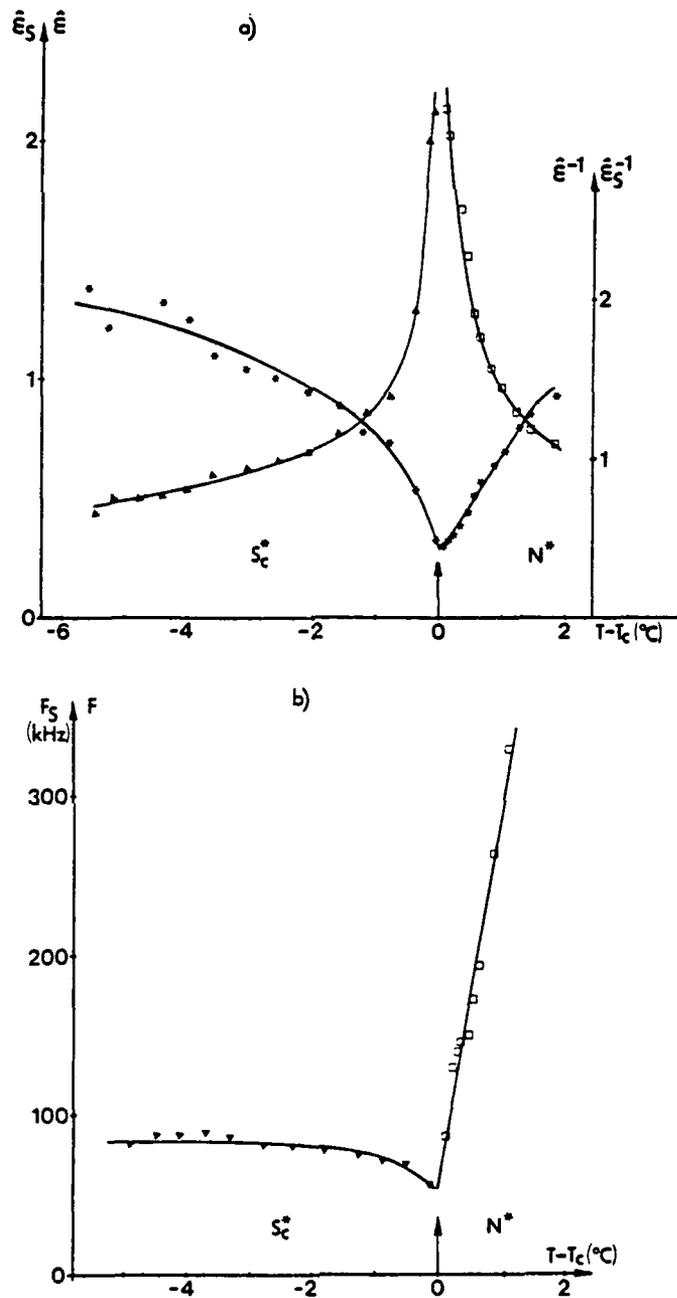
Figure 6 : Dielectric strength (a) and relaxation frequency (b)
temperature dependence of the soft mode (▲) and
of the relaxation process observed in the N* phase (□)
with bias=35V. The inverse dielectric strength is
also reported (*).

N* phase

Measurements, without and with bias, clearly detect a relaxation process in this phase. As we approach the N* $\overset{*}{S_C}$ phase transition, its dielectric strength increases whereas the relaxation frequency linearly decreases from several hundred kHz to several ten kHz (slopes ~ 200 kHz/° C with and without bias). The temperature dependence of the inverse of the dielectric strength is also linear (slopes 0.97 °C^{-1} with bias = 0 V and 0.64 °C^{-1} with bias = 35 V). In the case of the measurements under bias, the characteristic parameters of this relaxation process seems to be continuous with these of the soft mode in the $\overset{*}{S_C}$ phase. Different values of the dielectric strength and of the relaxation frequency are found in measurements with and without bias. Such a behaviour has already been reported [16]. Furthermore, the application of a D.C. bias may induce a N* $\overset{*}{S_C}$ phase transition [17]. In our case, the applied electric field is lower than 1V/μm ; taking into account the threshold voltage obtained by Andersson and al. the transition temperature is not significatively modified. Further experiments are in progress to precise the effect of the D.C. bias.

5 - Discussion and conclusion

The relaxation process observed in the N* phase of our compound has the same behaviour as the soft mode classically observed in the S_A phase (which corresponds to an electroclinic effect) :

- the inverse of the dielectric strength and the relaxation frequency linearly depend on the temperature,
- it seems continous with the soft mode observed in the $\overset{*}{S_C}$ phase under bias.

For this reason, we attribute this relaxation process to an electroclinic effect near a N^* S_C^* phase transition. An electroclinic effect in the N^* phase has recently been reported near N^* S_A [5, 7] and N^* S_C^* [7] phase transitions. The compounds have very large N^* pitch and the effect is measured by optical method using thin planar unwound samples. In our case, the pitch is low ($\leq$ 0,5 μm) and the method cannot be applied. As no effect is observed in Komitov experiments [7] when the N^* phase is wound, in our case optical light oscillations are clearly visible. They are related to rotatory power oscillations that can only be explained by a large amplitude electroclinic effect. Because of the lack of model for the N^* S_C^* sequence, we cannot estimate the electroclinic coefficient from the dielectric data of the unique n = 8 compound. Dielectric studies have been performed for other compounds (n = 9 $\rightarrow$ 11) ; a similar dielectric strength relaxation process is measured in the N^* phase [12]. We have estimated the electroclinic coefficient in the S_A phase of then = 10 compound near its S_A N^* transition : $3°/V.\mu m^{-1}$ at $T - T_C$ = 0.8° C. This coefficient is probably of the same order in the N^* phase. So the amplitude of the electroclinic effect in our compounds is much larger than this observed in [5 - 7]. The high polarization of the compound and the proximity of the N^* S_A S_C^* multicritical point which favours smectic fluctuations in the N^* phase are probably at the origin of an enhanced effect.

REFERENCES

[1]   S. GAROFF, R.B. MEYER,
       Phys. Rev. Lett., 38, 848 (1977).

[2]   G.ANDERSSON, I. DAHL, W. KUCLYNSKI, S.T LAGERWALL, K. SKARP, B. STEBLER,
       Ferroelectrics, 84, 285 (1988).

[3]   J. PAVEL, M. GLOGAROVA,
      Ferroelectrics, 84, 241 (1988).
[4]   L. KOMITOV and al., invited lecture at the 2nd Int. Topical
      Meeting on Optics of Liq. Cryst. TORINO, Italy (1988).
[5]   Z. Li, R.G. PETSCHEK, C. ROSENBLATT,
      Phys. Rev. Lett. 62, 796 (1989).
[6]   Z.U, G.A. DI USI, R.G. PETSCHEK, C. ROSENBLATT,
      Phys. Rev. A41, 1997 (1990).
[7]   L. KOMITOV, S.T. LAGERWALL, B. STEBLER, G. ANDERSSON,
      K. FLATISCHLER,
      Ferroelectrics, 114, 167 (1991).
[8]   M. BRUNET, N. ISAERT,
      Ferroelectrics, 84, 25 (1988).
[9]   Ph. MARTINOT - LAGARDE, R. DUKE, G. DURAND,
      Mol. Cryst. Liq. Cryst., 75, 249 (1981).
[10] J.M. BUISINE,
      Mol. Cryst. Liq. Cryst., 109, 143 (1984).
[11] C. LEGRAND, J.P. PARNEIX,
      J. Phys. 51, 787 (1990).
[12] N. ISAERT, J. HMINE, J.M. BUISINE, C. LEGRAND,
      J.P. PARNEIX, H.T. NGUYEN, C.DESTRADE , to be published
      J. HMINE, Thesis, University of Lille, France (1991)
[13] Ph. MARTINOT - LAGARDE, G. DURAND,
      J. Phys., 42, 269 (1981).
[14] T. CARLSSON, B. ZEKS, C. FILIPIC, A. LEVSTIK,
      Phys. Rev. A 42, 877 (1990).
[15] F. GOUDA, K. SKARP, S.T. LAGERWALL,
      Ferroelectrics, 113, 165 (1991).
[16] S.M. KHENED, S.KRISHNA PRASAD, B. SHIKUMAR,
      B.K. SADASHIVA,
      J. Phys. II, 2, 171 (1991).
[17] G.ANDERSSON, K. FLATISCHLER, L. KOMITOV,
      S.T. LAGERWALL, K.SKARP, B. STEBLER,
      Ferroelectrics, 113, 361 (1991).

A New FLC-EO Cell Showing Quasi-tristate Characteristics

M.Kimura, A.Mochizuki[*], M.Itoh, and S.Kobayashi

Division of Electronic and Information Engineering, Graduate School of Technology, Tokyo Univ. of Agri. & Tech., Koganei, Tokyo 184, Japan
*)Also with Fujitsu Lab. Ltd., Morinosato-Wakamiya, Atsugi 243-01, Japan

Abstract

A novel ferroelectric liquid crystal (FLC) EO (electro-Optic) cell showing a quasi-tristate has been demonstrated by using an FLC material ZLI-4139 (Merck) together with orientation films of polyimide RN-626 (Nissan Chem.Ind) which are rubbed in antiparallel way and are capable of generating a high pretilt angle.

The EO cell showing the quasi-tristates was characterized in term of the dynamic behavior of the dielectric constant, switching current, and D-E hysteresis.

Introduction

The EO device using surface stabilized ferroelectric liquid crystal (SSFLC) has attracted researchers' interests for its unique features such as bistability and fast response speed.[1]

It is, in general, still not easy to fabricate an ideal defect-free FLC EO device revealing good bistability accompanying good contrast ratio owing to the appearance of the so called zig-zag defects and owing to the degradation in the contrast ratio due to the formation of the depolarization fields. The former difficulty can be removed by using an appropriate FLC material as exemplified by the naphthalene based material[2], and the latter is resolved by using ultrathin or electrically conductive polymer films for molecular orientation[3,4,5]. Another

approach which is alternative to above methods is to use antiferroelectric LC[6], which is characterized by tristable EO performance and the existence of a DC threshold voltage. However, the condition for the appearance of the antiferroelectric phase is not clear yet.

This paper reports a quasi-tristable EO performance and other related characteristics of an FLC device using an FLC material ZLI-4139 (Merck) together with orientation films of polyimide RN-626 (Nissan Chem.Ind), which are capable of generating a high pretilt reaching above 5 degrees.

This device cell was shown to reveal a surface induced quasi-tristable EO performance when the antiparallel rubbing was performed. The additional measurements such as dynamic dielectric constant, polarization switching current, and D-E hysteresis were done to characterize the device.

2. Experimental
2.1 Samples

The structure of the FLC cell was the ordinary homogeneous sandwich type and consisted of two ITO-coated glass plates whose inner surfaces were coated with pre-rubbed polyimide (PI) films. We compared two types of sample cells which were rubbed in the antiparallel and parallel directions, respectively. The former is the standard type.

For comparison, we also prepared other sample cells using other kinds of orientation films of polyimide; they were RN-305 and RN-626 (Nissan Chem. Ind.). The former is widely utilized for aligning FLCs and the latter is also popular for aligning nematic LCs with a high pretilt angle. We also prepared an additional sample in which the FLC was aligned by using 85 degree obliquely evaporated SiO films.

The main FLC material used in this research was ZLI-

4139 (Merck), which exibits the the tilt angle of 28 degrees at 30 °C and shows the following phase sequences:

$$\text{Iso} \xrightarrow{\hspace{0.5cm} 82\,^\circ\text{C} \hspace{0.5cm}} \text{N}^* \xrightarrow{\hspace{0.5cm} 65\,^\circ\text{C} \hspace{0.5cm}} \text{SmC}^* .$$
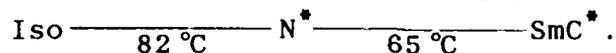
The lack of SmA phase is particularly remarkable in this material. The FLC layer thickness was 1.0μm. For comparison we also examined other FLC materials such as ZLI-3488, ZLI-3654 (Merck), CS-1014 (Chisso) and Felix-002 (Hoechst); all of these materials have the more common phase sequence that includes the SmA phase.
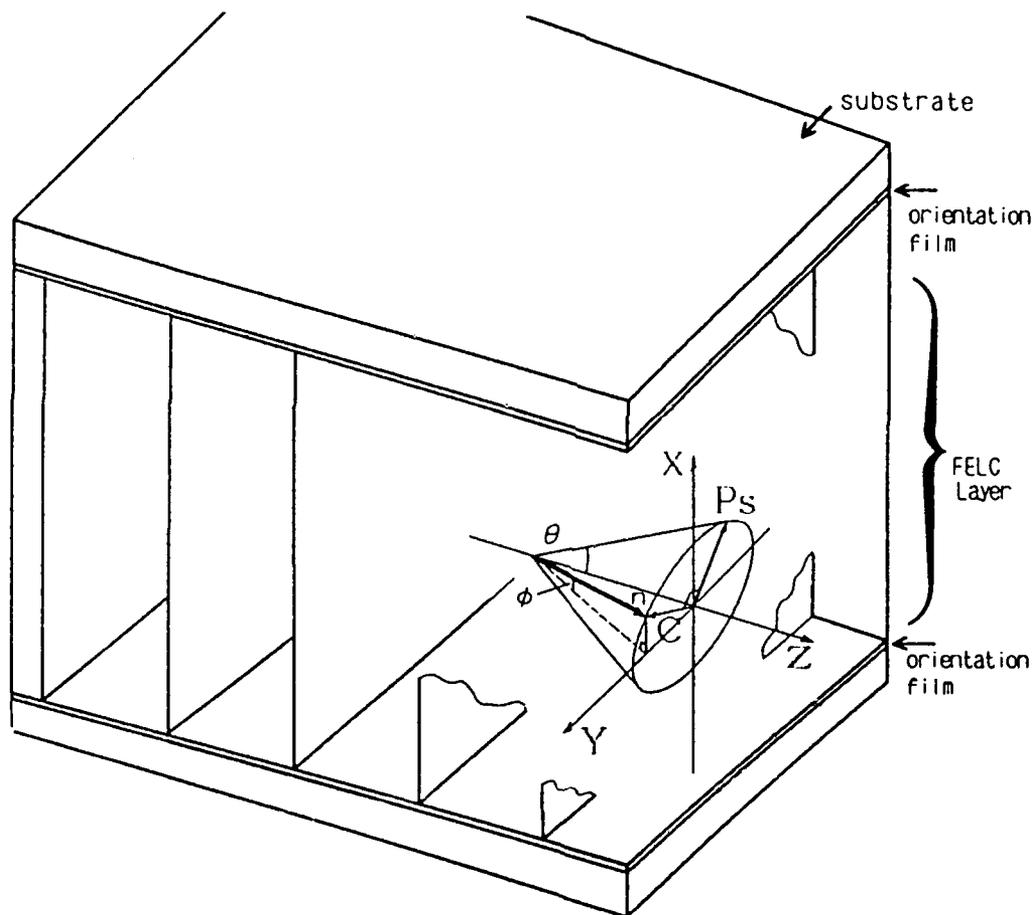
Figure 1   Schematic description for a cone model of chiral smectic liquid crystal in the sandwich cell. The z axis is set along the smectic layer normal direction, and ϕ(t) is the time-dependent angle between the long molecular axis and the electrode plane.

2.2 Measurements

The EO performance of the sample cells was measured. To characterize the cells the measurements of the transitional dielectric constants[7], polarization switching currents[8], and D-E characteristics (using Sawyer-Tower method[9]) were also conducted.

A note concerning the measurement of the transitional dielectric constant is given here as follows.

As the FLC medium has a dielectric anisotropy[7], the apparent dielectric constant of the FLCD cell varies with time during switching transitions due to molecular rotation (Goldstone mode). At each instant, the dielectric constant $\varepsilon(t)$ can be described as

$$\varepsilon(t) = \varepsilon_\perp \cos^2\phi(t) + \varepsilon_{//} \sin^2\phi(t), \qquad (1)$$

where $\varepsilon_\perp$ and $\varepsilon_{//}$ are the principal values for the dielectric constants perpendicular and parallel to the long molecular axis, respectively; and $\phi(t)$ is the time-dependent angle between the long molecular axis and the electrode plane as illustrated in Figure 1. Therefore, the temporal variation of the apparent dielectric constant $\varepsilon(t)$ reflects the molecular motion. We can obtain the information about the FLC molecular rotation characteristics by measuring the transitional dielectric properties. The details of this measuring system are given in a previous paper[7].

3. Results

Figure 2 shows the EO response (Fig.2(A)) of a sample cell using FLC ZLI-4139 and PI RN-626 orientation films which were rubbed antiparallel for a triangular-voltage waveform at 3Hz 10Vp-p (the top trace in Fig.2), also together with the transitional dielectric constant (Fig.2(B)) and polarization switching current (Fig.2(C)). The EO response exhibits three stable states denoted as (1) through (3). Particularly, the third state (3) appears in a low electric-field range. Furthermore it seems that
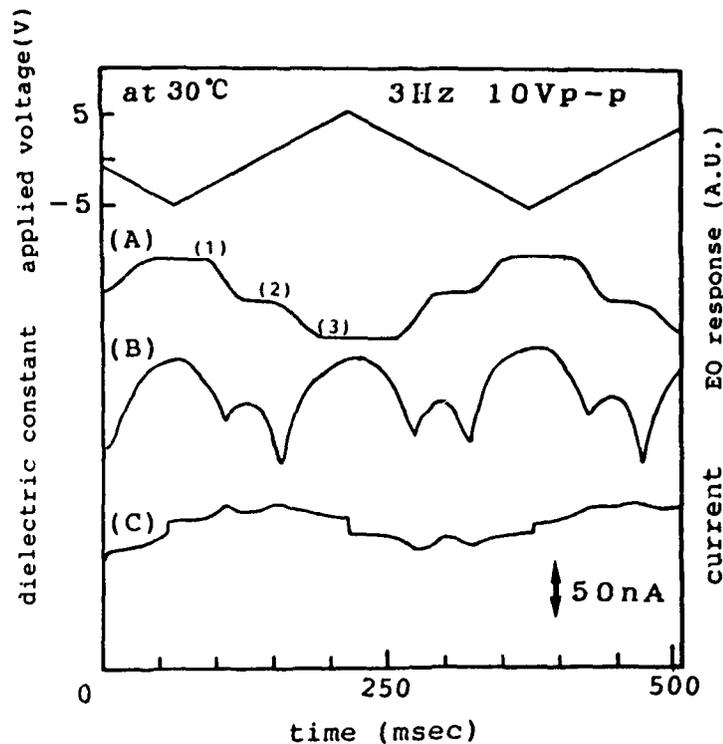
Figure 2   Cell using untiparallel rubbing of a
triangular-voltage waveform at 3Hz: trace of (A) EO re-
sponse, (B) transitional dielectric constant, and (B)
switching current.

both the dielectric constant (Fig.2(B)) and the switching
current (Fig.2(C)) typically show double peaks, and these
peaks coincide with variation of the EO characteristics.

However, even in the case where the same PI RN-626
orientation films were used, particularly when they were
rubbed in parallel, the quasi-tristate property does not
appear.

Regarding the textures of the sample that reveals the
quasi-tristate, the microphotographs that correspond to
these tristable states (shown in Fig.2(A)) are shown in
Figure 3(A) through 3(C) for the same applied triangular-

Rubbing direction

(A)

Rubbing direction

(B)

Rubbing direction

300μm

(C)

0
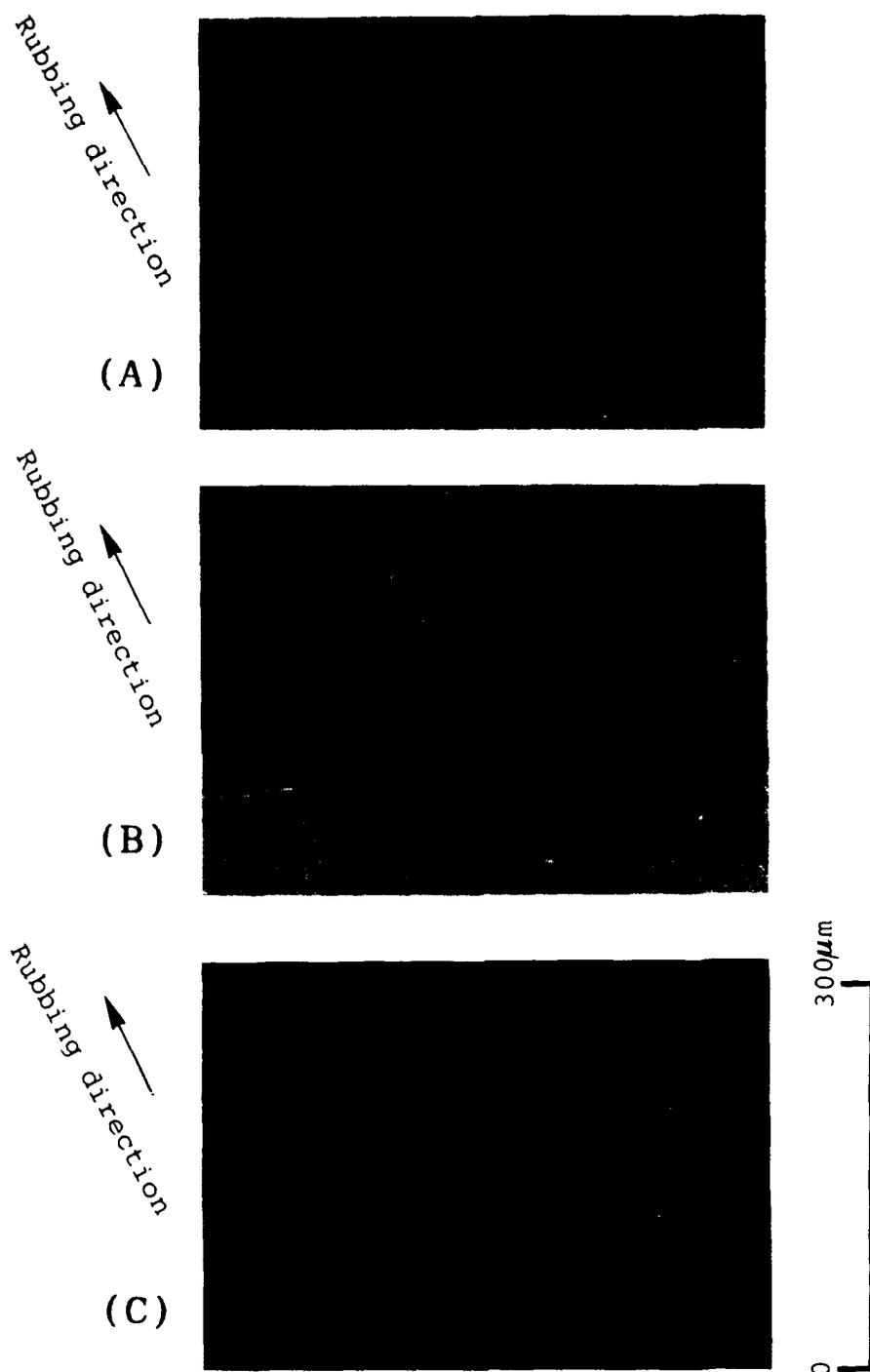
Figure 3 Microphotographs corresponding to these tristable
state (shown in Fig.2(A)) See Color Plate I.

voltage waveforms as shown in Fig.2. It is clear that these optical states are zig-zag defect free and totally uniform except for the existence of the line stripes, and the third state does not show any multidomain texture.

(A) 50 °C

(B) 30 °C

(C) 20 °C
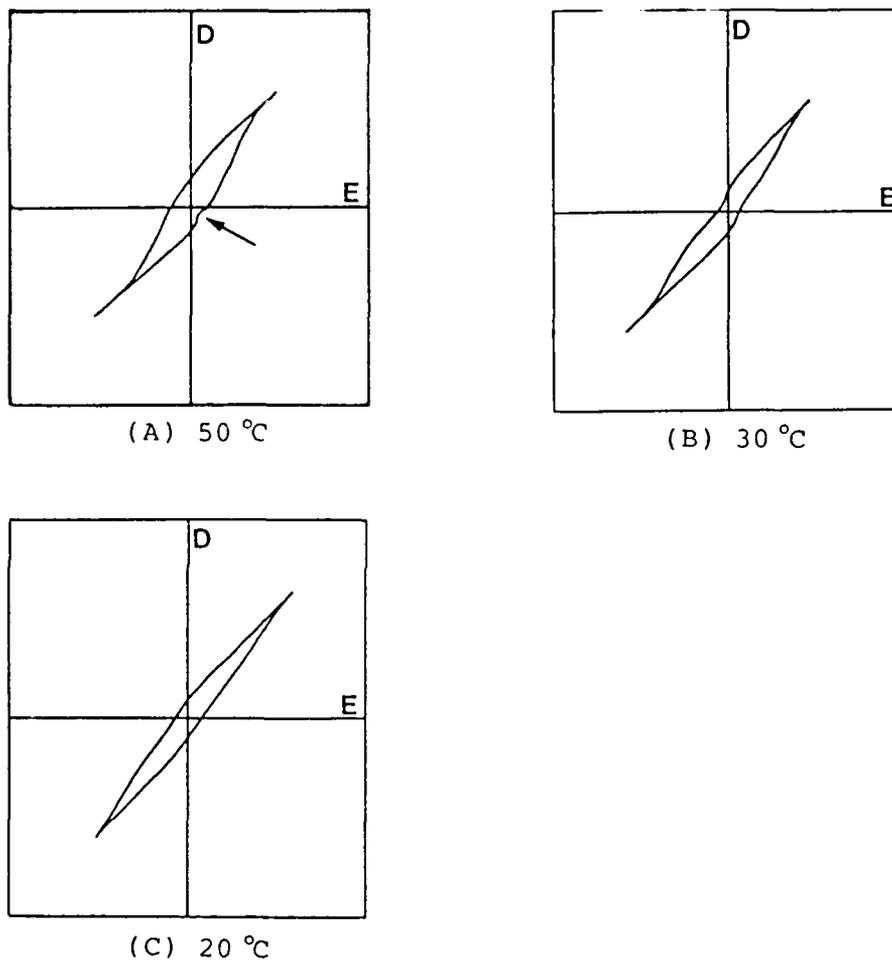
Figure 4   Sawyer-Tower Hysteresis property of a sample using antiparallel rubbing applying 50Hz 40Vp-p, at the temperature of 50°C(A), 30°C(B), and 20°C(C), respectively.

Figure 4 represents the result of the Sawyer-Tower hysteresis loop properties of the sample using FLC ZLI-4139 and PI RN-626 orientation films which were rubbed in antiparallel way, at three different temperatures: at $50^{\circ}C$ (Fig.4(A)), $30^{\circ}C$ (Fig.4(B)), and $20^{\circ}C$ (Fig.4(C)), respectively. It is noteworthy to point out that there exist a peculiar dent in the loop in Fig.4(A) as denoted by arrows. This dent was observed from $65^{\circ}C$ (N^*-SmC* phase transition point) through $20^{\circ}C$, and is getting bigger with cooling. At the temperature of $30^{\circ}C$ (Fig.4(B)), the shape of hysteresis is just like a peanut, however, the dent disappears at $20^{\circ}C$. These phenomenon are shown to occur completely in agreement with the EO characteristics, showing the quasi-tristate occurring from $65^{\circ}C$ (N^*-SmC* transitional point) through $20^{\circ}C$.

However, in a cell with parallel rubbing, the aforementioned dent did not appear, but only a usual hysteresis loop appeared.

We investigated the other orientation films to compare the EO characteristics; the result using FLC ZLI-4139 is shown in Table 1. It seems that the conditions of orientation films necessary to reveal the quasi-tristate are to use a particular PI for generating a high pretilt (in the nematic LC) and to perform rubbing in antiparallel direction.

In order to know how the morphology of the materials affects the appearance of the quasi-tristate, we examined

Table 1   Comparing the EO characteristics in the case of same orientation films.

Orientation Film	RN-626	RN-305	SiO
Antiparallel	tristable	bistable	good bistable
Parallel	bistable	bistable	good bistable

four other additional FLC materials besides ZLI-4139: ZLI-3488, ZLI-3654 (Merck), CS-1014 (Chisso), and Felix-002 (Hoechst AG); these materials have a conventional phase sequence including the SmA phase. As a result, none of the samples using these materials showed such quasi-tristate properties as the FLC material ZLI-4139 did. Consequently it is suggested that an LC material having no SmA phase as exemplified by ZLI-4139 may reveal a quasi-tristate, particularly when it is aligned in an antiparallel way accompanying a pretilt angle.

4. Illustrative description of the Model

Figure 5 compares two situations: in the case of (A) the SmC^* phase appears after the SmA phase in the course of cooling process down from the isotropic phase, while in (B) the SmC^* phase appears directly from the N^* phase. Furthermore, the tilted layer structures are drawn in both SmC^* phases which are formed by adopting orientation layers which are capable of pretilt angles.

According to Mochizuki et al., it is understood that an FLC material, which reveals a SmC^* phase after the SmA phase is likely to form a firm layer structure in the SmC^* phase and gives rise to good bistability, particularly when the temperature range of the SmA phase is wide[2]. Contrary to this situation, an FLC material that reveals SmC^* phase without passing through the SmA phase may not form a firm layer structure, and consequently the direction of the molecules near the surfaces may be intermingled but they are anchored rather tightly due to the nature of rubbed PI films. This kind of situation may allow the formation of an alternative arrangement of the spontaneous polarizations, as shown in Fig.5. Thus we suggest here a model for the quasi-tristable operation as follows: at the quiescent condition, when the layers are tilted as shown in Fig.5(B), the alternative arrangement of the horizontal components of Ps may be formed to reduce
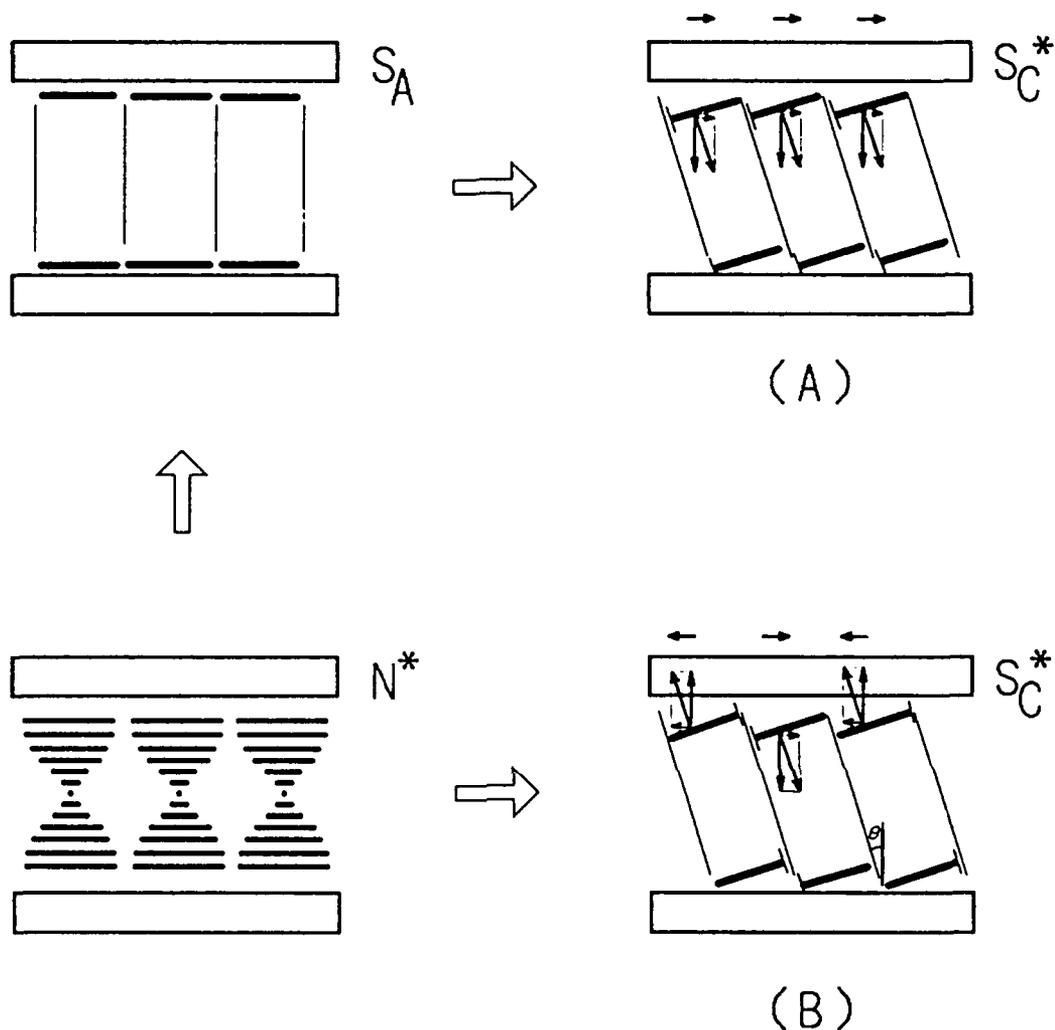
Figure 5   Illustrations of the tilted layer structure model, in the case of the FELC medium with SmA phase (A) and without SmA phase (B).

the free energy; thus an antiferroelectric arrangement may be formed; when a strong electric field is applied, all the Ps tend to the direction of the field; however, when the arrangement of the alternation in the horizontal components of the Ps is not perfect, the quasi-tristate response may occurs. The perfect tristability may occur in a system having the perfect alternation.

We did not observe the quasi-tristability in a sample cell with SiO orientation layers. This may be explained by considering the roughness of the SiO films surfaces that may considerably reduce the anchoring strength.

Therefore it seems that the quasi-tristate property is induced by surface effect particularly for a material having no SmA phase.

5. Conclusion

Surface induced quasi-tristate in the EO performance of an SSFLCD is confirmed by using FLC (ZLI-4139) and PI orientation films (RN-626) with $d < 1 \mu m$ and antiparallel alignment.

References

1. N.A.Clark and S.T.Lagerwall, Appl.Phys.Lett., 36, 899-903 (1980).

2. A.Mochizuki, T.Yoshihara, M.Iwasaki, M.Nakatsuka, Y.Takanishi, Y.Ouchi, H.Takezoe, and A.Fukuda, Proc. of SID, Vol. 31, No.2 123-128 (1990)

3. H.Ikeno, A.Ohsaki, M.Nitta, N.Ozaki, Y.Yokoyama, K.Nakaya, and S.Kobayashi, Jpn.J.Appl.Phys., 27, 475-476 (1988)

4. K.Nakaya, B.Y.Zhang, M.Yoshida, I.Isa, S.Shindoh, and S.Kobayashi, Jpn.J.Appl.Phys., 28, 116-118 (1989)

5. H.Maeda, M.Yoshida, B.Y.Zhang, M.Kimura, A.Mochizuki, and S.Kobayashi, Proceeding of EURODISPLAY'90, 360-363 (1990)

6. A.D.L. Chandani, T.Hagiwara, Y.Suzuki, Y.Ouchi, H.Takezoe, and A.Fukuda, Jpn.J.Appl.Phys.,27, 729-732 (1988)

7. M.Kimura, H.Maeda, M.Yoshida, A.Mochizuki, and S.Kobayashi, Rev.Sci.Instrum., 62,No.6, 1609-1613 (1991)

8. W.J.Merz, Phys.Rev.,95, 690, (1954)

9. K.Skarp and G.Andersson, Ferroelectrics,6, 67 (1986)

THE EFFECT OF BIASING ELECTRIC FIELD ON RELAXATIONS IN FLC
INVESTIGATED BY THE DIELECTRIC AND OPTICAL METHODS

J. PAVEL, M. GLOGAROVÁ
Institute of Physics, Czechoslovak Academy of Sciences,
Na Slovance 2, 18040 Prague 8, Czechoslovakia

Abstract   The dielectric and electrooptical responses within the
frequency range 30 Hz - 100 kHz are used to study the properties
of the soft and the Goldstone mode in dependence of bias electric
field. It is shown that the soft mode relaxation frequency
is linearly bias dependent in both SmA and SmC* phases, the
Goldstone mode relaxation frequency is constant for small bias.
After the modulated structure is unwound a low frequency mode
persists a relaxation frequency of which also linearly increases
with increasing bias. This mode is connected with vibration of
molecules around the layer normal keeping the constant tilt
angle, which could take place in surface layers. The Cole-
-Cole diagrams constructed from the optical response are obtained
for all studied modes in the shape of semicircles, showing all
the modes have relaxation character with well defined relaxation
frequencies. The bias field dependencies of both optical and di-
electric responses in the SmC* phase reflect the unwinding pro-
cess of the helicoidal and twisted structure.

INTRODUCTION

Two relaxation processes known as the soft mode and the Goldstone mode
are important to describe the origin of the ferroelectric phase tran-
sition in liquid crystals and the structural change at this transition
[1]. The soft mode, being fluctuations of the molecular tilt θ with res-
pect to the smectic layer normal, can be detected in dielectric
as well as in electroclinic properties in the vicinity of the phase
transition temperature[2]. The Goldstone mode which exists only in the
low temperature SmC* phase as a consequence of the spacely modulated
helicoidal structure corresponds to vibrations of molecules on the
surface of a cone defined by the helicoidal axis and the spontaneous
tilt θ. The Goldstone mode gives a great contribution to dielectric
susceptibility which overwhelms the soft mode contribution[3] and can be
also detected in electrooptical response[4,5,6]. In SmC* phase the soft
mode can be detected only when the Goldstone mode is suppressed for

instance by d.c. electric field[3].

In this contribution we compare advantages and limitations of both dielectric and electrooptic methods which are used to determine the properties of the soft mode as well as of the Goldstone mode. The influence of biasing electric field on both relaxation processes is also studied.

EXPERIMENTAL RESULTS

The studied material was ferroelectric liquid crystal 4-n-octyloxy benzoic acid 4'-[(2-methylbutyloxy) carbonyl] phenyl ester with the monotropic phase transition from SmA to SmC* at 29.7°C. The sample was sandwiched between two glass plates covered by transparent electrodes separated by a 12 μm thick spacer. To achieve the "book shelf" geometry the glasses had been rubbed on the velvet cloth and the liquid crystal in the SmA phase was exposed several hours to the a.c. electric field 20 Hz, 15 kV/cm. The alignment was checked by the observation under a polarizing microscope. The dielectric constant was measured by the HP 4192A impedance analyzer. The measuring field from the impedance analyzer served simultaneously as the source field for the measurement of the electrooptical response. Both responses have been measured in the frequency range 30 Hz - 100 kHz. The planar oriented sample has been placed between the crossed polarizers of the microscope the smectic layer normal containing the angle of 22.5 deg with the polarizer. In that geometry the optical response to the soft mode in the SmA phase is the largest[7]. Changes of the polarized light passing through the sample were detected by lock-in amplifier as an electric signal on a PIN photodiode.

In the SmA phase and under a sufficiently low applied field the detected signal linearly depends on the induced deviations of the molecules. It might not be true in the unwound SmC phase because we do not change the orientation of the sample regarding crossed polarizers in this phase. The spontaneous tilt of the molecules causes deviation of the optical axis from the optimal position for the electrooptical measurement and the detected signal becomes non-linear with respect to induced tilt angle. In the helicoidal SmC* structure the situation is even more complicated by the spatial modulation of the structure and by the existence of a twist along the sample thick-

ness[8] so that the measured electrooptical response gives only a qualitative picture.

To measure the soft mode contribution in the SmC* phase a strong d.c. electric field has to be applied to the sample to unwind the helix[4]. Figure 1 shows the temperature dependence of the reciprocal
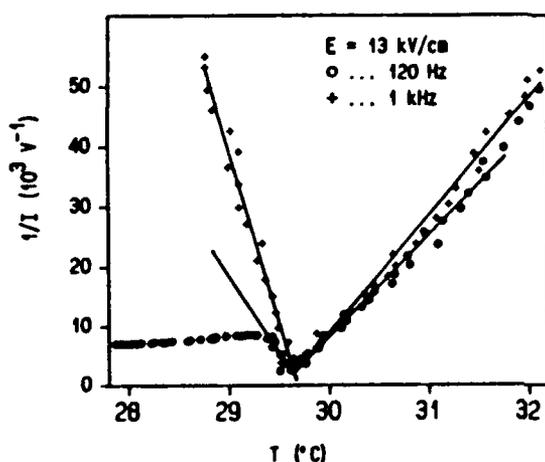
FIGURE 1

Reciprocal electrooptical response intensity in dependence of temperature for two denoted frequencies.

values of the optical response for two frequencies. During the experiment the d.c. electric field E = 13 kV/cm was applied. The field was about three times higher than the critical field for unwinding the helicoidal structure in the SmC* phase. It means the helix as well as the twist along the sample thickness were unwound in the whole SmC* phase which was checked by the direct observation in the microscope. It could be expected that in this case the electrooptical response corresponds only to the soft mode which could be verified by the fulfilling the Curie–Weiss law. As it can be seen in Figure 1 the Curie–Weiss law is fulfilled in the SmA phase, but in the SmC* phase for the higher frequencies only. For lower frequencies we detect a contribution from a low frequency mechanism similarly as in Ref.[6] which could correspond to vibrations of the molecules on the cone defined by the tilt angle. Above the relaxation frequency of this mode, which is close to the Goldstone mode relaxation frequency, this contribution vanishes. This low frequency contribution was observed also in the permittivity measurement.

As the electroclinic effect is linear, i.e. the induced tilt angle is linearly proportional to the electric field, it is not detected on the second harmonic frequency. It is apparently seen in Figure 2, where the temperature dependencies of intensities detected
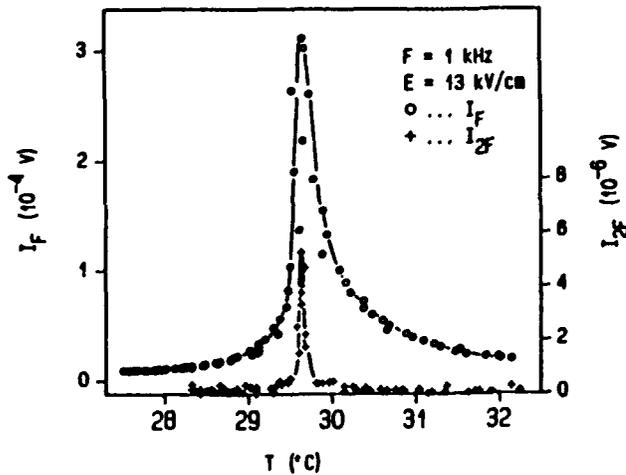
FIGURE 2

Temperature dependence of the electrooptical response intensity for the first (I_F) and the second (I_{2F}) harmonic measured at denoted bias and frequency.

on the single and on the double exciting frequency are shown. The second harmonic signal vanishes in both phases excluding a very narrow vicinity of the phase transition temperature, where the non-linearities strongly increase, because the exciting field (E = 0.8 kV/cm) has been too high. The experiment has been performed under the d.c. biasing electric field to eliminate the Goldstone mode contribution which would be detected in the second harmonic response, too.

Having measured the real and the imaginary part of the electrooptical response we can draw Cole-Cole diagrams, similarly as for dielectric response. For zero or small bias field, only one semicircle is obtained which corresponds to the Goldstone mode (Figure 3a). For
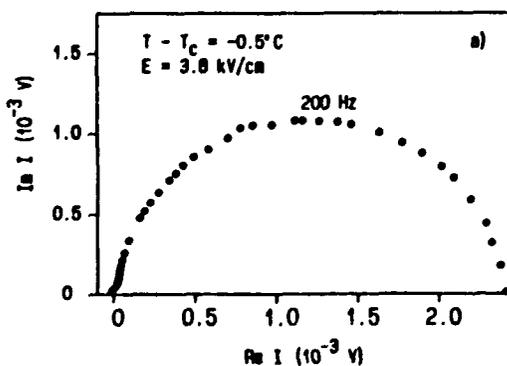
FIGURE 3a   FIGURE 3b

Cole-Cole diagrams constructed from real and imaginary parts of the electrooptical response for a) Goldstone mode, b) low frequency mode and soft mode. The temperature, bias field and relaxation frequencies are shown.
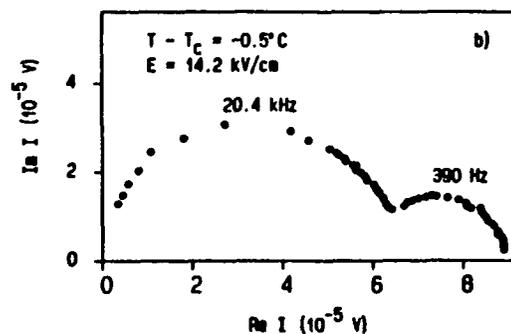
higher bias, when the Goldstone mode is suppressed, the semicircle of the soft mode appears (Figure 3b). Above the unwinding critical field the low frequency semicircle still exists. With increasing biasing field the amplitude of this low frequency mode decreases faster than the amplitude of the soft mode. Therefore the soft mode becomes more significant for higher biasing fields (Figure 3b). In the SmA phase, only one semicircle corresponding to the soft mode is observed in the Cole-Cole diagram.

From the Cole-Cole diagrams we can determine relaxation frequencies of the involved modes and their field dependencies. The temperature dependencies of the soft and the Goldstone modes were reported in Refs.[9,10,11]. Figure 4 shows the field dependence of the soft mode
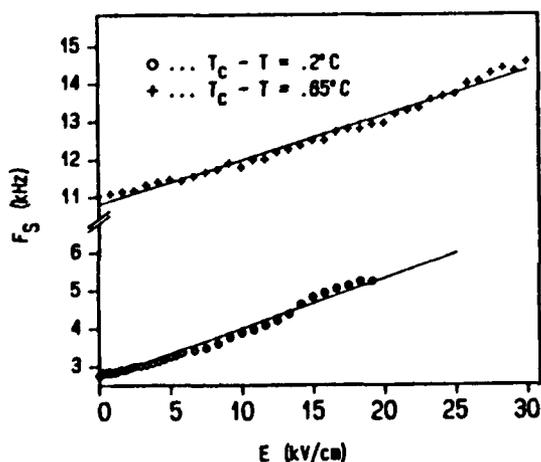
FIGURE 4

Relaxation frequencies of the soft mode in dependence of bias field for two temperatures in the smectic A phase.

relaxation frequency in the SmA phase for two temperatures. Both dependencies are linear with the same slope k = 125 Hz cm/kV. As it has been explained above, the relaxation frequency of the soft mode can be evaluated in the SmC* phase for the higher biasing fields only. It exhibits a linear field dependence, too, but with higher slope k = 700 Hz cm/kV (see Figure 5).

In the field dependence of the low frequency contribution we can found three regions (see Figure 5). From zero field to point A the relaxation frequency is only slightly influenced by the field, then, between points A and B it exhibits an anomaly, and above B it linearly depends on the applied bias field. From the direct observation of the liquid crystal texture during increase of the biasing field we can set points A and B to certain processes. In the field corresponding to A we have observed unwinding of the twist along the sample thickness
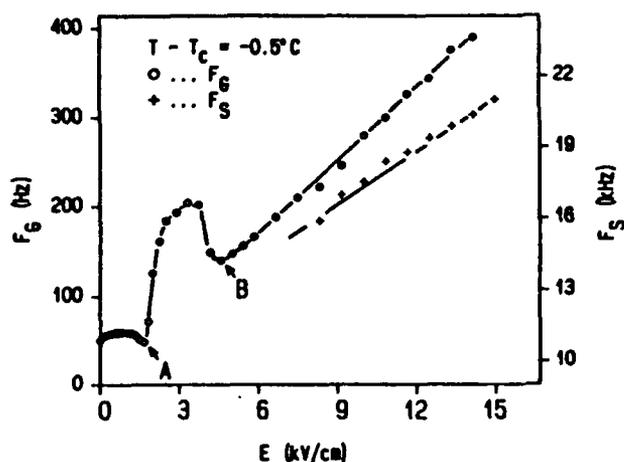
FIGURE 5

Soft mode (F_S) and Gold-
stone mode (F_G) relaxa-
tion frequencies in de-
pendence of bias field.
The points A and B show
the beginning of the
twist unwinding and the
completion of the helix
unwinding, resp.

which arose due to the polar anchoring of the molecules on the glass
surfaces[8]. After the twist unwinding the helicoidal structure persists
which is demonstrated by the existence of dechiralization lines[8]. In
the increasing field the helix is more and more deformed until it is
unwound at the critical field corresponding to the point B.

The significant points A and B can be found also in the field
dependence of electrooptical and dielectric responses for low (Figure
6a) and high (Figure 6b) frequencies. It is remarkable that the
permittivity and electrooptical response have the different behavior
during the transition from the twisted helicoidal to the homogeneous
structures. The shape of the field dependencies of the intensity
of transmitted light is independent on the frequency. Up to the
point A a sharp increase of the intensity is observed. In this region
the twist along the sample thickness and the helix are deformed[8].
After the twist vanishes further deformation of the helicoidal struc-
ture continues which is observed as the decrease of the intensity.
Similar dependence has been found in Ref.[5]. The explanation of this
behavior is not evident. The light passes through a strongly inhomo-
geneous medium where the adiabatic approximation cannot be used
and where the situation is moreover complicated by the presence
of dechiralization lines, which can scatter the light. For still
higher fields (above the point) the electrooptical response of
the homogeneous structure goes quickly to zero. The dielectric permit-
tivity is not very sensitive to the deformation of the twist, but
the deformation of the helix and its vanishing is observed as the
large decrease of ε in the low frequency region (suppresing of
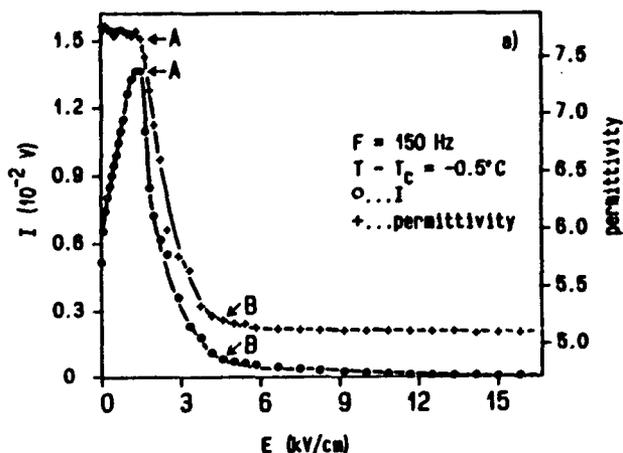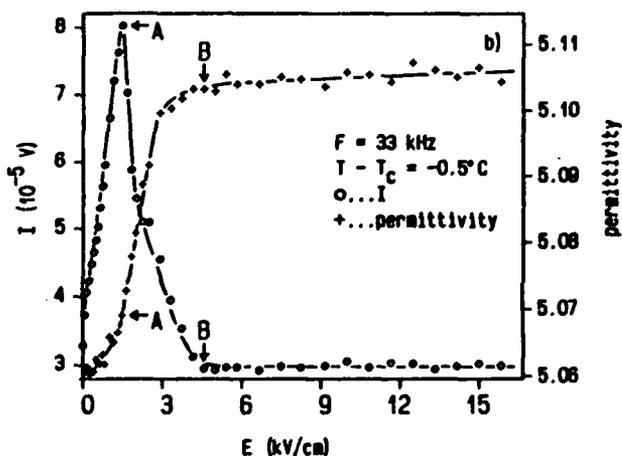
FIGURE 6a

FIGURE 6b

FIGURE 6   Optical response intensities and permittivities in
dependence of bias field measured at a) low frequency,
b) high frequency. The points A and B have the same meaning
as in Figure 5.

the Goldstone mode contribution) or by the increase of ε in the
high frequency region. The later case was discussed in Ref.[12]. Far
above the Goldstone and soft mode relaxation the permittivity of
the helicoidal structure can be expressed by the formula $\varepsilon_{hel.} =$
$= [\varepsilon_{\parallel}\sin^2\theta + \varepsilon_{\perp} (1 + \cos^2\theta)]/2$, where $\varepsilon_{\perp}$ resp. $\varepsilon_{\parallel}$ is the component
perpendicular resp. parallel to the molecule long axis. If the liquid
crystal exhibits the negative dielectric anisotropy ($\varepsilon_{\parallel} < \varepsilon_{\perp}$) as it is
the case, the permittivity of the unwound structure, which is given by
$\varepsilon_{\perp}$, is higher than $\varepsilon_{hel.}$ In fact, the source of the high frequency
permittivity contribution is the rotation of molecules along their

short axis[11].

DISCUSSION AND CONCLUSIONS

The dielectric study is a powerful tool to study the soft and the Goldstone modes in ferroelectric liquid crystals. As the dielectric response is isotropic in the sample plane, it is not very sensitive to the sample alignment. The disadvantage is relatively low contribution of the soft mode in comparison to the high frequency permittivity, which results in rather low sensitivity of the method especially far from T_c.

The electrooptical study is, on the contrary, enormously sensitive, because the high frequency contribution is identically zero. Therefore the soft mode contribution (electroclinic effect) can be detected even far from T_c. The anisotropy of the electrooptical response in the sample plane is a disadvantage when measuring the soft mode contribution in unwound SmC^* phase. Concerning the response of the Goldstone mode, the situation is still more complicated. It can be shown that the optical response from the ideal helicoidal structure would be averaged to zero. The measured electrooptical intensity is a result of electric field deformation of structure modulated in two directions, along the helicoidal axis and along the sample thickness. This hypothesis is confirmed by results shown in Figure 6a, where the intensity of electrooptical response is considerably increasing when the structure is more deformed by biasing field. The results allow to determine relaxation frequency precisely, but a quantitative analysis of intensities is practically impossible. On the other hand the electrooptical study can give some information about the switching process in the SmC^* phase (see Figures 5, 6a, b).

Both the Goldstone and the soft mode have a relaxation character with well defined relaxation frequency, which is documented by rather perfect semicircular shape of Cole-Cole diagrams (Figures 3a, b). The relaxation frequency of the soft mode increases linearly with increasing bias field in both SmA and SmC^* phases (Figures 4, 5). The electroclinic effect is linear in the measuring applied field intensity except for the vicinity of T_c where the second harmonic intensity exhibits a very narrow peak (see Figure 2).

The Goldstone mode relaxation frequency is nearly bias field independent up to the coercive field for the structure unwinding. When the SmC* structure is completely unwound a low frequency weak contribution is still detected corresponding probably to rotation of molecules around the layer normal keeping the constant tilt angle. This mode can exist in surface layers, where the molecules have not reached the saturated state corresponding to the unwound structure. The relaxation frequency of this mode also increases with increasing bias field (Figure 5).

REFERENCES

1. Ph. Martinot-Lagarde, G. Durand, Journ. de Physique, 42, 269 (1981).
2. M. Glogarová, Mol. Cryst. Liq. Cryst., 191, 71 (1990).
3. M. Glogarová, J. Pavel, Liquid Crystals, 6, 325 (1989).
4. W. Kuczynski, J. Hoffmann, B. Stryla, J. Malecki, Mol. Cryst. Liq. Cryst., 192, 295 (1990).
5. W. Kuczynski, J. Hoffmann, B. Stryla, J. Malecki, N. Shonova, Mol. Cryst. Liq. Cryst., 192, 307 (1990).
6. W. Kuczynski, J. Hoffmann, B. Stryla, and J. Malecki, Ferroelectrics, 114, 319 (1991).
7. G. Andersson, I. Dahl, W. Kuczynski, S. T. Lagerwall, K. Skarp, and B. Stebler, Ferroelectrics, 84, 285 (1988).
8. M. Glogarová, J. Pavel, Journ. de Physique, 45, 143 (1984).
9. J. Pavel, M. Glogarová, Ferroelectrics, 84, 241 (1988).
10. J. Pavel, M. Glogarová, Ferroelectrics, 114, 131 (1991).
11. J. Pavel, M. Glogarová, and R. Dabrowski, Ferroelectrics, 81, 413 (1988).
12. J. Pavel, M. Glogarová, and S. S. Bawa, Ferroelectrics, 76, 221 (1987).

THE STRONG TEMPERATURE DEPENDENT GOLDSTONE MODE RELAXATION FREQUENCY IN A BROAD RANGE SmC* PHASE

MATTHIAS PFEIFFER, GABRIELA SOTO*, STANISLAW WROBEL+ AND WOLFGANG HAASE

Institute of Physical Chemistry, Technische Hochschule Darmstadt, Petersenstrasse 20, 6100 Darmstadt, FRG.

ROBERT TWIEG, KATHLEEN BETTERTON

IBM Almaden Research Center, 650 Harry Rd., San Jose, California 95120-6099 USA

Abstract   Broad frequency range dielectric spectroscopy, X-ray diffraction, electro-optical methods and thermal analysis are used to characterize a single component liquid crystal with a monotropic broad range room temperature ferroelectric SmC* phase. The dielectric spectrum shows a Soft mode and a Goldstone mode. Unlike in other ferroelectric liquid crystals the Goldstone mode of this substance has a strongly temperature dependent characteristic frequency. It is proposed that glassy-state fluctuations are responsible for the appreciable increase of activation energy (from 37 to 91 kJ/mol) upon cooling from 318 K (T_{CA}) to 278 K. Beside these modes a Domain mode is detected. Measurements in the high frequency range 1 MHz to 450 GHz show an additional relaxation process.

INTRODUCTION

Ferroelectric liquid crystals (FLC's) have gained attention both from a theoretical[1-3] and a practical[4-8] point of view. In this context dielectric measurements are important since they contribute to characterize these materials. The results obtained using this method are valuable to understand the dynamics of the FLC phases and very recently some measurements on single compounds and mixtures were published[9-14]. Two collective processes, the Soft mode and the

Goldstone mode are detected by dielectric spectroscopy. In addition to these modes a new mode, the Domain mode, is also detected[15-16]. Usually the Goldstone mode is described as a relatively temperature insensitive process[9-14]. Our investigations on a new single compound FLC with a room temperature monotropic SmC* phase show that the Goldstone mode can be strongly temperature dependent. Our special attention to this observation is one aim of this contribution.

EXPERIMENTAL

The chemical formula and the phase sequence of the compound studied are as follows:

$$H-(CH_2)_{\overline{12}}-O-\langle\text{ring}\rangle-C(=O)-S-\langle\text{ring}\rangle-C(=O)-O-\overset{*}{C}H(CH_3)-C(=O)-O-(CH_2)_{\overline{2}}-H$$

$$Cr_1 \xrightarrow{\text{310.6 K}} SmA \xleftarrow{\text{331.2 K}} iso$$

$$Cr_1 \xrightarrow[\text{10 DAYS}]{\text{RT, AFTER}}$$

$$\text{308.8 K}$$

$$Cr_2 \xleftarrow{\text{274 K}} SmC^*$$
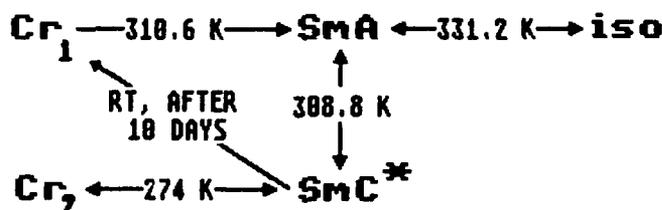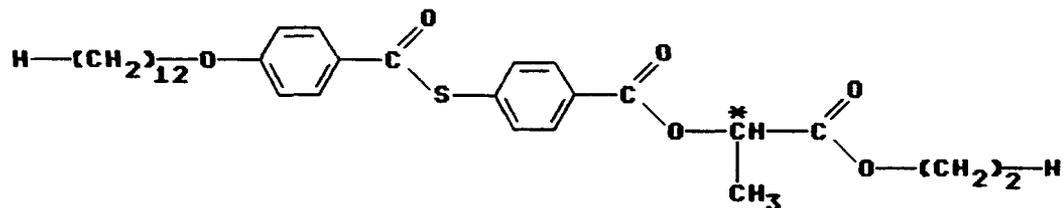
This compound is a member of a family of alkoxyphenylthiobenzoate FLC's having a chiral tail derived from an ester of lactic acid[17]. The structural variables in this family include the length of the alkoxy tail (octyloxy through penta-decyloxy) and the length of the lactic acid ester (methyl through octyl). These compounds are synthesized in a fashion identical to that utilized for the chiral 2-alkanol esters[18] exept that a lactic acid ester (e.g., (S)-ethyl lactate in this particular case) is substituted for the chiral 2-alkanol. The materials are purified by careful column chromatography with toluene as eluent and recrystallization from ethanol. This family of materials has a number of members, with a rich meso-morphic morphology with some remarkable properties. For example, many possess ferroelectric phases at or near ambient which in some cases readily supercool well below room temperature. In addition, it has been found that many of these com-pounds appear to possess the Sm A* phase[19] and the particular compound utilized in this study shows some evidence for this phase. Upon cooling from the isotropic

the following partially coexistant textures are observed by polarizing microscopy: cholesteric quickly followed by the charakteristic "spaghetti-like" strands of the SmA* phase followed by a more typical focal conic SmA texture. Further studies on the mesomorphic properties of this family of liquid crystals are under way[20].

The transition temperatures were obtained by standard techniques: polarizing microscopy (Leitz Orthoplan Pol) and differential scanning calorimetry (Du Pont 990 Thermal Analyzer) except for the transition temperature SmA - SmC* (T_{CA}). This transition temperature has been determined from X-ray measurements to be 308.8 +/- 0.2 K. The value agrees within +/- 0.4 K with the values obtained from our dielectric studies. Switching experiments as well as texture observations were not as clear in determining this transition temperature. The SmC* phase appears only on cooling the material (monotropic SmC* phase), and can be supercooled below 274 K.

Our dielectric spectrometer is based on a frequency response analyzer (Solartron Schlumberger 1250) and on impedance analyzers (HP 4191A, HP 4192A) covering a total frequency range of 10^{-4} to 10^9 Hz. The temperature is controlled by thermo/cryostats or electrically covering a possible range from 230 to 500 K. The whole setup is computer controlled, thus we are able to perform fully automatic measurements with frequency, voltage and temperature as variables. In this work only the impedance analyzers were used. A specially designed gold coated cell was employed (10 μm thickness) which enables anisotropic measurements up to about 500 MHz. The cell was first calibrated and then filled by capillary action. The planar alignment was obtained by slowly cooling down the material within a magnetic field of 1.2 T, which was proved to be strong enough by polarizing microscopy and X-ray diffraction. The details of these procedures and of those related to the dielectric measurements are described elsewhere[21,22].

The switching properties of the material were observed under a polarizing microscope using an ITO coated glass cell (thickness 2 and 10 μm, active area 0.66 cm^2). We used the same type of cell for the optical tilt angle measurements.

The X-ray experiments were performed on unoriented bulk samples contained in a 1.5 mm o.d. tubing according to procedures previously described[23] using a modified STOE STADI 2 X-Ray diffractometer.

RESULTS

The dielectric absorption spectra were taken over a wide temperature range from nearly the clearing point down to about 260 K to gain insight on the overall behaviour of this kind of substance.
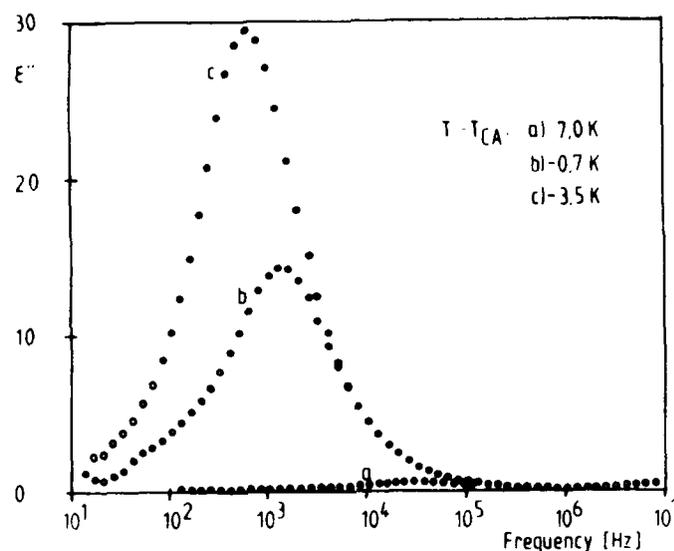
FIGURE 1   Dielectric absorption spectra in the SmC* and SmA phase at different temperatures.

Fig. 1 shows typical absorption curves of the dielectric absorption spectra obtained in perpendicular orientation (n E) in a) the SmA phase (T=315,2 K), b) near the transition point SmA-SmC* (T=312.6 K), and c) in the SmC* phase (T=305.3 K). All the measured spectra show a dielectric relaxation curve with a distribution characteristic similar to a Debye function (single relaxation)[24]. The weak process of the SmA phase has a maximum relaxation strength and a minimum relaxation frequency at T_{CA}. This is a typical Soft mode behaviour[25-28].

The strong process of the SmC* phase shows typical Goldstone mode relaxation behaviour[14,25-28]. It can be suppressed by an bias DC-field (Fig. 2). In that case two different weak processes can be seen. The one only close to the transition temperature is the SmC* Soft mode (but not visible in figure 2 due to the temperature of 303.3 K which is to far from the transition point). The other process seems to be a Domain mode[15-16] (curve 'e' in Fig. 2).
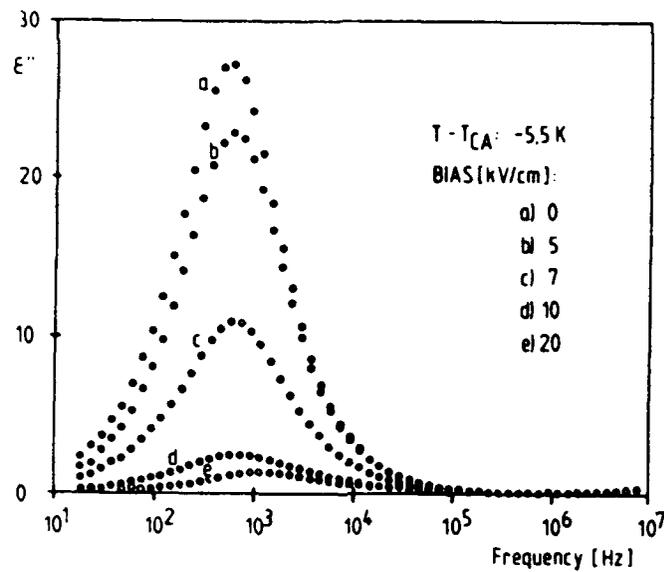
FIGURE 2   Dielectric absorption spectra in the SmC* phase. Suppression of the Goldstone mode by DC-fields.

Figure 3 shows the bias field dependence of the Goldstone mode relaxation strength at 303.3 K with increasing bias field. It was found that at this temperature a field strength of about 10 kV/cm suppresses the Goldstone mode nearly totally. We suppose that the residual weak intensity of less than 5 $\Delta\varepsilon$-units at
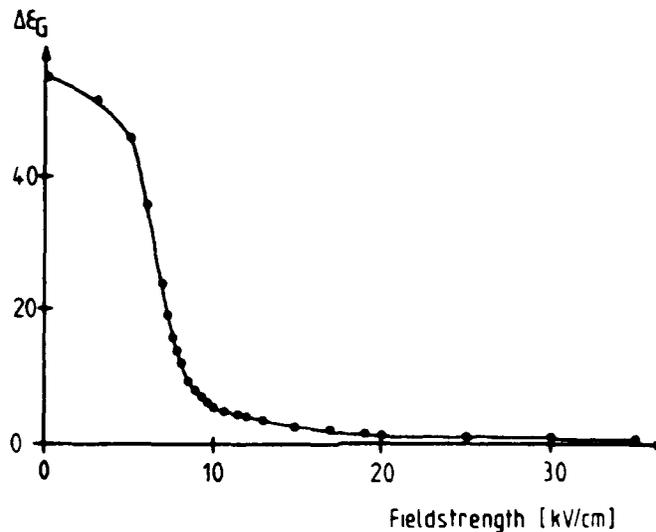
FIGURE 3   Suppression of the Goldstone mode. $\Delta\varepsilon_G$ is the relaxation strength. At field strengthes higher than 10 kV/cm the Domain mode appears.

>10 kV/cm results from the Domain mode. The use of higher field strengthes, up to 35 kV/cm, further suppresses its relaxation strength only slightly, which is typical for the Domain mode.

The temperature dependence of the Goldstone mode relaxation frequency is given in figure 4. The Goldstone mode of this substance shows an unexpected strong temperature dependence in its frequency. It is clearly an activated process.
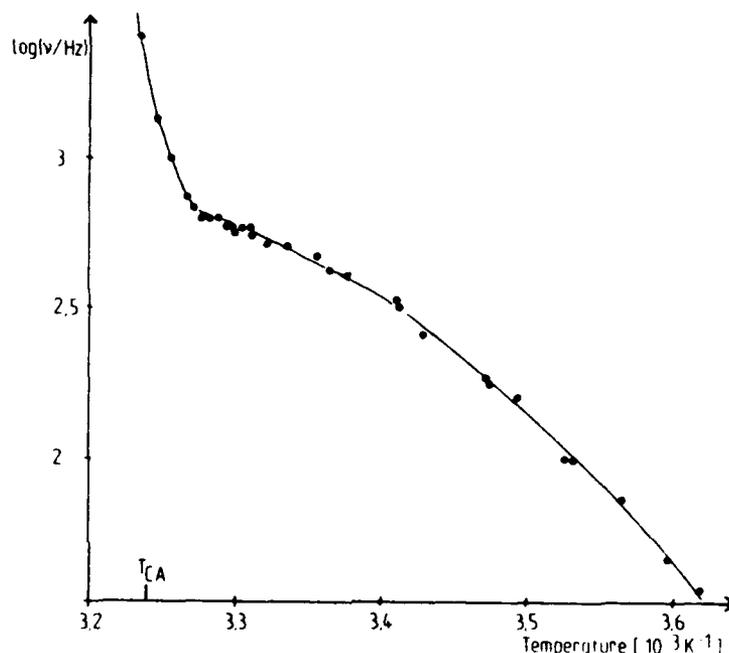
FIGURE 4   Activation energy plot of Goldstone mode relaxation frequency.

However the experimental values show a pronounced nonlinearity, this means non-Arrhenius behaviour in the activation energy plot. The strong increase in frequency near T_{CA} is due to the influence of the Soft mode.

Suppressing the Goldstone mode enables analysis of the Soft mode also in the SmC* phase[26]. However due to the Domain mode which could not be suppressed totally there were difficulties in separation of the two modes in the SmC* phase. Figure 5 shows the characteristic temperature dependence[25-28] of the inverse relaxation strength of the Soft mode in the vicinity of T_{CA}. It can be described with the typical 'V', which was predicted by theory[28].

The high frequency spectrum in the range 1 MHz to 450 MHz shows a weak absorption in the SmA and SmC* phase. This is shown in figure 6 for several temperatures between 277.5 K and 325.2 K. The relaxation frequency of that pro-
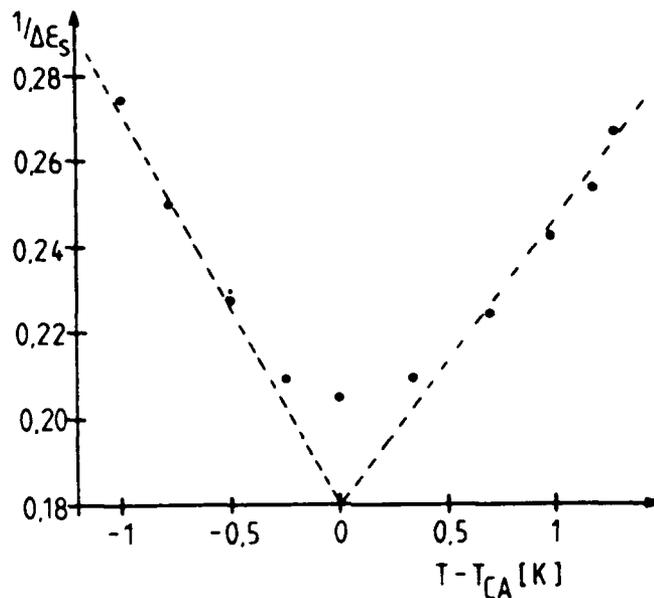
FIGURE 5   Temperature dependence of the characteristic Soft mode inverse relaxation strength.

cess seems not to be influenced by the phase transition (fig. 7a). It is an activated process, and like the Goldstone mode of this substance it has an temperature dependent activation energy. The ε''_{max} values increase with increasing temperature within the SmC* phase and decrease in the SmA phase (fig. 7b).
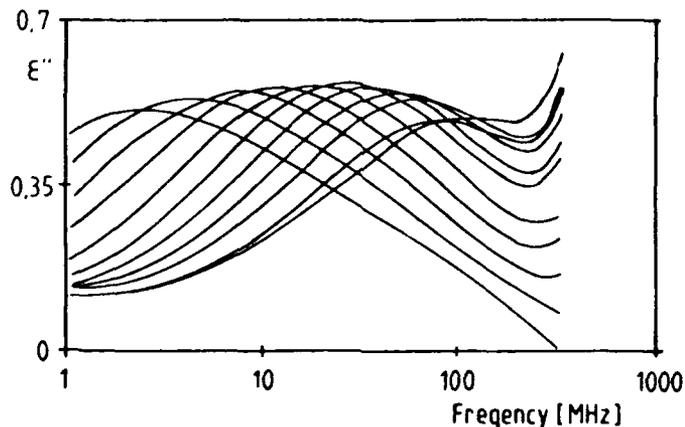
FIGURE 6   Dielectric absorption spectra in the high frequency region at different temperatures in the SmC* and SmA phase. The temperatures are (maxima from left to right): 278.6, 282.8, 287.3, 297.1, 301.7, 306.3, 310.9, 315.2, 320.1, 324.6 K.
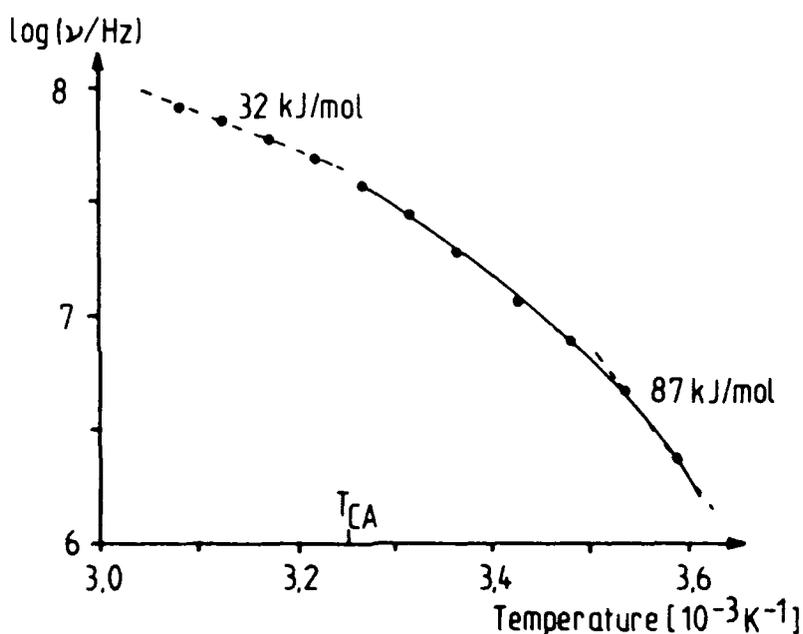
FIGURE 7a   Activation energy plot of the high frequency process
relaxation frequency. The broken lines indicate local activation energies.
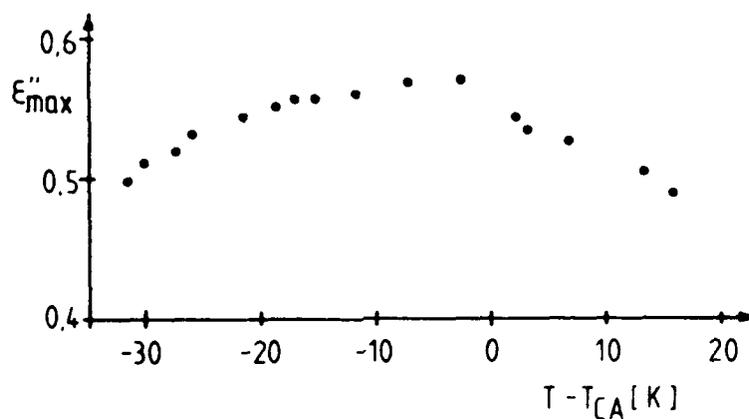
FIGURE 7b   Temperature dependence of the high frequency process
relaxation strength.

To find an explanation for the temperature dependent activation energy of
the Goldstone mode we made some further experiments. The tilt angle θ has been
determined by the measurement of 2θ between bistable SSFLC states and was
calculated from the layer spacing obtained from the X-ray diffraction experiment

(fig. 8). Both techniques provide experimental data with expected temperature dependence (fig. 9). The θ varies up to a maximum of 25° (278 K). The small optical tilt angle in the SmA phase has a linear dependence on the voltage and is
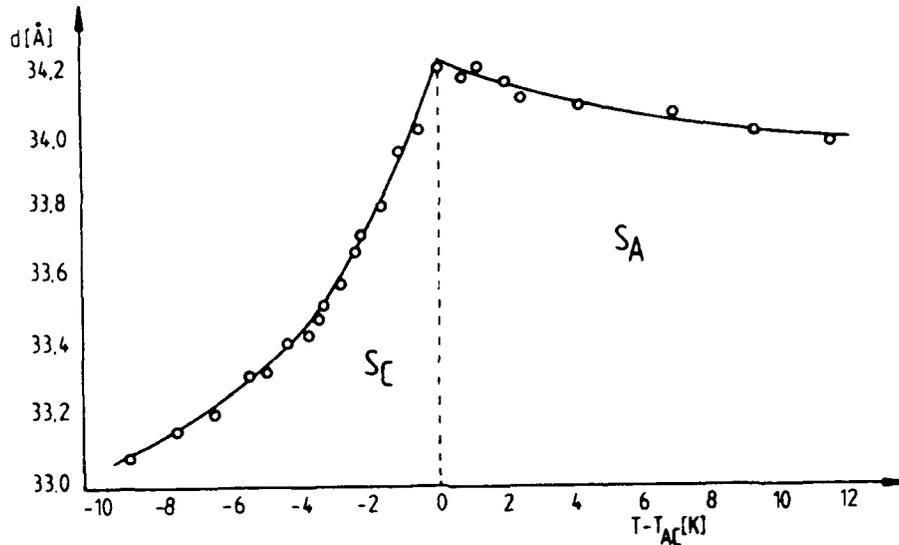
FIGURE 8   Temperature dependence of the layer spacing in SmA and SmC* phase.
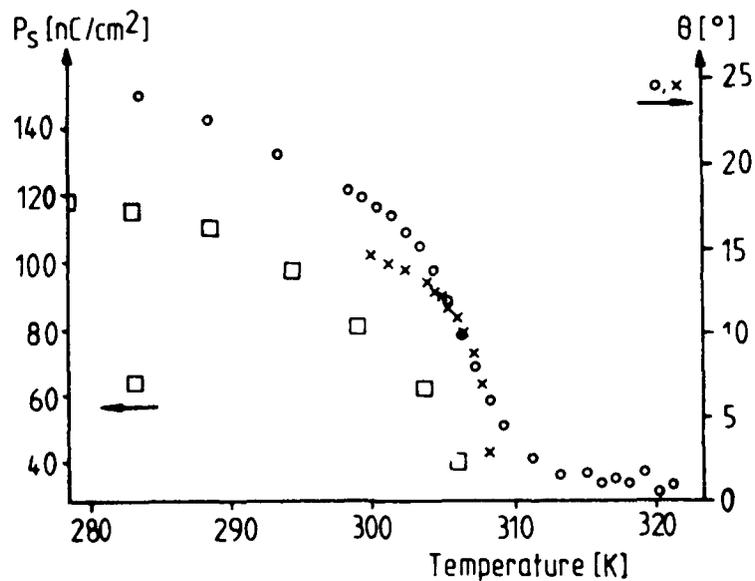
FIGURE 9   Temperature dependence of the spontaneous polarization (o) and the tilt angle (x obtained from X-ray diffraction, o optical tilt angle).

therefore an electroclinic effect[29]. The same effect generates the deviation between the two techniques at low temperatures where field strengthes up to 50 kV/cm have been used to switch the material into extreme positions on the cone. The spontaneous polarization increases with decreasing temperature up to a maximum value of about 120 nC/cm^2. Unfortunately we could not determine the temperature dependence of the helical pitch due to its small value of about 0.6 to 0.7 μm. This values are obtained from the color of the selective reflected light.

DISCUSSION

The strong SmC^* phase relaxation process can be identified as a Goldstone mode. The area of its relaxation frequency, the strength and the suppressibility in an bias DC-field are typical for Goldstone mode behaviour[14,25-28]. The strong temperature dependence of the relaxation frequency and the temperature dependent activation energy (37-91 kJ/mol, 278-308 K) have not been observed on other compounds or mixtures so far. The low temperature range of the SmC^* phase, which distinguishes this material from the others, may be a reason for this behaviour. The nonlinearity in the Arrhenius diagram is well known for molecular processes when approaching a glass transition[30,31]. Collective modes having a much higher correlation length should be more sensitive to a glass transition. Extrapolation in the activation energy plot to lower temperatures would give a hypothetical glass temperature not less then 263 K. Unfortunately the material crystallized at 271 K before a glass was formed. To check the assumption of a glass transition we calculated[32] the Goldstone mode rotational viscosity γ_G using equation (1).

$$\gamma_G = \frac{1}{4\pi\varepsilon_0} \frac{P_s^2}{\theta^2 \Delta\varepsilon_G f_G} \tag{1}$$

The absolute values of the rotational viscosity (fig. 10) agree well with published data of other FLC[33]. Its average activation energy in the high temperature range of the SmC^* phase is about 70 kJ/mol which is slightly higher than that of e.g. DOBAMBC (49 kJ/mol)[32].
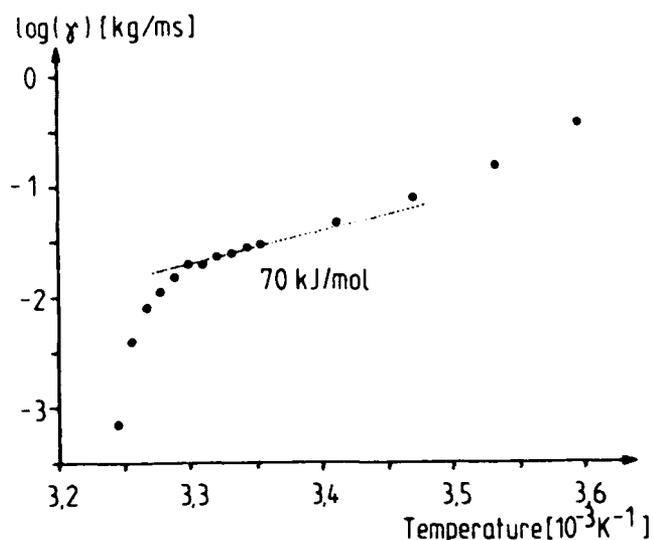
FIGURE 10   Temperature dependence of the Goldstone mode rotational viscosity. The line corresponds to an activation energy of 70 kJ/mol.

In equation (1) there are 4 temperature dependent variables (P_s=spontaneous polarization, Θ=tilt angle, $\Delta\varepsilon_G$=Goldstone mode relaxation strength and f_G= Goldstone mode relaxation frequency). which influence the temperature dependence of the Goldstone mode rotational viscosity (γ_G). ε_o is the dielectric constant in vacuum. This means at the same time, that a nearly temperature independent Goldstone mode relaxation frequency can result from a compensation of the temperature dependences of four parameters. In a rough approach P_s/Θ is proportional to the piezoelectric coefficient (μ_p) and should therefore be nearly temperature independent. As the Goldstone mode relaxation strength $\Delta\varepsilon_G$ also shows no strong temperature dependence, the unusual behaviour of the rotational viscosity should appear in the temperature dependence of f_G. It can be seen from figure 8 that neither the spontaneous polarization nor the tilt angle are responsible for the temperature dependence of the Goldstone mode relaxation frequency due to their similar temperature dependence. It was found that γ_G usually shows a linear behaviour in the activation energy plot[33]. This substance shows a slight deviation from linearity at low temperatures in a sense that the increase of viscosity with decreasing temperature is stronger than expected. This behaviour could be explained by approaching the glass transition. Temperature dependent measurements of the elastic constant K_3 and the helical pitch should give additional information.

The SmA phase relaxation process is clearly identified as a Soft mode[25-28]. It was also observed in the SmC* phase after suppression of the Goldstone mode. Its characteristic parameters and their temperature dependence agrees well with that predicted by theory[28] and described in literature for other substances.

The weak SmC* phase process which appears after the suppression of the Goldstone mode in the whole SmC* phase is identified as a Domain mode[15-16]. This mode appears due to the high spontaneous polarization of this substance. It is caused by fluctuations of a modulated planar structure which forms due to the tendency of the spontaneous polarization to compensate itself, at least partially, when the helix is suppressed.

The high frequency process could not be identified clearly. Nevertheless it was also observed by Vallerien[13] et al. and Kresse[34] et al. in other FLC's. It can be interpreted either as a molecular mode (reorientation of the molecules around their long molecular axis) or as a collective mode (stiff mode: out of phase fluctuations of tilt angle and spontaneous polarisation). A comparable molecular mode is known from measurements on non-chiral substances, the collective mode is predicted by theory. Nevertheless a splitting up in the SmC* phase as is predicted[28] for the stiff mode could not be observed. Further measurements and chemical variations (chiral/nonchiral substance) have to be done in order to solve this problem. It is an interesting result that this process is only slightly influenced by the phase transition SmA-SmC*. The temperature dependence of its activation energy again gives evidence for a glass transition not far below 273 K.

Permanent addresses:

* Institute of Physical Chemistry, University of Concepcion, Concepcion, Chile

$^+$ Institute of Physics, Jagellionian University, 30-059 Krakow, Reymonta 4, Poland

REFERENCES

1. A. Levstik, T. Carlsson, C. Filipic, I. Levstik and B. Zeks, Phys. Rev. A, 35, 3527 (1987).
2. C. Filipic, T. Carlsson, A. Levstik, B. Zeks, R. Blinc, F. Gouda, S.T. Lagerwall and K. Skarp, Phys. Rev. A, 38, (1988).
3. T. Carlsson, B. Zeks, B. Filipic and A. Levstik, Ferroelectrics, 84, 223 (1988).
4. N.A. Clark and S.T. Lagerwall, Appl. Phys. Lett., 36, (1980).
5. S.T. Lagerwall, B. Otterholm and K. Skarp, Mol. Cryst. Liq. Cryst., 152, 503 (1987).
6. K. Skarp and M.A. Handschy, Mol. Cryst. Liq. Cryst., 165, 439 (1988).
7. G.A. Andersson, I. Dahl, W. Kuczynski, S.T. Lagerwall, K. Skarp and B. Stebler, Ferroelectrics, 84, 285 (1988).
8. F. Kremer, S.U. Vallerien, H. Kapitza and R. Zentel, Phys. Lett., A146, 273 (1990).
9. J. Hoffmann, W. Kuczynski, J. Malecki, Mol. Cryst. Liq. Cryst., 44, 287 (1978).
10. A. Levstik, B. Zeks, I. Levstik, R. Blinc and C. Filipic, J. Phys., C3, 303 (1979).
11. C. Legrand, J.P. Parneix, A.M. Kadmi, N.H. Tinh, C. Destrade, C. Salleneuve and N. Isaert, Ferroelectrics, 84, 249 (1988).
12. S.U. Vallerien, F. Kremer, H. Kapitza, R. Zentel and W. Frank, Phys. Lett., A138, 219 (1989).
13. S.U. Vallerien, F. Kremer, T. Geelhaar and A.E. Wächtler, Phys. Rev. A. Rap. Commun., 42, 2487 (1990).
14. M. Pfeiffer, S. Wrobel, L.A. Beresnev and W. Haase, Mol. Cryst. Liq. Cryst., (1991), in print.
15. L.A. Beresnev, M. Pfeiffer, W. Haase, S.A. Pikin, L.M. Blinov, Ferroelectrics, (1991), presented at FLC-91.
16. L.A. Beresnev, M. Pfeiffer, W. Haase, M.V. Loseva, N.I. Chernova, P.V. Adomenas and E.P. Pozhidaev, Pis'ma Zh. Eksp. Teor. Fiz., 53, 170 (1991).
17. R. Twieg, K. Betterton, W. Hinsberg, C. Nguyen and P. Wong, 13th Int. Liq. Cryst. Conf. Vancouver, 1990.
18. R.J. Twieg, K. Betterton, W. Hinsberg, P. Wong, W. Tang and H.T. Nguyen, Ferroelectrics, 114, 295 (1991).
19. A.J. Slaney, J.W. Goodby, Liq. Cryst., 9, 849 (1991) and references therein.
20. R. Twieg, K. Betterton, C. Nguyen and H.T. Nguyen, unpublished results.
21. W. Klämke, Z.X. Fan, W. Haase, H.J. Müller and H. Gallardo, Ber. Bunsenges. Phys. Chem., 93, 478 (1989).
22. W. Haase, H. Pranoto, F.J. Bormuth, Ber. Bunsenges. Phys. Chem., 89, 1229 (1985).
23. W. Haase, F.J. Bormuth, M. Pfeiffer and E. Jakob, Ber. Bunsenges. Phys. Chem., 95, (1991), in print.
24. C.J.F. Böttcher, Theory of Electric Polarization, Elsevier Publ. Co., London 1952.
25. A.M. Biradar, S. Wrobel and W. Haase, Phys. Rev. A, 39, 2693 (1989).
26. F. Gouda, K. Skarp and S.T. Lagerwall, Ferroelectrics, 113, 165 (1991).
27. R. Blinc, M. Copic, I. Drevensek, A. Levstik, I. Musevic and B. Zeks, Ferroelectrics, 113, 59 (1991).
28. R. Blinc and B. Zeks, Phys. Rev. A, 18, 741 (1978).
29. S. Garoff and R.B. Meyer, Phys. Rev. Lett., 38, 848 (1977).
30. H. Kresse, K. Jahn and D. Demus, Phys. Stat. Sol., 119, 632 (1976).

31. M.L. Williams, R.F. Landel and J.D. Ferry, J. Am. Chem. Soc., 77, 370 (1955).
32. A. Levstik, Z. Kutnjak, C. Filipic, I. Levstik, B. Zeks and T. Carsson, Ferroelectrics, 119, 207 (1991).
33. C. Escher, H.D. Dübal, W. Hemmerling, I. Müller, D. Ohlendorf and R. Wingen, Ferroelectrics, 84, 89 (1988).
34. H. Kresse, C. Tschierske, D. Joachimi, F. Kremer and S.U. Vallerien, Cryst. Res. Technol., 26, 245 (1991).

COLLECTIVE AND MOLECULAR RELAXATIONS IN POLYMERIC FERROELECTRIC LIQUID CRYSTALS AND EXPERIMENTAL PROOF OF PIEZOELECTRICITY IN CHIRAL SMECTIC C–ELASTOMERS

A. SCHÖNFELD, F. KREMER, S.U. VALLERIEN

Max–Planck–Institut für Polymerforschung, Postfach 31 48,
W–6500 Mainz, FRG

H. POTHS, RUDOLF ZENTEL[*]

Institut für Organische Chemie der Universität Mainz, Becherweg 18–20,
W–6500 Mainz, FRG

[*] present address: Institut für Organische und Makromol. Chemie der
Universität, Universitätsstr. 1, W–4000 Düsseldorf, FRG

Abstract Broadband dielectric spectroscopy (10^{-1} Hz $-$ 10^{9} Hz) was used to study the collective and molecular dynamics in polymeric side–chain FLC. In the frequency window under study collective (Goldstone–mode) and molecular (β–relaxation) relaxations are observed. By crosslinking combined main–chain side–group polymers an elastomeric FLC can be prepared which exhibits a Goldstone–mode as well. The piezoelectricity in these elastomeric materials is experimentally proven.

INTRODUCTION

Broadband dielectric spectroscopy is a powerful tool to study the collective and molecular dynamics in (polymeric) FLC. By varying the chemical structure ingoing from low molecular to polymeric side–chain, "combined" main–chain side–group and to elastomeric systems its influence on the dynamics can be analysed in detail. This allows to envisage possible new applications of FLC.

EXPERIMENTAL

To study the collective and molecular dynamics in ferroelectric liquid crystalline side–chain polymers broadband dielectric spectroscopy (10^{-1} Hz – 10^9 Hz) was employed. To cover this frequency regime three different measurement systems were combined: (i) a frequency response analyser (10^{-3} Hz – 10^4 Hz), (ii) an Ac–bridge (10 Hz – 10^7 Hz) and (iii) a coaxial line reflectometer (10^6 Hz – 10^9 Hz). Rubbed polyimid coated metal electrodes ($\emptyset$: 5 mm, spacing: 20 μm) were used which enabled us to measure in the entire regime from 10^{-1} Hz – 10^9 Hz with <u>one</u> capacitor arrangement. Additionally, the spontaneous polarization could be measured in this sample cell.

Two side–chain polymers were used having a siloxane main–chain:

$$CH_3 - \underset{\underset{n}{\overset{|}{\lfloor}}}{\overset{\overset{\lceil}{\overset{O}{|}}}{Si}} - (CH_2)_{11} - O - \langle O \rangle\langle O \rangle - OOC - R^*_{1/2}$$

$$R^*_1: \quad \langle O \rangle \overset{NO_2}{} - O - \overset{\overset{CH_3}{|}}{\underset{*}{CH}} - C_6H_{13}$$
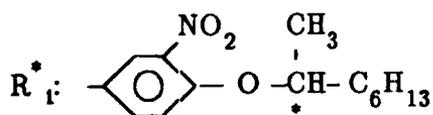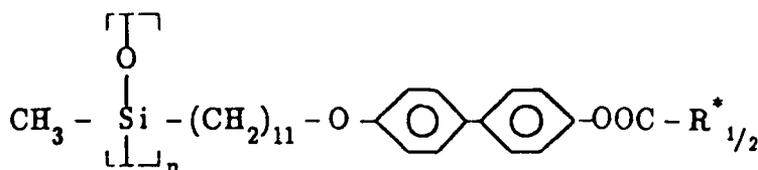
g 294 K   330 SmC* 434 SmA 456 i   (polymer 1)

$$R^*_2: \quad \langle O \rangle \overset{Cl}{} - O - \overset{\overset{CH_3}{|}}{\underset{*}{CH}} - C_6H_{13}$$
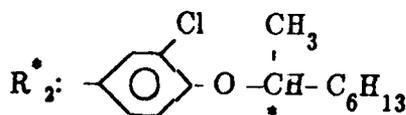
k 334 SmC* 442   (polymer 2)

The phase sequences were determined by DSC. For details see refs. 7 10.

The frequency and temperature dependence of the dielectric loss ϵ' (Fig. 5) for the elastomer shows a loss process having a strong dielectric strength. Presumably it has to be assigned to the Goldstone—mode, thus indicating towards the existence of a chiral smectic C*—phase. In its dielectric strength and its frequency position it is comparable with our recent studies on polymeric ferroelectric liquid crystals[2].
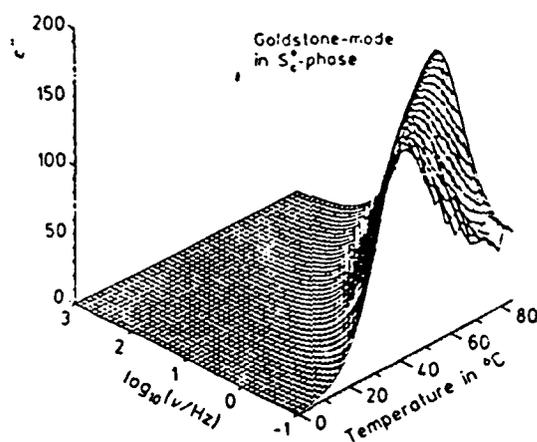
FIGURE 5   Dielectric loss ϵ' vs. temperature and decadic logarithm of frequency ν for the elastomer.

Temperature—dependent measurements of the piezosignal registered at a frequency of 7 Hz and an amplitude of 10 μm (corresponds to 10% change in sample thickness) are shown in Fig. 6a. Entering the smectic C*—phase at a temperature around 81°C leads to a continuous increase of the signal until a nearly 1000—fold value compared to the isotropic signal is reached. The plateau—level signal of about 10 mV might not be saturated, since the elastomer was crosslinked in the isotropic state. Thus, a better orientation of the sample by crosslinking the precursor polymer in the smectic phase in the presence of an orienting magnetic field should strongly improve the observed piezoelectricity. Fig. 6b shows the linear—amplitude dependence of the piezosignal at different temperatures inside the smectic C*—phase.
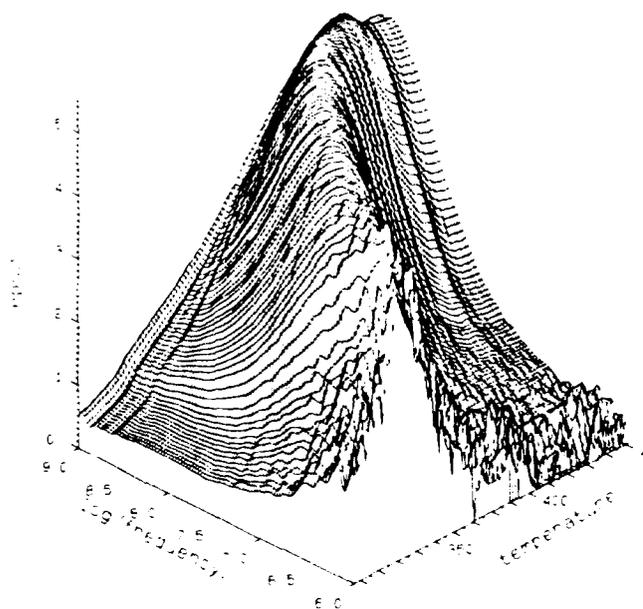
FIGURE 2   Dielectric loss ϵ' vs. temperature and decadic logarithm of frequency for polymer 2 (sample not macroscopically aligned).

At the phase transition SmA/SmC* this process does not split or broaden. Its dielectric strength does not decrease, as suggested by the (generalized) Landau theory of the phase transition SmA/SmC* in FLC[3,4]. Instead the dielectric strength changes slightly at this phase transition which can be explained by the change of the aspect angle of the lateral dipole moments with respect to the outer electrical field. The temperature dependence of the β–relaxation is Arrhenius–like with a slope which changes slightly in the different mesophases (Fig. 3). These experimental findings are in full accordance with our results in low molecular weight systems[5]. They require a reformulation of the Landau theory of the phase transition in FLC as discussed in detail in the contribution of F. Kremer et al. in these proceedings.
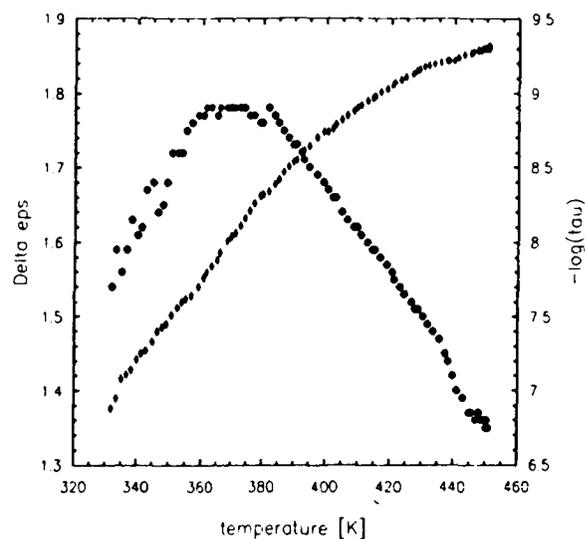
FIGURE 3 $\Delta\epsilon$ (•) and decadic logarithm of the relaxation time τ (♦) vs. temperature for polymer 2.

Experimental proof of piezoelectricity in chiral smectic C elastomers

Low–molar–mass liquid crystals (LC) with chiral smectic C*–phases show ferroelectric properties and act therefore also as piezo–elements. However, since they are liquid–like, they cannot support stress and relax immediately after mechanical deformation. LC–elastomers[6] and especially LC–elastomers with S_C^*–phases[7,8] can be prepared by crosslinking of LC–polymers. These polymers show the ferroelectric modes typical for low–molar–mass liquid crystals in the uncrosslinked state[9,10]. Since they are soft solids after crosslinking, they can support stress under equilibrium conditions. Therefore, these elastomers should be interesting as piezo–sensors[7]. Since they are in rubbery state, they should have piezoelectric features which are different from classical piezoelectric polymers such as poly(vinylidene difluoride) (PVDF)[11].

For our investigations we selected LC–elastomers based on combined main–chain/side–group polymers[7], because it can be assumed that a deformation of the network is most effective on mesogenes, which are incorporated into the polymer chain (in combined polymers one half of the

A. SCHÖNFELD *et al.*

mesogenes is incorporated in the polymer chain, but all mesogenes orient parallel to each other and to the polymer chain)[12]. As chiral group we selected a chiral ether of 4–hydroxy–3–nitrobenzoic acid, which gives rise to a very high spontaneous polarization in LC–side–group polymers[2]. The phase sequence was measured by DSC.

For the measurement of the piezoelectric effect[13] the liquid–crystalline elastomer was mounted between two ITO–coated glass plates (area 4 x 10 mm²) which had a separation of about 100 μm being maintained by two spacers of polyimide (Fig. 4). The two glass plates could be pressed together by use of a piezotransducer equipped with a ceramic tip. In order to compensate for its hysteresis, it was provided with an internal position sensor which was connected to a feed–back loop of the electronic piezocontroller. The temperature of the piezotransducer was held between 40° C and 50° C by use of a housing which was temperature–controlled by an air jet. The sample temperature was controlled by placing the whole sample holder in a cryostat which was temperature–controlled by a temperature–controlled nitrogen gas jet. The oscillator (frequency: 7 Hz) of the lock–in–amplifier was used to control the piezocontroller. The lock–in amplifier was employed to detect the electrical response of the mechanical excitation. The actual experimental set–up does not include a force sensor, thus the conclusions concerning the piezoelectricity of the different mesophases are qualitative only. A quantitative approach is in progress.
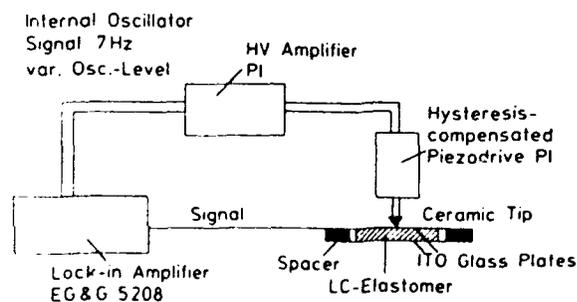
FIGURE 4   Experimental sep–up for the investigation of piezoelectricity in LC–elastomers
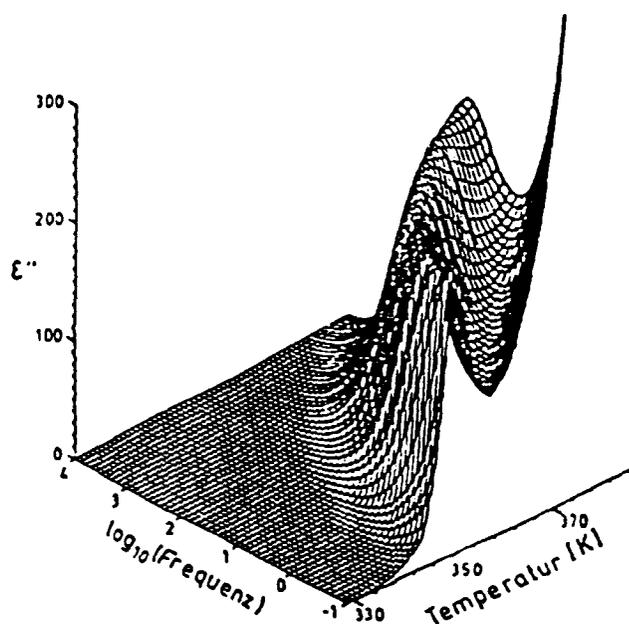
FIGURE 1 Dielectric loss ϵ' vs. temperature and decadic logarithm of frequency for polymer 1.

RESULTS AND DISCUSSION

In the low frequency regime ($\lesssim 10^4$ Hz) beside the conductivity contribution an additional strong dielectric loss process is observed. Its strength proves the collective nature of this process. It has to be assigned presumably to a Goldstone mode.

(The soft—mode was not studied in this system because of the high SmC*/SmA transition temperature.) For the spontaneous polarization measured in the identical capacitor arrangement a value of about 400 nC/cm^2 is found, which compares well with measurements in a commercial FLC—cell (EHC—cell). Between 10^6 Hz and 10^5 Hz the β—relaxation is observed (Fig. 2). It is assigned to a hindered rotation (libration) of the mesogenes around their long molecular axis.
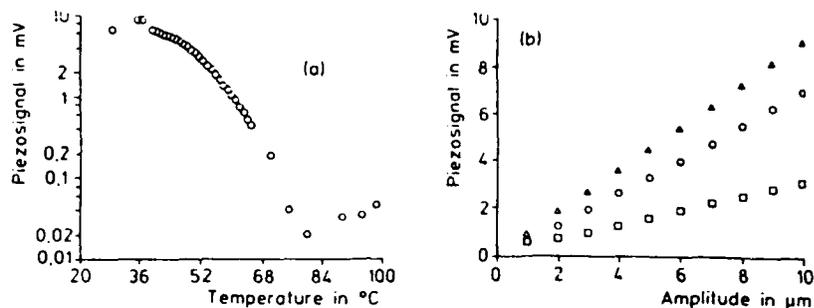
FIGURE 6   (a) Decadic logarithm of piezosignal vs. temperature for the elastomer with an amplitude of 10 μm.   (b) Amplitude dependence of the piezosignals inside the smectic C*–phase of the elastomer at 35° C (Δ), 39° C (o) and 52° C ($\square$).

CONCLUSION

Broadband dielectric spectroscopy delivers for a polymeric FLC in the frequency regime between 10^{-1} Hz to 10^9 Hz a highly collective processes (Goldstone–mode) and a molecular relaxation (β–relaxation). This is in full accordance with our studies in low–molecular weight systems[5]. By crosslinking combined main–chain side–group polymers elastomeric FLC can be prepared. In these systems the mechanical properties of the rubbery state and the dielectric (and electrical) properties of an FLC are combined. The theoretically discussed[14] piezoelectricity is experimentally proven.

ACKNOWLEDGEMENT

REFERENCES

1. F. Kremer, D. Boese, G. Meier and E.W. Fischer,
    Progr. Colloid & Pol. Sci., 80, 129 (1989).
2. H. Kapitza, R. Zentel, R.J. Twieg, C. Nguyen, S.U. Vallerien, F. Kremer
    and G. Wilson, Adv. Mat., 2, 539 (1990).
3. R. Blinc and B. Žekš, Phys. Rev., A 18, 740 (1978).
4. T. Carlsson, B. Žekš, C. Filipič and A. Levstik,
    Phys. Rev., A 42, 877 (1990).
5. F. Kremer, A. Schönfeld, S.U. Vallerien, A. Hofmann and N. Schwenk,
    Ferroelectrics, this issue.
6. H. Finkelmann, H.J. Kock, G. Rehage, Makromol. Chem., Rapid
    Commun., 2, 317 (1981); J. Schätzle, W. Kaufhold, H. Finkelmann,
    Makromol. Chem., 190, 3269 (1989).
7. R. Zentel, Angew. Chem., Adv. Mater., 101, 1437 (1989); R. Zentel,
    G. Reckert, S. Bualek, H. Kapitza, Makromol. Chem., 190, 2869 (1989).
8. H. Kapitza, Dissertation, Mainz (1990); H. Kapitza, R. Zentel,
    S.U. Vallerien, F. Kremer, in: Liquid Crystalline Polymers, edited by
    R.A. Weiss and C.K. Ober, ACS Symp. Ser. No. 435, to be published.
9. S.U. Vallerien, R. Zentel, F. Kremer, H. Kapitza, E.W. Fischer,
    Makromol. Chem., Rapid Commun., 10, 333 (1989).
10. S.U. Vallerien, R. Zentel, F. Kremer, H. Kapitza, E.W. Fischer,
    Proceedings of the 2nd Ferroelectric Liquid Crystal Conference,
    Göteborg/Sweden (1989), Ferroelectrics, in press; S.U. Vallerien,
    F. Kremer, H. Kapitza, R. Zentel, E.W. Fischer,
    Ferroelectrics , 109, 273 (1990).
11. T. Furukawa, Phase Transitions, 18, 143 (1989).
12. R. Zentel, G.F. Schmidt, J. Meyer, M. Benalia, Liq. Cryst., 2, 651
    (1987); S. Diele, M. Naumann, F. Kuschel, B. Reck, H. Ringsdorf,
    Macromolecules, 21, 1620 (1988).
13. S.U. Vallerien, F. Kremer, E.W. Fischer, H. Kapitza, R. Zentel,
    H. Poths, Makromol. Chem., Rapid Commun., 11, 593 (1990).
14. H.R. Brand, Makromol. Chem., Rapid Commun., 10, 441 (1989).

SECTION B
FLC PHYSICS

SMECTIC C* LOCAL LAYER STRUCTURE WITHIN TEXTURE LINES STUDIED WITH A (SUB)MICROMETER OPTICAL MEASURING SPOT

A.G.H. VERHULST AND F.J. STOMMELS
Philips Research Laboratories, P.O.Box 80.000, Eindhoven, The Netherlands

Abstract   The smectic layer structure within texture lines is investigated with a (sub)micrometer optical measuring spot. The property that the SmC-cone is perpendicular to the smectic layer is used to measure the in-plane rotation angle of the local smectic layers. From the measurements and observations it is concluded that texture lines, either spontaneously present or field induced, which run parallel to the rubbing direction in a virgin area, consist of two parts which are equivalent to zig-zag lines. These texture lines can be removed with a small low-frequency electric field, indicating that the smectic layers at the FLC—solid interfaces are not rotated or displaced. The texture which results after a prolonged treatment with a large low-frequency field consists of a dense structure of parallel texture lines, modified in such a way that the in-plane smectic layer rotation is extended from the bulk to the FLC—solid interfaces. Texture lines from DC electric fields, running obliquely to the rubbing direction, show an in-plane smectic layer rotation of a few degrees, which reasonably agrees with the layer rotation calculated from existing theory. Oblique lines created with a low frequency field exhibit an internal fine-structure which originates from the two polarities of the AC field. From this structure the electro-optical properties can be understood.

INTRODUCTION

Surface Stabilized Ferroelectric Liquid Crystals [1] (SSFLC) usually exhibit a chevron type smectic layer structure as is found by X-ray diffraction experiments.[2] This layer structure can give rise to zig-zag defects [3], and texture change under the application of low-frequency electric fields.[4] It has been shown, that irreversible texture change can be used to create an analogue grey-scale in the bistable SSFLC system (the texture method).[5] From optical spot measurements on such textures we concluded that bistability is maintained at every position, but that the threshold voltage for latching is distributed as a result of local variation in the uprighting of the smectic layers.

Smectic layer structures can be studied both by optical and X-ray techniques. X-ray studies provide direct information on the layer structure. In this work we present an optical method which has high lateral resolution due to the use of a submicron measuring spot. This allows us to measure within texture lines to reveal the local layer structure in an indirect way. Generally, optical methods are indirect methods, as for their interpretation one relies on presumptions on the local director pattern. As will be explained, this drawback is not very severe with respect to rotation of the smectic layers in a plane parallel to the bounding plates. Therefore, optical spot measurements yield useful information on the in-plane rotation angle of the local smectic layers.

In this paper results will be given for texture lines of different types, either spontaneously present or field induced with a DC or AC electric field. The different

types are divided into two main groups: texture lines running parallel to the rubbing direction and texture lines obliquely to it. Comparisons will be made with the results of local smectic layer structures as proposed and modelled by the Boulder group.[5,7,8,11] We start with a description of the microscope set-up and the measuring method.

EXPERIMENTAL

Microscope set-up
Local small spot measurement of the transmission is in principle not different from large spot measurement. Practical limitations on the lower limit of the spot size arise from the noise of the photomultiplier (PM), from the mechanical stability of the set-up with respect to spot position and from the optics with respect to focusing and cone angle of the light focused by the condenser onto to the substrate.

The measuring set-up consists of a Leitz microscope with PM-unit, temperature-controlled stage, drive electronics, TV-camera and recorder and a personal computer (PC). The PM-unit is equipped with an interchangeable pin-hole diaphragm. The diameter of the measuring spot is determined by the diameter of the pin-hole and the objective in use. For most measurements we used a 125x objective and a pin-hole of 0.1 mm resulting in a circular measuring spot of $1.2\mu m$ diameter at the FLC layer. A number of measurements were done with a spot $< 1\mu m$, resulting in about the same values, but possessing a higher inaccuracy due to the increased PM noise. With a built-in illumination and reflection system the measuring spot is made visible in the image of the sample.

In the case of a small measuring spot it is difficult or even impossible to keep the spot in position during rotation of the substrate table. Therefore we modified the microscope in such a way that not the substrate table but the polarizer (P) and analyzer (A) are rotated simultaneously. As an advantage of this system, a pin-hole diaphragm can be used with translation possibilities to precisely adjust the position of the spot.

With respect to the optics, it is important to create a sharp image, otherwise the detail in the image on which the measuring spot is focussed contains too much light from the surrounding area, which consequently results in a large measuring error. In addition, the cone angle of the light focused by the condenser onto the substrate has to be small, which is achieved by decreasing the aperture of the condenser diaphragm, but unfortunately this also lowers the light level and consequently increases the PM noise.

Measuring method
To determine the in-plane smectic layer rotation (in the plane parallel to the glass plates) we make use of the property that the SmC-cone is perpendicular to the smectic layer. By measuring the extinction angles when the director is on the side of the cone (saturated states, S-states), the direction of the smectic layer normal (projected onto the glass plate) is found as the bisector of the angle between the two S-states. For this measurement we use a drive voltage consisting of a set of 2 bipolar pulses of $\pm 25V$ repeated every 20ms. During each of these 4 pulses of 0.5ms each, the director is driven to an S-state. The angles of these states can easily be measured by rotating the polarizer/analyzer (P/A) to minimum PM output at the positive and the negative pulses respectively. It turned out that these angles, which are averaged values over the thickness of the FLC layer, are almost independent of the amplitude of the measuring volt-

age (for V > 15V). This indicates that if a splay or twist deformation of the director pattern is present, it is concentrated into a relative thin part of the FLC layer.

In principle, the in-plane rotation angle of the smectic layers can also be found by rotating the P/A to the point where the transmissions at the plus and minus pulses are equal. However, even without a test-cell in the system, the output of the PM depends on the angle of the polarized light. This would result in a certain measuring error. For that reason the extinction angles were used and not the transmission levels, which has the additional advantage that also the angle between the S-states is obtained.

The general way to measure extinction angles accurately is by determination of two angular positions with equal transmission close to the extinction point. Due to the symmetrical (sin²) function of the transmission in this respect, the extinction angle is equal to the average value of the two angles. In our measurements this method resulted in an accuracy of $\pm0.2°$.

In the case of a narrow texture line, the measuring result depends on the precise spot position. Although the position of the spot can be observed under the microscope, optical positioning turned out to be inaccurate. Reliable and accurate spot positioning is obtained with the help of the measuring pulses described before. This is explained in Fig.1.
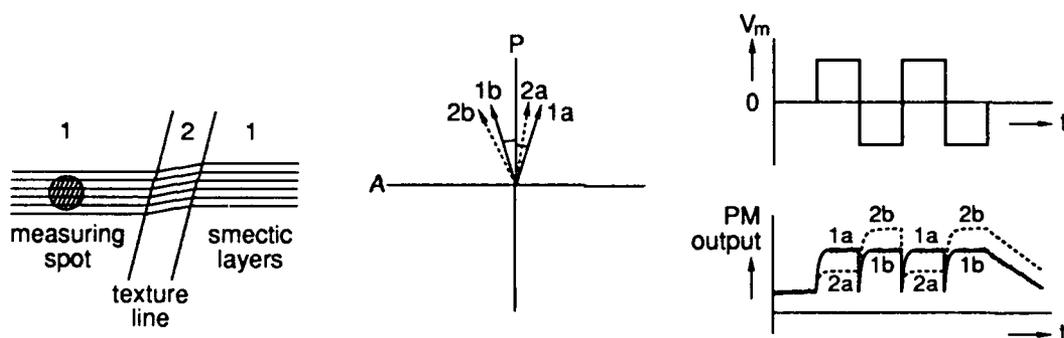
FIGURE 1   Positioning of the measuring spot. When the spot is moved across the texture line (2), the PM output exhibits a minimum (2a) at the positive pulses of V_m and at the same time a maximum (2b) at the negative pulses. The measuring position of the spot is defined by this minimum/maximum.

On the left part of the figure a texture line (2) is drawn with slightly rotated smectic layers. As shown in the polar plot (middle part), the S-states are then also rotated (2a, 2b). When the measuring spot is moved across the texture line, the PM output at the positive pulses of V_m exhibits a minimum (2a), while for the same spot position at the negative pulses a maximum occurs (2b) (right part). Before each measurement, the spot is positioned exactly on this minimum/maximum, which corresponds with the position of maximum layer rotation.

Test-cells

The test-cells consist of 1.1mm glass plates with ITO on which the alignment layers, consisting of chemically modified PVA, are spin-coated. After drying, the layers are strongly rubbed and the cell is assembled with the rubbing directions parallel using $1.6\mu m$ spacer spheres of SiO_2. The cells are filled with the FLC mixture ZLI-3654 from Merck (in the isotropic phase) and slowly cooled down to room temperature. All measurements are carried out at 25°C.

TEXTURE LINES PARALLEL TO THE RUBBING DIRECTION

One type of texture lines parallel to the rubbing direction is often present after cooling down to the SmC* phase (texture-I lines). The presence of these lines depends on the properties of the alignment layer, the rubbing density and the FLC mixture. These lines shorten or remove upon application of a small low-frequency voltage ($\pm$1V 25Hz).[6]

Under the application of a medium to high voltage (5-30V), in general two types of texture lines can occur: lines running obliquely to the rubbing direction (texture-II lines) and lines running parallel to it (texture-III lines).[4] The oblique lines nucleate at a lower threshold field, they will be described in the next chapter. During the voltage treatment, texture-III develops from a mixture of parallel and oblique lines to the well known parallel striped texture. We succeeded in field creating single parallel texture lines in a virgin area, thus without the crossing oblique lines, making it possible to investigate their properties.

Parallel lines in a virgin area

Photographs of a texture-I line and of parallel texture lines generated with +25V, −25V and $\pm$ 25V 25Hz square wave voltage, are shown in Fig.2.
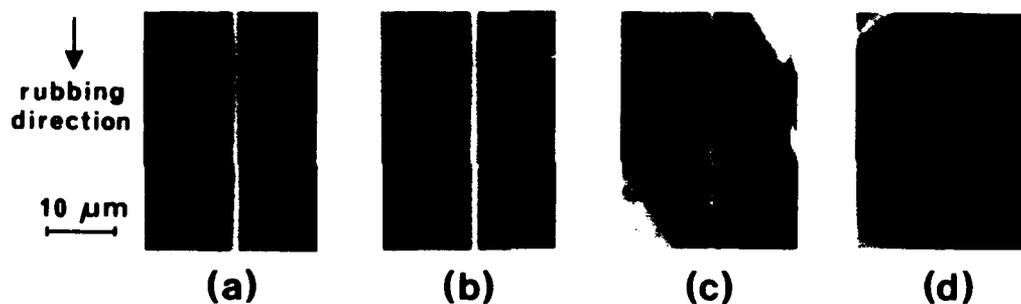
FIGURE 2   Photographs of parallel texture lines (parallel to the rubbing direction). (a) Texture-I line, present after cooling to SmC*. (b) Line, generated with +25V 0.5s. (c) Generated with −25V 1.5s. (d) Generated with $\pm$ 25V sq.w. 25Hz 2.5s.

The similarity between the four lines is striking. For the measurements, we selected texture lines with both ends pinned, because other lines sometimes disappeared under the influence of the measuring pulses. The lines consist of two halves although on the photographs more lines are visible, which may be caused by a complicated director pattern of the memory state in combination with microscope effects. It turned out that the director patterns on both halves are monostable. On the two halves we have measured the director angles of the S-states, θ_S. For the four texture lines, the values of θ_S and the derived in-plane smectic layer rotation χ are given in Table I. The angles θ_S are given relative to the z-axis, which is defined as the direction of the smectic layer normal in the virgin area, projected onto the glass plate. This direction is measured separately via the angles of the S-states in the virgin area using a measuring spot of 10μm diameter. The positive z-axis points in the same direction as the chevron kink (anti-parallel to the rubbing direction).

From the results two things directly show up: 1. the angles measured on the four lines are of the same magnitude and 2. the χ values of the two parts are approximately

TABLE I   Measured director angles of the S-states (θ_S) and derived in-plane smectic layer rotation (χ) for the different texture lines parallel to the rubbing direction. Angles are given in degrees.

line or voltage	left part (L)			right part (R)		
	θ_S	χ		θ_S	χ	
texture-I	−31.4	+14.2	−8.6	−18.1	+35.4	+8.7
+25V DC 20s	−31.5	+17.3	−7.1	−16.8	+35.7	+9.5
−25V DC 20s	−31.9	+14.5	−8.7	−18.4	+35.4	+8.5
±25V 20Hz 2s	−34.4	+15.2	−9.6	−19.7	+36.4	+8.4

symmetric, being negative for the left part and positive for the right part. The variation in the values of θ_S from line to line is also present, to a certain extent, within texture lines of the same type. When the angle between the S-states, $\Delta\theta_S$, is compared with the cone angle θ, it turns out (for most cases) that $\Delta\theta_S < 2\theta$ for the left part and $\Delta\theta_S > 2\theta$ for the right part ($\theta = 24.5°$). This phenomenon is not yet understood. Furthermore. it is found that the field generated (parallel) texture lines, if not pinned at both ends, can be shortened or removed with a small low-frequency voltage (±1V 25Hz), in the same way as the texture-I lines. *From the measurements and observations it is concluded that there is no real difference between the four lines of Table I and from now on this type of line will be denoted as "parallel texture line" (parallel to the rubbing direction),* shortened to "PT-line". The property that only a very small AC voltage is needed to shorten or remove the line (±1V) indicates that the smectic layers are not displaced or rotated at the FLC−solid interfaces but only in the bulk of the FLC layer.

Comparison with zig-zag lines

We observed that under certain circumstances (fields, way of pinning, temp.) PT-lines can split up in two parts forming conventional zig-zag lines of the lightning type. In addition, as is shown in Fig.3 (different sample), two zig-zag lines which approach each other look the same as a PT-line.
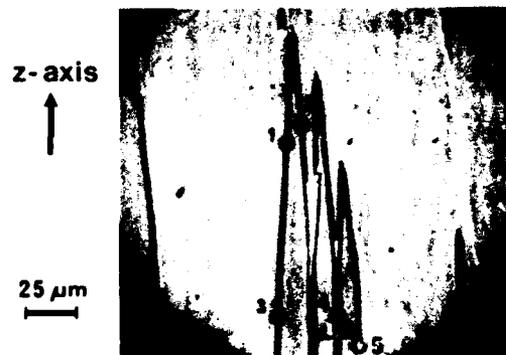
FIGURE 3   Zig-zag lines of the lightning type. The positions 1 to 5 indicate the measuring positions given in Table II.

Small spot measurements are applied on the different lines of Fig.3 and the results obtained on the positions 1 to 5 are given in Table II.
As expected, the direction of the layer rotation is the same for the positions 1, 3 and 4R and for 2, 4L and 5. Comparing 4L and 4R with the results of Table I, it turns out

TABLE II   Measured director angles of the S-states (θ_S) and derived in-plane smectic layer rotation (χ) for the positions on the lines indicated in Fig.3. Angles are given in degrees.

position	θ_S		χ
1	−31.3	+16.4	−7.5
2	−18.2	+34.8	+8.3
3	−32.1	+15.2	−8.5
4L	−16.6	+33.7	+8.6
4R	−31.1	+14.8	−8.2
5	−18.7	+34.2	+7.8

that the signs of the χ values are interchanged. As will become clear, this is due to the chevron direction within the zig-zag area.

The model structure of a zig-zag line, as described in refs.7 and 8, is drawn in Fig.4a.

(a)   (b)
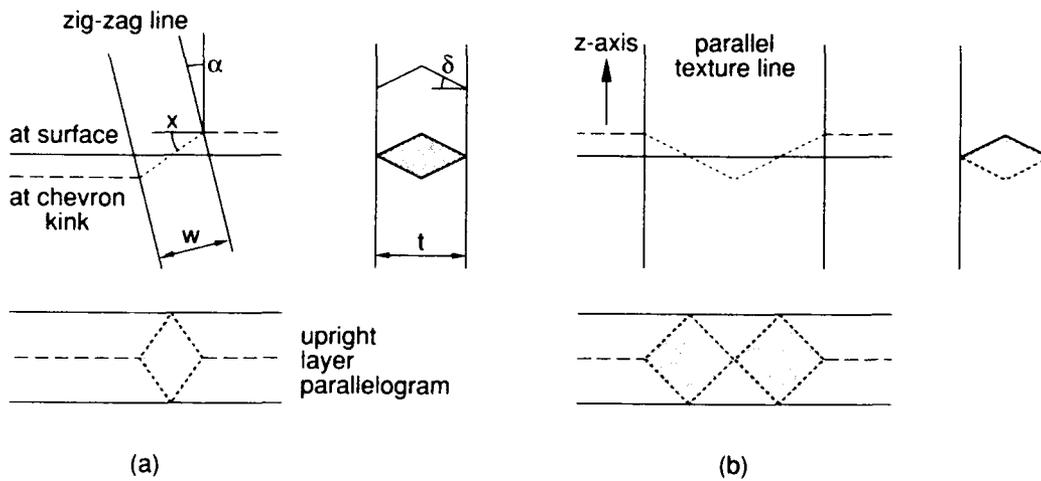
FIGURE 4   (a) Simplified model of a zig-zag line, illustrated by means of a top-view and two side-views. On both sides of the line the chevrons point in opposite direction. (b) Model of a parallel texture line (parallel to the rubbing direction and to the z-axis). On both sides of the line the chevrons point in the same direction.

The top-view and the two side-views give an impression of the 3-dimensional layer structure. The upright layer parallelogram is a plane smectic layer, rotated in the plane of the cell over an angle χ. From this model the following equations hold [7]

$$\frac{\cos(\alpha - \chi)}{\cos \alpha} = \cos \delta \qquad\qquad w = t \, \frac{\cos \alpha \sin \delta}{\sin \chi} \qquad\qquad (1)$$

The parameters α, χ, δ, w and t are defined in Fig.4a. For $\alpha = 0$ this reduces to $\chi = \delta$ and $w = t$. For planar director orientation, the layer angle δ, the cone angle θ and the angle of the memory state (M-state) θ_M, are in general related by

$$\cos \delta = \frac{\cos \theta}{\cos \theta_M} \qquad\qquad (2)$$

With $\theta = 24.5°$ (ZLI-3654) and $\theta_M = 5°$ (measured value) this results in $\delta = 24°$. The measured values of χ are much smaller than 24°. From the structure of the smectic layers (Fig.4a) it follows that we always measure a certain averaged value over the thickness of the FLC layer which is smaller than the real layer rotation.

The step from the model for a zig-zag line to the model for a parallel texture line is straightforward. This is sketched in Fig.4b. The upright layer parallelogram in the left half is rotated clockwise ($\chi < 0$) and in the right half counter-clockwise ($\chi > 0$), which corresponds to the signs of χ in Table I. Within a zig-zag area the chevrons point in the opposite direction, which results in an in-plane rotation of the parallel texture line of 180°. This agrees with the signs of χ on the measuring positions 4L and 4R in Table II. The width of the PT-line is expected to be two times the cell thickness, which agrees with the width as estimated from Fig.2. The absence (in the model) of layer displacement at the FLC—solid interfaces favourably agrees with the observation that only a small low-frequency field is needed to shorten or remove the texture line. From this and from the structure of the smectic layers, it can be stated that extra energy is involved in the layer and director structure of the line.

Texture-III

The texture which is induced by a prolonged treatment with a high low-frequency voltage ($\pm 25V$ 25Hz) (texture-III),[4] contains lines parallel to the rubbing direction which look, at a first glance, as a dense structure of PT-lines described before. The main differences, however, are found in the angle between the M-states and in the impossibility to remove the lines with a small AC field. As mentioned earlier, the director patterns in both parts of a PT-line are monostable. On the other hand, the measured M-state angles of a texture-III line result in $\Delta\theta_M > 35°$. For $\Delta\theta_M = 35°$ eq.(2) gives $\delta = 17°$, so, in chevron terms, the layers are strongly uprighted, which is known already from X-ray diffraction experiments.[9] When generating texture-III, the first occurrence is a dense structure of (reversible) PT-lines. These lines are transformed by the prolonged field into (irreversible) texture-III lines. Although it is still under investigation, we assume that the in-plane smectic layer rotation, which is already present within the body of the PT-lines, is extended then to the FLC—solid interfaces. This gives a zig-zag like smectic layer structure (in-plane chevrons), which is in accordance with recent X-ray results.[10]

TEXTURE LINES OBLIQUE TO THE RUBBING DIRECTION

The texture which is induced by a low-frequency voltage of medium amplitude (5-15V 25Hz) is known as texture-II [4] and contains line pairs (roof tops) running obliquely to the rubbing direction. Oblique texture lines can also be generated with a $\pm$DC field.[11] In that case they occur as single lines. We generated and investigated DC as well as AC oblique texture lines (OT-lines).

Oblique texture lines from DC fields

OT-lines generated with +15V and −15V , are shown in Fig.5a and b respectively. These lines nucleate at positions where the smectic layer system is distorted (e.g. a PT-line or a zig-zag line). The line parts indicated with A and B grow in opposite direction, with line A growing roughly in the direction of the positive z-axis.

(a) **(b)**
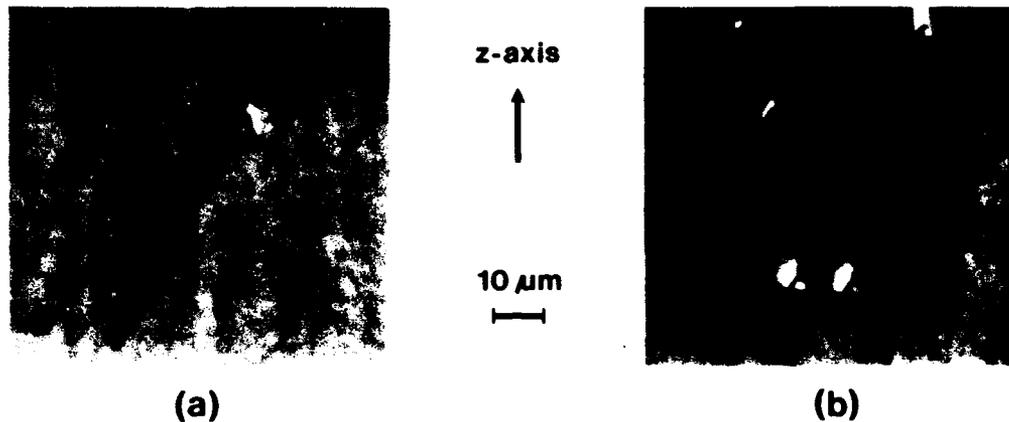
FIGURE 5   Texture lines running obliquely to the rubbing direction, generated with (a) +15V 1s and (b) −15V 1s. Indicated are the two line types A and B.

A number of such lines were generated with different DC voltages. In most cases when the spot (for positioning) was moved across the texture line, a "flat part" was found in the PM output when the spot was at the centre part of the line. The following parameters were measured: the angle α of the lines with respect to the z-axis, the extinction angles of the S-states, θ_S, from which the in-plane smectic layer rotation χ is derived, and the angles of the M-states, θ_M. The M-states were measured by rotating the crossed polarizer analyzer set to minimum PM output at the end of the 20ms driving cycle, once with normal pulse polarities and once with the pulses inverted. It has to be mentioned here that the M-states, measured in this way, are less well defined than the S-states. The experimental results are summarized in Table III. The values of α are averaged values over a number of lines. The other at.' 's are the result of single line measurements.

TABLE III   Experimental results obtained on oblique texture lines generated with a DC voltage. Angles are given in degrees.

voltage	line	α	θ_S		χ	θ_M	$\Delta\theta_M$		χ_{CAL}
−15V 1s	A	+17	−28.3	+21.2	−3.6	−8.1	+10.0	18.1	−1.7
"	B	−151	−27.2	+21.7	−2.8	−10.6	+10.9	21.5	−1.5
−20V 0.5s	A	+30	−28.1	+20.7	−3.7	−12.2	+13.6	25.8	−2.1
"	B	−150	−28.1	+20.9	−3.6	−12.7	+12.7	25.4	−2.1
+20V 0.5s	A	−30	−23.0	+27.8	+2.4	−12.3	+13.9	26.2	+2.2
"	B	+150	−22.5	+27.6	+2.6	−13.1	+15.2	28.3	+2.6
−25V 0.4s	A	+35	−27.0	+22.3	−2.4	−13.6	+12.3	25.9	−1.8
"	B	−149	−27.6	+21.2	−3.2	−12.1	+12.4	24.5	−1.8

The in-plane smectic layer rotation χ is of the order of 3° and the angle between the M-states, $\Delta\theta_M$, is 18-28°, which is much larger than the 9° in the virgin area. This is in qualitative agreement with uprighting and in-plane rotation of the smectic layers as has been measured by X-ray diffraction.[12] Following the Boulder model for oblique texture lines [11], adapted to our situation, the following equation holds

$$\frac{\cos \alpha}{\cos(\alpha - \chi)} = \frac{\cos \delta'}{\cos \delta} \tag{3}$$

in which δ' is the angle of the smectic layers within the texture line with respect to the glass plate normal. With eq.(2) this results in

$$\frac{\cos \alpha}{\cos(\alpha - \chi)} = \frac{\cos \theta_M}{\cos \theta'_M} \tag{4}$$

The prime indicating the texture line again. With $\theta'_M = 0.5(\Delta\theta_M)$, and $\theta_M = 4.5°$ in the virgin area, the values of χ for the different texture lines in Table III were calculated. The results are shown as χ_{CAL} in the last column of the table. The direction of the layer rotation corresponds with the model, but the calculated values are for most lines smaller than the measured ones. One of the reasons for this difference can be that the M-states, as stated before, are less well defined when measured within the 20ms driving cycle.

In addition, transmission voltage (Tr-V) curves are measured on these lines using a reset drive scheme. The bipolar reset pulse is fixed at $\pm25V$, $256 + 256$ μs, and the bi-polar switch pulse is increased from 0 to $\mp25V$ at a width of $128 + 128$ μs. The transmission value is measured at about 7ms after the switch pulse. The Tr-V curve shown in Fig.6 is obtained on a B-line generated with $+20V$ 0.5s.
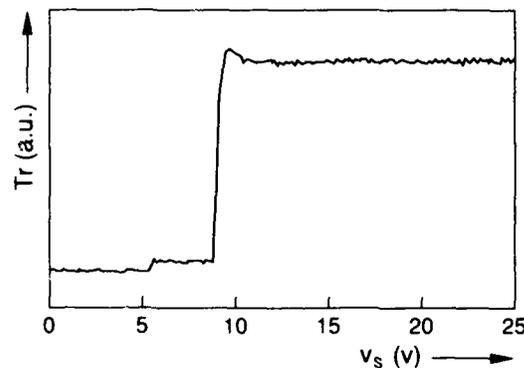
FIGURE 6   Transmission voltage curve obtained with a reset drive scheme on a B type oblique texture line generated with $+20V$ 0.5s.

The small Tr jump at 5.5V comes from latching of the virgin area which surrounds the texture line. The large Tr jump at 9V is from the texture line itself. The higher threshold voltage of the texture line is in qualitative agreement with the larger angles between the M-states, which is connected to the uprighting of the smectic layers. This effect is used in the "Texture Method" [5] to create an analogue grey-scale in the bi-stable SSFLC effect. The relative heights of the two jumps give information on the spot size in relation to the width of the texture line. In all the measurements the relative Tr jump from the virgin area is kept below 10%.

Oblique texture lines from AC fields

When generating OT-lines with an AC voltage of a very low frequency, the internal structure of the line becomes visible. The parts originating from the successive polarities of the voltage can be identified. An example is shown in Fig.7a where a square wave voltage has been used of $\pm20V$ 1.5Hz 4 periods, starting with a positive phase.
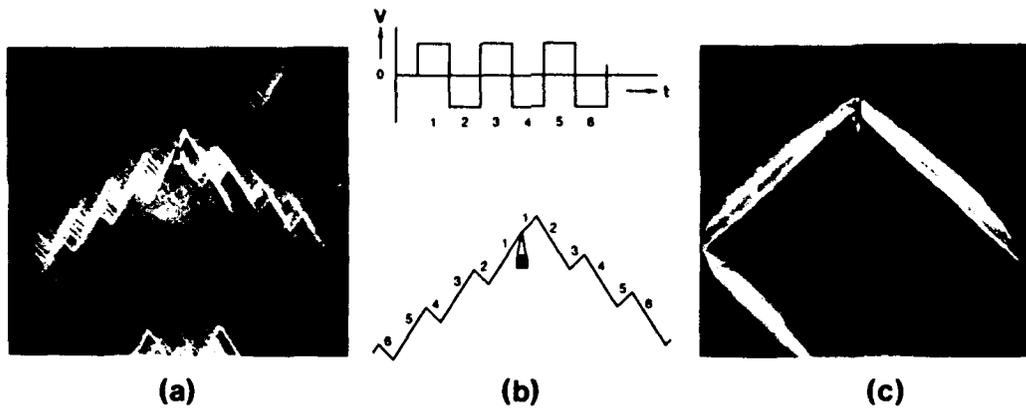
FIGURE 7   Oblique texture lines generated with a square wave voltage of (a) ±20V 1.5Hz 4 periods and (c) ±20V 25Hz 3s. The structure of the lines in (a) is drawn schematically in (b) together with the generating voltage to indicate the successive phases of the generation process.

In Fig.7b the essential parts of the lines are drawn. They are numbered according to the successive phases of the AC voltage. The shorter parts are A-lines and the longer parts B-lines (see Fig.5). When generated at 25Hz, the internal structure cannot be resolved any more. This is shown in Fig.7c. On the other hand, the electro-optical properties integrated over some area remain the same. The measuring spot then covers A-lines and B-lines, which are created by the two different polarities of the generating voltage, respectively. From the opposite smectic layer rotations of these lines it can be understood that the measured average smectic layer rotation is small or even absent. For this reason the M-states are symmetric with respect to the rubbing direction.[5]
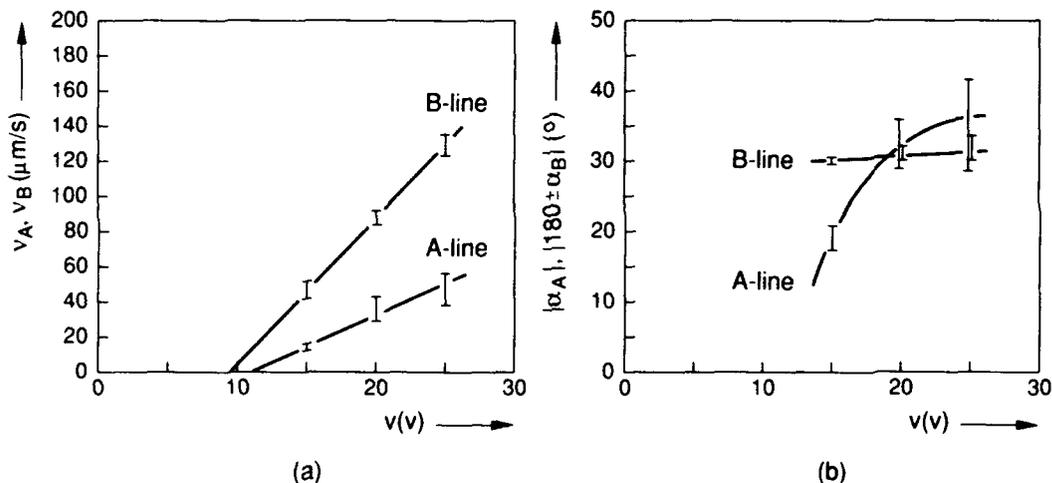
FIGURE 8   Growth velocities v_A and v_B (a) and growth angles α_A and α_B (b) of DC oblique texture lines as a function of the generating voltage V. The line types A and B are defined in Fig.5.

As will be shown, the growth angle and growth velocity of an AC OT-line is determined by the growth properties of the different DC parts. For this purpose we have

measured the growth velocities v_A and v_B and growth angles α_A and α_B of the line types A and B as a function of the generating voltage V. The results are shown in Fig.8.

The construction of the AC OT-line is given in Fig.9, together with the definition of the different angles.
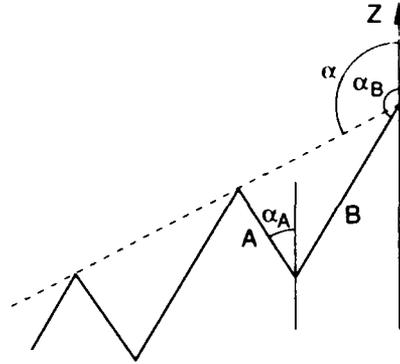
FIGURE 9   Construction of the AC oblique texture line from DC oblique texture lines. The A and B refer to the line types A and B as defined in Fig.5.

From this, the goniometric relations are derived for the average growth angle α and the average growth velocity v, which are given by

$$\tan \alpha = \frac{v_A \sin \alpha_A + v_B \sin \alpha_B}{v_A \cos \alpha_A + v_B \cos \alpha_B} \tag{5}$$

$$v = 0.5\sqrt{\left(v_A \sin \alpha_A + v_B \sin \alpha_B\right)^2 + \left(v_A \cos \alpha_A + v_B \cos \alpha_B\right)^2} \tag{6}$$

Table IV gives the measured and the calculated values of α and v for AC OT-lines generated with $\pm 15V$, $\pm 20V$ and $\pm 25V$ 1.5Hz square wave voltage. The calculated values are obtained from the eqs.(5) and (6) using the values of v_A, v_B, α_A and α_B as given in Fig.8.

TABLE IV   Measured and calculated values of the growth angle α and the growth velocity v of AC oblique texture lines generated with a square wave voltage of 1.5Hz.

generating voltage (V)	$\alpha(°)$ meas.	$\alpha(°)$ calc.	$v(\mu m/s)$ meas.	$v(\mu m/s)$ calc.
± 15	127	135	23	19
± 20	126	127	42	40
± 25	127	127	64	59

From this comparison it can be concluded that the model of Fig.9 is reasonably good.

CONCLUSIONS

From local optical spot measurements on different texture lines it is concluded, that texture lines parallel to the rubbing direction, created with a +DC, −DC or AC field and running in a virgin area, are identical to the lines which are present directly after

cooling down into the SmC* phase (texture-I lines). These so called parallel texture lines or "PT-lines" can be removed by application of a small low-frequency field, indicating that the measured smectic layer rotation is only present in the bulk of the FLC layer and not at the FLC—solid interfaces. The PT-lines consist of two halves which are found to be equivalent to zig-zag lines of the lightning type. The existing model for zig-zag lines could therefore directly be applied to the PT-line.

The texture which results after a prolonged treatment with a high low-frequency field (texture-III), contains parallel lines which look the same as PT-lines. From the measurements and observations we assume that this texture consists of a dense structure of PT-lines in which the smectic layer rotations are extended from the bulk to the FLC—solid interfaces.

Texture lines which run obliquely to the rubbing direction (OT-lines) and which are created with a DC field, exhibit a smectic layer rotation of a few degrees, which reasonably agrees with the layer rotation as calculated from existing theory. These lines cannot be removed by a small low-frequency field, indicating smectic layer rotation at the FLC—solid interfaces.

OT-lines created with a low-frequency field, exhibit an internal structure which originates from the two polarities of the AC field. From this the electro-optical properties (e.g. the symmetric memory states) can be understood. The growth angle and growth velocity of these lines can be calculated from the growth properties of DC lines.

ACKNOWLEDGEMENT

REFERENCES

1. N.A.Clark and S.T.Lagerwall, Appl. Phys. Lett. 36 , 899 (1980).
2. T.P.Rieker, N.A.Clark, G.S.Smith, D.S.Parmar, E.B.Sirota, and C.R.Safinya, Phys. Rev. Lett. 59 , 2658 (1987).
3. N.A.Clark and T.P.Rieker, Phys. Rev. A 37 , 1053 (1988).
4. H.-R.Dübal, C.Escher and D.Ohlendorf, Proc. 6th Int. Symp. on Electrets, Oxford, England, sept. 1988, p. 344.
5. A.G.H.Verhulst, W.J.A.M.Hartmann, F.J.Stommels and A.M.M.Luyckx- Smolders, Proc. Eurodisplay'90, 10th Int. Display Res. Conf., Amsterdam, The Netherlands, sept. 1990, p. 150.
6. W.J.A.M.Hartmann and A.M.M.Luyckx-Smolders, J. Appl. Phys. 67 , 1253 (1990).
7. T.P.Rieker, PhD Thesis, University of Colorado (1988).
8. N.A.Clark, T.P.Rieker and J.E.Maclennan, Ferroelectrics 85 , 467 (1988).
9. Y.Sato, T.Tanaka, H.Kobayashi, K.Aoki, H.Watanabe, H.Takeshita, Y.Ouchi, H.Takezoe and A.Fukuda, Jpn. J. Appl. Phys. 28 , L483 (1989).
10. G.Srajer, R.Pindak and J.S.Patel, submitted to Phys. Rev. A.
11. J.-Z.Xue, PhD Thesis, University of Colorado (1989).
12. P.C.Willis, N.A.Clark and J.-Z.Xue, SID 90 Digest , 114 (1990).

THE IMPORTANCE OF DIELECTRIC BIAXIALITY FOR FERROELECTRIC LIQUID CRYSTAL DEVICES.

J.C.JONES, M.J.TOWLER AND E.P.RAYNES
Electronics Division of the Defence Research Agency
RSRE, St Andrews Rd, Malvern, Worcestershire. WR14 3PS U.K.

Abstract   The dielectric biaxiality of SCE13, a commercially available ferroelectric liquid crystal (FLC) mixture, has been measured. The results have been used to compare theoretically predicted AC field stabilization effects and the voltages for response time minima with experiment.

INTRODUCTION

Planar homogeneous alignment of S_C materials with the N - S_A - S_C phase sequence leads to a chevron layer structure[1]. Most ferroelectric S_C^* liquid crystal devices use a combination of this phase sequence and extended cholesteric pitch[2] to produce this geometry, and device behaviour is influenced by the chevron layer structure. The condition of director continuity across the chevron interface forces the director to lie parallel to the plane of the cell[3] and twisted away from the preferred alignment direction through an angle β_0:

$$\cos \beta_0 = \frac{\cos\theta}{\cos \delta} .\tag{1}$$

where θ is the S_C cone angle and δ the layer tilt angle. Optical measurements[4] suggest that the director profile is approximately uniform from one surface to the other, as shown in figure 1a). When observed between crossed polarizers using a microscope, the sample is
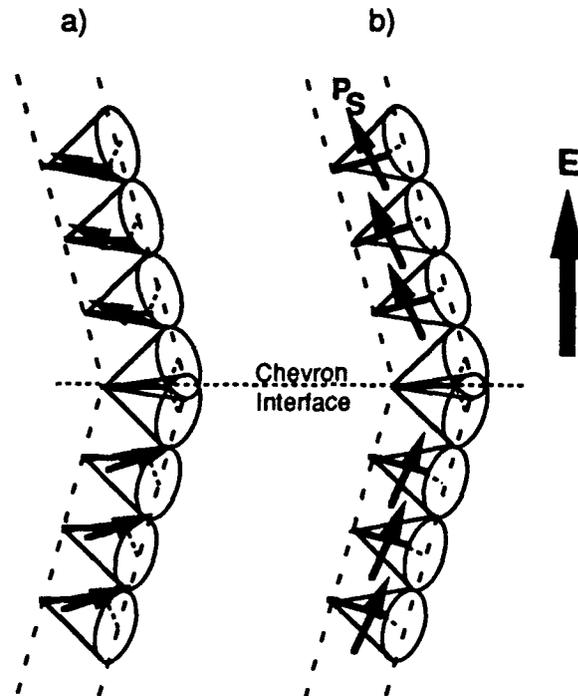
FIGURE 1 The chevron layer geometry with a) an approximately uniform director profile in the surface stabilized state, and b) the fully switched state, assuming that there is no change in the layer structure.

divided into two types of domains with extinction at approximately β_0. For most materials, the ratio (δ/θ) is independent of temperature and is in the range (0.85 - 0.9), so that β_0 is typically $10°$. Applying a DC electric field which couples to the ferroelectric spontaneous polarisation P_S, induces reorientation of the director out of the plane of the cell, as shown in figure 1b), and the extinction angle increases towards β_s:

$$\tan\beta_s \quad = \quad \frac{\tan\theta}{\cos\delta} \cdot \qquad\qquad (2)$$

Removal of the applied field causes the director to reorientate to the surface stabilized state of figure 1a) and the extinction angle to decrease. This lack of complete bistability causes a significant contrast reduction; the fully switched state, and therefore the device contrast, may be maintained if a high frequency AC field is applied across the cell after the

DC switching field has been removed[5]. The existence of this AC field stabilization in chevron layer geometries suggests that there is a significant dielectric biaxiality $\partial\epsilon$[6]; this has been confirmed by permittivity measurements on several host and commercial FLC mixtures[7].

The DC switching of FLC devices can show a minimum in the response time voltage curve[8], particularly in low to medium P_S materials. The presence of this minimum is important for the successful multiplexing of FLC devices[9,10]. Although uniaxial dielectric anisotropy provides a satisfactory explanation[11,12] of the minimum in bookshelf layers ($\delta = 0$), in tilted layers a minimum is not predicted[13] unless dielectric biaxiality is included[14].

In the present work, the method for determining the biaxial S_C permittivities is reviewed. The biaxiality is shown to be sufficiently large to cause the observed AC field effects and the minima in the FLC switching times.

MEASUREMENT OF THE BIAXIAL PERMITTIVITIES OF HOSTS

The S_C principal axes are defined such that ϵ_3 is parallel to the n director, ϵ_2 parallel to the C_2 symmetry axis and ϵ_1 normal to these as shown in figure 2. Defining two S_C anisotropies as $\Delta\epsilon = (\epsilon_3 - \epsilon_1)$ and $\partial\epsilon = (\epsilon_2 - \epsilon_1)$, the measured permittivity of a uniform sample is[7]:

$$\epsilon = \epsilon_1 + \Delta\epsilon.(\cos\delta.\sin\varphi.\sin\theta - \sin\delta.\cos\theta)^2 + \partial\epsilon.\cos^2\delta.\cos^2\varphi \qquad (3)$$

Measurement of the three S_C host permittivities requires at least three alignment geometries in which the director profile is known accurately. At present, only two geometries meet this requirement: the planar homogeneous chevron geometry of figure 1a), and the homeotropic geometry in which the layers are parallel to the plane of the cell. The permittivities measured in these two geometries are ϵ_p and ϵ_h:

$$\epsilon_p = \epsilon_2 - \partial\epsilon.\frac{\sin^2\delta}{\sin^2\theta}, \qquad (4)$$

$$\epsilon_h \quad = \quad \epsilon_1 + \Delta\epsilon.\cos^2\theta \quad . \tag{5}$$
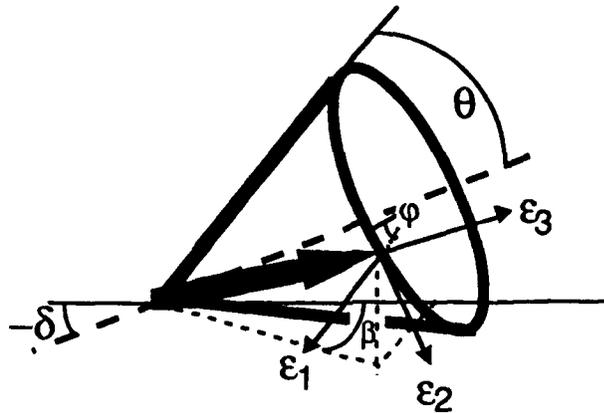
FIGURE 2   Definition of the S_C permittivities, cone angle (θ), layer tilt (δ) and azimuthal angle (ϕ) and in-plane twist angle (β).

In FLC materials, a possible third geometry is the fully switched state of figure 1b). However, this option is not practical in hosts, and even with FLC materials the director profile for a given voltage is uncertain. Therefore, a method was developed which uses an extrapolation of the mean permittivity $\bar{\epsilon}$ from the uniaxial nematic and smectic A phases[7] (where $\bar{\epsilon} = 1/3\,\epsilon_{\parallel} + 2/3\,\epsilon_{\perp}$). In the biaxial S_C phase:

$$\bar{\epsilon} \quad = \quad \frac{\epsilon_1 + \epsilon_2 + \epsilon_3}{3} \quad , \tag{6}$$

and simultaneous solution of equations (4), (5) and (6) allows ϵ_1, ϵ_2 and ϵ_3 to be extracted, providing the cone angle and layer tilt angle are known. Both θ and δ were determined from optical critical angle measurements[15] and θ assumed to be equivalent at optical and dielectric frequencies. Achiral hosts and racemic analogues of FLC mixtures were studied to avoid complications associated with either the chirality or ferroelectricity,

such as the formation of half-splayed states or Goldstone mode switching of P_S about the cone. Several materials have been measured[7], including the racemic analogue of the commercially available SCE13 (available from Merck Ltd), and the results are summarised in table 1:

TABLE 1 S_C Permittivities at T_C-T = 30°C for Several Host Mixtures [7].

Host Mixture	T_{C-A} /°C	ε_1 ($\pm$ 1%)	$\Delta\varepsilon$ ($\pm$ 0.06)	$\partial\varepsilon$ ($\pm$ 0.1)
R-⬡-⬡-CO_2-⬡(F)-R'	73.3	3.842	-0.61	+0.26
RO-⬡-⬡-CO_2-⬡(F)-R'	107.3	3.938	-0.73	+0.48
R-⬡(N,N)-⬡-O-R'	55.0	2.894	+0.50	+0.10
R(O)-⬡-⬡(F)-⬡-R'	66.8	3.134	+0.08	+0.13
R-⬡(F,F)-⬡-⬡-R'	91.5	4.624	-1.55	+0.76
DiFTP Mixture (R)	62.0	5.141	-1.07	+0.97
SCE13(R) BDH	60.8	4.756	-1.03	+0.30

The temperature dependence of the SCE13(R) permittivities measured at 1kHz are shown in figure 3. Clearly, there is a significant dielectric biaxiality, which depends on the temperature below the S_A to S_C phase transition and values of $\partial\varepsilon$ up to +2.0 have been measured at room temperature[7] for some materials.
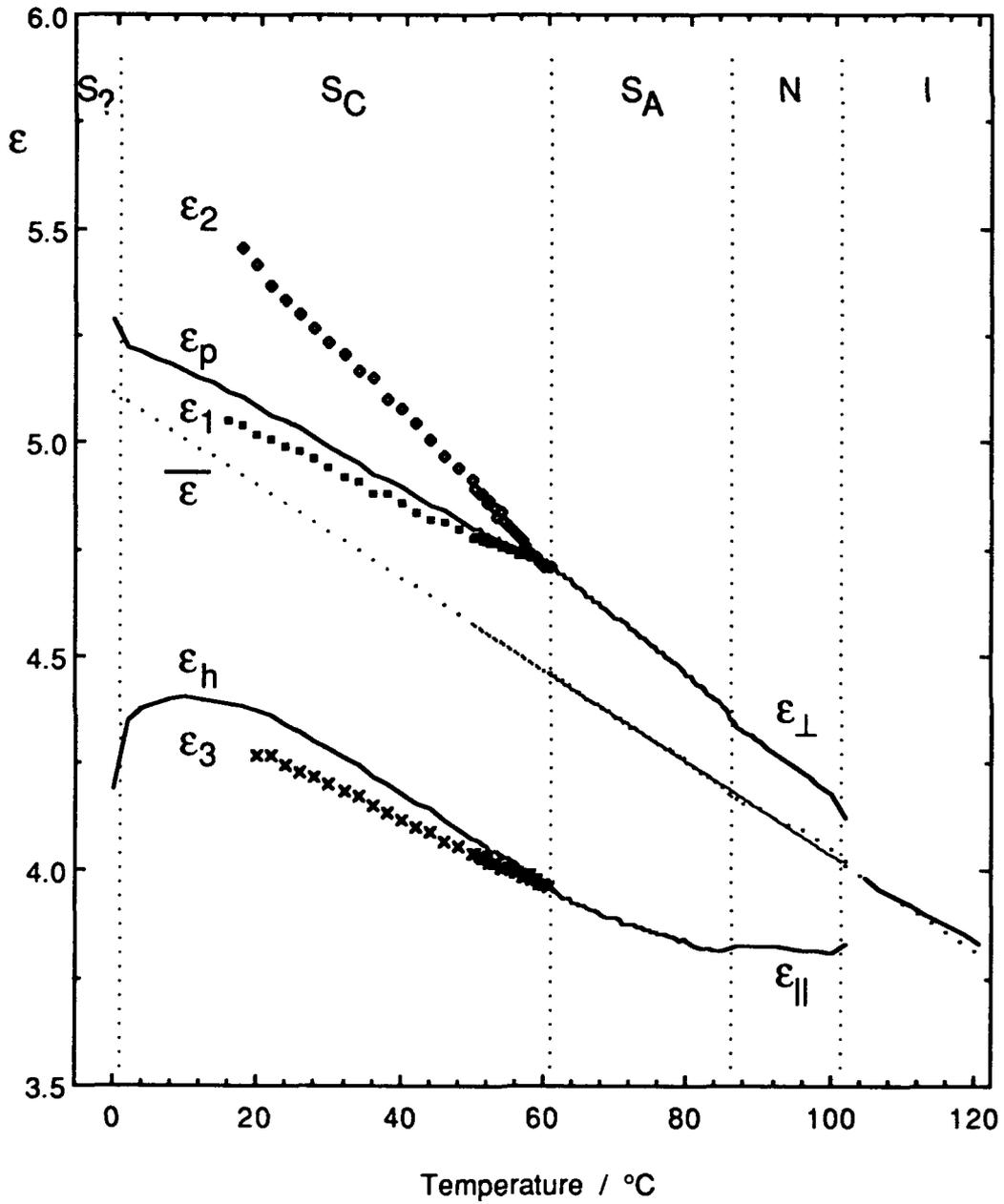
FIGURE 3   Temperature dependence of the low frequency
permittivities for SCE13(R), the racemic analogue of the
commercially available FLC SCE13.

AC FIELD STABILIZATION.

If $\partial\varepsilon$ is large, the electric field behaviour of achiral S_C materials, and of FLC mixtures at AC frequencies too high to couple to the ferroelectric polarisation P_S, is strongly influenced by the dielectric biaxiality. For a finite electric field, the degree of director reorientation will depend on both dielectric anisotropies ($\Delta\varepsilon$ and $\partial\varepsilon$) and the appropriate elastic constants. At infinite fields, the director will be completely reorientated so that the maximum permittivity is parallel to the applied field. Assuming there are no field induced changes in either θ or δ, the azimuthal angle of the fully stabilized state φ_∞ is:

$$\sin\varphi_\infty \quad = \quad \frac{\tan\delta \,.\, \cos\theta \,.\, \sin\theta}{\sin^2\theta \; - \; \dfrac{\partial\varepsilon}{\Delta\varepsilon}} \quad , \tag{7}$$

and the director twist angle (and therefore extinction angle in the fully stabilized case) is:

$$\tan\beta_\infty \quad = \quad \frac{\cos\varphi_\infty . \sin\theta}{\sin\delta . \sin\varphi_\infty . \sin\theta + \cos\delta . \cos\theta} \quad . \tag{8}$$

The predicted temperature dependence of β_∞ for SCE13(R) is shown in figure 4. Extinction angles cannot be measured for voltages above $\approx 10V_{rms}$ due to the occurrence of "needle" defects [16], however, β_∞ may be estimated by extrapolation of the extinction angle voltage dependence. This extrapolation leads to the satisfactory agreement in figure 4 between the experimental data and the values predicted by equation (8).
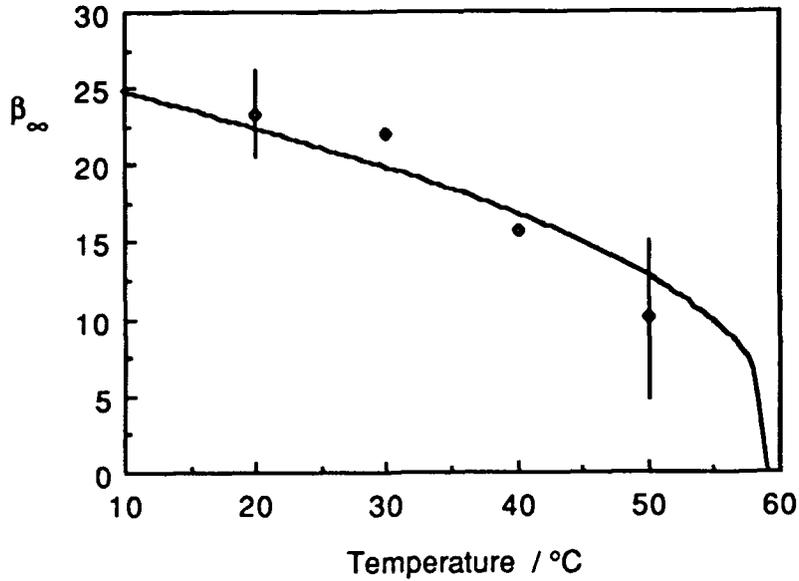
FIGURE 4   Temperature dependence of the fully AC stabilized extinction angle β_∞ for SCE13(R). The points show experimental data determined by extrapolation of the extinction angle versus voltage curve and the solid line is from equation (8).

FERROELECTRIC SWITCHING.

The effect of layer tilt and dielectric biaxiality on FLC switching have recently been analysed[14]. Reorientation of the director through change of azimuthal angle ϕ is described by:

$$\eta\frac{d\phi}{dt} = P_s\left(\frac{V}{d}\right)\cos\delta\sin\phi + \varepsilon_0\left(\frac{V}{d}\right)^2\left[(\Delta\varepsilon\sin^2\theta - \partial\varepsilon)\cos^2\delta\sin\phi\cos\phi - \frac{\Delta\varepsilon}{4}\sin2\theta\sin2\delta\cos\phi\right]$$

(9)

where η is the rotational viscosity, V the applied voltage and d the cell spacing. Defining $\alpha = \frac{\varepsilon_0\Delta\varepsilon V}{P_s d}$, the response time τ is then given by:

$$\left(\frac{P_s^2\cos\delta}{\varepsilon_0\Delta\varepsilon\eta}\right)\tau = \frac{1}{\alpha}\int_{\phi_0}^{\pi/2}\frac{d\phi}{\sin\phi + \alpha\left[\left(\sin^2\theta - \frac{\partial\varepsilon}{\Delta\varepsilon}\right)\cos\delta\sin\phi - \sin\theta\cos\theta\sin\delta\right]\cos\phi} \qquad (10)$$

where ϕ_0 is the initial azimuthal angle. Equation (10) requires numerical integration for most practical values of θ, δ, $\Delta\varepsilon$ and $\partial\varepsilon$. However, Towler *et al* [14] quote an approximation for V_{min} when switching from $\phi_0 = \phi_\infty$:

$$\left|V_{min}\atop{\phi_\infty\to\frac{\pi}{2}}\right| = 0.62\left|\frac{P_s d}{\varepsilon_0\cos\delta((\Delta\varepsilon\sin^2\theta-\partial\varepsilon)^{2/3} - (\Delta\varepsilon\sin\theta\cos\theta\tan\delta)^{2/3})^{3/2}}\right| \qquad (11)$$

A comparison of the V_{min} found by numerical solution of equation (10) and the approximation of equation (11) is shown in figure 5, and there is excellent agreement for a range of $\Delta\varepsilon$ and $\partial\varepsilon$.

2μm parallel rubbed polyimide cells were vacuum filled with SCE13 and switched using alternating positive and negative pulses with amplitude V, duration t and a 1:100 mark space ratio. A seperate high frequency AC signal could be gated with the switching pulses to effect AC stabilization. The response time τ was taken as the pulse duration at which there was "clean switching"[12]. No V_{min} was detected experimentally in the FLC mixture SCE13 due to the high P_S of $\approx$30 nCcm^{-2}. The P_S was lowered to $\approx$5nCcm^{-2} at 30°C to provide a measurable V_{min} using a 20% mixture of chiral SCE13 with its racemic analogue SCE13(R). The 30°C $\tau(V)$ dependence is shown in figure 6 for the low P_S version of SCE13 at several levels of applied high frequency AC voltage. A preliminary comparison, figure 6, between the V_{min} measured with a 10Vrms AC field applied and the Vmin predicted by equation (11) and using the SCE13(R) permittivities of figure 3 shows good agreement across the temperature range. The measured values were slightly higher than those predicted, because the 10V$_{rms}$ applied AC is insufficient to cause complete AC field stabilization. Above 10V$_{rms}$, however, needle defects began to nucleate and response time measurements became inaccurate.
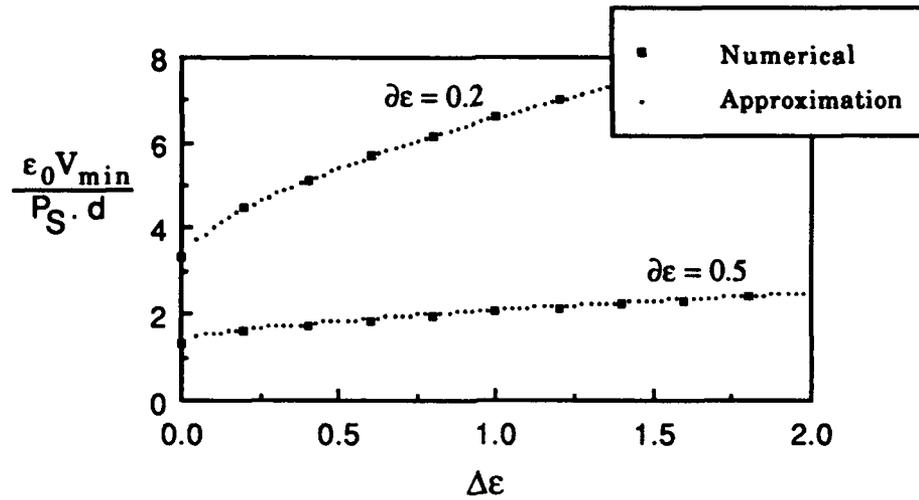
FIGURE 5   Comparison of the theoretical values for Vmin
calculated from numerical solution of equation (10) and the
approximation of equation (11).
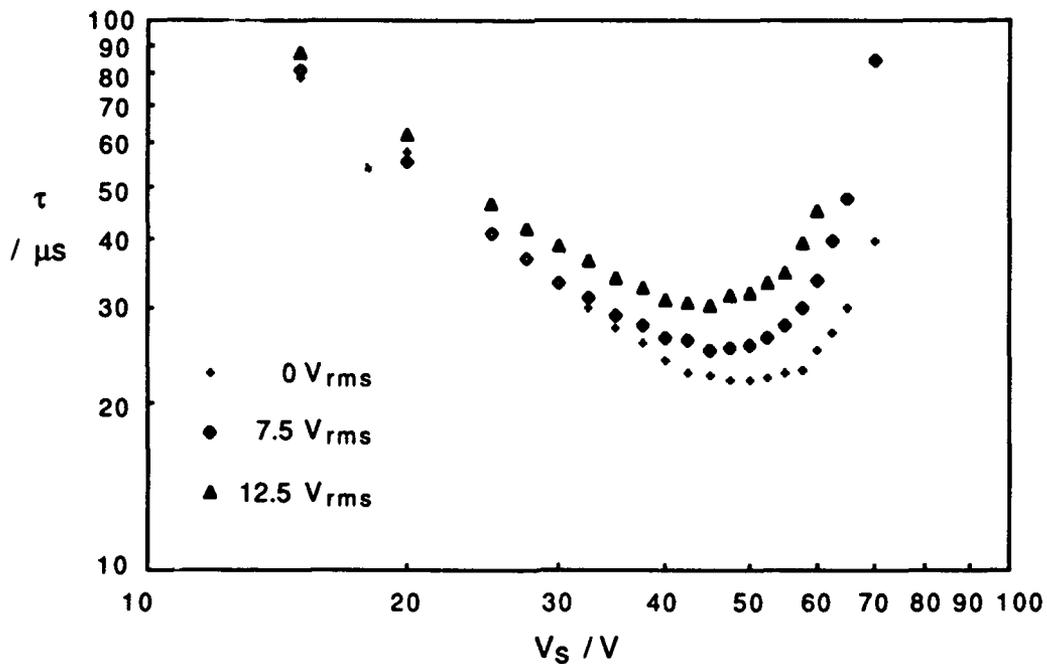
FIGURE 6   Pulse voltage dependence of the switching time at 30°C
for several levels of high frequency AC field.
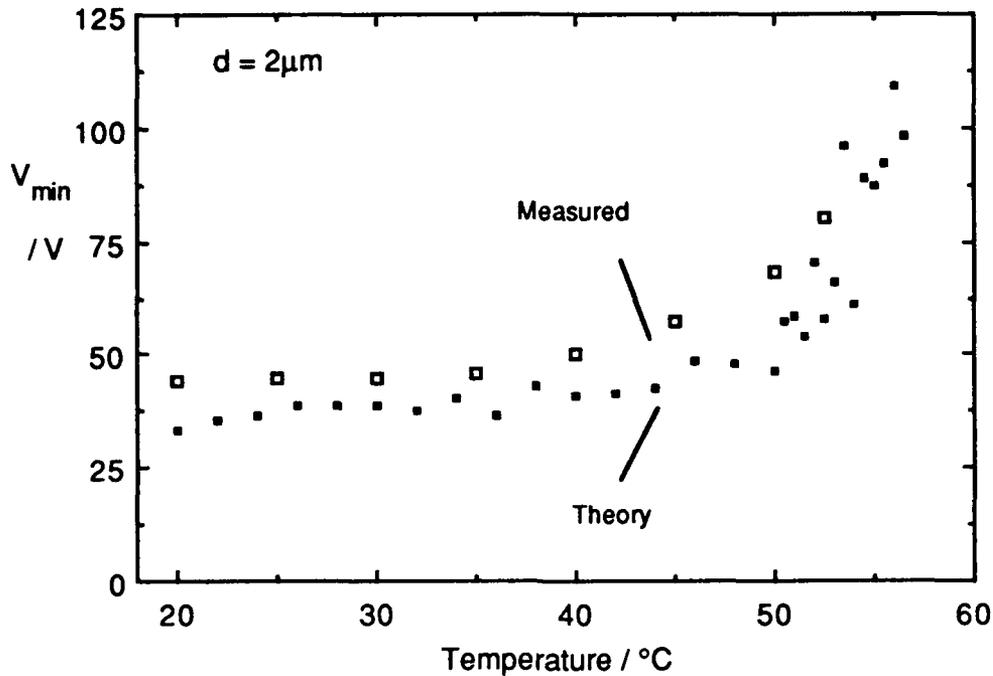
FIGURE 7   Comparison of the measured (□) and predicted (■)
Vmin for the low Ps version of SCE13.

CONCLUSION

The dielectric biaxiality of S_C liquid crystals has been measured for
several host and racemic FLC mixtures and shown to be significant. It
has also been shown that the dielectric biaxiality plays an important role
both in S_C and S_C^* AC field behaviour and for FLC switching in cells with
chevron and tilted layer geometries. It is therefore important to know the
dielectric biaxiality of other commercially available mixtures and to
formulate new mixtures with increased biaxiality.

REFERENCES

1. T. P. Rieker, N. A. Clark, G. S. Smith and C. R. Safinya, Liquid Crystals, 6, 565 (1989).

2. M. J. Bradshaw, J. Constant and E. P. Raynes, Liquid Crystals, 2, 107 (1987).

3. N. A. Clark, T. P. Rieker and J. E. Maclennan, Ferroelectrics, 85, 79 (1988).

4. J. R. Sambles, S. Elston and M. G. Clark, J. Mod. Opt., 36, 1019 (1989).

5. J. P. LePesant, J. N. Perbet, B. Mourey, M. Hareng, G. Decobert and J. C. Dubois, Mol. Cryst. Liq. Cryst., 129, 161 (1985).

6. J. C. Jones, E. P. Raynes, M. J. Towler and J. R. Sambles, Mol. Cryst. Liq. Cryst. Lett., 7, 91 (1990).

7. a) J. C. Jones and E. P. Raynes, Submitted to Liquid Crystals.
b) J. C. Jones, E. P. Raynes, M. J. Towler and J. R. Sambles, Presented at The 13th International Liquid Crystal Conference, Vancouver, July 1990. Mol.Cryst.Liq. Cryst, 199 277 (1991).

8. H. Orihara, K. Nakamura, Y. Ishibashi, Y. Yamada, N. Yamamoto and Y. Yamawaki, Jap. J. Appl.Phys. 25 L839 (1986).

9. M. F. Bone, I. Coulson, J. R. Hughes, P. W. Ross, F. C. Saunders and P. W. H. Surguy, European Patent Application No: 88307804.0.

10. P. W. H. Surguy, P. J. Ayliffe, M. J. Birch, M. F. Bone, I. Coulson, W. A. Crossland, J. R. Hughes, P. W. Ross, F. C. Saunders and M. J. Towler, Presented at this conference.

11. J. Z. Xue, M. A. Handschy and N. A. Clark, Ferroelectrics, 73, 305 (1987).

12. F. C. Saunders, J. R. Hughes, H. A. Pedlingham and M. J. Towler, Liquid Crystals, 6, 341 (1989).

13. J. Z. Xue, M. A. Handschy and N. A. Clark, Liquid Crystals, 2, 707 (1987).

14. M. J. Towler, J. C. Jones and E. P. Raynes Submitted to Liquid Crystals.

15. J. C. Jones and E. P. Raynes, British Liquid Crystal Society Conference, Reading, UK, April 1991.

16. Sato, Y., Tanaka, T., Nagata, M., Takeshita, H., and Morozumi, S., Proceedings of the SID, 28, 189 (1987).

ION TRANSPORT IN SSFLCD's

B. Maximus,* E. De Ley,† A. De Meyere,‡ H. Pauwels

Laboratory of Electronics, Ghent State University

Sint-Pietersnieuwstraat 41, B-9000 GENT, Belgium

Abstract

An essential feature of surface stabilized ferroelectric liquid crystal displays (SSFLCD) is their bistability. Experiments and theory show however that this bistability can be destroyed by ionic charges building up at both electrodes. In this article a better understanding of the ion concentration distribution and their transport behavior is obtained through leakage current measurements on FLC cells with bipolar voltage driving. We also present a model for the ionic transport that can explain the measured current curves. Simulations according to this model fit the experimental data. In this way we derive some important parameters concerning the ionic behavior.

1 Introduction

A ferroelectric liquid crystal material has a relatively large polarization P. The two most important states in a SSFLC cell are configurations with the polarization either pointing up or down. Switching between these two states can be done very easily by applying a voltage, the electric field will pull the polarization in the desired direction. In ideal circumstances, the polarization will hold its direction, even when the voltage is set back to zero after a short time, presuming that the pulse area exceeds the dynamical threshold.

Several phenomena can destroy this effect called bistability. In fig. 1, we consider the basic structure of a SSFLCD. The following symbols are used:
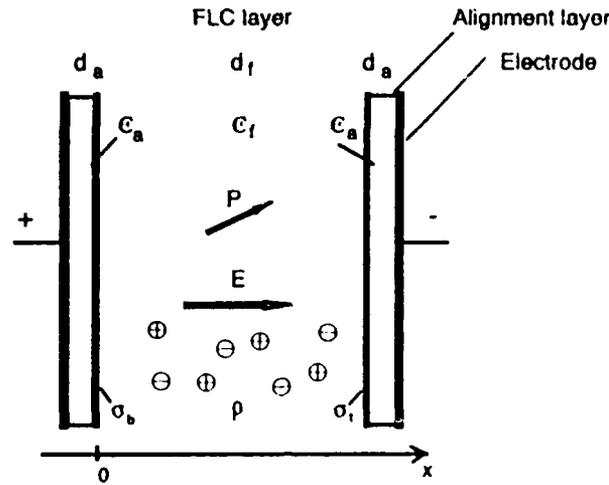
Figure 1: Cross-section of SSFLC-cell.

d_a, d_f: the thickness of one alignment layer and of the FLC, respectively.

ϵ_a, ϵ_f: the relative permittivities of the alignment layers and the FLC, respectively. The inhomogeneity of ϵ_f can be neglected in the present applications.

$\sigma_b(t), \sigma_t(t)$: the surface charge densities, accumulated at the interface between bottom and top alignment layers and the FLC. The alignment layers themselves are non-conductive.

$\rho(x,t)$: the space charge density in the bulk

If V stands for the voltage over the total display, one can deduct an expression for the electric field $E(x,t)$ as follows. (see also [1])

$$E(x,t) = \alpha \frac{V(t)}{d_f}$$
$$- \frac{1}{\epsilon_0\epsilon_f}\{(1-\alpha)\sigma_t(t) + \int_x^{d_f} \rho(x,t)dx - \frac{\alpha}{d_f}\int_0^{d_f} x\rho(x,t)dx\}$$
$$- \frac{1}{\epsilon_0\epsilon_f}\{P_x(x,t) - \frac{\alpha}{d_f}\int_0^{d_f} P_x(x,t)dx\} \tag{1}$$

Here, $P_x(x,t)$ stands for the component of the polarization which is perpendicular to the glass substrate.

α is a correction factor which takes the alignment layers into account: $\alpha = \frac{\epsilon_a d_f}{\epsilon_a d_f + 2\epsilon_f d_a}$

Typically, α has a value close to 1, e.g. 0.94.

During the derivation of the expression 1, we considered charge neutrality:

$$\sigma_b(t) + \sigma_t(t) + \int_o^{d_f} \rho(x,t)dx = 0 \qquad (2)$$

Analysis of the formula 1 leads to important conclusions. If the FLCD is switched in the so-called UP-state ($P_x > 0$) and is in short circuit ($V = 0$), there are basically three reasons why there still can exist an electrical field in the liquid crystal.

1. Inhomogeneity of the polarization profile in the stable state causes the existence of an inhomogeneous electrical field.

2. Without the presence of ions, the alignment layers are responsible for the presence of a reversed field, which tends to pull the display out of the stable state. Especially when the alignment layers are too thick and, consequently α is too small, the polarization contribution in $E(x,t)$ becomes strongly negative. For discussion of this topic we refer to [2].

3. There is enough evidence however that ions do exist in the FLC [3] [4] [5]. In the simple model with $\rho = 0$ (all charges have drifted towards the interfaces) one can easily see that the ions, accumulated at the interfaces, can cancel the reversed field. Considering this situation, if one switches the display to the DOWN -state and short-circuits it again, this ion field remains in the first instance, since the migration of the ions is rather slow. Now the ion field adds up to the depolarizing field which has changed sign together with the polarization. The accumulative effect can destroy the stability of the DOWN-state (for example). The importance of the surface charge σ has already been pointed out by some of us in [2].

One may conclude that the ion concentration is important. Ions moving through a FLC cell submitted to a constant voltage, cause an external leakage current which can be measured in a simple way. The magnitude of the current density gives information about the number of moving ions. We also studied the time-dependent current curves in detail, in order to get more accurate information, not only on the concentration of the ions, but also on their mobility, the interaction with the alignment layers and the ion generation speed.
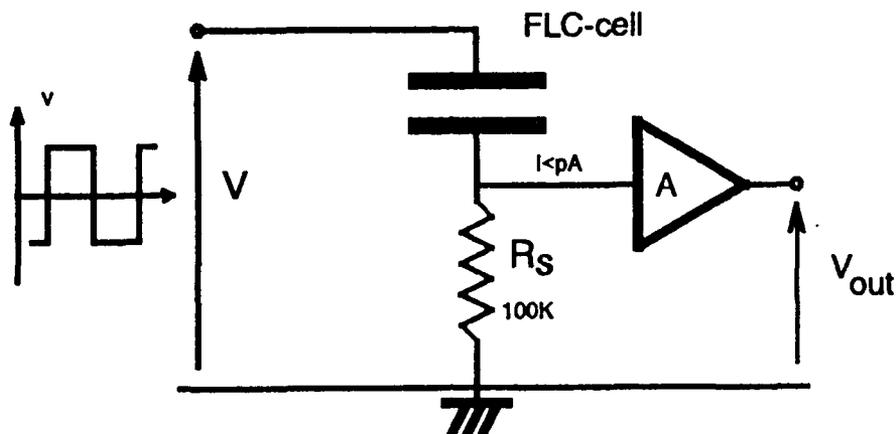
Figure 2: Measurement set up.

2   Measurements

We fabricated several $5 \times 5cm^2$ SSFLC-cells with $0.7cm^2$ pixels, using different materials: Merck ZLI 3654 and Merck ZLI 3488 for the FLC layer, nylon-6 and JSR Al 1254 polyimide for the alignment layer.

The measurement set up is shown in fig. 2. The applied bipolar voltage has an amplitude V and a period of $200ms$. That way we not only avoid a long time dc-voltage over the cells, but we also allow the ions to move to and fro between the electrodes, so that we can get information about their transport time. Using a resistor R_s and an amplifier with a very high input impedance, an output voltage can be created, proportional to the leakage current through the FLC cell. The value of the resistor R_s is small enough so that it does not disturb the leakage current measurement. We therefore made sure $R_s I_L \ll V$ and $R_s C_{pix} dI_L/dt \ll I_L$.

A small disadvantage of this measurement set up is the large current peak that is produced each time the voltage is altered. This is caused by the charging of the pixelcapacitor and by the changing polarization. However, since the polarization of the FLC switches very quickly and because the RC-time constant in the measuring circuit is kept small ($R_s C_{pix} \leq 1ms$) this effect has already vanished after a few milliseconds, and only the ionic transport current remains.

Fig. 3 shows an example of half a cycle in a current measurement on a FLC-cell with liquid crystal Merck ZLI 3488 and nylon-6 for the alignment layer. The second part of the cycle is identical, except for its negative sign. The different curves correspond with different applied voltage amplitudes (12V, 10V, 8V, 6V and 4V as indicated).
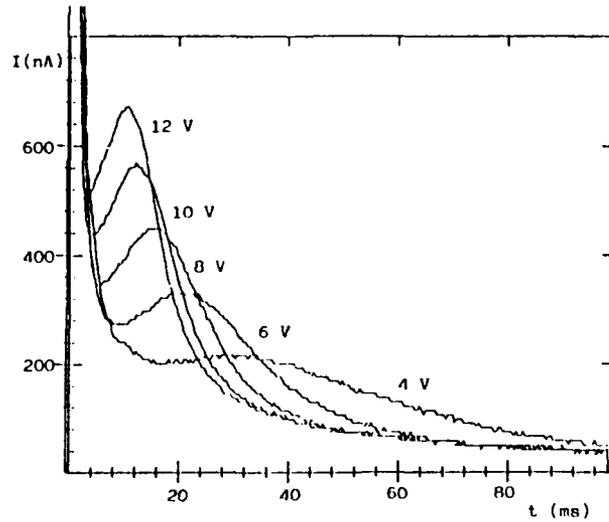
Figure 3: Leakage current measurement.

Materials		I_{max}	Q
FLC	AL	(nA)	(nC)
ZLI3488	Nylon	400-1000	16-28
"	Polyimide	120-170	5-7
ZLI3654	Nylon	200-1000	8-25
"	Polyimide	40-60	1-1.5

Table 1: Measurements

In table 1 two characteristics of the current profile, the peak current and the total amount of charge transported in 100ms, being $\int I_L dt$, are compared for the different materials. In this case the applied voltage is 12V.

3   Model for the ion transport

In order to get a better understanding of the leakage current behavior, we tried to simulate the motion of ionic charges in the liquid crystal layer. Our one dimensional model is a more detailed and improved version of the model proposed by Chieu and Yang [3].

Starting with a charge distribution $\rho(x, t)$ and an applied voltage V, we can determine the field distribution $E(x, t)$ according to equation 1. For the factor $P_x(x, t)$

we made the following considerations. Since we study ion behavior after the switching of the polarization, we can neglect the time dependence in $P_x(x,t)$. According to a simple homogeneous model we may drop the x-dependence as well. Considering a chevron structure, we then get $P_x = P cos\phi cos\delta$ (ϕ describes the position of the director on the smectic cone, δ is the angle that the smectic layers make with the substrate normal). Assuming horizontal director alignment and $\delta = 17°$, the correction factor $cos\phi cos\delta$ becomes 0.722, the number we used in our further calculations.

With these data, one can find $E(x,t)$ from equation 1. This electric field will cause a current density $J(x,t)$ due to the motion of the ionic charges:

$$J = J^+ + J^- \tag{3}$$

with

$$J^\pm = q\mu^\pm n^\pm E \mp q D^\pm \frac{\partial n^\pm}{\partial x} \tag{4}$$

Here $n^\pm(x,t)$ is the ionic density, $\mu^\pm$ is the mobility and $D^\pm$ the diffusion constant of positive and negative ions respectively. q is the unit charge.

In our model we assume that the present positive and negative ions come from the dissociation of a number of neutral impurities N_{tot} in the liquid crystal. So we have to consider the chemical equilibrium between the ionized products and the neutral molecules. This means that in the ion continuity equations both an ion generation term and an ion recombination term has to be taken into account. This way we find:

$$\frac{\partial n^\pm}{\partial t} = \beta n_0 - \gamma n^+ n^- \mp \mu^\pm \frac{\partial(n^\pm E)}{\partial x} + D^\pm \frac{\partial^2 n^\pm}{\partial x^2} \tag{5}$$

for the ions and:

$$\frac{\partial n_0}{\partial t} = -\beta n_0 + \gamma n^+ n^- \tag{6}$$

for the neutral molecules. (β is the ion generation rate coefficient, $n_0(x,t)$ the number of neutral molecules per m^3 and γ the recombination rate coefficient.) At this point, we have not considered any E-dependence of β (see [3]). Simulations fit the measurements without it.

Furthermore, our simulation results were improved when we assumed that one kind of ion is much more mobile than the other. It seems reasonable that the ionization of neutral molecules gives rise to small mobile radicals of one charge type and larger slower residual ions of the other type. Without loss of generality we choose the positive ions to be the most mobile: $\mu^- \ll \mu^+$. If one would assume both ion types to be equally mobile, the ion current profile would be different than the one

observed: the local electric field generated by two equally mobile ion types which pass each other, causes a double ion current peak in our simulations.

The necessary boundary conditions to solve the equations are obtained by stating that the ions can get trapped at the interfaces between the liquid crystal layer and the alignment layers. They will build up a surface charge $\sigma(t) = \sigma^+(t) + \sigma^-(t)$. This trapping is described in correspondence to the theory of surface states:

$$J^\pm(0) = -\frac{\partial \sigma_b^\pm}{\partial t} = \frac{\sigma_b^\pm}{\tau} \mp q k_{trap} n^\pm(0) \tag{7}$$

$$J^\pm(d_f) = \frac{\partial \sigma_t^\pm}{\partial t} = -\frac{\sigma_t^\pm}{\tau} \pm q k_{trap} n^\pm(d_f) \tag{8}$$

Here τ represents the life time of the interface charges, while k_{trap} stands for the trapping factor. We consider no interaction between the positive and negative ions that are trapped in the surface states.

Finally the external leakage current density J_L is calculated from the rate of change in charge on the electrodes, but naturally also the dielectric displacement can be used:

$$J_L = -\frac{\partial D_x}{\partial t}\bigg|_{electrode} \tag{9}$$

4   Results

The characteristic current behavior, shown in fig. 4, can now be explained using the model:

1. At the end of a period most of the ions are located near the interfaces with the alignment layers, and some of them are trapped there. When the voltage is altered the free ions suddenly begin to move towards the opposite electrode and this transport immediately causes a certain external leakage current. This current then increases because of the release of the trapped ions, gradually building up the number of moving ions.

2. When the first ions reach the opposite electrode, the current starts to decrease. In this way the current peak position is related to the ion transit time, but because of the diffusion process it is not exactly the same. For
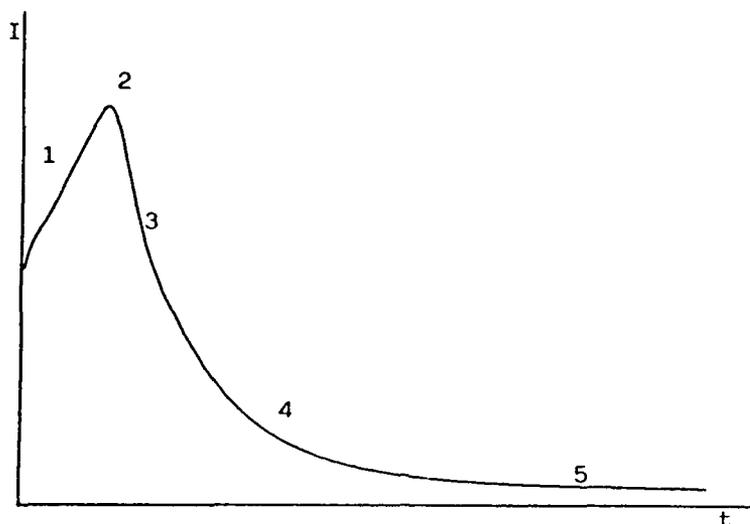
Figure 4: Explanation of the current behavior.

example in the case when the voltage is 12V, the current peak occurs after about 12.5ms, but the transport time is $\frac{d_l}{\mu <E>} \approx \frac{d_l^2}{\mu \alpha V} = {}^{1}6ms$

3. The leakage current now drops quickly. Indeed, the ior.. .hat were not trapped in the beginning, arrive almost all together, be. aust ney started moving at the same time. In fact the slope of this der   nly determined by the diffusion proces. It is at this print that our s   ons sometimes disagree with the measurements: in sor..   .ses we woun   .   to increase the diffusion factor to obtain a perfect match. But of cours   u do not agree with such a solution because then the Einstein relation $D/\mu = kT/q$ is no longer fulfilled.

4. Further on the current decays more smoothly: the ions that were trapped at the ..aterfaces are gradually released. So their arrival at the opposite electrode will also be more spread out in time. It can be proved that in this part of the curve the slope of the decay is determined by the life time constant τ.

5. Finally, when most of the trapped charge has been transported, the leakage current decays to an almost constant level, depending only on the ion generation and the very slow motion of the negative ions. This should not be thought of as a DC current, considering the bipolar applied voltage. In fact, the frequency of the signal is too high to observe the total extinction of the external current. If one tries to explain this non-zero current with the small conductivity of the alignment layers, the values in the literature do not allow such a large off-set of the measured current.

These considerations can be used to get a rough estimation for the parameters. For example, using items 1 and 4 the values of k_{trap} and τ can be obtained, items 2

$d_f =$	$2.1\mu m$	$d_a =$	$50nm$
$\epsilon_f =$	5	$\epsilon_a =$	4
$P_x =$	$21 \times 10^{-5} C/m^2$		
$\mu^+ =$	$2.4 \times 10^{-11} m^2/Vs$	$D^+ =$	$25mV \times \mu^+$
$\mu^- =$	$0.1 \times 10^{-11} m^2/Vs$	$D^- =$	$25mV \times \mu^-$
$\beta =$	$5s^{-1}$	$\gamma =$	$3 \times 10^{-21} m^3 s^{-1}$
$k_{trap} =$	$2 \times 10^{-6} m/s$	$\tau =$	$12 \times 10^{-3} s$
$N_{tot} =$	$1.4 \times 10^{15} m^{-2}$		

Table 2: Parameters for the simulation in fig 5.

and 3 give the mobility, and item 5 can help to find the value for β and μ^-. These values then can be corrected using the calculated results.

As can be seen in fig. 5 the simulations now match the measurements shown in fig. 3.
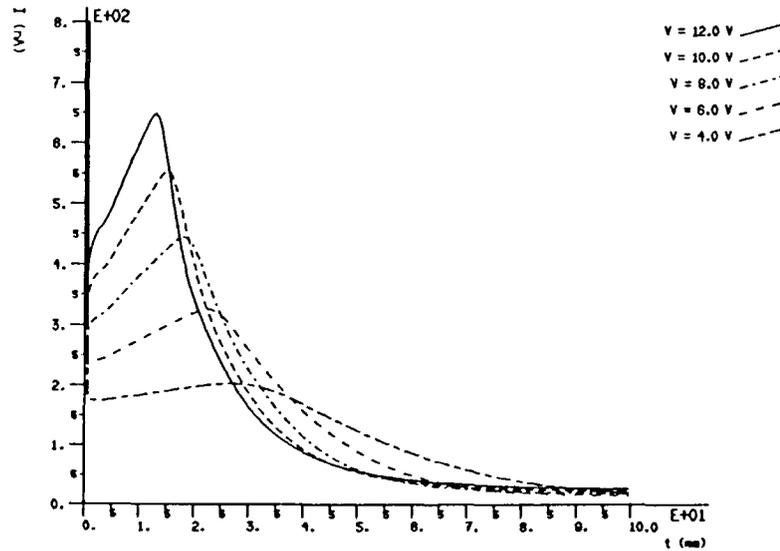
Figure 5: Simulations of leakage current.

In table 2 we show the values of the parameters used for the simulation in fig. 5. In this case the two most important properties of the ion behavior are:
Ionic density (averaged value): $6 \times 10^{20} m^{-3}$
Mobility of the fast ions (at $20°C$): $2.4 \times 10^{-11} m^2/Vs$

One should realize that the shape of the current curve is strongly dependent on the applied voltage amplitude (see also fig. 3). At lower voltages the ion concentration at the interface between FLC and alignment layer is not so high (diffusion tends to spread the ion population). Consequently, the trapped ions are not so numerous. Their release during the following cycle is smaller, so the current rise is less pronounced. The longer transit time causes the current peak to shift to the right in the considered profile. Moreover, during the longer transit time, diffusion is capable of flattening the curve peak. At high voltages the ions move so fast through the FLC-layer that the resulting peak is not visible anymore: it has been 'absorbed' by the initial peak which is caused by charging the capacitor and switching the polarization. The voltage range in which the current peak is visible depends predominantly on the ion mobility. In fact, we sometimes observed three kinds of ions, each of them having a different mobility and showing up at different voltages.

5   Conclusions

Ionic charges can contribute to destruction of the bistability of SSLC displays. Leakage current measurements on SSFLC-cells are useful to examine the ionic presence and transport. They can be used as a tool to evaluate the quality of the FLC- and alignment layer materials used in SSFLCD production.

We presented a model that can explain the leakage current behavior. In this model the presence of a strongly ionized species is accepted. The ionization gives rise to one mobile type of ion and an almost immobile background charge. Moreover the ions can be trapped at the interfaces with the alignment layers. These assumptions allow an agreement of the simulations with the experiments.

References

[1] K.A. Neyts, *IEEE Transactions on Electron Devices*, to be published

[2] E. De Ley and H. Pauwels, *Proceedings Eurodisplay '90*, pp 264-268 (1990)

[3] T.C. Chieu and K.H. Yang, *Japanese Journal of Applied Physics I* , (nov. 1989)

[4] C. Escher et al., *Japan Display '89*, pp 348-351.

[5] J. Dijon et al., *SID 88 digest*, pp 246-249.

The Surface Anchoring Dependence of the Dielectric Constant of an FLC Material Showing Electroclinic Effect

Y.B.Yang, T.Bang, A.Mochizuki and S.Kobayashi
Division of Electronic and Information Engineering, Graduate School of Engineering, Tokyo University of Agriculture and Technology, Koganei, Tokyo 184, Japan.

Abstract : In an LC material 764E(BDH), which shows strong electroclinic effect both in SmA and SmC* phase, the phase transition points between SmA and SmC* phase observed through the divergent behavior of the dielectric constant are shown to vary remarkably depending on the surface anchoring potential. It is shown that the non polar part of the potential plays a role in determining the critical temperature, while the polar part contribute to determine the width of the curves. Actually the value of the surface potential is controlled in terms of the rubbing strength for polyimide orientation films and the thickness of the LC medium.

INTRODUCTION

The electroclinic (EC) effect of smectic LCs is of interesting both for its important properties of pre-phase-transition and for its high potentiality in a fascinating application to optical processing and optic computation because it posscesses a fast electro optic response[1]. In a previous paper we showed that a mixtured material 764E (BDH) shows a large EC effect even in SmC* phase as is so in the SmA phase[2].

It is well known that the temperature dependence of the dielectric constant of some LC materials, which contain chiral dopant, measured at the soft mode freqency shows a divergent behavior at a critical temperature between SmA and SmC* phase [3,4]. This phenomenon can be explained by a theory along to Landau theory of the phase transition.

However, no research was done, as far as the authors know, on the effect of the surface anchoring potential affecting on this phase transitional phenomenon yet.

This paper reports the effect of the surface potential on the phase transition phenomenon in an LC material 764E (BDH) in terms of the dielctric constants in the Goldstone mode at 100Hz and in the soft mode at 2kHz. In the temperature dependence of the dieletric constant in the soft mode, the phase transition temperature between SmA and SmC* phase and the width of the curves were shown to strongly depend on the surface potential which were controlled by changing the rubbing strength on the polyimide orientation films and the thickness of the LC medium.

The observed results were explained in terms of the Mayer-Garoff-Okano formula but taking account the surface potential consisting of the polar and non polar parts[5].

EXPERIMENTAL

In this research we utilized a liquid crystal (LC) material 764E(BDH) containing a chiral dopant. This material is widely used in the research of electroclinic effect for its wide SmA temperature range and a large electroclinic coefficient. According to the data sheet of BDH, its phase sequence is as follows:

$$
\begin{array}{cccc}
& 28^\circ C & 72^\circ C & 92^\circ C \\
SmC^* ----- & SmA ---- & N^* ------ & I
\end{array}
$$
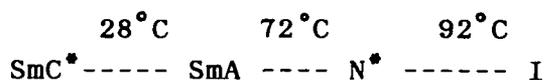
We prepared the sample cell by filling the LC material into a narrow space of 2um thick between two pieces of ITO-glass substrates whose inner surface were coated with pre-rubbed polyimide RN-305 (Nissan Chem.Ind.) films of a thickness of about 50nm.

The strength of rubbing was controlled by changing the repeated number of the rubbing, which is used as a parameter for the rubbing strength. Fig.1 shows the relation between the retardation of the substrate due to
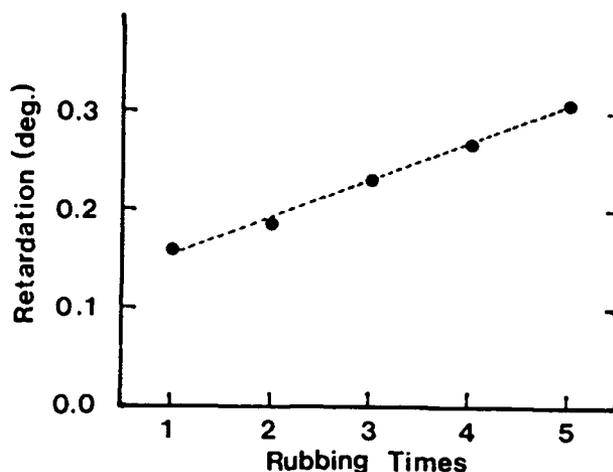
Fig.1 An experimental result for retardation of substrate and Rubbing times.

the rubbing and this parameter. As reported by our colleagues, the surface anchoring energy is strongly dependent on the rubbing strength which is characterized by the induced retardation of the orientation films [7].

The cell gaps were controlled by choosing the diameters of the space beads ranging from 0.7um to 50um. In this way we succeded in preparing the samples having LC medium thickness from 0.7um to 20um. To controll the intensity of the surface anchoring potential we adopted two methods simutaneously: one is to change the rubbing strength and the other is to vary the thickness of the LC medium.

The molecular alignment of the LC and its layer structure in the cell both in SmA and SmC* phases were examined with a polarizing microscope and also an X-ray diffractometer. The dependence of the dielectric constant both on the freqency and the temperature was measured with a system shown in Fig.2 consisting of YHP4274A LCR meter(5HZ-100KHZ) and the temperature control unit, a hot-stage (Mettler 80) which was controlled with a microcomputer. Fairly good temperature stability was achieved with an accuracy of $\pm 0.01°C$ during the data-collection period (5 seconds). The collection of data was carried out for only cooling process. The data of the capacitance and temperature were transferred to the microcomputer and then
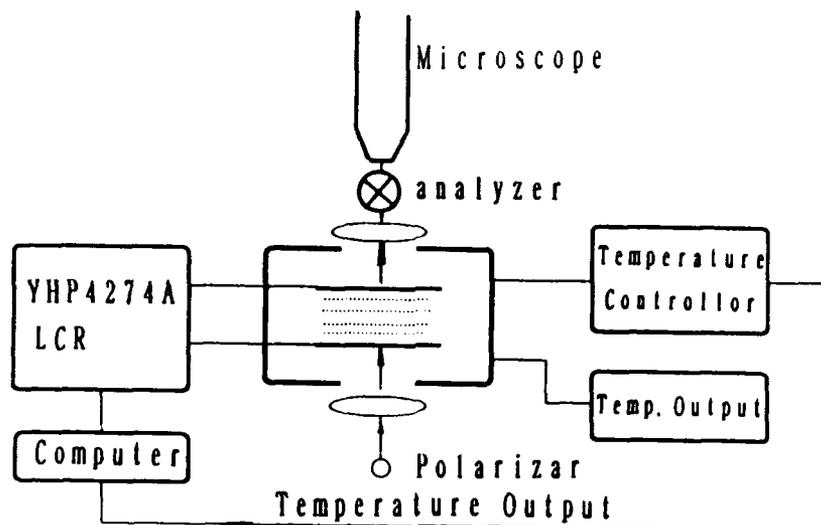
Fig.2   A layout of measuring system.

they were processed and the result was displayed on a display unit.

RESULTs

In the SmC* phase, the orientation of the director of this FLC material in the sample cell is found to be zigzag defect free and uniformly oriented to a direction with a angle between zero and the peculiar tilt angle to the rubbing direction. Its layer structure is found to be an almost bookshelf geometry by X-ray diffraction as we have reported earlier[2]. In the SmA phase, the layer normal of this material is directed to the rubbing direction.

As we have reported in a previous paper[2], this material shows remarkable electroclinic effects both in SmA and chiral SmC phase.

The dielectric constant was measured in a frequency from 100HZ to 100KHZ. At 100HZ a dielectric response related to the Goldstone was obtained below the SmA-SmC* transition. To suppress dielectric response of Goldstone mode in SmC* phase a DC field was applied over the sample.
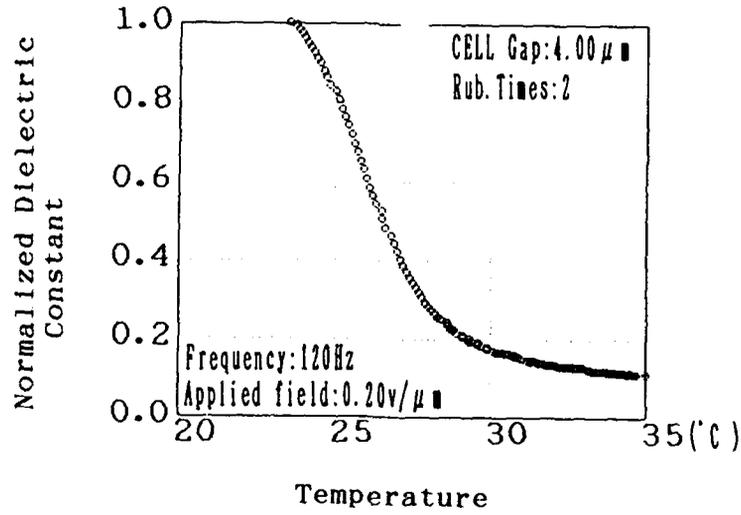
(a) For low frequency
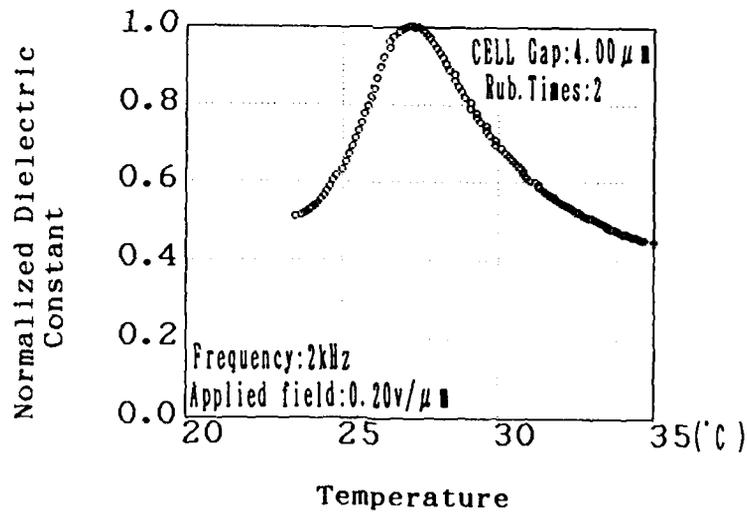
(b) For high frequency

Fig.3 The relation between standardized dielectric constant and temperature of the sample.
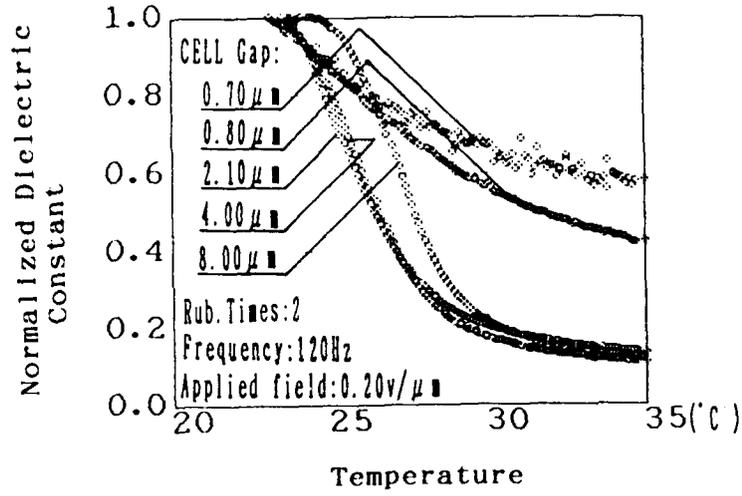
Fig.4 The thickness dependence of the relation between   and temperature, for low frequency.
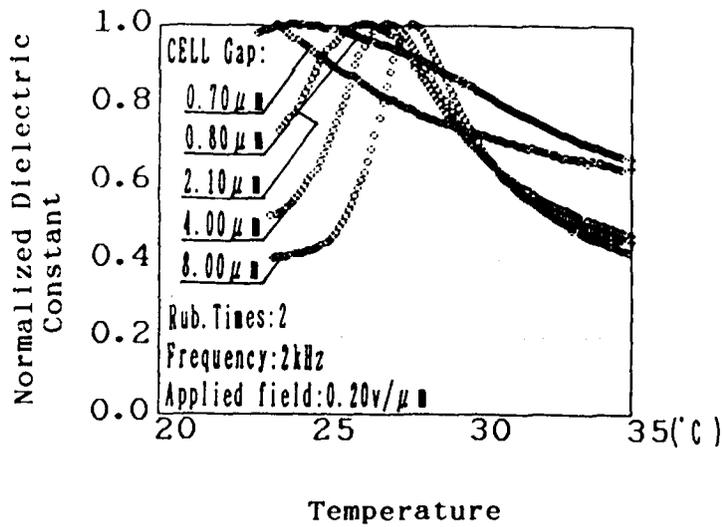
Fig.5 The   thickness dependence of the relation between standardized   and temperature, for high frequency.
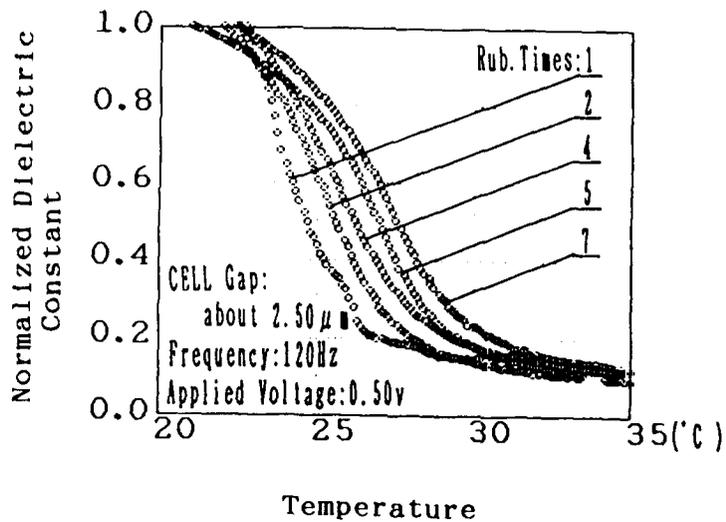
Fig.6   The   influence   of rubbing   times   on   the
standardized dielectric constant as a function   of
sample temperature, for low frequency.
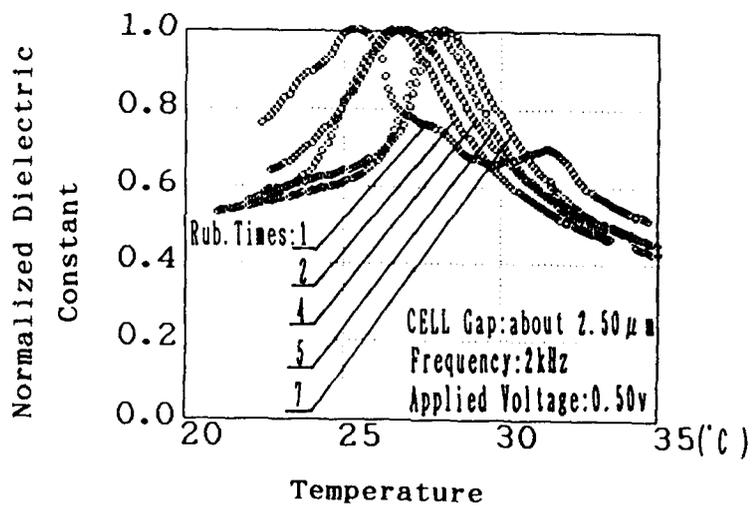
Fig.7 The   influence   of   rubbing   times   on   the
standardized dieletric constant   as a function   of
temperature, for high frequency.

The temperature variation of dielectric constant is shown in Fig.3 (a) and Fig.3 (b). For a low frequency (a) (corresponding to the Gold stone mode) it increases with decreasing of the temperature of the cell under the transition point; however for the high frequency (b) (corresponding to the soft mode, for soft mode a frequency dependence of dielectric constant was found, a striking divergence at the transition point was found at a region from 1-10KHz.) even though it is imperfect, a divergence of the dielectric constant is observed at the transition point.

In Fig.4 we show the influence of the cell thickness on the observed dielectric constant. From this figure we can understand that in a thick sample the dielectric constant, corresponding to Goldstone mode, increases faster than in a thin sample as the temperature of the samples decreases. The relation between dielectric constant and temperature can be written as $(Tc-T)^n$, where n increases with the thickness of the sample in a region from 0.5 to 1.

Contrast to Fig.4, Fig.5 shows the dielectric constant corresponding to the soft mode. Two facts can be found in this result. The first is that the width of the curve of a thin sample is larger than that of a thick one; the second one is that the positions of peaks (critical temperatures) shift to low temperature region when the samples become thiner.

To investigate the influence of surface anchoring potential furthermore, we controlled the surface anchoring strength by changing the rubbing times of polyimide orientation films. As mentioned before the surface potential increases with rubbing times. Fig.6 and Fig.7 show the dependence of the dielectric constant on the rubbing times as a function of temperature. Similar to Fig.4, the low-frequency dielectric constant varies as a function $(Tc-T)^n$, but contrast to that case remains a constant, while the transition points shift to higher values with the rubbing times i.e. increase with surface potential. Furthermore, the high-frequency dielectric constant (Fig.7) varies as a function of $(T-Tc)^{-1}$, analogous to what happens as shown in Fig.5.

DISCUSSION

To explain the experimental results we shall derive some analytical formulae for the dielectric constants. For this purpose , we adopted Mayer-Garoff-Okano formulation for the bulk free energy of the LC medium Fb[8], and Fs for the surface energy[5,6]. The total energy Ft is the sum of them:

$$F_b = F_0 + \frac{1}{2}A\theta^2 + \frac{1}{4}B\theta^4 + \frac{1}{2}\chi^{-1}P^2 - PE - t\theta P \tag{1}$$

$$F_s = -(U\theta + \frac{1}{2}G\theta^2) \tag{2}$$

$$F_t = F_b + F_s \tag{3}$$

where A= a(T-Tc).

In the following we will assume that θ is uniform along the thickness direction. This is because in the smectic phase, particularly in the SmA phase, the variation of θ necessarily accompanies the variation of the thickness of the layer, since this is not easily allowable in the SmA phase. A more detailed treatment by considering the spatial variation of θ is now underway and the result will be published elsewhere.

To consider the influence of surface anchoring potential, we will divide the discussion into two parts, at first we will consider the dielectric constant with no surface effect. Then a surface anchoring potential will be taken into account.

1. No Influence of surface be considered

As showed in previous paper[2], for a free standing smectic film, where the surface energy is negleted, the state variables θ and P can be obtained by minimizing the free energy Fb with respect to both θ and P. This results in the

existence of a spontaneous polarization Ps and a tilt angle expressed in the SmC* phase (eq.(5)),

$$\frac{\partial F_1}{\partial P} = \chi^{-1}P - t\theta = 0$$

$$\frac{\partial F_1}{\partial \theta} = A\theta + B\theta^3 - tP = 0 \tag{4}$$

$$\theta_0^2 = -\frac{A'}{B} \tag{5}$$

$$Ps = \chi t\theta_0$$

where $A' = A - \chi t^2 = a(T-T_0) - \chi t^2 = a(T-Tc)$. Therefor $Tc = T0 + \chi t^2 /a$. For a low-frequency ac field, the dielectric constant of a free stand FLC film varies as a function of $(Tc-T)^{1/2}$, because in this frequency region the Ps would contribute to the dielectric constant. This is qualitatively in coincidence with the result of experiment shown in Fig.3 (a).

For high frequency ac field the Ps would never contribute, the dielectric constant almost owe to the increase of dP, resulted from the applying of electric field. Letting the tilt angle as $\theta = \theta_0 + \delta\theta$ when a field was applied, the formulae (4) become

$$A(\theta_0 + \delta\theta) + B(\theta_0 + \delta\theta)^3 - tP = 0$$

$$\chi^{-1}P - E - t(\theta_0 + \delta\theta) = 0 \tag{6}$$

then P can be obtained as

$$P = \chi t\theta_0 + \chi \left\{ 1 + \frac{t^2\chi}{2a(T-T_c)} \right\} E \tag{7}$$

the incremental part dP can be written as

$$\delta P = \left\{ \chi + \frac{\chi^2 t}{2a(T-T_c)} \right\} E \tag{8}$$

The dielectric constant can be written as

$$\varepsilon_c = (1+\chi) + \frac{\chi^2 t^2}{2a(T-T_c)} \tag{9}$$

similarly the dielectric constant of SmA phase reads as

$$\varepsilon_A = (1+\chi) + \frac{\chi^2 t^2}{a(T-T_c)} \tag{10}$$

Each of ps shows a diverging maximum at T=Tc, however the coefficients differ by the factor 2.

However, in the actual data(e.g. that of Fig.3(b)), no perfect divergence in the $\varepsilon-$ T observed; this may be due to actual situation where the value of the electric field is not ideally null[9].

2. Surface energy be considered

If we consider a surface anchoring energy given in the formula (2), then the equation (4) becomes

$$\chi^{-1}P - t\theta = 0$$

$$-(U+G\theta) + d(A\theta + B\theta^3 - tP) = 0 \tag{11}$$

where d is the sample thickness. The spontaneous polariztion can be derived from the following equation (12).

$$\theta^3 + (A - G/d - t\chi^2)/B\theta - U/dB = 0$$

$$3a = a(T-T_s) - G/d - t\chi^2 = a(T-T_c)$$

$$\beta = -U/dB \qquad T_c = T_s + \frac{G}{ad} + \frac{t\chi^2}{a}$$

$$\theta^3 + 3a\theta + \beta = 0 \tag{12}$$

The root of this equation is shown as

$$\theta'_1 = \sqrt[3]{\mu} + \sqrt[3]{\nu} \tag{13}$$

$$\mu = \frac{1}{2} \{-\beta + \sqrt{\beta^2 + 4a^3}\}$$

$$\nu = \frac{1}{2} \{-\beta - \sqrt{\beta^2 + 4a^3}\}$$

For low frequency singal(for Goldstone mode) ; if U=0, that means there is no polar surface potential, Ps would varies as $(T-Tc)^{1/2}$, but the transition point would shift according to dT=-G/ad; if U≠0, there exist a polar surface potential, Ps would varies as $(T-Tc)^n$ with n greater than 1/2, and also the predicated shift in the transition point is dt= -G/ad.

On the other hand, the dielectric constant of high frequency(for the soft mode) is given as follows:

$$-U - G(\theta'_1 + \delta\theta') + d\{A(\theta'_1 + \delta\theta') + B(\theta'_1 + \delta\theta')^3 - tP'\} = 0 \tag{14}$$

$$\chi^{-1}P' - E - t(\theta'_1 + \delta\theta') = 0$$

$$\varepsilon_c' = (1+\chi) + \frac{t^2\chi^2}{(A + 3B\theta'^2_1 - t^2\chi + G/d)} \tag{15}$$

For high frequency signal, if U=0 the dielectric permitivity would proportional to $(T-Tc')^{-1}$, where Tc' is Tc the critical temperature accompaning an incremental part dT=-G/ad, where U≠0, it would not varies as $(T-Tc)^{-1}$, but a broad peak can be predicated, and also a incremental part of transition point would be found. It is worth to note that no more divergence occurs in the EPc at the critical temperature.

CONCLUSION

From above discussions several conclusions can be drawn; first the temperature dependence of the dielectric constant

would be affected strongly by the surface anchoring potential; Second the surface anchring potential can be divided into a polar part and a non polar part. The polar part would contribute to change the broadness of the curve of dielectric constant with temperature, and the non polar part would contribute to the shift of the critical temperature.

By comparing the results of experiment with the analytical consideration done in this paper we claim that both the two parts of the surface anchoring potential increases with decreasing the thickness of the sample; However the rubbing strength may not contribute to change the polar part.

References
----

1) G.Andersson,I.Dahl,P.Keller,W.Kuczynski,S.T.Lagerwall, K.Skarp, and B.Stebler: Appl.Phys.Lett.51 (1987) 1653.

2) Y.B.Yang,N.Nakamura, and S.Kobayashi:Jpn.J.Appl.Phys. 30(1991)L612.

3) F.Gouda,K.Skarp,G.Andersson,H.Kresse and S.T.Lagarwall: Jpn.J.Appl.Phys. 30 (1989) 1887.

4) J.P.Parneix, C.Legrand: Ferroelectrics 84 (1988) 199.

5) N.A.Clark, M.A.Handschy, and S.T.Lagerwall:Mol.Cryst. Liq.Cryst. 94,(1983) 213.

6) H.Yokoyama: J.Chem.Soc., Faraday Trans.2 84(8) (1988) 1023

7) S.Kuniyasu, H.Fukuro, S.Maeda, K.Nakaya, M.Nitta, N.Ozaki and S.Kobayashi: Jpn.J.Appl.Phys. 27(5)(1988) 827.

8) R.B.Meyer: Mol.Cryst.Liq.Cryst. 40 (1977) 33

9) Y.Maruyama: private communication.

THE FIELD INDUCED STRIPE TEXTURE IN SURFACE STABILIZED FERROELECTRIC LIQUID CRYSTAL CELLS

Ren Fan Shao, Paula C. Willis and Noel A. Clark
Condensed Matter Laboratory, Department of Physics and Opto-electronic Computing System Center, University of Colorado Boulder, Colorado 80309 USA

abstract: We investigate the texture which appears as parallel stripes perpendicular to the smectic layers in SSFLC cells. When the temperature approaches the smectic A to smectic C* transition from above in the smectic A phase, a DC field induces the chevron structure due to the electroclinic effect and then the stripe texture is formed. We have identified the stripes to be parallel zig-zag walls. We show that a reasonably high DC voltage changes the structure of the cell from chevron to book-shelf in the smectic C* phase and we show how this happens. We have experimentally found that the width of the stripes is approximately equal to the thickness of the cell and we present a theoretical explanation of the equivalence. We have measured the layer tilt angles in the plane of the cell as a function of temperature and have found them to be the same as the chevron tilt angles determined by X-ray scattering. The result confirms the chevron layer structure and stripe texture models and also gives a simple way to measure chevron layer tilt angles.

INTRODUCTION

Due to the fast response and bistability of surface stabilized ferroelectric liquid crystals (SSFLC's), discovered by Clark and Lagerwell in 1980[1], a large number of studies on FLC's in thin cells have been carried out. An understanding of the structure of the SSFLC is important not only for fundamental study, but also for practical application. From the viewpoint of application to display devices, defects are a serious problem since they influence the contrast ratio of the display.

Recently several papers [2-6] have discussed a new type of layer structure defect in the chiral smectics that appears as a stripe-shaped texture perpendicular to the smectic layers as observed under a polarizing microscope. This kind of texture can be created in samples of varing thickness [2][4] after the application an AC electric field with a certain frequency in the smectic A or

the smectic C*. There are several models like parabolic focal conics, curva-
ture walls, smectic layer deformations and electromechanical effects used to
explain the causes of the stripe-shaped texture. However, they are not able
to indicate the relationship between the stripe width and the cell thickness.
According to the model of layer deformation, the width of stripes seems to
be connected with the pitch value[4]. One paper [2] suggested the width of
the stripes to be related to the cell thickness, but there was no theoretical
explanation.

In this paper we present results of observation of the stripe texture in
SSFLC cells under a polarizing microscope (see Figure 1). We investigated
the procedure of forming the texture and identified the stripes to be parallel
zig-zag walls. We also give the internal relation between the width of stripes
and the thickness of cell. The experimental results and theoretical explana-
tions will be presented in the next sections.
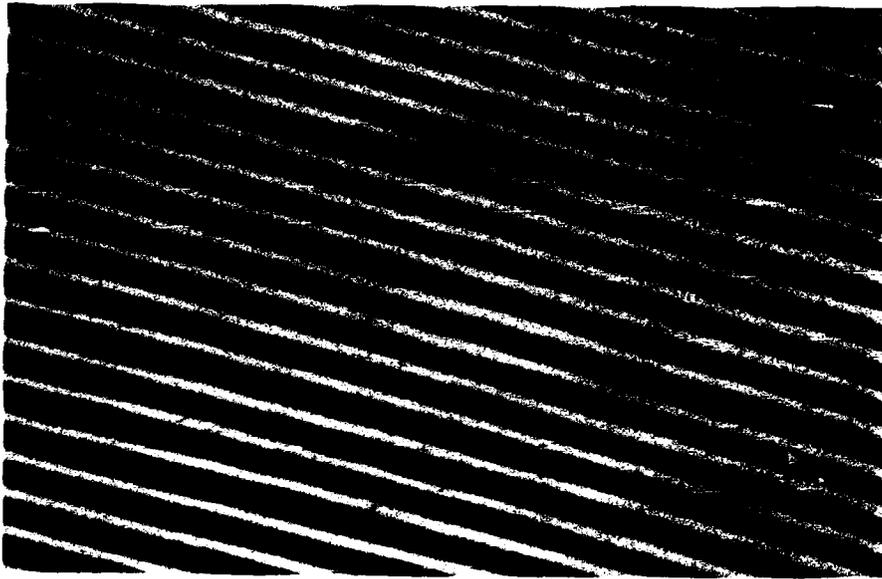
Fig.1: The parallel stripe texture in SSFLC in the smectic C* phase.
The smectic layers run perpendicularly to the stripes. See Color Plate II.

EXPERIMENTAL

The FLC used in our experiment was the commercial chiral smectic mixture ZLI 3654 from Merck. It has the following phases and transition temperatures:

C < -30 Smectic C* 62 Smectic A 76 Nematic 86 Isotropic

The cells were made by sandwiching the ZLI 3654 between two glass plates coated with Indium-Tin Oxide(ITO). The cells were prepared by rubbing after the glass plates were coated with a thin nylon 6,6 layer. The ZLI 3654 was filled between the two plates by capillary action in the isotropic phase and cooled down very slowly to get a good planar alignment. When the temperature approached the smectic A to smectic C* transition from above, a DC field of 20 V was applied to the cells and a stripe-shaped texture appeared suddenly after the application of the field. The stripes often began to build up at the places where the spacers were located. The shape of early stripes was sword-like (see Figure 2.a). Then they grew up quickly and spread over the whole cell. The stripes were strictly parallel to the smectic layer normal. When the cells cooled down to the smectic C* phase region, the stripes still remained even after the DC field was turned off. We observed the texture using a polarized light microscope equipped with a rotating stage. The cells were located in a hot stage between the crossed polarizers. The colors of the neighboring two stripes can be exchanged by rotating the cell, so the stripe texture has a pair structure. That is, the neighboring two stripes combine as a unit, which repeats to form the whole texture. We measured the width of stripes to be about 3.5μm. Also we used transmission spectroscopy to measure the thickness of the cells with the sample in the smectic A phase and found that the width of stripes was approximately equal to the thickness of the cells. We measured the layer tilt angles in the plane of the cell as a function of temperature and found them to be the same as the chevron layer tilt angles determined by X-ray scattering (see Figure 4).

DISCUSSION

We use the chevron layer structure model to explain the stripe-shape

texture. We expect the electroclinic effect to be the strongest just above the smectic A to smectic C* transition (as demonstrated in other materials [7,8])and that field applied to the cell will induce a phase transition from smectic A to Smectic C*. In this case, the molecular directors will tilt away from the smectic layer normal and therefore establish a chevron structure in the smectic A phase. A chevron layer structure was observed in the smectic A phase of another FLC material by Takanishi et al [9]. We explain the stripe-shaped texture as electroclinically induced zig-zag walls.

a   b
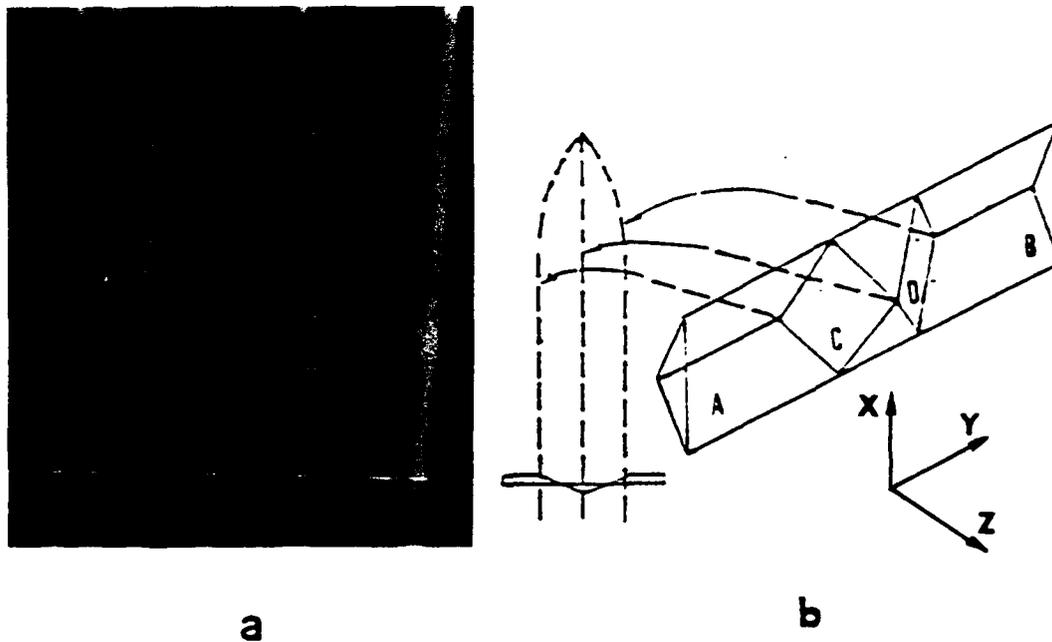
Fig.2: (a) Photomicrograph of the early shape of the stripes. (b) Layer structure of the stripes: part A and part B are chevron layer structure. Diamond shape C and D are in two planes rotated about the x axis from z. See Color Plate III.

According to the chevron layer structure model, the zig-zag defects are the regions mediating the transition zones between chevron shaped layers

pointing in opposite directions [11]. In our case, two zig-zag walls are combined together as an unit to form a stripe. The layer structure is shown in Figure 2.b. Parts A and B are chevron layer areas. The diamond-shape areas C and D are two zig-zag walls immediately adjacent to one another. Area C is tilted in some direction from the layer normal, and the diamond D is tilted to the other. The geometry of the layer structure mentioned above results in the undulation of the smectic layers in the plane of the cell and the appearance of zig-zag walls in parallel stripes perpendicular to the layers. Notice that the layers are not displaced at the substrates by the presence of this stripe defect, meaning that it can in principle be reversibly removed.
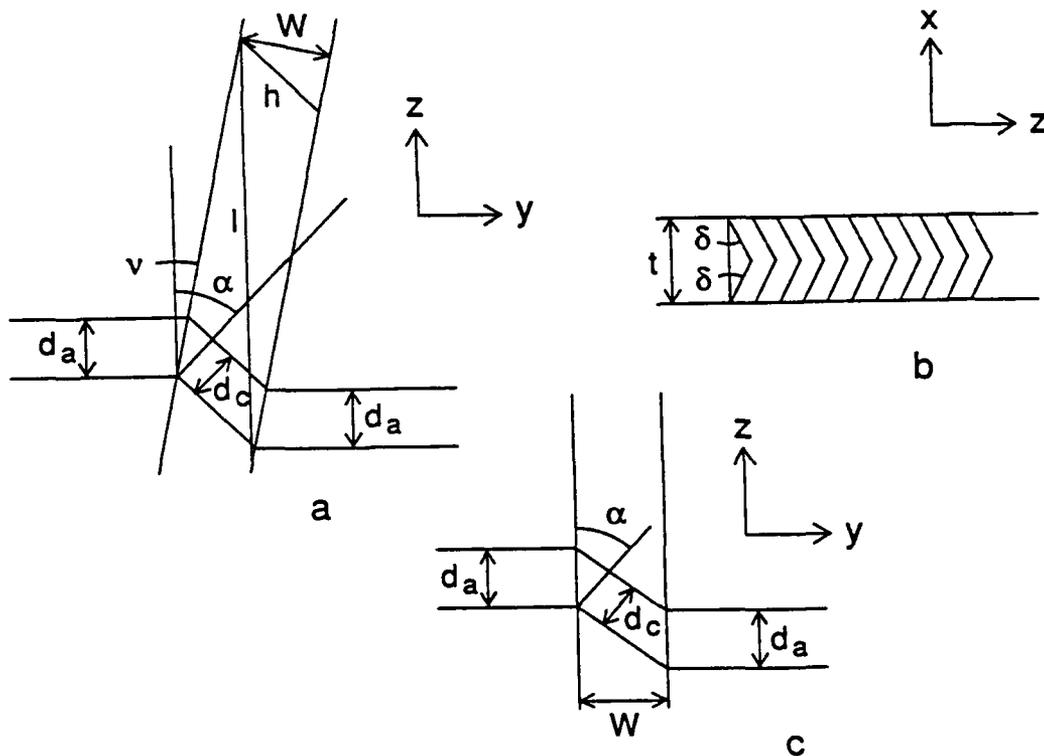
Fig.3: Schematic diagram of the layer structure of the narrow zig-zag wall defect (a) top view: the zig-zag wall is tilted by an angle α from the layer normal. (b) side view of the zig-zag wall, (c) special case: $\alpha=0$. The zig-zag wall is perpendicular to the smectic layer.

The narrow zig-zag walls having the general construction [10-12] are illustrated in Figure 3. As an aid to understand the zig-zag wall structure and the relations between the parameters of the layer structure, we define the geometry: the z axis lies in plane of the glass and normal to the upright smectic A layer, the y axis is parallel to the smectic layers. As delineated in Figure 3, γ is the angle between z and the zig-zag wall. α is the angle between z and the layer normal in the zig-zag wall . d_c and d_a represent the smectic C* and smectic A layer spacing. δ is the angle of the smectic layer with respect to the x axis. The zig-zag wall has width w. The SSFLC cell has fixed thickness t.

From Figure 3, three significant geometrical relations are easily obtained[13].

$$\frac{\cos(\alpha - \gamma)}{\cos\gamma} = \cos\delta \tag{1}$$

$$h \sin\alpha = t \tan\delta \tag{2}$$

$$l \tan\gamma = h \cos\delta \tag{3}$$

Using the above three equations, we can get the relation between the width of the zig-zag wall and the thickness of the cell as

$$w = \frac{t\cos\gamma\sin\delta}{\sin\alpha} \tag{4}$$

We are interested in the case of narrow walls running parallel to Z. In this case, $\gamma=0$, we get the following two equations:

$$\alpha = \delta \tag{5}$$

$$w = t \tag{6}$$

The equations reveal that the width of the stripes is equal to the thickness of the cell and that the tilt angle in the plane of the cell is equal to the chevron tilt angle. The facts were proved by our experiment. In our case, $\gamma=0$, the diagram of the layer structure is shown in Figure 3.c. Since $d_c=d_a \cos\alpha$ and d_c decreases as the temperature is decreased, the inclination angle α of smectic layer in the plane of cell will be a function of temperature. Thus, the smectic layer should be inclined more when the temperature is cooled down but still in the smectic C* (see Figure 4). This result is verified by
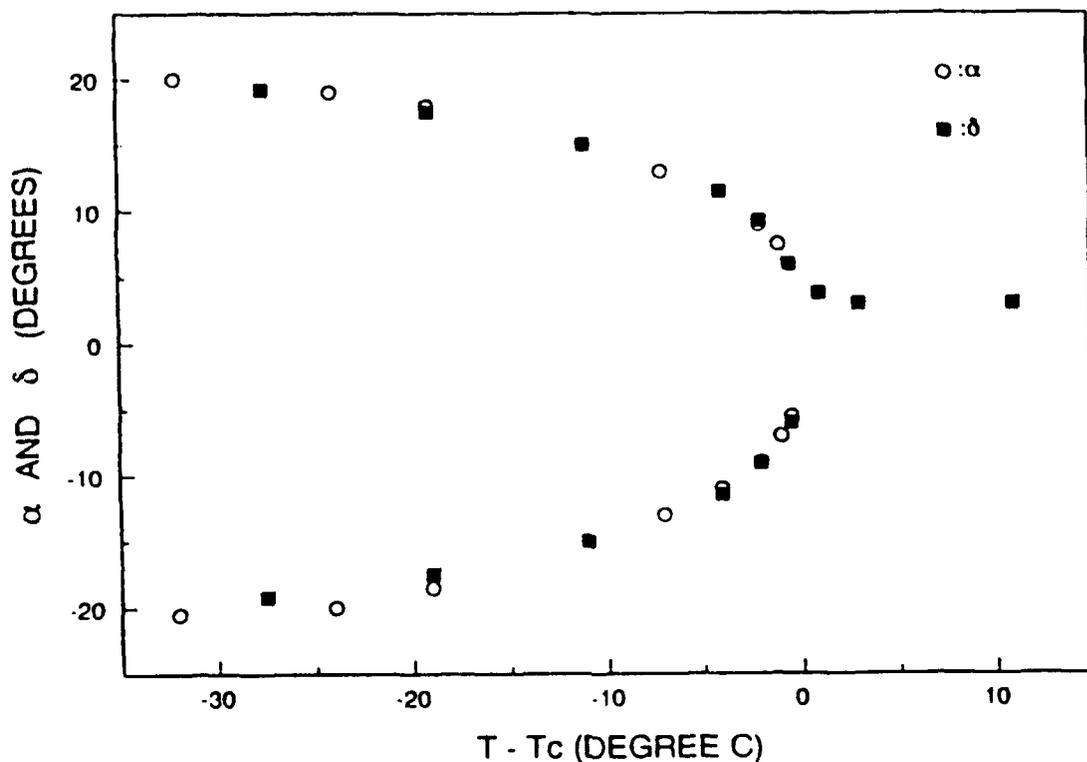
Fig.4: The chevron layer tilt angle (δ) and the optically observed layer inclination angle (α) in the plane of the cell plotted as a function of T-T$_c$.

our experiment, but is different from reference[6] where the smectic layer inclination angle in the plane is constant (6 degrees). The chevron tilt angles are usually determined by X-ray scattering, but it is still complicated. Our experiment also gives a simple way to measure the chevron layer tilt angles.

A reasonably high DC voltage can change the structure of the cell from chevron to book-shelf in the smectic C* phase. The change of the layer structure is illustrated in Figure 5. Figure 5.a shows that the stripes contain two parts: part A is the book-shelf area and part B is the chevron structure area. Since the chevron exists in part of the stripe the molecular orientation is splayed and the stripes never appear dark with rotation of cell. When the applied DC voltage reaches 67 V at 30°C, the chevron area partly begins
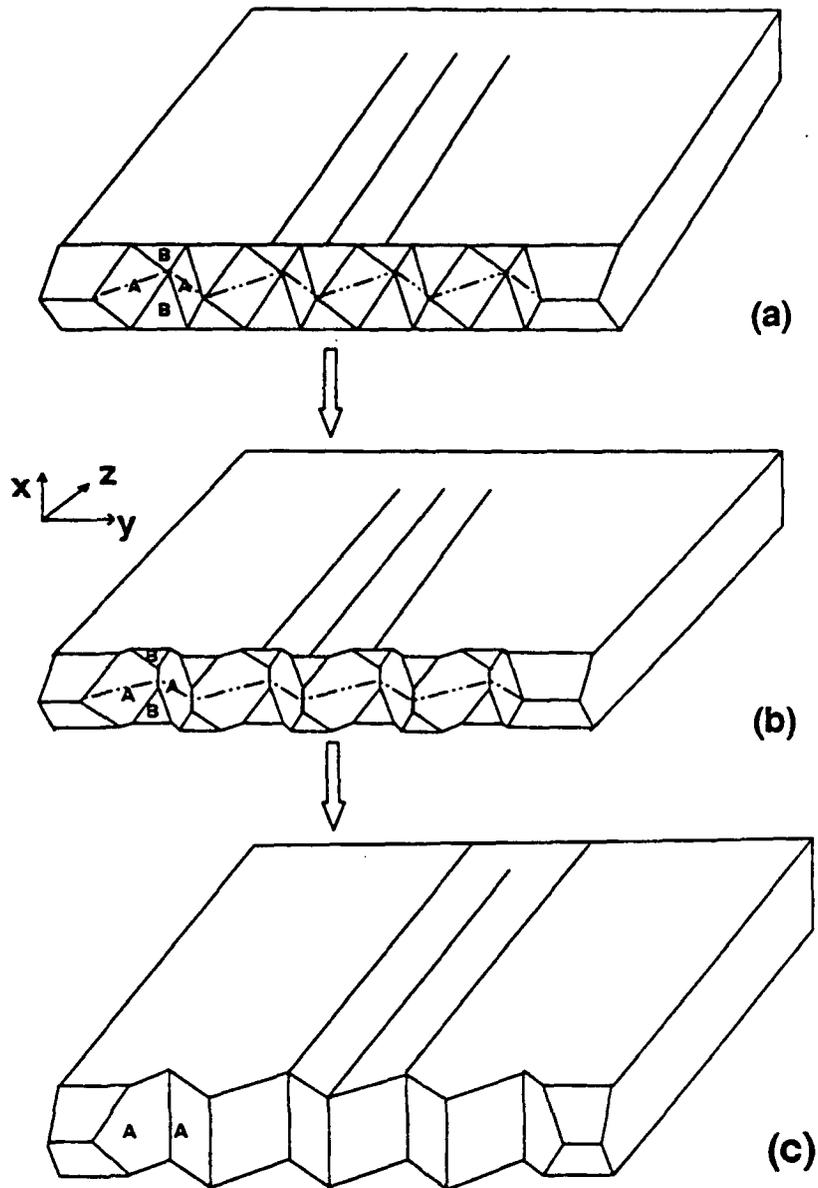
Fig.5: The layer structure within stripes changing from chevron to book-shelf with increasing electric field. (a) The initial structure of the stripes: part B is chevron, part A is book-shelf normal to the bounding surfaces. (b) The area of chevron structure is decreased as the applied DC voltage is increased. (c) The book-shelf structure of the stripes.

to change to book-shelf structure because the electric field forces the layers
to straighten up (see Figure 5.b) increasing areas A at the expense of areas
B, until the voltage reached 90 V, the layer structure completely changes
to book-shelf, the undulation of the smectic layers in the plane remaining
as shown in Figure 5.c. The layer structure of Figure 2.a maintains the
layer pitch (number of layers per length along z) constant. Maintaining this
constant during the increase of A areas and decrease of B areas requires the
scenario shown in Figure 5 wherein the chevron interfaces between the A
and B regions are always parallel to their initial condition (Figure 5.a). This
leads to a finite intersection of A areas with the surfaces and therefore a layer
rotation at the surface. This restructuring of the layers at the surface locks in
the A regions, the undulating texture being irreversibly formed and having a
strong memory: even when the cell is heated to the smectic A phase, the layer
undulation still remains. These book-shelf cells have a strong bistability.

There are two clues that the final structure is book-shelf. One is that
the patterns of the switching domains are totally different from the starting
chevron structure. The appearance of "speed boat" domains for the chevron
indicates that the layer structure is chevron. For book-shelf structure, surface
switching domains were observed instead of the speed boats. Another clue is
that we have observed the dark state of the stripes for the book-shelf structure
at low DC voltage indicating that the molecular orientation is uniform.

CONCLUSION

We have observed and explained the structure and formation of the stripe
defects in SSFLC cells. The chevron layer structure model and zig-zag walls
can be used to explain the stripe texture in the sectic A and smectic C*
phases. This paper also describes the switching behavior and layer struc-
ture of the stripes under a varying electric field. We propose a measurement
method, using these defects, for obtaining the chevron tilt angles without X-
ray scattering. Details of the memory effect described above are still under
inverstigation.

ACKNOWLEDGEMENTS

References

[1] N.A. Clark and S.T. Lagerwall, *Appl. Phys. Lett.*, **36**, 899 (1980)

[2] J. Pavel and M. Glogarova, *Ferroelectrics*, **113**. 619 (1991) and *Liquid Crystals*, **9**, 87 (1991)

[3] M. Kleman, Points, Lines and Walls in Liquid Crystals, Magnetic systems and Various Ordered Media (wiley) (1983)

[4] L. Lejcek and S. Pirkl, *Liquid Crystals*, **8**, 871 (1990)

[5] A. Jakli and A. Saupe, *Proc. Third Int. Conf. on Ferroelectric Liquid Crystals*, Boulder,*Ferroelectrics* (to be published in 1991)

[6] A. Verhulst and F. Stommels, *Proc Third Int. Conf. on Ferroelectric Liquid Crystals*, Boulder, *Ferroelectrics* (to be published in 1991)

[7] L. Dupont,M. Glogarova,J.P. Marcerou,H.T. Nguyen,C. Destrade and L. Lejcek, *J. Phys. II France* , **1**, 831 (1991)

[8] G. Andersson, I. Dahl,W. Kuczynski,S.T. Lagewall,K. Skarp and B. Stebler *Ferroelectrics*. **84**, 285 (1988)

[9] Y. Takaniski, Y. Ouchi, H. Takezoe and A. Fukuda,*Jpn. J. Appl. Phys.*, **28**. L487 (1989)

[10] T.P. Rieker, N.A. Clark, D.S. Parmer, E.B. Sirota and C.R. Safinya, *Phys. Rev. Lett.*, **59**, 2653 (1987)

[11] N.A. Clark and T.P. Rieker, *Phys. Rev.*, A **37**, 1035 (1988)

[12] T.P. Rieker, N.A. Clark and C.R. Safinya, *Ferroelectrics*, **113**, 245 (1991)

[13] N.A. Clark, T.P. Rieker and J.E. Maclennan. *Ferroelectrics*, **85**, 79 (1988)

OPTICAL STUDIES OF THIN LAYERS OF SMECTIC C MATERIALS

M.J.TOWLER, M.H.ANDERSON, J.C.JONES and E.P.RAYNES
Electronics Division of the Defence Research Agency, RSRE, St Andrews Rd, Malvern,
Worcestershire. WR14 3PS. U.K.

Abstract Surface stabilised ferroelectric liquid crystals (SSFLC) provide fast, bistable, optical modulators suitable for display and other applications. The effect of surface alignments and the resulting director profiles are not fully understood, but can be probed by studying the wavelength dependent optical transmission properties. 5° and 30° evaporated SiO alignments are investigated and it is shown that the surface pretilt affects markedly the director profile.

INTRODUCTION

FLC materials are formulated by mixing an achiral S_C host with a small amount of chiral dopant[1]. In this manner, mixtures are designed which exhibit the phase sequence (I-N-S_A-S_C) necessary for good alignment and suitable physical properties. Studies of host systems are therefore relevant to FLC understanding, avoiding complications due to the chiral bulk and surface energy terms and the spontaneous polarisation (P_S). For example polar surface terms have been used to explain the origin of splayed[2] and half-splayed[3] states. However, we have only observed these asymmetric splayed states in cells using high P_S materials, and most SSFLC cells show only two types of domains, corresponding to P_S up and P_S down. Similar domains occur in equivalent samples of the host. Rotation of a cell produces minimum transmission for a given domain at an angle from the rubbing direction which is significantly lower than the S_C cone angle θ_0, suggesting tilted layers[4]. However, complete extinction of white light between crossed polarisers is not observed for any cell orientation. Clearly, the director profile is not uniform and transmission spectra contain information about it.

THEORY

The Director Profile Within The Chevron Layer Geometry.

X - ray studies indicate a chevron layer structure[5] which successfully explains the zig-zag defect[6] and certain electric field effects[7]. In parallel aligned cells the chevron structure is present for both low and high surface pretilt[8]. In a symmetric structure the chevron interface is at the cell centre and at a twist (in-plane-tilt) angle ϕ_m from the alignment direction, given by:

$$\cos\phi_m = \frac{\cos\theta_0}{\cos\delta}$$

where θ_0 is the cone angle and δ is the layer tilt angle.
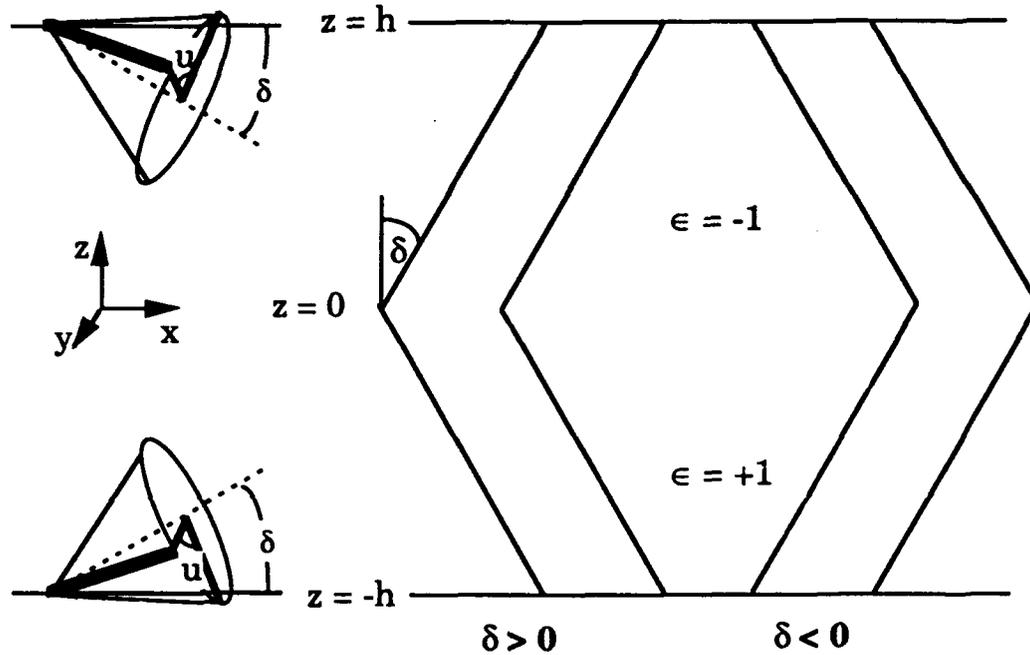
Figure 1. the Sc coordinate geometry.

At the liquid crystal-alignment layer interface there is a balance between surface and bulk couples. For simplicity we neglect polar surface terms and consider the orientation of the n-director which minimises the non-chiral surface energy density (Ws)

$$2Ws = \alpha\,(n.v)^2 - \beta\,(n.t)^2 - 2\gamma\,(n.v)(n.t) \qquad ....(1)$$

where n is the director, v the surface normal and t the anchoring direction. We choose the coordinate system (Fig. 1) such that

$n = (\sin\theta_0.\sin\delta.\cos u + \cos\theta_0.\cos\delta,\ \sin\theta_0.\sin u,\ \epsilon(\cos\theta_0.\sin\delta - \sin\theta_0.\cos\delta.\cos u))$

$v = (0, 0, \epsilon)$ $t = (1, 0, 0)$

$\epsilon = -1$ for $z > 0$, $\epsilon = +1$ for $z < 0$ and u is the azimuthal angle measured from the top/bottom of

the cone. Then Ws is an extremum for u given by

$$\sin u = 0 \qquad\qquad\qquad ....(2a)$$

or

$$\cos u = \frac{1}{\tan\theta_0}\left[\frac{(1 + \frac{\beta}{\alpha})\sin\delta.\cos\delta. - \frac{\gamma}{\alpha}\cos2\delta}{\cos^2\delta - \frac{\beta}{\alpha}\sin^2\delta + \frac{\gamma}{\alpha}\sin2\delta}\right] \qquad ....(2b)$$

It is clear from this naive argument that the preferred director position at the surface depends upon both the alignment layer (characterised by α, β and γ) and the sign of the chevron angle. In parallel aligned cells, differing surface treatments will give rise to n-director profiles in which the twist (in-plane tilt) angle at the cell surface can be either greater or less than that at the chevron interface.

Optical Transmission of Symmetric Structures Between Crossed Polarisers.

For light normally incident on symmetric structures (i.e. $u(z) = u(-z)$) the normalised transmission between crossed polarisers has the general form

$$T = A(\lambda)\sin^2 2(\theta - \theta_{ext}(\lambda)) \qquad\qquad ....(3)$$

where $A(\lambda)$ and $\theta_{ext}(\lambda)$ will depend on the director profile present in the cell. Normal incidence polarised microscopy is not sensitive to out-of-plane tilt in thin S_C cells, but can be sensitive to the twist present in the system.

Ignoring out-of-plane tilt a simple director configuration, giving a wavelength dependent extinction angle, is a triangular director profile (TDP). In a TDP the n - director twists linearly from a surface value ϕ_s to a twist angle ϕ_m in the middle of the cell and back to ϕ_s at the second surface. For such a system it is easily shown that the extinction angle $\theta_{ext}(\lambda)$ (measured with respect to the anchoring direction in the S_A phase) is given by[9]

$$\tan 2(\theta_{ext} - \phi_s) = \frac{\tan\left[(\phi_m - \phi_s)\sqrt{1 + \alpha^2}\right]}{\sqrt{1 + \alpha^2}} \qquad ....(4)$$

where $\alpha = \Delta n h \pi / (\phi_m - \phi_s)\lambda$ and h is half the cell thickness. Figure 2 shows equation (4) plotted for a cell of thickness 2.5μm (h = 1.25 μm) for the two cases of positive ($\phi_m > \phi_s$) and negative ($\phi_m < \phi_s$) TDPs, using the measured $\Delta n(\lambda)$. Taking both ϕ_m and $\phi_s > 0$, for both curves the extinction angle is positive at long wavelengths; as the wavelength is shortened

the extinction angle initially increases for a positive TDP but decreases in the negative case.
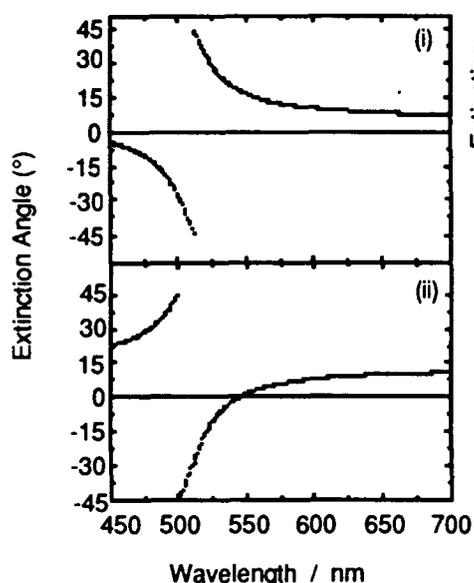
Fig.2 Theoretical extinction angle behaviour
(i) $\phi_m = 9°$, $\phi_s = 1°$ (ii) $\phi_m = 9°$, $\phi_s = 17°$.
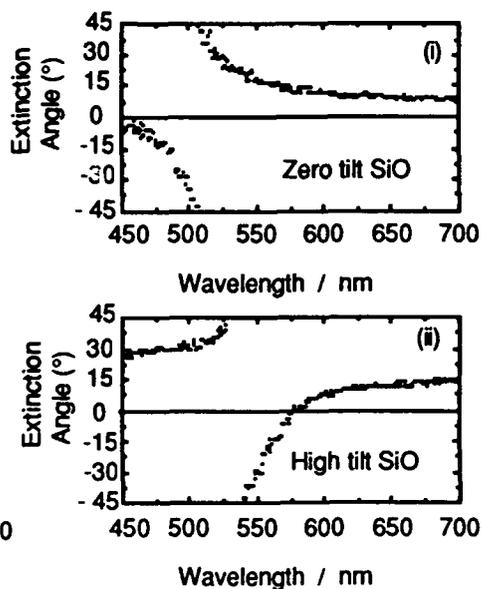
Fig.3 Measured extinction angles for
(i) ≈2.5μm 30° SiO cell, (ii) ≈3μm 5° SiO cell

EXPERIMENT.

Parallel aligned cells of approximately 2-3μm thickness fabricated using either 30° or 5° evaporated SiO alignment were filled with a mixture of biphenyl esters of the general structure:
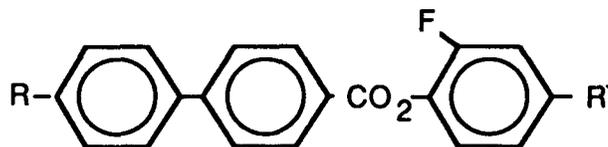
and phase transition temperatures (°C):

K   25 S_B 32 S_C 73.3 S_A 84   N   135   I

and cooled slowly into the S_C phase. A small amount of chiral dopant was also added to induce a small P_S (< 0.5 nC/cm^2) to allow the use of an electric field to form reasonable sized single domains. The P_S was kept small to minimise any asymmetry due to chiral bulk and surface terms, and to limit the influence of P_S on the director profile.

Transmission spectra of defect free single domains between crossed polarisers were obtained using an Optical Multichannel Analyser and a Nikon Optiphot-pol Polarising Microscope. The data were collected over the wavelength range 450-700 nm as a function of cell orientation and the extinction angles extracted. The extinction angle was measured as the angle between the first polariser and the anchoring direction in the S_A phase. Further details of the method can be found in the earlier paper [9] on polyimide aligned samples.

RESULTS and DISCUSSION.

Figure 3 shows the measured extinction angle data for 30° and 5° evaporated SiO alignments, these results are seen to show the same qualitative behaviour as the theoretical predictions in Figure 2. It is clear that in the case of low surface pretilt alignments that the twist (in-plane tilt) angle at the surface is likely to be smaller than that at the chevron interface, whilst for high surface pretilt alignments the opposite will be the case.

REFERENCES.

1. W. Kuczynski and H. Stegemeyer. **Chem. Phys. Lett., 70**, 123 (1980)

2. M.J. Handschy and N.A. Clark. **Ferroelectrics., 59**, 69 (1984)

3. J.E. Maclennan, N.A. Clark, M.J. Handschy and M.R. Meadows. **Liq.Cryst.,7**, 753 (1990)

4. G. Pelzl, P. Kolbe, U. Preukschas, S. Diele and D. Demus. **Mol.Cryst.Liq.Cryst., 53**, 117 (1979)

5. T.P. Rieker, N.A. Clark, G.S. Smith, D.S. Parmar, E.B. Sirota and C.R. Safinya. **Phys.Rev.Lett., 59**, 2658 (1987)

6. N.A. Clark, T.P. Rieker and J.E. Maclennan. **Ferroelectrics., 85**, 79 (1988)

7. S.J. Elston and J.R. Sambles **Appl.Phys.Lett., 55**, 1621 (1989)

8. Y. Ouchi, J. Lee, H. Takezoe, A. Fukuda, K. Kondo, T. Kitamura and A. Mukoh., **Jap.J.Appl.Phys., 27**, L1993 (1988)

9. M.H. Anderson, J.C. Jones, E.P. Raynes and M.J. Towler., **J.Phys.D:Appl.Phys., 24**, 338 (1991)

LARGE ELECTROCLINIC EFFECT IN
NEW LIQUID CRYSTAL MATERIAL*

Paul A. Williams[*†], Noel A. Clark[†], M. Blanca Ros[‡],
David M. Walba[‡], and Michael D. Wand[§]

*National Institute of Standards and Technology
Boulder CO 80303-3328

†Department of Physics, Condensed Matter Laboratory,
University of Colorado, Boulder CO 80309-0390

‡Department of Chemistry and Biochemistry
and Optoelectronic Computing Systems Center,
University of Colorado, Boulder CO 80309-0215

§Displaytech Inc.
2200 Central Avenue, Suite C
Boulder CO 80301

ABSTRACT We report a new liquid crystal material (W317) which
has an unusually large electroclinic effect in a phase tentatively
identified as smectic A. We show electroclinic tilt angles as large as
21°, and measurable tilt angles over a 40°C temperature range.

The electroclinic effect was first described by Garoff and Meyer in 1977.[1,2]
We will consider the effect as it occurs in the chiral smectic A phase, where the
liquid crystal molecules are oriented with their long molecular axis or director (n)
parallel to the layer normal. An electric field E applied parallel to the smectic layers
couples to the transverse component of the molecule's permanent electric dipole (p).
This biases the rotation of the molecules about their long axes since p tends to be
parallel to the applied field. The chirality of the molecules requires that the plane
defined by p and n is not a mirror plane. The result is that the free energy of the
molecule is not a symmetric function of molecular tilt. So, for a non-zero applied
electric field, the average molecular tilt in the plane perpendicular to E is non-zero.
It also turns out that the tilt is a linear function of the field (for small fields).

We recently measured an unusually large electroclinic effect in a newly synthesized material (which we refer to as W317). This material has the structure
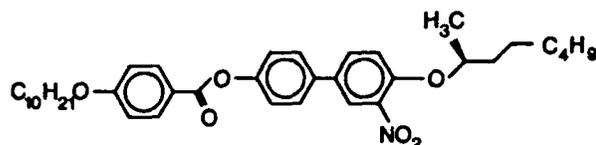
The electroclinic effect is seen in what has been tentatively identified as the smectic A phase. The texture as viewed through a microscope resembles a smectic A phase. However, preliminary x-ray scattering data does not seem to support this identification.[b] With this in mind, we describe the phase diagram as

$$X \rightarrow (41°C) \rightarrow Sm \ A? \rightarrow (76°C) \rightarrow Iso.$$

It should be noted that the so-called smectic A phase can be supercooled to temperatures lower than 41°C for short times. This was done to take some of the data shown in this paper. The polarization of W317 was measured to be around -130 nC/cm^2.[c]

For this experiment, a homogeneously aligned W317 cell was prepared using patterned indium-tin-oxide coated glass slides which were spin-coated with a nylon alignment layer and buffed unidirectionally. We measured the cell to be between 2 and 3μm thick.

Using the apparatus shown in figure 1, we measured the electroclinic tilt angle as a function of both applied field and temperature. The temperature was controlled by placing the cell in a computer controlled hot stage. A sinusoidal voltage of amplitude V_0 and frequency 200Hz was applied to the cell. This caused the molecules to tilt between $+\theta_0$ at $V = +V_0$ and $-\theta_0$ at $V = -V_0$. The applied voltage and the output signal from the detector were monitored on an oscilloscope. We rotated the cell in figure 1 until the transmission was a minimum at the point in time corresponding to $V = +V_0$. This meant that the molecular axis was parallel to one of the polarizers when the applied voltage was a maximum ($V = +V_0$). We then rotated the cell until a minimum transmission at $V = -V_0$ was reached. We measured the angle through which the cell was rotated to find $2\theta_0$. By changing the amplitude of the sine wave and the temperature of the cell, we measured θ as a function of V and T. Results are shown in figures 2 and 3.

---

[b] A. Rappaport, Department of Physics, Condensed Matter Laboratory, University of Colorado, Boulder CO 80309-0390, private communication.

[c] Measured by R. Shao, Department of Physics, Condensed Matter Laboratory, University of Colorado, Boulder, CO 80309-0390.
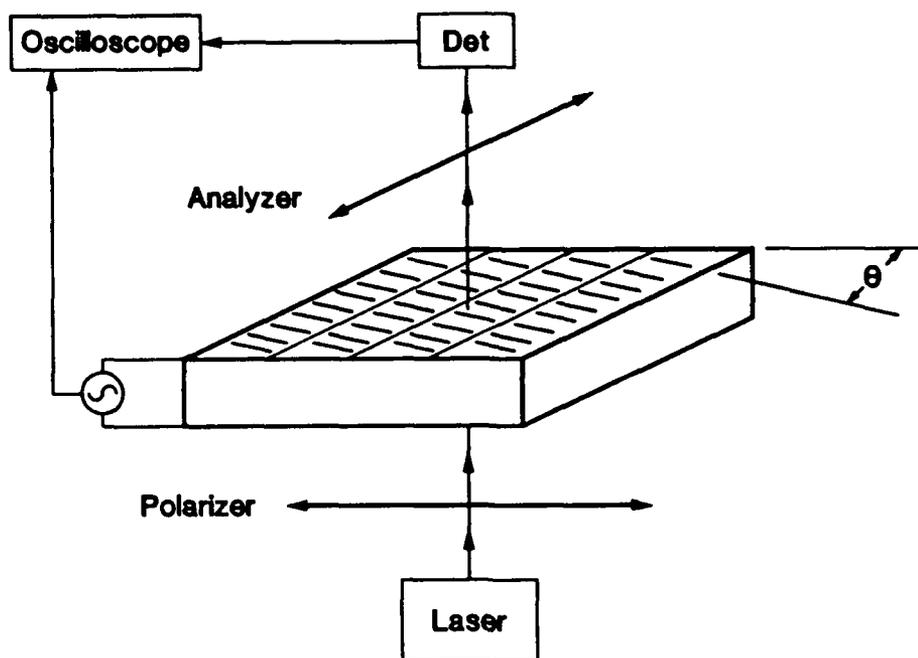
Figure 1. Experimental orientation of the cell between crossed polarizers.
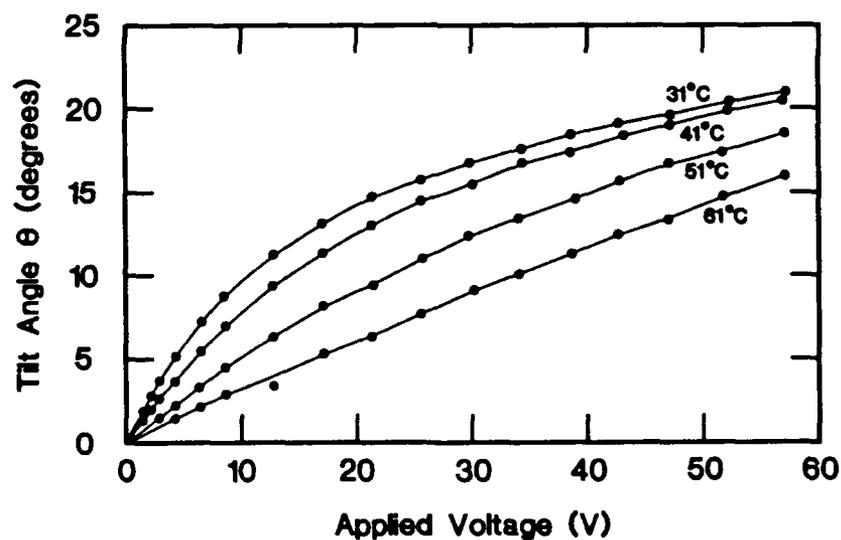
Figure 2. Electroclinic tilt vs applied voltage at several temperatures.

Figure 2 shows that unusually large tilt angles are achieved by relatively small voltages (fields) and that tilt angles in excess of 21° are possible. The measured tilt as a function of field is linear in field for small fields or high temperatures, and nonlinear for larger fields or lower temperatures. This agrees qualitatively with theoretical predictions[3,4] and experimental work on other
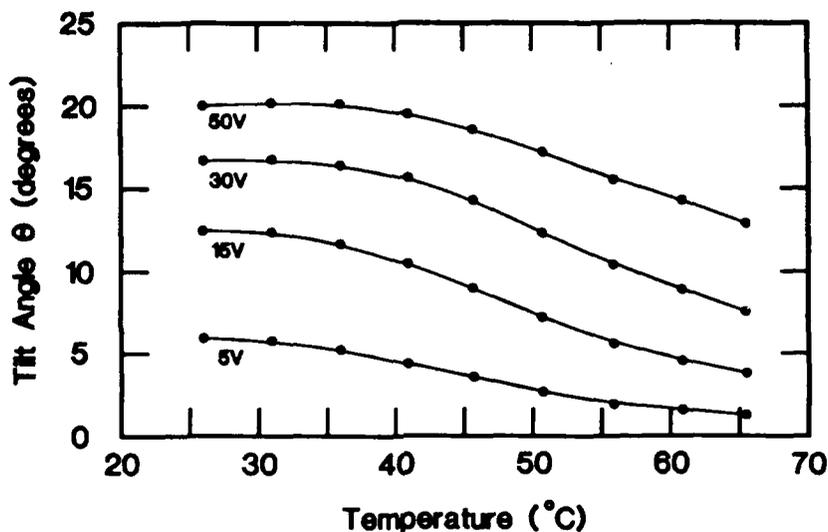
Figure 3. Electroclinic tilt vs temperature at various applied voltages.

electroclinic materials.[3,5,6] However, the behavior of the tilt vs temperature plots of figure 3 was unexpected. Typically, an electroclinic tilt vs temperature graph is concave up, with the tilt increasing dramatically as the temperature is reduced toward the bottom of the smectic A phase.[4,5,6] Although W317 shows this concave-up behavior at higher temperatures, the steep increase at lower temperatures is not seen. As a matter of fact, the tilt becomes almost independent of temperature at the lowest temperatures. This unusual behavior will be explored in the future.

REFERENCES

1.   S. Garoff and R.B. Meyer, Phys. Rev. Lett., **38**, 848 (1977).
2.   S. Garoff and R.B. Meyer, Phys. Rev. Lett., A **19**, 338 (1979).
3.   S.D. Lee and J.S. Patel, Appl. Phys. Lett., **54**, 1653 (1989).
4.   I. Abdulhalim and G. Moddel, Liquid Crystals, **9**, 493 (1991).
5.   S. Nishiyama, Y. Ouchi, H. Takazoe, and A. Fakuda, Jpn. J. Appl. Phys., **26**, L1787 (1987).
6.   G. Anderson, I. Dahl, W. Kuczynski, S.T. Lagerwall, K. Skarp, and B. Stebler, Ferroelectrics, **84**, 285 (1988).

IONIC TRANSPORT EFFECTS IN SSFLC CELLS

Zhong Zou, Noel A.Clark, and Mark A. Handschy[†]
Department of Physics and Center for Optoelectronic Computing Systems
University of Colorado, Boulder, Colorado 80309-0390
[†]*Displaytech Inc. 2200 Central Ave., Boulder, Colorado 80301*

<u>Abstract</u> In the surface stabilized ferroelectric liquid crystal cells, low frequency square waves with different DC offsets are applied in order to study the ionic transport properties. Transport equations have been solved numerically, and the results agree with the measurements qualitatively. By using a simple model, we clarify the fact that the measured current is different from the ionic flow current at the interfaces. Our calculation shows that, in cells with insulating alignment layers, due to the existence of ions, the fields at the interfaces can be many times larger than $\frac{V}{d}$, where V is the applied voltage and d is the spacing. From the calculations we get that the current peak time is roughly $\frac{d^2}{2\mu V}$ instead of the previous published $\frac{d^2}{\mu V}$, where μ is the mobility of the ions.

INTRODUCTION

Since the discovery of the Surface Stabilized Ferroelectric Liquid Crystal[1] (SS-FLC) device, its bistability and high switching speed has attracted attention to both its basics physics and applications.[2] It is known that there are always some ionizable molecules as impurities in SSFLC cells. The distribution and the transport processes of the ionic impurities modify the electric field distribution in FLC. Therefore, they can affect the device performance significantly. Current measurement is a common technique to study the electrical transport behavior of ions[3–7], but the fact that the measured current is different from the ionic drift current itself at the Liquid Crystal (LC) - Alignment Layer (AL) interfaces has been ignored[3–6]. In this paper, we first present our current measurement results, then using a very simple model illustrate that the measured current is not simply equal to $\mu E n|_{x=d}$. Next we use a computational method to solve the
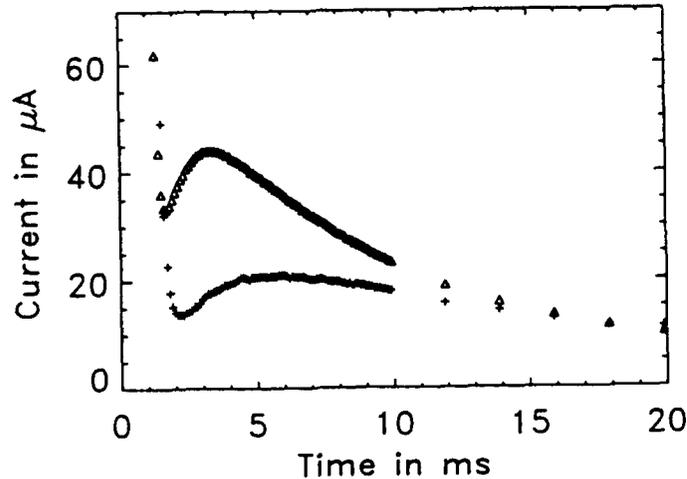
Figure 1: *SSFLC cell current vs time following a sign change in applied voltage from $-10V$ to $+10V$, (2Hz SQWV). $\triangle$ corresponds to the DC offset $V_0 = 0$, $+$ corresponds to the DC offset $V_0 = -5$.*

ionic transport equation to get the current and field distribution. The parameters used in this calculation are either from our experiment or from Chieu and Yang[4]. The calculated current curves qualitatively agree with our experiments. Finally, we conclude our observations in the last section.

EXPERIMENT

The SSFLC cells are filled with LC ZLI3654, doped with 0.2% by weight TMTTF-ODTCNQ. The AL is nylon and spacing is $1.8\mu m$. We measure the current with various applied voltages. In figure 1 and 2, the applied voltage is a $-10V$ to $+10V$ $2Hz$ Square Wave (SQWV) with DC offset $V_0 = 0$ or $-5V$. Fig.1 shows the current response following the transition from $-10V$ to $+10V$ in the applied voltage, while Fig.2 is case for the transition from $+10V$ to $-10V$. In figure 3, we measure the current with the applied voltage from $-10V$ to $+10V$ $2Hz$ SQWV with $V_0 = 0$ at $T = 27$ °C and $T = 37$ °C respectively. In all the three figures, the initial high values of the current curves are due to the switching of the polarization $\vec{P_s}$, which is well within $1ms$ of the voltage switching at time $t = 0$. The following current bumps are believed to be contributed by the
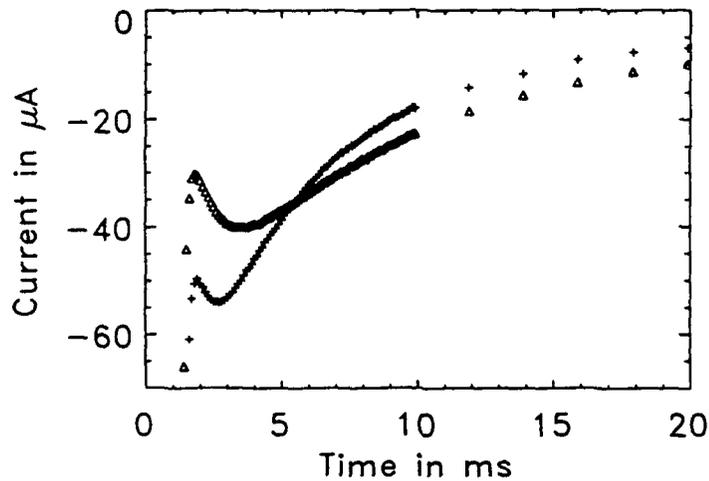
Figure 2: *SSFLC cell current vs time following a sign change in applied voltage from +10V to −10V, (2Hz SQWV). $\triangle$ corresponds to the DC offset $V_0 = 0$, + corresponds to the DC offset $V_0 = -5$.*
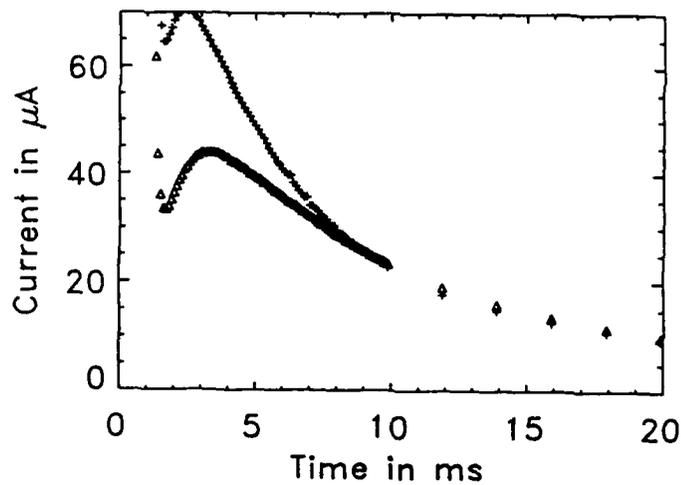
Figure 3: *SSFLC cell current vs time following a sign change in applied voltag from −10V to +10V, (2Hz SQWV), with zero DC offset. $\triangle$ corresponds tc $T = 27^0C$, + corresponds to $T = 37^0C$.*

(a)   **(b)**   **(c)**
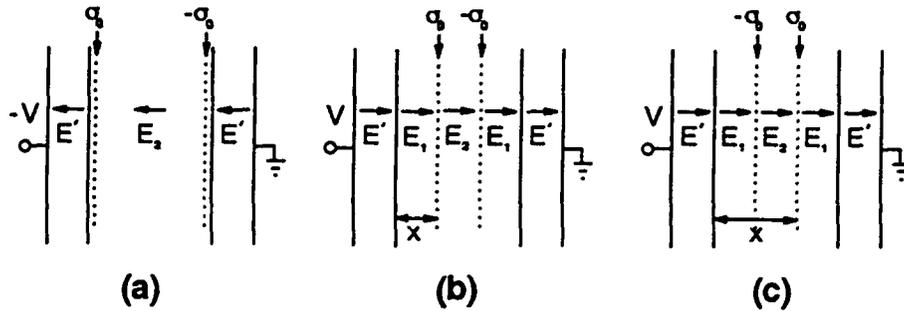
Figure 4: *With no diffusion, recombination and generation, the ion transport in the cell can be described by a simple model. (a) For $t < 0$, (b) for $0 < t \leq t_{1/2}$, (c) for $t_{1/2} < t < t_d$.*

transport of ions in the cell. The rest of this paper is aimed at explaining the ionic current bump. Due to the finite DC resistance of the cell, all the current finally decays to different constant values depending on the applied voltage.

A SIMPLE MODEL

The ionic drift current at the interfaces of LC and AL has been taken to be the measured current directly[3,4]. In this section, we illustrate, using a simple model in which approximation is not necessary, that the measured current and the ionic drift current are different. With the assumption that there are no diffusion, recombination and generation, the ion transport in the cell can be described by a simple model as shown in Fig.4. At $t < 0$, $-V$ voltage is applied to the cell. The ions accumulate at the LC and AL interfaces, shown in Fig.4(a). The applied voltage changes sign at $t = 0$, then the ionic charge sheets begin to move to the opposite interfaces. Fig.4(b) is the situation before the two sheets of charge meet at the cell middle while Fig.4(c) is after. The symbols and notations used are as following: E', ϵ', and d' are the electric field, dielectric constant and thickness of the AL; σ_0 is the ion sheet charge density; x is the distance between the left interface and σ_0 sheet; E_1 and E_2 are the electric field near the interfaces and at the middle respectively; ϵ is the dielectric constant of LC and d is the

spacing. For $t = 0^-$, we have the following equations:

$$\begin{cases} V = 2d'E'(0^-) + dE_2(0^-), \\ \sigma_0 = \epsilon'E' - \epsilon E_2(0^-), \end{cases} \tag{1}$$

which lead to

$$E_2(0^-) = \frac{V - \frac{2d'}{\epsilon'}\sigma_0}{d + 2d'\frac{\epsilon}{\epsilon'}}. \tag{2}$$

The direction of $E_2(0^-)$ must point to the left in Fig.4(a), therefore

$$\sigma_0 < \frac{\epsilon'}{2d'}V. \tag{3}$$

For $t = 0^+$, we have

$$\begin{cases} V = 2d'E' + dE_2 \\ \sigma_0 = -\epsilon'E' + \epsilon E_2, \end{cases} \tag{4}$$

which lead to

$$E' = \frac{V - \frac{d}{\epsilon}\sigma_0}{2d' + d\frac{\epsilon}{\epsilon}}. \tag{5}$$

Notice that when $\frac{\epsilon V}{d} < \sigma_0 < \frac{\epsilon'}{2d'}V$, Eq. (5) gives E' a negative value. That is when V changes sign, the electric field in the AL does not follow the sign change immediately. In the next section our calculation shows this situation.(c.f. Fig.11.)

Let $t_{1/2}$ be the time when two sheets of charge meet at middle, and t_d the time when they reach the opposite interfaces. For the time range $0 < t \le t_{1/2}$, shown in Fig.4(b), we have the following equations:

$$\begin{aligned} V &= 2d'E' + 2xE_1 + (d - 2x)E_2 \\ &= 2d'\frac{\sigma}{\epsilon'} + 2x\frac{\sigma}{\epsilon} + (d - 2x)\frac{\sigma + \sigma_0}{\epsilon}, \end{aligned} \tag{6}$$

$$\dot{x} = \mu E = \mu(\sigma + \frac{\sigma_0}{2}), \tag{7}$$

where σ_0 is the ionic sheet charge; μ is the mobility; σ is the free electron surface charge density accumulated on the electrode. The factor $\frac{1}{2}$ in Eq. (7) is due to the fact that $+\sigma_0$ charge sheet cannot feel the field produced by itself. For the time range $t_{1/2} < t < t_d$, shown in Fig.4(c), the following equations must be obeyed:

$$\begin{aligned} V &= 2d'E' + 2(d - x)E_1 + (2x - d)E_2 \\ &= 2d'\frac{\sigma}{\epsilon'} + 2(d - x)\frac{\sigma}{\epsilon} + (2x - d)\frac{\sigma - \sigma_0}{\epsilon}, \end{aligned} \tag{8}$$

$$\dot{x} = \mu E = \mu(\sigma - \frac{\sigma_0}{2}). \tag{9}$$
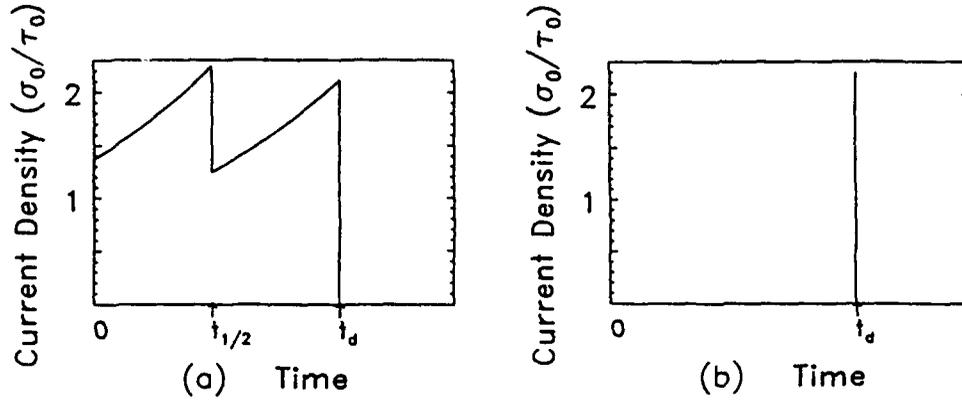
Figure 5: *Results of the simple model of Fig.4.* (*a*) *Space charge current* $J(t) = \dot{\sigma}$. *The first peak is corresponding to that the two sheets of ionic charge meet at the cell middle.* (*b*) *This is the ionic drift current at the interfaces.*

One can get the following solutions from equations (6) − (9):

$$\begin{cases} J(t) = \dot{\sigma} = J_0 e^{t/\tau_0} & 0 < t \le t_{1/2}, \\ J(t) = \dot{\sigma} = J_{1/2} e^{(t-t_{1/2})/\tau_0} & t_{1/2} < t < t_d, \end{cases} \quad (10)$$

where $\tau_0 = \frac{\epsilon d}{2\sigma_0 \mu}(1 + \gamma_1)$, and $\gamma_1 = \frac{2d'\epsilon}{\epsilon'd}$, $t_{1/2} = \tau_0 ln\frac{1+\frac{\gamma_2}{2}(1+\gamma_1)}{1-\frac{\gamma_2}{2}(1-\gamma_1)}$, and $\gamma_2 = \frac{d\sigma_0}{V\epsilon}$, $t_d = t_{1/2} + \tau_0 ln\frac{2+\gamma_2(1-\gamma_1)}{2-\gamma_2(1+\gamma_1)}$, $J_0 = \frac{\sigma_0}{\tau_0}\frac{1-\frac{\gamma_2}{2}(1-\gamma_1)}{\gamma_2(1+\gamma_1)}$, $J_{1/2} = \frac{\sigma_0}{\tau_0}\frac{1-\frac{\gamma_2}{2}(1+\gamma_1)}{\gamma_2(1+\gamma_1)}$.

The measured current in this simple model should be given by equations (10). When taking $\gamma_1 = 0.147$ and $\gamma_2 = 0.5$, we have the measured current as shown in Fig.5(a). The discontinuity at $t = t_{1/2}$ is due to the fact that the field produced by the ion charge sheets changes sign when they cross over each other at $t = t_{1/2}$. This gives rise to the first peak in the current shown in Fig.55(a). The ionic drift current at the interface $x = d$ is simply $J(t) = \sigma_0 \delta(t - t_d)$, Fig.5(b).

THEORY

In order to describe the transport properties of ions, the following coupled e-quations have been solved numerically.

$$\dot{n}^+ = Dn^+_{xx} + \mu n^+_x \phi_x + \mu n^+ \phi_{xx} + G - R \quad (11)$$

$$\dot{n}^0 = Dn^0_{xx} + R - G \tag{12}$$

$$\phi_{xx} = -\frac{q}{\epsilon}[n^+ - n^-] \tag{13}$$

$$R = \alpha n^+ n^- \tag{14}$$

$$G = \beta n^0 \tag{15}$$

The following boundary conditions have been used

$$J_{n^+} = \mu n^+ \phi_x + Dn^+_x = 0 \qquad x = 0, d, \tag{16}$$

$$J_{n^0} = Dn^0_x = 0 \qquad x = 0, d, \tag{17}$$

$$\phi - \frac{\epsilon d'}{\epsilon'}\phi_x = \frac{V(t)}{2} \qquad x = 0, \tag{18}$$

$$\phi + \frac{\epsilon d'}{\epsilon'}\phi_x = -\frac{V(t)}{2} \qquad x = d, \tag{19}$$

where n^+ and n^- are the positive and negative ion density respectively; n^0 is the neutral ionizable molecule density; ϕ is the electrical potential; G and R are the generation rate and the recombination rate of ions respectively. The diffusion constant D is given by $\mu\frac{kT}{q}$, where q is the unit charge, k is Boltzmann constant, and T is the temperature. The coefficient β is given by[4] $\beta = \beta_0 e^{-\frac{U_0 - \Delta U}{kT}}$ and $\Delta U = q(\frac{qE}{\pi\epsilon})^{\frac{1}{2}}$, where $E = |\phi_x(x, t)|$. The conservation of particles is guaranteed by

$$N_0 d = \int_0^d (n^+ + n^0)dx, \tag{20}$$

where N_0 is the total ionizable molecule density. The measured current is calculated from

$$J(t) = \dot{\sigma} = -\epsilon\dot{\phi}_x(0, t). \tag{21}$$

Eqs.(11) and (12) are the continuity equations for n^+ and n^0 with the generation and recombination terms included. Eq.(13) is the Poisson equation. Eqs.(16) and (17) simply mean that there are no ions and neutral molecules flowing in and out of the cell. Since we have observed a very similar current behaviour for different ALs and for both doped LC and undoped LC, the ion trapping at the interfaces has not been included to explain the ionic transport current. Eqs.(18) and (19) are the boundary conditions for the electrical potential.

In this paper we consider only one dominant ionizable molecule. Furthermore, we assume that the mobilities for both negative and positive ions are the
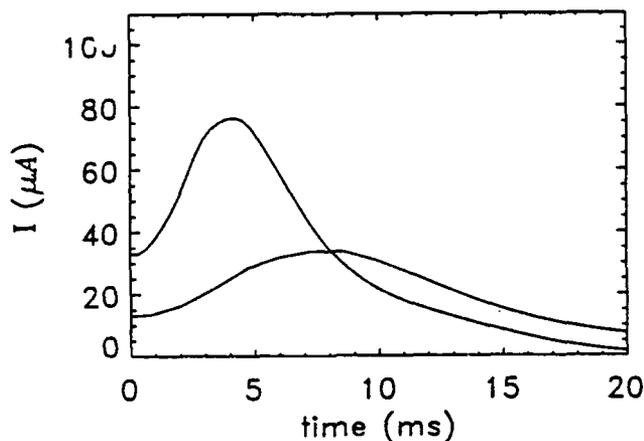
Figure 6: *The calculated current curves correspond the cases in Fig.1.*

same. Under the above assumptions, by symmetry, we have

$n^-(x,t) = n^+(d-x,t)$.

Under the conditions that, $G = 0$, $R = 0$, and $T \to 0$, the transport equations with the boundary conditions should reduce to the simple model in the previous section. Due to the numerical difficulties, we cannot let $T = 0$ in our program. So, we test our program with $T = 100K$, and get a very similar current shape (with two peaks) to that shown in Fig.5(a). When we raise temperature to the room temperature, and include the G and R terms with large enough recombination coefficient α, we get rid of the second peak with only the first peak in Fig.5(a) remaining. The remaining peak position $t_{1/2}$ is roughly equal to $\frac{d^2}{2\mu V}$, while in the previous publications[3-6] the peak position is taken to be $\frac{d^2}{\mu V}$.

There are many parameters in the transport equations, and most of them are unknown for our material. In order to measure those parameters directly or even indirectly we need better designed experiments. Our main goal in this paper is to have a correct qualitative physical picture of the ion transport process. In our calculations we use Chieu and Yang's parameters[4] except for d, N_0, and μ. We use that $d = 1.8\mu m$, $N_0 = 1.33 \times 10^{18} cm^{-3}$ estimated from 0.2% doping, and $\mu = 4 \times 10^{-7} \frac{cm^2}{V \cdot s}$ estimated from $t_{1/2} = \frac{d^2}{2\mu V}$.
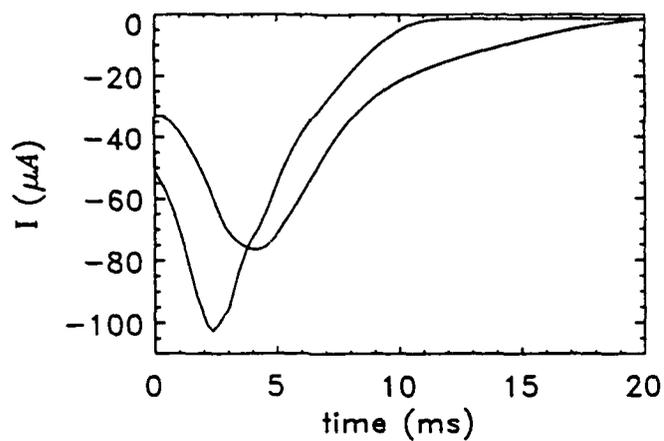
Figure 7: *The calculated current curves correspond the cases in Fig.2.*
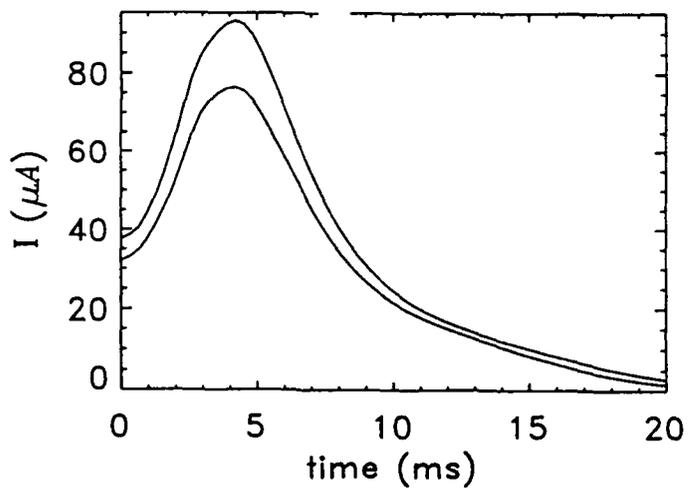
Figure 8: *The calculated current curves correspond the cases in Fig.3. The top curve is for $T = 310K$, the other is for $T = 300K$.*
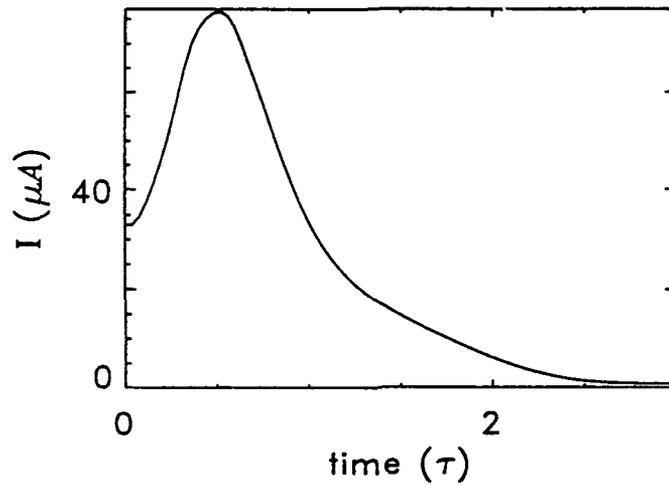
Figure 9: *This same curve as shown in Fig.6 with $V_0 = 0$, where $\tau = \frac{d^2}{\mu V}$. It is very clear that the peak position is not at $t = \tau$.*
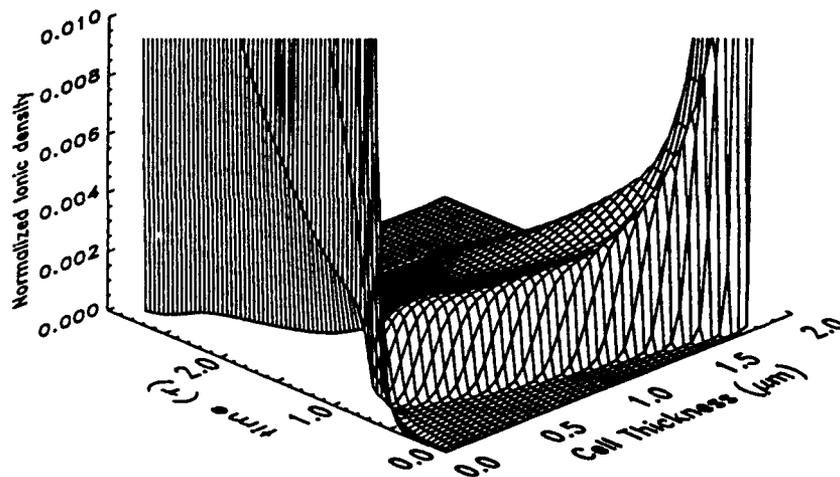
Figure 10: *The transport of positive ion density (with normalization $N_0 = 1$) corresponding to the current curve in Fig.9.*
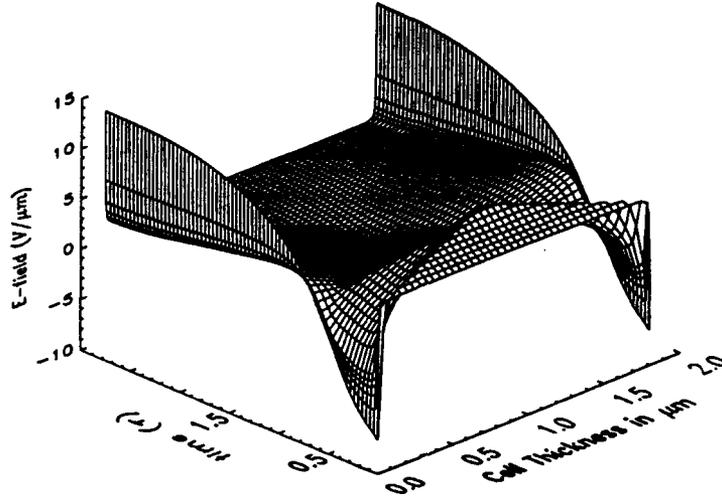
Figure 11: *The field distribution corresponding to Fig.9. In the steady state, the fields at the interfaces are a few times larger than $\frac{V}{d}$.*

The calculated current in Figs.6, 7, 8 are corresponding to the experimental measurements in Figs.2, 3, 4 respectively. We see that our calculations only qualitatively agree with the experiments. In order to get quantitative agreement between the measurements and the calculations, we need to include the field produced by the permanent polarization $\vec{P}_s(x,t)$ and also the finite DC resistivity of the ALs and the LC, in addition to have the correct parameters in the transport equations. We may also need to include the temperature and field dependence of the mobility. The current curve in Fig.9 is the same as that shown in Fig.6 with the DC offset $V_0 = 0$, but with the time unit τ, where $\tau = \frac{d^2}{\mu V}$. Here we see clearly that the current peak position is roughly at $\frac{1}{2}\tau$. The $n^+(x,t)$ and $E(x,t)$ corresponding to the current shown in Fig.9 are plotted in Figs.10 and 11 respectively. Notice that the field near the interface (therefore in the ALs) does not follow the sign change of the applied voltage immediately, (c.f. Fig.11), due to the existence of ions. In the previous section, we have illustrated the possibility of this case. Our calculation, Fig.11, also shows that, due to the very nonuniform distributions of the ions, in the steady state the fields at the interfaces are much larger than the field at the cell center. This shall have importance in the interface properties of AL and LC, and have a strong effect

on the molecular orientation dynamics on the LC and AL interfaces.

CONCLUSIONS

We have proved that for cells having insulating ALs the measured current is not the ionic flow current at the interfaces. We have also shown that the ionic current bump occurs when the two sheets of ionic charge meet at the middle of the cell, and the peak time is roughly $\frac{1}{2}\tau$ instead of τ as believed before by other authors. Our calculation also shows clearly that at the steady state the fields at the interfaces are much larger than $\frac{V}{d}$.

ACKNOWLEDGMENT

REFERENCES

[1] N. A. Clark and S. T. Lagerwall, Appl. Phys. Lett., 36, 889 (1980).
[2] Proceedings of the International Ferroelectric Liquid Crystal Conferences:
First, Ferroelectrics, Vol.84-85;
Second, Ferroelectrics, Vol.113-114;
Third, Ferroelectrics, to be published.
[3] J. Vaxiviere, B. Labroo, and Ph. Martinot-Largarde, Mol. Cryst. Liq. Cryst., 173, 61 (1989).
[4] T. C. Chieu and K. H. Yang, Jpn. J. Appl. Phys., 28, 2240 (1989).
[5] B. Y. Zhang, M. Yoshida, H. Mada, M. Kimura, H. Sekine, and S. Kobayashi, The XIII International Liquid Crystal Conference (Vancouver, Canada, 1990).
[6] K. Saxena, S. S. Bawa, A. M. Biradar, S. Chandra , and R. Rup, Jpn. J. Appl. Phys., 29, 2041 (1990).
[7] B. Maximus, E. Deley, A. DeMeyere, and H. Pauwels, presented in the Third International FLC Conference, Boulder, Colorado, (1991), to be published in Ferroelectics.

SECTION C
NEW MATERIALS

DESIGN, SYNTHESIS AND PROPERTIES OF NEW FERROELECTRIC LIQUID CRYSTALLINE COMPOUNDS HAVING A CHIRAL CENTER DIRECTLY CONNECTED TO THE CORE AROMATIC RING

TAMEJIRO HIYAMA*, TETSUO KUSUMOTO
Sagami Chemical Research Center
4-4-1 Nishiohnuma, Sagamihara, Kanagawa 229, Japan

SADAO TAKEHARA
Central Research Laboratories, Dainippon Ink Chemicals, Inc.
631 Sakado, Sakura, Chiba 285, Japan

Abstract Synthesis and opto-electrical properties of new chiral dopants α-aryl-γ-alkyl-γ-lactones, 3-aryl-5-alkyl-oxazolidin-2-ones and 2-alkyl-1-aryl-1-cyanocyclopropanes for ferroelectric liquid crystals are discussed.

INTRODUCTION

In 1980 Clark and Lagerwall suggested that thin cells containing ferroelectric liquid crystals (FLCs) might be applicable to high-speed switching devices.[1] The switching time depends on the magnitude of spontaneous polarization (Ps) and viscosity of the FLCs. The FLC materials are usually prepared by mixing a chiral dopant possessing large Ps values with achiral smectic C (S_C) host liquid crystal mixtures of low viscosity. For chiral dopants various optically active compounds have been designed. In particular, we have proposed chiral dopants having commonly a chiral center connected directly both to a core aromatic ring and to a polar group and have shown that these actually exhibit large Ps values.[2] We discuss the synthesis and opto-electrical properties of α-aryl-γ-alkyl-γ-lactones 1[3] and 1', 3-aryl-5-alkyloxazolidin-2-ones 2 and 2-alkyl-1-aryl-1-cyanocyclopropanes 3.[4]

1 (R = H)
1' (R = Me)

2

3
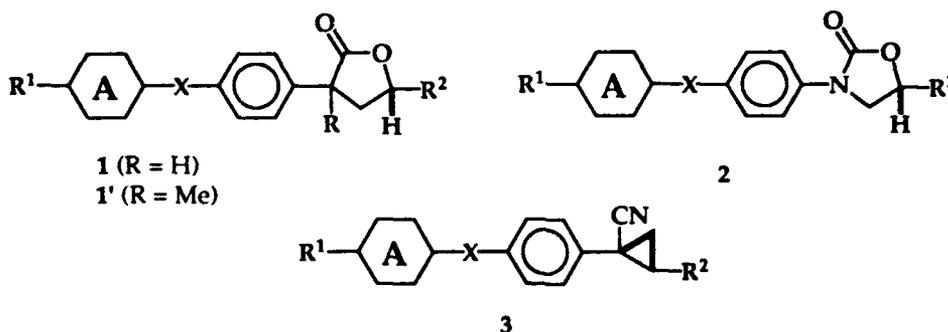
host liquid crystals mixture A (see the footnote a of Table 1). The results summarized in Table 1 demonstrate that the cis-isomer of 1 exhibits Ps over +4 nC/cm^2 when added by 2 wt%. In particular a mixture containing 4 wt% of 1a showed +12.7 nC/cm^2 and response time (τ_{0-90}) less than 100 µs. In sharp constrast, the trans-isomer 1b did not show any measurable Ps. The striking difference may be ascribed to the conformation of each isomer as shown in Fig 1. The diople moment of the cis-lactone directs nearly perpendicular to the plane of the axes of the core and alkyl chain, whereas that of the trans-lactone is closely parallel to the planes of the core and alkyl side chain. In view of the well-discussed zig-zag model of FLC molecules, the former conformation should be particularly important for high Ps to be realized.

cis   trans
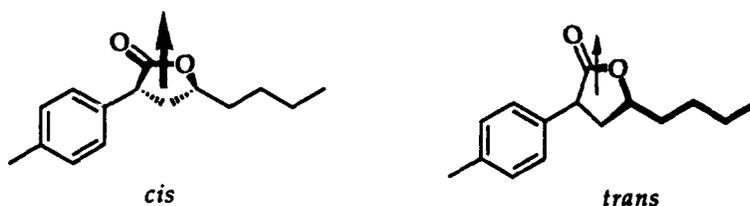
FIGURE 1   Conformation of cis- and trans-lactones Computed by MM2 and MOPAC.

The lactones 1' having methyl at its α- or benzylic position induced less Ps than the unsubstituted ones. To our surprise, the trans-lactone exhibited larger Ps than the cis-lactone. We prepared cis- and trans-δ-lactones 1" also, both of which exhibited small Ps's.

1'   1"
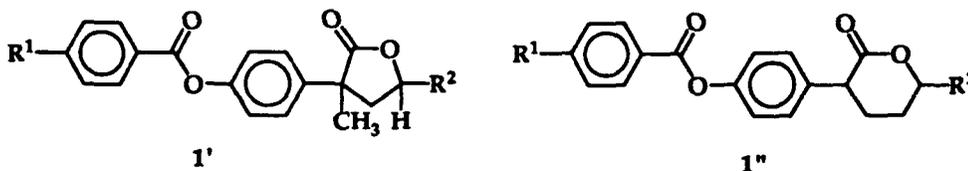
OXAZOLIDINONES

In order to reduce the stereoisomeric problem of 1, we designed and synthesized 3-aryl-5-alkyloxazolidin-2-ones 2 according to Scheme 2. The synthesis is straightforward. N-Anisylurethane was reacted with a chiral epoxide to give the target material in a single step. Deprotection followed by esterification gave the desired materials 2a-2c, which showed better liquid crystallinity, exhibiting higher order of smectic, S_A and/or

The ferroelectric liquid crystal mixtures doped with one of these exhibited high spontaneous polarizations and short response times of high level. The sign of Ps was found to correlate well to the absolute configuration of the benzylic chiral center of the dopant.

γ-LACTONES

Synthesis of the lactones 1 is carried out according to the procedures shown in Scheme 1. The enolate of 4-methoxyphenylacetonirile or the dienolate of 4-methoxyphenylacetic acid was allowed to react with (R)-1,2-epoxyoctane. Subsequent lactonization afforded a mixture of cis- and trans-γ-butyrolactones. Each was separated by column chromatography and demethylated to give a phenol which upon esterification with various aroyl chlorides yielded the desired lactones 1a-1c. Using an optically active epichlorohydrin, the γ-lactones 1d and 1e were prepared.

i: n-BuLi, (R)-1,2-epoxyoctane; ii: KOH
iii: $SOCl_2$; iv: p-$CH_3C_6H_4SO_3H$
v: EtSH, $AlCl_3$ or Me_2S, $AlCl_3$
vi: 4-(n-C_8H_{17}O)C_6H_4COCl, pyridine
vii: n-BuLi, (R)-epichlorohydrin
viii: NaH; ix: n-PrMgBr, CuI
x: 4-(n-C_8H_{17})C_6H_4COCl, pyridine
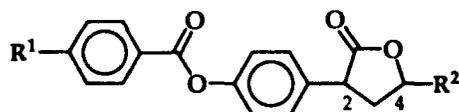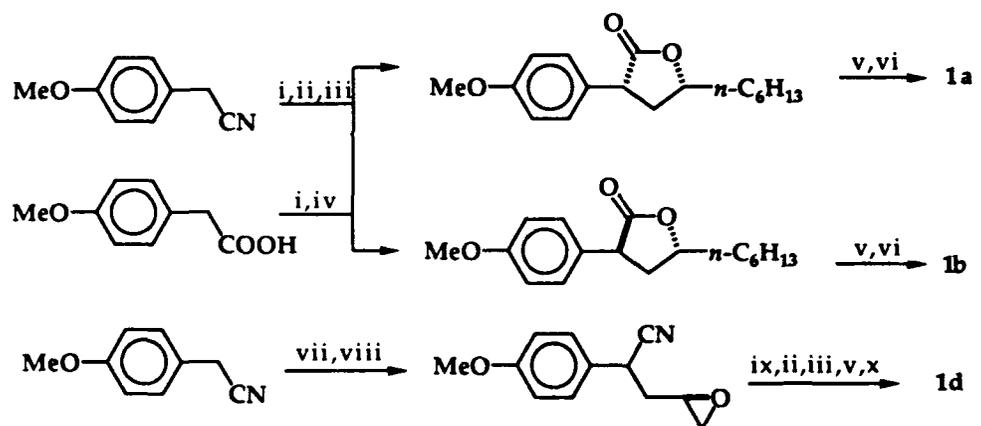
1a: 2R,4R (cis), R^1 = n-C_8H_{17}O, R^2 = n-C_6H_{13}
1b: 2S,4R (trans), R^1 = n-C_8H_{17}O, R^2 = n-C_6H_{13}
1c: 2R,4R (cis), R^1 = n-C_8H_{17}, R^2 = n-C_6H_{13}
1d: 2S,4S (cis), R^1 = n-C_8H_{17}, R^2 = n-C_4H_9
1e: 2S,4S (cis), R^1 = n-C_8H_{17}, R^2 = n-CH_3

SCHEME 1   Synthetic Route to γ-Lactones 1.

As compounds 1a-1e did not exhibit chiral smectic C (Sc*) phase, we employed them as chiral dopants for achiral Sc liquid crystals. Thus, each lactone was added to a

chiral nematic (N*) phase but no S$_C$*. The oxazolidinone 2a was added to Host A or B by 5 or 10 wt%. As compared with 1a, the Ps of the mixture was about half and accordingly response time was roughly doubled at 5 wt% in Host B. Taking into account that trans-lactone 1b did not exhibit measurable Ps, the conformation of 2a seems to be the one in between cis-lactone 1a and trans-isomer 1b, resulting in roughly half of Ps. That at higher concentrations 2a-2c did not realize fast switching as compared 1 should be ascribed to high viscosity of the oxazolidinone moiety.

i: (R)-1,2-epoxyoctane, NEt$_3$　　2a: R = n-C$_8$H$_{17}$O　　　Cr 109 S$_X$ 147 I
ii: BBr$_3$　　　　　　　　　　　2b: R = n-C$_8$H$_{17}$　　　Cr 107.5 S$_A$ 127 N* 127.1 I
iii: ArCOCl, pyridine　　　　　　2c: R = (S)-CH$_2$CHMeEt Cr 93 N* 99 I
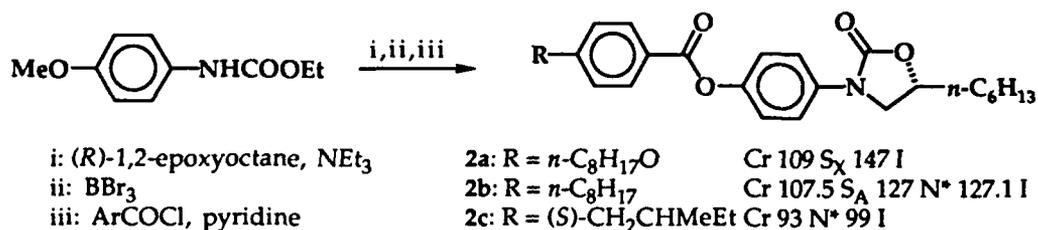
SCHEME 2　Synthesis of Oxazolidinones 2.

CYANOCYCLOPROPANES

Synthesis of cyanocylopropanes 3a-3c and 3e is achieved according to Scheme 3, which involves addition of the lithium enolate of 4-methoxyphenylacetonitrile to (R)-1,2-epoxyoctane, tosylation of the resulting hydroxyl group, ring closure with a base, demethylation, followed by esterification. The cis/trans isomer ratio was controllable by a proper choice of the base: sodium hydride gave the trans-isomer as a nearly exclusive product, whereas potassium t-butoxide gave a 1 : 1 mixture. Benzyl ether 3d was prepared by benzylation in stead of esterification. The nitriles 3a-3e were added to Host B or C to show relatively large Ps as summarized in Table 1. It is noteworthy that 3a and 3b showed similar opto-electrical properties, only the difference being the sign of Ps. Response times in Host B are short enough. Particular attention should be paid to 3e which upon addition by 10 wt% to Host B realized extremely fast response time of 67 μs.

3a: 1R,2S, R = 4-[4-(n-C$_8$H$_{17}$O)C$_6$H$_4$]C$_6$H$_4$COO　　　　　　Cr 70 S$_X$ 114 S$_A$ 136 I
3b: 1S,2S, R = 4-[4-(n-C$_8$H$_{17}$O)C$_6$H$_4$]C$_6$H$_4$COO　　　　　　Cr 48 S$_X$ 50 I
3c: 1R,2S, R = 4-(n-C$_8$H$_{17}$O)C$_6$H$_4$COO　　　　　　　　　　　Cr 25 I
3d: 1R,2S, R = 4-[4-(n-C$_8$H$_{17}$O)C$_6$H$_4$]C$_6$H$_4$CH$_2$O　　　　　Cr 61 S$_{X2}$ 74 S$_{X1}$ 97 S$_A$ 101 I
3e: 1R,2S, R =4-[4- [(S)-n-C$_3$H$_7$OCHMeCOO]C$_6$H$_4$]C$_6$H$_4$COO Cr 49 (S$_A$ 47) I

In addition, the helical pitch of this mixture at N* phase was extremely large. Accordingly, this may find practical application to FLC display material.
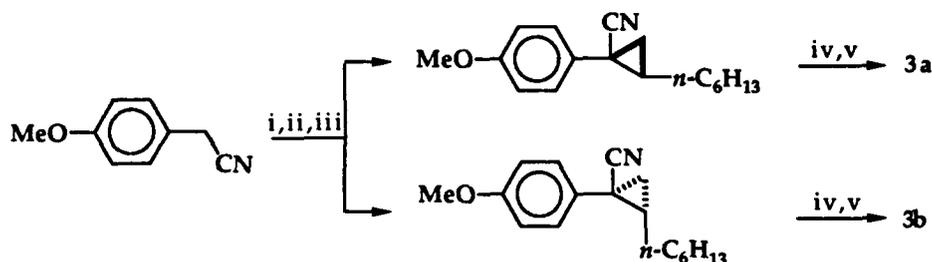
i: n-BuLi, (R)-1,2-epoxyoctane; ii: TsCl, pyridine, 4-Me$_2$NC$_5$H$_4$N
iii: NaH or t-BuOK; iv: Me$_2$S, AlCl$_3$; v: 4-[4-(n-C$_8$H$_{17}$O)C$_6$H$_4$]C$_6$H$_4$COCl, pyridine

SCHEME 3   Synthesis of Cyanocyclopropanes 3.

CORRELATION OF THE SIGN OF Ps TO THE ABSOLUTE CONFIGURATION

We have reviewed synthesis and opto-electrical properties of FLC materials containing a ring structure with a chiral center at the benzylic position.[2-4] During these studies we have observed that the sign of Ps correlates well to the absolute configuration of the benzylic chiral center. The results are summarized in Fig 2. Those having a polar functional group of α-configuration at benzylic chiral center showed +Ps, whereas those of β-configuration exhibited -Ps. This empirical rule is attributed to the zig-zag model[5] of FLCs shown in Fig 3. The FLC materials are so aligned as that the polar group is disposed parallel to the applied electric field. Due to the restricted free rotation around the chiral benzylic center, large Ps is induced as we anticipated. Thus, the benzylic chiral center mainly contributes to Ps, other chiral center(s) to less extent. Based on the empirical rule, we can determine the absolute configuration of a benzylic chiral center. For example, we prepared (3R)-2-(4-methoxyphenyl)-3-methylnonanenitrile (Scheme 4) whose C-2 configuration remained unknown. The FLC material **4a** derived from the nonpolar isomer, when added by 5 wt% to Host C, exhibited -5.7 nC/cm^2; the other **4b** derived from the polar isomer exhibited +5.9 nC/cm^2. Based on the empirical rule, the absolute configurations of **4a** and **4b** were deduced to be (2S,3R) and (2R,3R) respectively. This assignment was supported by chemical synthesis. Nmr spectra of (2S*,3R*)- and (2R*,3R*)-nitriles prepared by the hydrogenation of structurally well-defined unsaturated nitriles (Scheme 5) were identical with the precursors of **4a** and **4b** respectively.

Ps (+)

Ps (-)
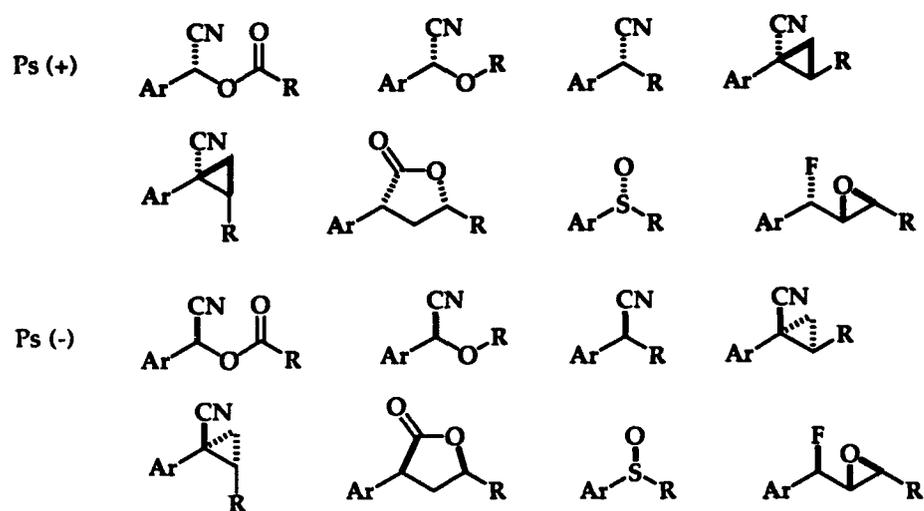
FIGURE 2   Sign of Ps *vs* Absolute Configuration.

Ps +

Ps -
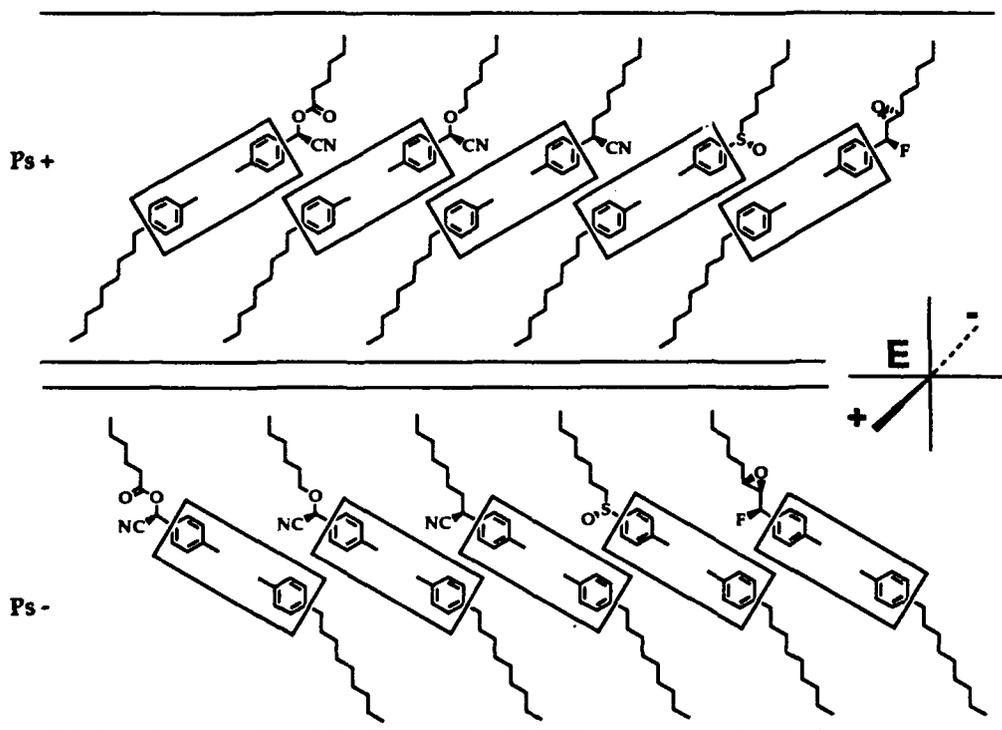
FIGURE 3   Alignment of FLC molecules in an Electric Field.

MeO—⬡—CN —i→ MeO—⬡—CN

n-C$_8$H$_{17}$O—⬡—⬡—C(=O)—O—⬡—CN

ii,iii

4a (nonpolar) Cr 104 S$_A$ 122 I

n-C$_8$H$_{17}$O—⬡—⬡—C(=O)—O—⬡—CN

4b (polar) Cr 106 S$_A$ 111 I

i: n-BuLi, (S)-TsOCHMen-C$_6$H$_{13}$; ii: Me$_2$S, AlCl$_3$
iii: 4-[4-(n-C$_8$H$_{17}$O)C$_6$H$_4$]C$_6$H$_4$COCl, pyridine
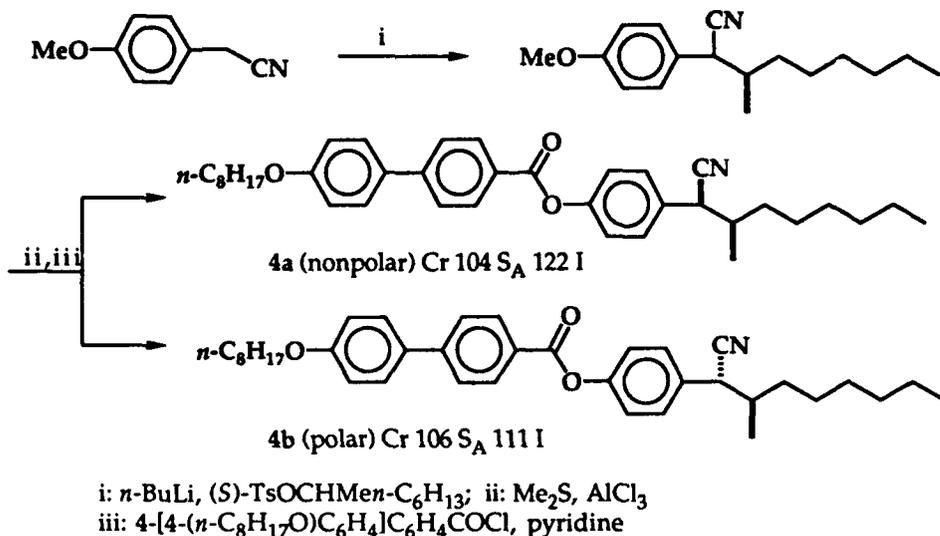
SCHEME 4 Preparation of Cyano-Substituted FLC 4.

MeO—⬡—C(CN)=C(CH$_3$)— —i→ MeO—⬡—CN

MeO—⬡—C(CN)=C(CH$_3$)— —i→ MeO—⬡—CN

i: H$_2$, Rh/C
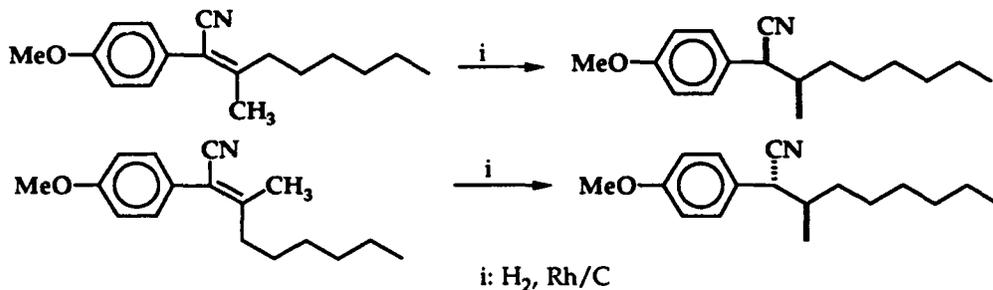
SCHEME 5 Preparation of Authentic Diastereomers.

CONCLUSION

Our study on the design and synthesis of new FLC materials led to a ring structure which connects directly to core aromatic rings and contains chiral center(s) and a polar functional group therein. This design principle may allow us to explore further advanced materials.

REFERENCES

1. N. A. Clark and S. T. Lagerwall, *Appl. Phys. Lett.*, 1980, *36*, 899.
2. T. Kusumoto, T. Ueda, T. Hiyama, S. Takehara, T. Shoji, M. Osawa, T. Kuriyama, K. Nakamura, and T. Fujisawa, *Chem. Lett.*, 1990, 523; K. Nishide, A. Nakayama, T. Kusumoto, T. Hiyama, S. Takehara, T. Shoji, M. Osawa, T. Kuriyama, K. Nakamura, and T. Fujisawa, *Chem. Lett.*, 1990, 623; T. Kusumoto, T. Hanamoto, T. Hiyama, S. Takehara, T. Shoji, M. Osawa, T. Kuriyama, K. Nakamura, and T. Fujisawa, *Chem. Lett.*, 1990, 1615; T. Kusumoto, T. Hanamoto, K. Sato, T. Hiyama, S. Takehara, T. Shoji, M. Osawa, T. Kuriyama, K. Nakamura, and T. Fujisawa, *Tetrahedron Lett.*, **31**, 5434 (1990).

3. T. Kusumoto, A. Nakayama, K. Sato, K. Nishide, T. Hiyama, S. Takehara, T. Shoji, M. Osawa, T. Kuriyama, K. Nakamura, and T. Fujisawa, *J. Chem. Soc., Chem. Commun*, **1991**, 311.
4. T. Kusumoto, A. Nakayama, K. Sato, T. Hiyama, S. Takehara, T. Shoji, M. Osawa, T. Kuriyama, K. Nakamura, and T. Fujisawa, *Tetrahedron Lett.*, **32**, 939 (1991).
5. J. W. Goodby, E. Chin, T. M. Leslie, J. M. Geary, and J. S. Patel, *J. Am. Chem. Soc.*, **108**, 4729 (1986); D. M. Walba, S. C. Slater, W. N. Thrumes, N. A. Clark, M. A. Handschy, and F. Supon, *ibid.*, **108**, 5210 (1986).

TABLE 1   Opto-electrical properties of **1**, **2**, and **3** in achiral host at 25 °C.

Compound	(wt%)	Host[a]	Ps (nC/cm^2)[b]	τ_{0-90} (μs)[c]	Tilt Angle (deg)	Twist Sense[d]
1a	(2)	A	+4.5	162	25	left
1a	(4)	A	+12.5	98	24	left
1a	(5)	B	+14.5	119	25	left
1b	(10)	A	-~0	891	14	left
1c	(2)	A	+4.4	153	26	left
1d	(2)	A	-4.2	169	24	right
1e	(2)	A	-4.1	171	23	right
2a	(5)	B	+7.7	235	21	left
2a	(10)	B	+26.3	139	21	left
2b	(2)	A	+3.2	192	24	left
2b	(5)	B	+8.2	178	21	left
2b	(10)	B	+20.6	121	22	left
2c	(5)	B	+4.8	181	18	left
3a	(5)	C	+3.3	200	27	left
3b	(5)	C	-3.1	228	24	left
3c	(5)	C	+7.4	158	26	e
3d	(5)	C	+7.0	154	26	left
3d	(5)	B	+4.3	128	15	left
3e	(5)	B	+8.8	82	19	e
3e	(10)	B	+20.5	67	19	e

[a]Host A: Cr 14 S_C 56 S_A 65 N 70 I; Host B: Cr -3 S_C 43 S_A 65 N 77 I; Host C: Cr 13 S_C 69 S_A 74 N 84 I.

[b] The liquid crystal mixture was sealed in a polyimide rubbing cell of 2 μm thickness, and a square wave of 10 V_{p-p}/μm was applied to the cell. Ps was measured by the triangular wave method.

[c]The change of transmittance (from 0% to 90%) of light was observed.

[d]Helical sense was observed with respect to N* phase of the mixture.

[e]The helical pitch was too large to be measured.

SYNTHESIS AND PHYSICAL PROPERTIES OF NOVEL PHENYLBENZOATE TYPE FERROELECTRIC LIQUID CRYSTALS

K.FUJISAWA*, C.SEKINE*, Y.UEMURA*, T.HIGASHII**, M.MINAI** AND I.DOHGANE**

*Tsukuba Research Laboratory, Sumitomo Chemical Co., LTD.
6 Kitahara, tukuba, Ibaraki 300-32, Japan

**Organic Synthesis Laboratory, Sumitomo Chemical Co., LTD.
10-1,2-chome, Tsukahara, Takatsuki city, Osaka 569, Japan

ABCTRACT

A relationship between molecular structure and physical properties of novel 2- and 3-ring phenylbenzoate derivatives is reported. In these compounds, the chiral carbon is directly linked to the core aromatic ring, or to the methylene unit which is linked to the core aromatic ring.The internal methylene unit plays an important role to exhibit the liquid crystal phases in 2-ring phenylbenzoate.

$$R_1 \left(\text{\textcircled{}} \right)_l X \left(\text{\textcircled{}} \right)_m (CH_2)_n \overset{CH_3}{\underset{|}{\overset{*}{C}HO}} R_2 \quad (\,I\,)$$
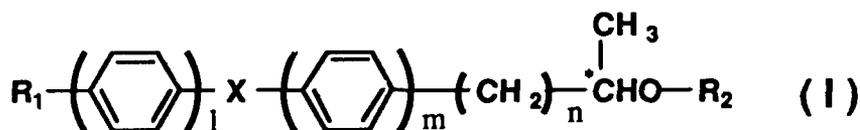
where X=-COO- or -OCO-
l+m=2 or 3, l≥1, m≥1, n≥1
R1=alkyl or alkoxyl
R2=alkyl or alkanoyl

INTRODUCTION

With the increase of interest of ferroelectric liquid crystals, there has been considerable amount of efforts in the sysnthesis and evaluation of the compounds exhibiting Sc* phase.   Many kinds of phenylbenzoate derivatives are reported elsewhere [1,2,3,4].   But those phenyl benzoate derivatives usually have hetero atom between the core aromatic ring and the chiral carbon.

We have prepared new series of 2- and 3- aromatic ring phenylbenzoate derivatives (I) and examined their physical properties as ferroelectric liquid crystals.   In these compounds, there is no ester or ether group between core aromatic ring and chiral carbon atom, that is, the chiral carbon atom is directly linked to aromatic ring in the mesogenic core, or to internal methylene unit which are linked to the aromatic ring.   Various structural modification of mesogenic core, terminal chain and internal methylene chain in such a phenylbenzoate derivatives have been made to investigate the relationship between molecular structure and physical properties.

The purpose of this paper is to study the relationship between molecular structure and physical properties in 2- and 3-ring phenylbenzoate derivatives, and the effect of introduction of methylene -CH_2- unit between the mesogenic core and the chiral c? bon.

In this paper, we focus ...y on same interesting relationship between molecular structure and physical properties of our phenylbenzoate derivatives. Complete FLC properties of all these materials will be reported elsewhere.

Experimentals
Synthesis

Synthetic route is given in SCHEME 1 and 2, and the details of synthetic procedures were reported already[5].   The optically active alcohols were prepared from the corresponding acetete compounds by the method of asymmetric hydrolysis using lipase.   The selectivities of asymmetric hydrosis on the substrate depend on the length of internal methylene chain in the
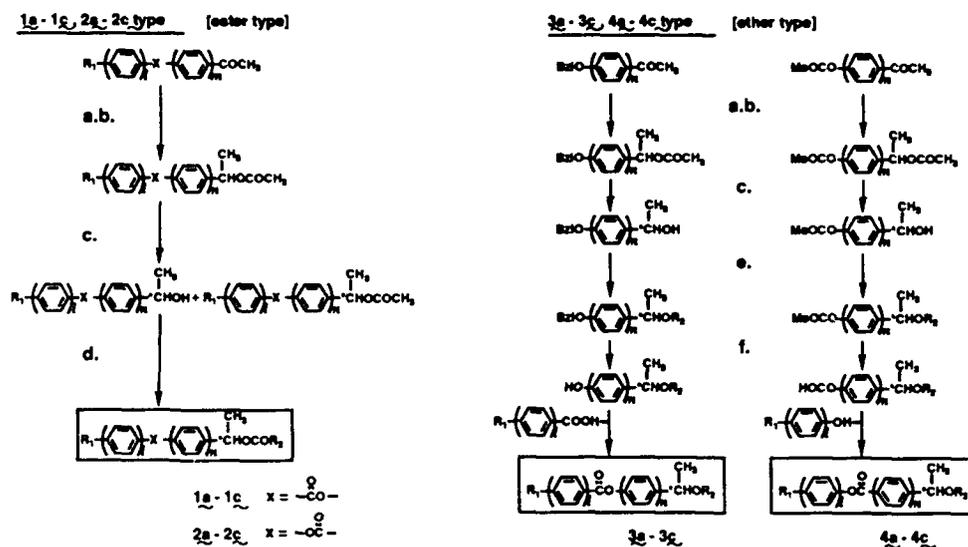
(a)NaBH4, (b)CH3COCl-Pyr., (c)lipase, (d)R2COCl-Pyr., (e)NaH-R2X, (f)deprotection

SCHEIME 1

i.)R2l/Ag2O ii.)MCPBA→OH⁻ iii)NaBrO
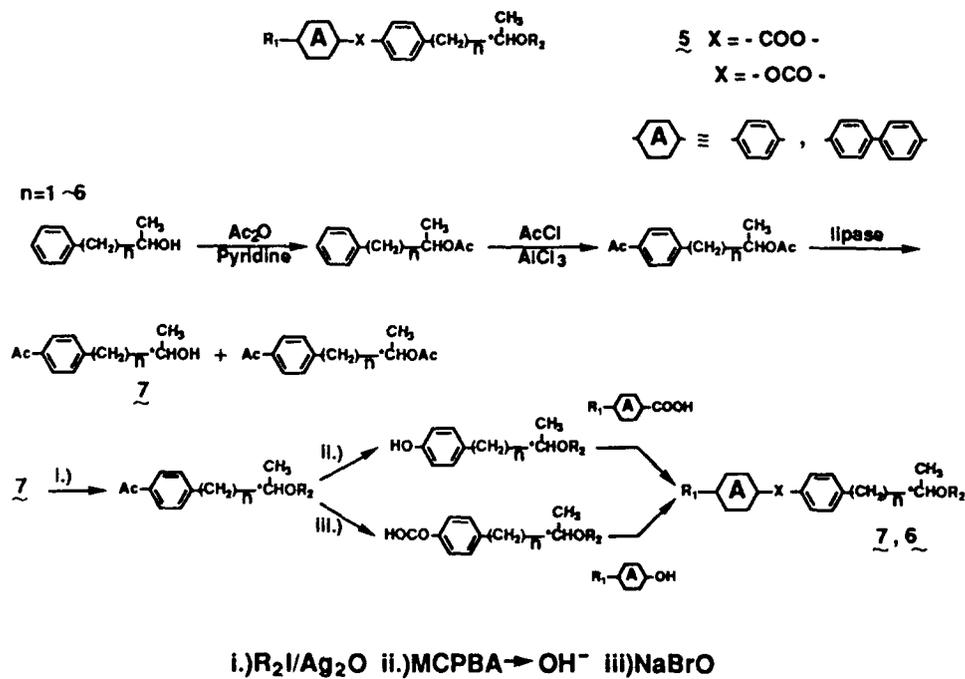
SCHEME 2

acetate compounds.   Final products obtained by these procedures were purified by a column chromatograph on silica gel and by recrystallization from ethyl alcohol.   The optical active purities of these compounds were more than 95%ee.

Measurements

Physical parameters were measured by using homogeneously aligned ITO coated glass cells of 2.0μm thickness which were prepared by rubbing thin polyimide films coated on the substrate plates.

The phase sequence and the transition temperature were measured by using DSC and a polarizing optical microscope with a hot stage. The spontaneous polarization was evaluated by using the triangle wave method[6]. The frequency was 100Hz and the amplitude was ±10V/μm. The rotational viscosity was evaluated by the method of Fukuda et al[7]. Response time was measured from the full width at half maximum of polarization current peak.

RESULTS AND DISCUSSION

We have most extensively examined the structure/ properties relationship of 2- and 3-ring phenylbenzoate derivatives with the chiral carbon directly linked to core aromatic ring. TABLE 1 shows the relationship between the mesogenic core structure and the physical properties in a series.   In this series the achiral alkyl tail and the chiral alkyl tail were fixed, and the number and position of aromatic rings, the direction of ester group against chiral carbon and the magnitude of dipole moment near chiral center were varied.   2-ring phenylbenzoates in which the chiral carbon is directly linked to core aromatic ring do not exhibit mesophase regardless of the direction of ester group against chiral carbon and the structure near the chiral carbon, ester group or ether group.   3-ring phenylbenzoates exhibit liquid crystal phases regardless of the core structure, i.e., the position of aromatic ring and the direction of ester group. The direction of ester group against chiral carbon determines the type of phase sequence.   Those compounds which have -COO- type ester group exhibit S_A phase without exception in this case.   The sign of the

TABLE1 The effect of mesogenic core structure on physical properties.

R_1	$-(\text{ring})_l$ X $-(\text{ring})_m$	$\overset{CH_3}{\underset{\cdot}{\cdot}CHO(CO)C_6H_{13}}$	Phase Series	θ	Ps [nC/cm²]
$C_8H_{17}O-$	-⬡ OCO-⬡-⬡-	$\overset{CH_3}{\cdot}CHOC_6H_{13}$	K———Sc*———Ch—I	37.5	76.0
	-⬡-⬡ OCO-⬡-		K———Sc*————I	42.0	48.0
	-⬡ COO-⬡-⬡-		K————SA————I	—	—
	-⬡-⬡ COO-⬡-		K———Sc*-SA————I	27.0	76.8
	-⬡ OCO-⬡-		K————————I	—	—
	-⬡ COO-⬡-		K————————I	—	—
$C_8H_{17}O-$	-⬡ OCO-⬡-⬡-	$\overset{CH_3}{\cdot}CHOCOC_3H_{11}$	K—S₁————————I	—	—
	-⬡-⬡ OCO-⬡-		K———Sc*————I	20.0	114.0
	-⬡ COO-⬡-⬡-		K————SA———I	—	—
	-⬡-⬡ COO-⬡-		K————SA———I	—	—
	-⬡ OCO-⬡-		K————————I	—	—
	-⬡ COO-⬡-		K————————I	—	—

TABLE 2 Signs of spontaneous polarization and absolute conformation

types	absolute conformation	signs of Ps	dipole moment
$R_1-\square-\overset{CH_3}{\underset{\cdot}{}}CHOR_2$	R	-	
	S	+	
$R_1-\square-\overset{CH_3}{\underset{\cdot}{}}CHOCOR_2$	R	+	
	S	-	

spontaneous polarization for the compounds is determined by (R) or (S) configuration and the structure near chiral carbon as shown in TABLE 2. Temperature dependence of tilt angle and spontaneous polarization in 3-ring phenylbenzoate derivatives are shown graphically in FIGURE 1 and FIGURE 2 respectively.

FIGURE 1 shows the relationship between the magnitude of tilt angle and the direction of ester group, -COO- or -OCO- as the achiral or the chiral tail structure is varied while holding the number and position of
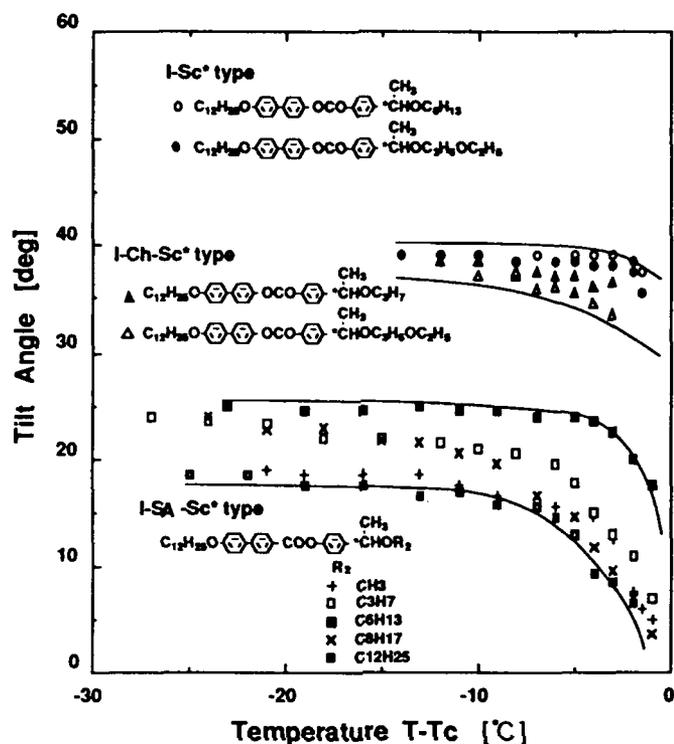
FIGURE 1 The effect of the direction of ester group against chiral carbon on tilt angle.

aromatic rings constant. The direction of ester group against chiral carbon determines primarily the magnitude of tilt angle.

In FIGURE 2 the effect of carbonyl group to the magnitude of polarization is shown. Compounds which have the ester group in the neighborhood of chiral carbon exhibit larger value of polarization than those of ether types as already reported[8].

Dependence of tilt angle and spontaneous polarization on the achiral tail length is shown in FIGURE 3 in the case of 3-ring derivatives. Figure 3 shows that the magnitude of tilt angle and spontaneous polarization have maximum value with the increase of alkyl chain length. This phenomena are also observed in different families of compounds such as phenylpirimidine derivatives.
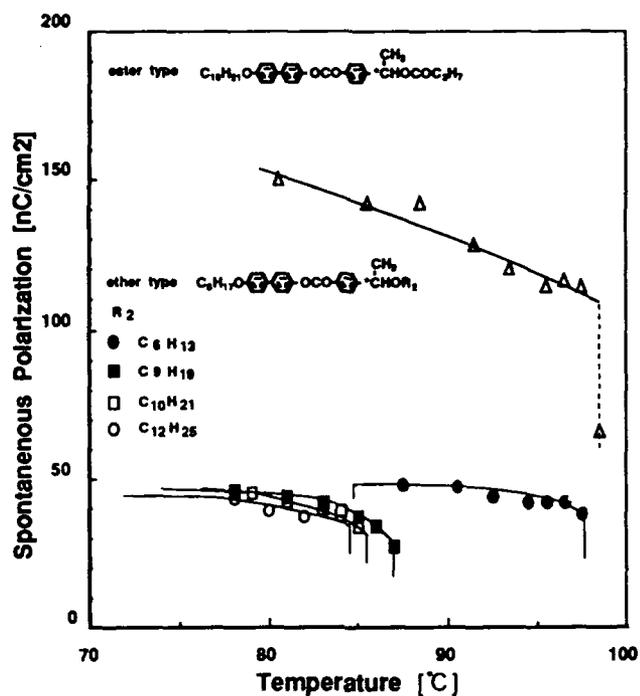
FIGURE 2 The effect of polar group in the neighborhood of
chiral carbon on spontaneous polarization.
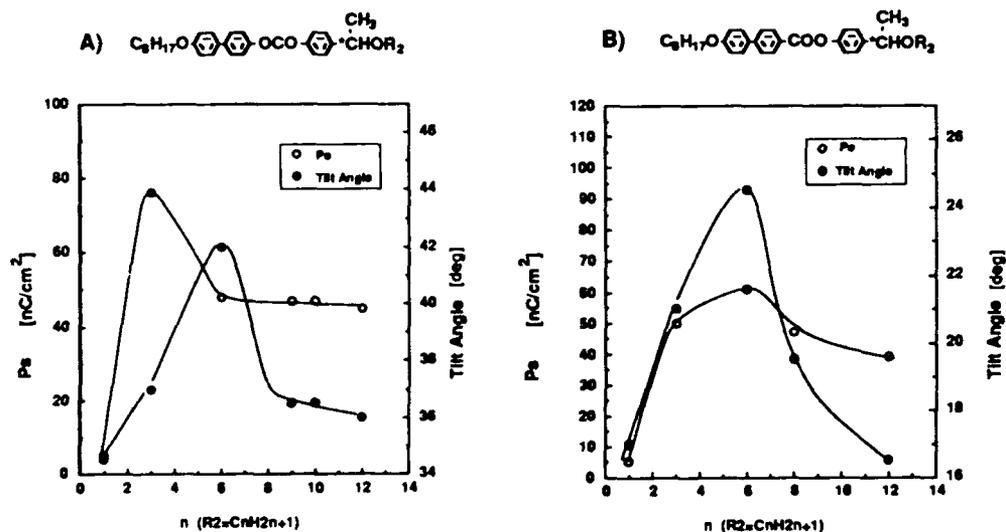
FIGURE3 The effect of chiral chain length on spontaneous polarization and tilt angle.

As shown in TABLE 1, 2-ring phenylbenzoate derivatives whose chiral carbons are directly connected to core aromatic ring do not exhibit liquid crystal phase. But the introduction of methylene -CH_2- unit between the chiral carbon and the core aromatic ring is effective for the exhibition of liquid crystal phase. The results of introduction of methylene unit are summarized in TABLE 3. These results show that the internal methylene units play an important role for exhibiting mesophase.

TABLE 3 The effect of internal methylene unit on physical properties.

A)

-(CH₂)ₙ	Phase sequence	tw [1] $[\mu s]$	Ps [2] $[nC/cm^2]$	$\eta 0$ [3] $[Pa \cdot s]$
n =1	K ←$\frac{29.0}{-1.0}$ SA ←$\frac{}{5.0}$→ I	—	—	—
n =2	K ←$\frac{18.0}{0.0}$ Sc* ←$\frac{}{8.0}$→ I	54.3(11℃)	-40.0	0.36(20℃)
n =3	K ←$\frac{16.2}{-14.0}$ Sc* ←$\frac{}{-4.0}$ SA ←$\frac{}{15.2}$→ I	—	-11.9	—
n =4	S I ←$\frac{9.2}{7.5}$→ Sc* ←$\frac{33.6}{24.3}$ SA ←$\frac{}{28.3}$→ I	33.2(15℃)	-16.0	0.13(20℃)

B)

-(CH₂)ₙ	Phase sequence	Ps $[nC/cm 2]$	$\eta 0$ $[Pa \cdot s]$
n =0	K ←$\frac{77.5}{S_1}$← SA ←Ch $\frac{97.0}{}$← I	—	—
n =1	S2 $\frac{66.0}{62.0}$ S1 $\frac{70.5}{65.3}$ Sc* $\frac{104.5}{104.8}$ Ch $\frac{125.9}{124.1}$ I	-29.8	1.48(20℃)
n =2	S2 $\frac{30.2}{54.0}$ S1 $\frac{72.3}{70.3}$ Sc* $\frac{110.4}{108.9}$ Ch $\frac{128.6}{127.2}$ I	-27.2	0.96(20℃)
n =3	K $\frac{50.9}{54.0}$ S1 $\frac{62.2}{60.3}$ Sc* $\frac{64.1}{62.9}$ Ch $\frac{129.2}{127.9}$ I	-18.3	0.76(20℃)

1) Response time (10V/μm) was measured by polarization current peak
2) Spontaneous Polarization was measured by using triangle wave method
3) Rotational Viscosity was estimated by Fukuda method; $\eta_0 = Ps \cdot E \cdot tw / 1.76 \sin^2\theta$

Generally speaking, it is necessary to introduce more than two methylene units $-CH_2CH_2-$ for the exhibition of Sc^* phase in 2-ring phenylbenzoates. The internal methlene unit plays an important role for exhibiting Sc^* phase not only 2-ring system but also 3-ring system as shown in TABLE 3 (B). TABLE 3 also shows the interesting phenomena conserned with the rotational viscosity, i.e., the increase of the number of methylene unit decrease the magnitude of rotational viscosity in 2-ring and 3-ring phenylbenzoate derivatives.

Compound which has two methylene units between the chiral carbon and the ether group also show Sc^* phase. But such a compound exhibit smaller tilt angle and spontaneous polarization than the compounds shown in TABLE 3.

The comparison of physical properties for two types of 2-ring phenylbenzoate derivatives is shown in TABLE 4. Although Sc^* phase of two type compounds are both monotoropic, the temperature range of the

TABLE 4 Comparison of physical properties for two types of phenylbenzoate derivatives.

$$C_{10}H_{21}O - \text{⟨◯⟩} - COO - \text{⟨◯⟩} - A - \overset{CH_3}{\underset{|}{^*CHOC_2H_5}}$$

Parameters	$A \approx -CH_2-CH_2-$	$A = -O-CH_2-$
Sc^* Temp. Range	-10.0 ~ 21.1 (Monotropic)	8.5~ 24.5 (Monotropic)
Ps [nC/cm^2]	-15.0	-13.6
η_0 [Pa·s]	0.43 (16℃)	0.74 (20℃)
Response Time [μs]	92 (16℃)	138 (20℃)

internal methylen type compund is wider than that of the compound in which oxygen atom is directly connected to the core aromatic ring instead of methylene unit, i.e., ether type compound. And the internal methylene type compound exhibits smaller magnitude of rotational viscosity and response time compared with the ether type compound.

In FIGURE 4 the relationship between the magnitude of rotational viscosity and temperature range for 2- and 3-ring phenylbenzoate derivatives is shown.
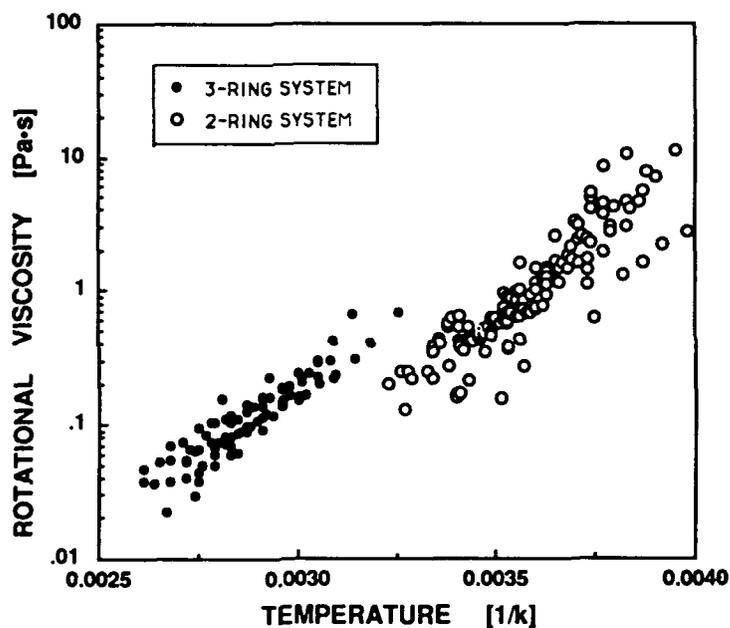
FIGURE 4 Arrhenius plot of rotational viscosities. All the measured results are plotted without the restrictionon molecular structure in 2-ring and 3-ring phenylbenzoatederivatives studied here.

The slopes of two groups are nearly same. This shows that 2-ring and 3-ring derivatives have almost same activation energy of switching process between two states. And the reason why the viscosity of 2- ring derivatives is lower than 3-ring derivatives comes from the difference of oscillation factor.

SUMMARY

The ferroelectric properties of novel 2-ring and 3-ring phenylbenzoate deriva-
tives have been examined. These series of compounds have not hetero
atom between the core aromatic ring and the chiral carbon. The introduc-
tion of methylene unit is efficient at exhibiting Sc* phase and reducing the

REFERENCES

1. B. I. Ostrovskii, A. Z. Rabinovich, A. S. Sonin and E. L. Sorkin,
    Ferroelectrics, 24, 309 (1980)
2. J. W. Goodby, T. M. Leslie, Proceedings of American Chemical
    Society Symposium, Las Vegas, March 29 - April 1, 1982
3. G. W. Gray, D. G. McDonnel, DE - OS 2736722, (1978)
4. H. R. Brand, P. E. Cladis, J. de. Phys. Lett. 45, L217 (1984)
5. EP-0284371A, EP-0297745A, EP-0357435A
6. K. Miyasato, S. Abe, H. Takezoe, A. Fukuda, and E. kuze, Jpn. J.
    Appl. Phys. 22, L661 (1983)
7. S. Kimura, S. Nishiyama, Y. Ouchi, H. Takezoe, and A. Fukuda, Jpn.
    J. Appl. Phys, 26, L255 (1987)
8. K. Yoshino, H. Taniguchi, and M. Ozaki, Ferroelectrics, 91, 267 (1989)

NOVEL OPTICALLY ACTIVE COMPOUNDS HAVING 2-ALKANOYLOXYPROPYL MOIETY AS CHIRAL DOPANTS

KAZUTOSHI MIYAZAWA, SHINICHI SAITO,
KANETSUGU TERASHIMA, MAKOTO KIKUCHI,
and TAKASHI INUKAI*
Chisso Petrochemical Corporation, 5-1, Goi Kaigan, Ichihara, 290 Japan
*Chisso Corporation, 2, Kamariya, Kanazawa-ku, Yokohama, 236 Japan

Abstract Novel optically active compounds having 2-alkanoyloxypropyl moiety were synthesized. By use of these compounds as chiral dopants in an achiral smectic C mixtures, Sc* mixtures exhibiting quick response and a long N* pitch suitable for the SSFLC displays could be obtained.

INTRODUCTION

Improved working characteristics of the chiral smectic C (Sc*) dielectrics are still in demand for the surface-stabilized liquid crystal (SSFLC) display mode[1] to be industrialized. One of the important technological elements for attainment of suitable properties of such liquid crystals, namely quick response, wide Sc* temperature range, good alignment and so on, is the selection of the chiral dopant as well
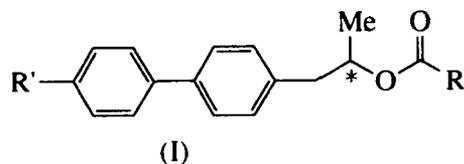
R ; alkyl, 1-butoxyethyl
R'; alkoxy

(I)

known, and this work concerns this point. We report the syntheses and properties of the compounds (I), together with working characteristics of the Sc* mixtures obtained by using them as chiral dopants.

EXPERIMENTAL

Syntheses

The compounds (I) were synthesized by the route shown in SCHEME 1.
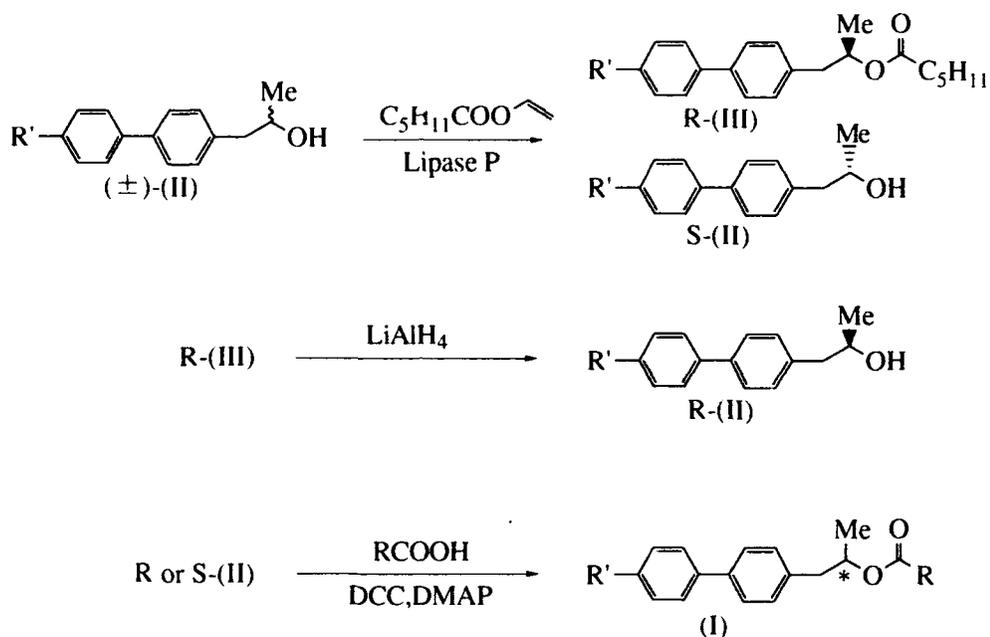
SCHEME 1. General synthetic route to (I)

Optically active 1-aryl-2-propanols R-(II) and S-(II) were prepared by optical resolution of racemic alcohol $(\pm)$-(II)[2] via enantioselective acylation in organic media, catalyzed by the lipase from *pseudomonas fluorescens* (Lipase P, Amano Pharmaceutical Co., Ltd.). Under the enzymatic condition, only R-(II) was converted to ester R-(III), S-(II) remaining unchanged. After separating R-(III) and S-(II) by column chromatography, the compound R-(III) was reduced to the alcohol R-(II) with LiAlH4. The compounds (I) were obtained by esterification of R or S-(II) with appropriate carboxylic acids by DCC and DMAP.

High enantiomeric purity (> 99 %ee) of alcohol R-(II) and S-(II) was found by the analysis of 400 MHz ^{1}H-NMR spectrum of respective (R)-α-methoxy-α-trifluoromethylphenylacetic acid (MTPA) esters (Mosher's method[3]).

Measurements

Evaluation of compounds (I) as chiral dopants was made on the mixtures containing 15 mol% of (I) in an achiral Sc mixture (base mixture A : phase sequence; Cr 4° , Sc 65° , Sa 79° , N 90° , Iso) of phenylpyrimidines. The transition temperatures were measured with a polarizing microscope, Nikon XTP-11, in conjunction with a Mettler hot stage FP 82 and control unit FP 80. The magnitude of Ps was measured with the triangular wave method [4]. The sign of Ps was determined according to the convention by Lagerwall in the field reversal method by optical observation of the director motion[5]. The tilt angle was determined, under crossed Nicol, as a half of the rotation angle between the two extinction positions, associated with the oppositely directed polarization[6]. The helical pitch in Sc* phase was determined by measuring the distance between the dechiralization lines corresponding to the full pitch by using a homogeneously aligned cell. The helical pitch in the N* phase was determined by the Cano-wedge method. The helical twist sense was determined by observation of textures of a contact preparation using specimen of known twist sense as a component of the binary system. (S) DOBAMBC was usually used as the authentic reference of right-handed twist [7]. The response time (τ) was measured from the transmission characteristics, as determined by photodiode, through crossed polarizers on application of square wave voltage. We defined τ as the time from field reversal to 90 % response.

RESULTS AND DISCUSSION

Phase transition temperatures of (I)

The chemical structures of synthesized compounds and their transition temperatures are listed in TABLE 1. None of the compounds prepared showed any mesophase, but the melting points are favorably low: This is what was expected from the outset, because the wing group is branched while the core is rather short. The compounds (Ih) and (Ii) with double branchings show lower melting points than those with a single branch.

TABLE 1. The structures and transition temperatures of compounds (I)

Compounds	R'	R	Abs.Config.	C-I ($^\circ$C)
Ia	$C_8H_{17}O$	C_2H_5	S	31.2
Ib	$C_8H_{17}O$	C_3H_7	S	33.6
Ic	$C_7H_{15}O$	C_3H_7	R	34.8
Id	$C_8H_{17}O$	C_4H_9	S	28.7
Ie	$C_8H_{17}O$	C_5H_{11}	R	31.4
If	$C_8H_{17}O$	C_6H_{13}	S	30.2
Ig	$C_8H_{17}O$	C_7H_{15}	S	34.4
Ih	$C_8H_{17}O$	$C_4H_9O\overset{*}{C}H(CH_3)$	S,S	10.0
Ii	$C_8H_{17}O$	$C_4H_9O\overset{*}{C}H(CH_3)$	S,R	-0.5

Properties of Sc* mixtures containing (I)

The transition temperatures, response time, Ps value, tilt angle, and helical pitches of Sc* mixtures containing 15 mol% of the compounds (I) in the base mixture A are

TABLE 2. Properties of compounds (I) in the base mixture A [a,b]

	Transition temperatures ($^\circ$C)				τ	Ps	θ	pitch (μm) [c]	
	Sc*	Sa	N*	Iso	(μsec)	(nC/cm2)	($^\circ$)	N* [d]	Sc*
Ia	• 48.2	• 63.6	• 75.6	•	97	+3.3	17.5	2.1 (L)	2.1 (L)
Ib	• 50.2	• 64.2	• 75.5	•	87	+5.0	19.5	1.3 (L)	2.1 (L)
Ic	• 48.3	• 60.0	• 75.4	•	92	-5.2	20.0	1.3 (R)	1.8 (R)
Id	• 49.4	• 64.1	• 75.1	•	88	+4.2	18.5	1.4 (L)	2.1 (L)
Ie	• 49.0	• 63.4	• 74.1	•	77	-5.7	18.0	1.3 (R)	2.1 (R)
If	• 46.5	• 63.7	• 74.8	•	80	+5.0	17.8	1.2 (L)	2.1 (L)
Ig	• 44.0	• 63.0	• 74.5	•	76	+4.7	17.0	1.2 (L)	2.1 (L)
Ih	• 42.2	• 67.0	• 75.7	•	71	+4.5	14.5	1.2 (L)	2.4 (L)
Ii	• 40.0	• 63.1	• 75.2	•	---	very small	13.0	---	15.7 (L)

a) base mixture A ; Cr 4°, Sc 65°, Sa 79°, N 90°, Iso.
b) at 25°C, unless otherwise indicated.
c) L and R indicate left- and right-handed, respectively.
d) measured at just above the N*-Sa phase transition temperature.

shown in TABLE 2. The Sc* mixtures containing (Ia)-(Ig) (R is alkyl) showed 15 to 20 degree depression of Sc*-Sa transition temperature. R absolute configuration induces Ps of negative sign and right-handed helical twist in both N* and Sc* phases. It is puzzling that the compound (Ii) with S,R configuration shows very small Ps value while (Ih) with S,S configuration shows a Ps value comparable to that of (Ia) to (Ig).

If we compare the Ps values shown in TABLE 2 with that of a mixture containing (S)-4'-octyloxy-4-(2-methylbutyl)biphenyl (IV) (Ps $\simeq 0$, 15 mol% in base mixture A)[8], the role of the ester linkage in the optically active wing of

$$\text{(S)} \quad C_8H_{17}O \text{—} \underset{\text{Me}}{\overset{\text{Me}}{\diagdown}}$$

(IV)
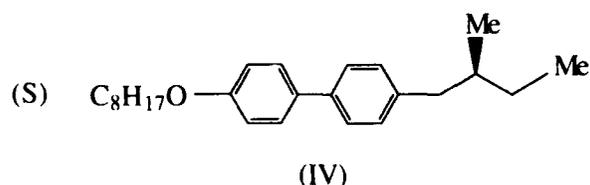
compound (I) in enhancement of Ps will be clear.

All of the Sc* mixtures containing compounds (I) exhibited quick response; less than 100 μ sec at electric field of 10 V/μ m. The helical pitches were short both in N* and Sc* phases.

FLC mixtures having long N* helical pitches

We previously reported syntheses and properties of kindred optically active compounds having 2-alkanoyloxypropyloxy moiety[9], for example, the compound of formula (V)[9a,d]. As shown in the insert, the Sc* mixtures containing (V) gave a negative high Ps value and exhibited quick response. However, they showed a short

$$\text{(S,S)} \quad C_5H_{11}$$

Ps = $-$ 46.3 nC/cm^2 (25°C)
τ = 31 μ sec (25°C)
15mol% in base mix. A

(V)
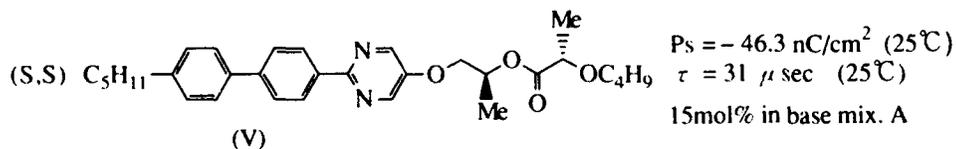
helical pitch in N* phase (1.8 μ m, left-handed) . Therefore, further doping with an optically active compound having right-handed helical twisting power is required in

K.MIYAZAWA ET.AL.

order to prepare an Sc* mixture having a long N* pitch for good alignment. The compounds (I) of R configuration and compound (V) present a good combination for this purpose, because the former exhibits negative Ps value and right-handed helical twist in N* and Sc* phases while compound (V) exhibits same sign of Ps and left-handed helical twist in N* and Sc* phases.

TABLE 3 shows transition temperatures, response time, Ps value, tilt angle, and helical pitches both in N* and Sc* phases of Sc* mixtures containing (Ie) and (V) in base mixtures A and B. Both of the Sc* mixtures listed in TABLE 3

TABLE 3. The properties of FLC mixtures containing (Ie) and (V) [a].

Transition temperatures (°C)				τ	Ps	θ	Pitch (μ m) [b]	
Sc*	Sa	N*	Iso	(μ sec)	(nC/cm^2)	(°)	N* [c]	Sc*
FLC mix. A [d] • 54.5 •	62.2 •	79.6 •		37	−30.0	23.3	35.7 (R)	2.4 (L)
FLC mix. B [e] • 60.8 •	84.8 •	96.7 •		26	−28.1	19.3	31.5 (R)	3.0 (L)

a) at 25°C, unless otherwise indicated.
b) L and R indicate left- and right-handed, respectively.
c) measured at just above the N*-Sa phase transition temperature.
d) FLC mix A containing 10 wt% of (Ie) and 12 wt% of (V) in base mixture A.
e) FLC mix B containing 10 wt% of (Ie) and 12 wt% of (V) in base mixture B. (phase sequence; Cr 2°, Sc 61°, Sa 105°, N 114°, Iso).

exhibit remarkably long N* pitch, lager than 30 μ m, which is long enough to realize an Sc* mixture with a good alignment in SSFLC displays. The Sc* mixtures show rather wide Sc* phase and quick response, less than 30 μ sec, indicating that these mixtures are usefull for display applications.

CONCLUSION

Optically active compounds (I) having 2-alkanoyloxypropyl moiety did not show any mesophase, but Sc* mixtures containing (I) in an achiral Sc mixture exhibited a large Ps and quick response. Moreover, by using compound (I) in combination with

the kindred chiral dopants having 2-alkanoyloxypropyloxy moiety (for example (V)), Sc* mixtures showing quick response and a long N* pitch could be obtained.

REFERENCES

1. N.A.Clark and S.T.Lagerwall, Appl. Phys. Lett., 36, 899 (1980).
2. Prepared from 4'-alkoxy-4-biphenylylmagnesium bromide and propylene oxide according to the method of E.E.Dreger, Org. Synth., I,306 (1941).
3. J.A.Dale, D.L.Dull and H.S.Mosher., J.Org.Chem., 34,2543 (1969).
4. K.Miyasato, S.Abe, H.Takezoe, A.Fukuda and E.Kuze, Jpn. J. Appl. Phys., 22, 1661 (1983).
5. S.T.Lagerwall and I.Dahl, Mol. Cryst. Liq. Cryst., 114, 151 (1984).
6. Ph.Martinot-Lagarde, R.Duke and G. Durand, Mol. Cryst. Liq. Cryst., 75, 249 (1981).
7. J.Billard, A.Dahlgen, K.Flatischler, S.T.Lagerwall and B.Otterholm, J. Physique, 46, 1241 (1985).
8. Unpublished result.
9. a) S.Saito, K.Miyazawa, M.Ushioda, K.Ohno, H.Inoue, K.Furukawa and T.Inukai, Proceeding of the 1988 International Display Research Conference San Diego, P. 107 (1988).
    b) M.Ichihashi, K.Kikuchi, F.Takeshita, K.Terashima, K.Furukawa, S.Saito, K.Miyazawa and T.Inukai, Sen-i-Gakkai Symp. Preprints, B-09 (1988).
    c) K.Ohno, M.Ushioda, H.Inoue, K.Miyazawa, S.Saito, K.Furukawa and T.Inukai, The 14th Symposium on Liquid Crystals 1B 101 (1988).
    d) K.Miyazawa, M.Ushioda, H.Inoue, K.Ohno, S.Saito, K.Furukawa, and T.Inukai, The 14th Symposium on Liquid Crystals 1B 119 (1988).

HELICAL SMECTIC A* PHASE (TGB$_A$ PHASE) IN SOME TOLAN SERIES

H.T. NGUYEN*, R.J. TWIEG+, M.F. NABOR•, N. ISAERT•,
C. DESTRADE*
*Centre de Recherche Paul Pascal, Avenue A. Schweitzer,
F33600 Pessac Cedex, France
+ IBM Almaden Research Center, 650 Harry Road,
San Jose, CA 95120-6099, USA
• Laboratoire de dynamique et structure des matériaux
moléculaires, Université de Lille 1, U.F.R. de Physique,
F59655 Villeneuve d'Ascq Cedex, France

Abstract : A helical smectic A* phase between the isotropic liquid and the ferroelectric smectic C* phase is found in three new series with very long alkoxy chains. The materials belong to the optically active series : (R) and (S) 1-methylheptyl 4'-(4"-alkoxybenzoyloxy)tolan-4-carboxylates, 4'-(4"-alkoxy-3"-fluorobenzoyloxy)tolan-4-carboxylates, 4'-(4"-alkoxy-2",3"-difluorobenzoyloxy)tolan-4-carboxylates. This new phase has two typical textures: filament texture when the helix pitch is large and cholesteric texture (Grandjean texture) with a short pitch.

INTRODUCTION

Recently the discovery of a new helical smectic A* phase was reported by Goodby et al[1,2] in a series of compounds having the general formula:

$$H(CH_2)_nO - \bigcirc - C \equiv C - COO - \bigcirc\bigcirc - COO - \overset{*}{C}H - C_6H_{13} \quad \underset{\sim}{I}$$
$$\underset{CH_3}{|}$$
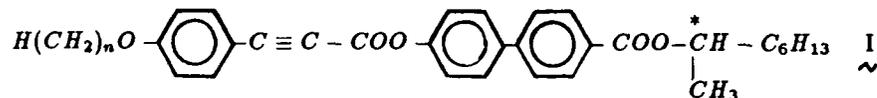
In this series, there are three compounds which display this phase with a texture similar to the cholesteric one (n=13 → 15). The existence of this phase was predicted earlier by De Gennes and he proposed the term S_A^* to identify this mesophase[3]. In this phase, the molecules are packed in layers and the blocks of the S_A^* rotate around the direction normal to the long axes of the molecules and parallel to the layers in forming a helical structure[4]. Renn and Lubensky[5]suggested that the

formation of a helix would be possible if a lattice of screw or edge dislocations is incorporated between the different individual blocks of the helical smectic A* layers. They call this phase a twist grain boundary A phase (TGB$_A$ or S_A^*)[6].

Initially Renn and Lubensky predicted that the TGB$_A$ phase could be observed between the cholesteric and S_A phases but the compounds of the series I exhibit directly the helical S_A^* phase below the isotropic liquid. The new $N^* - S_A^* - S_A$ phase sequence was reported at first in a mixture by Lavrentowich et al[7] then in a pure compound by Slaney et al[8,9]. These pure materials have the general formula:

$$n - C_9H_{19}O - \langle\bigcirc\rangle - COO - \langle\bigcirc\rangle\langle\bigcirc\rangle - COO - CH_2 - \overset{*}{C}H - R \quad \underset{Cl}{|} \quad \text{II}$$
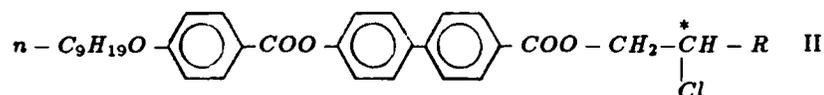
where the chiral primary alcohols were obtained from chiral amino-acids.

In this study, we explore the influence of the tolan core (instead of the biphenyl core) and the influence of fluorine substitution on polarity or steric hindrance in the first phenyl ring on the stabilization of the S_A^* phase (TGB$_A$) in the series of compounds III.

$$H(CH_2)_nO - \overset{X \quad Y}{\langle\bigcirc\rangle} - COO - \langle\bigcirc\rangle - C \equiv C - \langle\bigcirc\rangle - COO - \overset{*}{C}H - C_6H_{13} \quad \underset{CH_3}{|} \quad \text{III}$$

where   X = Y = H   (A)
        X = F, Y = H   (B)
        X = Y = F   (C)
        n = 6 - 20
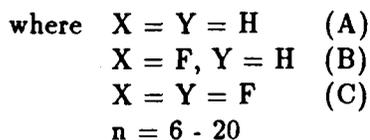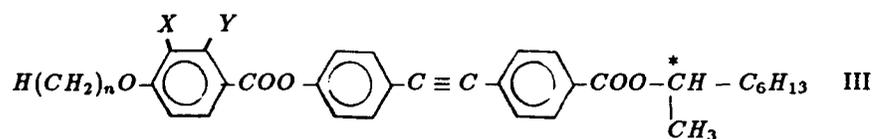
RESULTS AND DISCUSSION

Synthesis

The compounds of series III A,B,C were prepared following the scheme .

4-Iodophenol 1 is protected with 3,4-dihydro-2H-pyran (DHP) in presence of the p-toluensulfonic acid (PTSA) as catalyst. The palladium-catalyzed coupling reaction between 2 and ethynyltrimethylsilane gives the intermediate 3 which yields 4 after removal of the trimethylsilyl group with $NaOH$ 50% at ambient temperature[10]. Diisopropylamine is not only used as the solvent but also as a scavenger for the hydrogen halide generated during the ethynylation reaction. The same palladium catalyzed coupling reaction is used for preparing 5.

$$HO-\!\!\langle\bigcirc\rangle\!\!-I \quad \xrightarrow{a} \quad THPO-\!\!\langle\bigcirc\rangle\!\!-I$$

$$\downarrow b$$

$$THPO-\!\!\langle\bigcirc\rangle\!\!-C\equiv CH \quad \xleftarrow{c} \quad THPO-\!\!\langle\bigcirc\rangle\!\!-C\equiv C-Si(Me)_3$$

$$\downarrow d$$

$$THPO-\!\!\langle\bigcirc\rangle\!\!-C\equiv C-\!\!\langle\bigcirc\rangle\!\!-CO_2-\overset{*}{C}H-C_6H_{13}$$
$$\underset{CH_3}{|}$$

$$\downarrow e$$

$$HO-\!\!\langle\bigcirc\rangle\!\!-C\equiv C-\!\!\langle\bigcirc\rangle\!\!-CO_2-\overset{*}{C}H-C_6H_{13}$$
$$\underset{CH_3}{|}$$

$$\downarrow f$$

$$\overset{X\quad Y}{H(CH_2)_nO-\!\!\langle\bigcirc\rangle\!\!-COO-\!\!\langle\bigcirc\rangle\!\!-C\equiv C-\!\!\langle\bigcirc\rangle\!\!-CO_2-\overset{*}{C}H-C_6H_{13}} \quad IV$$
$$\underset{CH_3}{|}$$
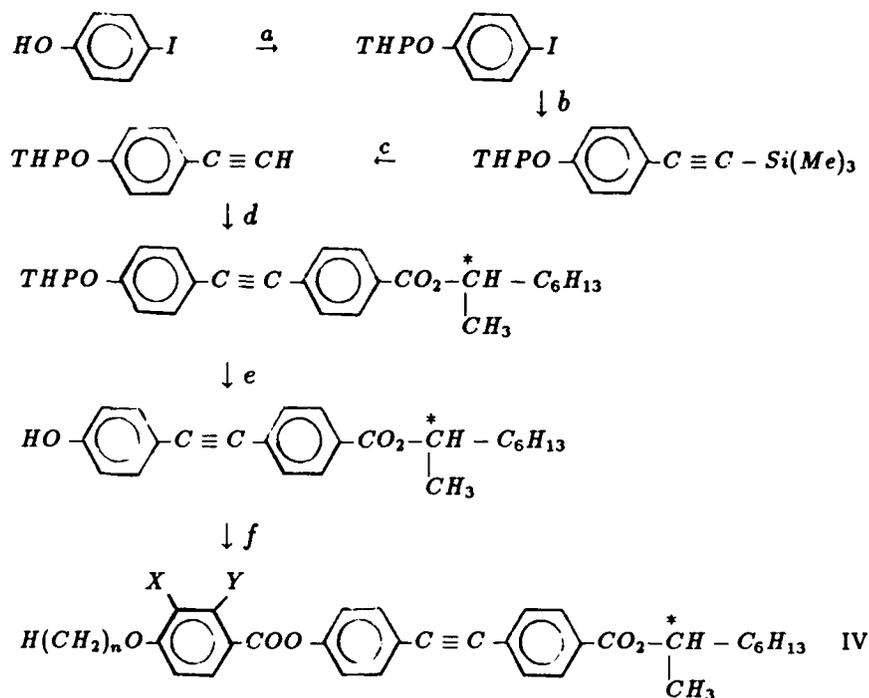
a : $DHP, PTSA, CH_2 Cl_2$

b : $HC\equiv C\,Si\,Me_3, PdCl_2, Cu(AcO)_2, Ph_3P, iPr_2NH$

c : $NaOH\,50\%, MeOH$

d : $Br-\!\!\langle\bigcirc\rangle\!\!-CO_2-\overset{*}{C}H-C_6H_{13}(7), PdCl_2, Cu(AcO)_2, Ph_3P, iPr_2NH$
$$\underset{CH_3}{|}$$

e : $PTSA, THF, MeOH$

f : $H(CH_2)_nO-\!\!\langle\bigcirc\rangle\!\!-COOH(8), DCC, DMAP, CH_2Cl_2$
$$\underset{X\quad\quad Y}{}$$

Scheme 1

The compounds 7 used in this reaction, are obtained by esterification reaction between 4-bromobenzoic acid and (R)- or (S)-2-octanol in presence of 1,3 dicyclohexylcarbodiimide (DCC) and 4-dimethylamino-pyridine (DMAP). The deprotection of the phenol group is made with PTSA in tetrahydrofuran (THF), methanol mixture, affords the phenols 6. The final compounds III are obtained by a classical esterification reaction between 6 and 8. The mono and difluoroalkoxy benzoic acids are prepared following the well known methods[11,12].

All the final compounds were purified by chromatography on silica gel with toluene as eluent and were recrystallized from absolute ethanol. Their chemical structures were checked by a combination of nuclear magnetic resonance spectroscopy (Bruker 270 MHz spectrometer), infra red spectroscopy (Perkin Elmer 78 spectrophotometer) and elemental analyses.

Mesomorphic properties

All the compounds III A,B,C are mesogenic. The phase assignments and corresponding transition temperatures were determined both by thermal optical microscopy (Mettler FP5) and by differential scanning calorimetry (Perkin Elmer 7). The liquid crystal transition temperatures and enthalpies of these new materials are presented in Tables 1A,B and C.

* Series III A

TABLE 1A :   Transition temperatures (°C) of compounds III A

$$H(CH_2)_nO - \bigcirc - COO - \bigcirc - C \equiv C - \bigcirc - COO - \overset{*}{C}H - C_6H_{13} \quad (n)$$
$$| \atop CH_3$$
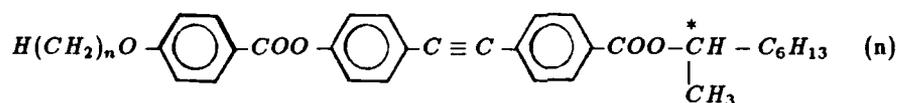
n	K	$S_?$	S_C^*	S_A	S_A^*	I
6	. 75	-	-	. 135	-	.
7	. 84	-	-	. 131.7	-	.
8	. 102	-	-	. 133.8	-	.
9	. 87	-	-	. 130	-	.
10	. 83	(. 73)	-	. 130	-	.
11	. 88	(. 70)	-	. 126	-	.
12	. 66	(. 69)	. 79	. 123	-	.
13	. 77	(. 75)	. 100	. 120	-	.
14	. 80	(. 75)	. 102	. 118	-	.
16	. 76	(. 69)	. 104	-	. 114[+]	.
18	. 79	-	. 103	-	. 110[+]	.
20	. 86	·	. 105	-	. 109[+]	.

The meanings of the signs used in this table and in the following are :

K : crystalline phase ; I : isotropic phase ; - : the phase does not exist
S : smectic phases A, C ..., smectic phases S_A, S_C ... ;
● : the phase exists
( ) : monotropic transition ; + : S_A^* with filament texture

We can see in Table 1A that the first four derivatives (n = 6-9) only display the S_A phase with focal conic or homeotropic textures. In the two next derivatives (n = 10,11), in addition to this S_A phase, an unidentified smectic $S_?$ phase is observed at lower temperature which persists until n = 16. The ferroelectric S_C^* phase appears from n = 12 with striated fan shaped or schlieren textures. The helical S_A^* phase is only observed with very long chains (n = 16, 18, 20) with filament or focal conic textures. On cooling from the isotropic phase, one can observe the filament or worm which partially disappear on cooling down (Figure 1). This indicates that the pitch of the S_A^* helix is short near the isotropic phase but is longer at low temperature. As Goodby et al[1,2] mentionned about their compounds, in this series III A we cannot observe the $S_A - S_A^*$ transition.
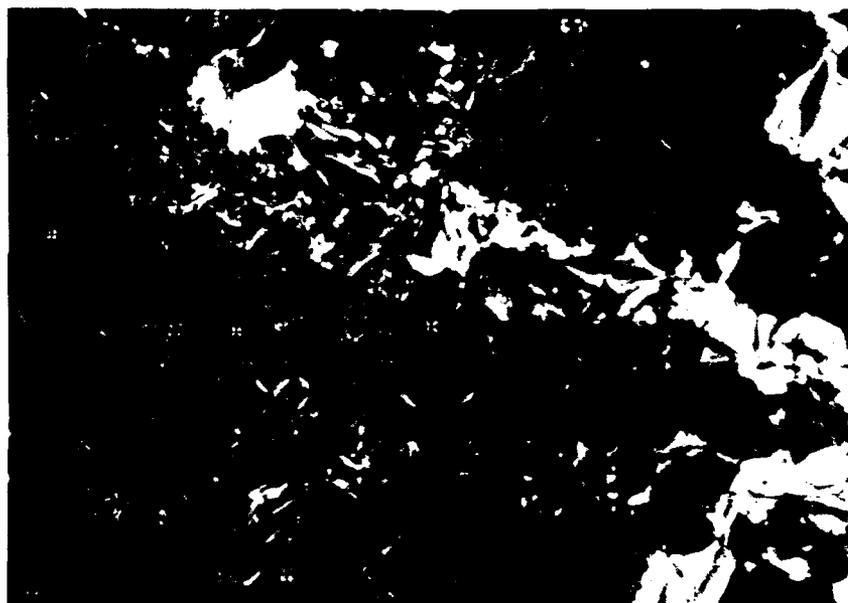
FIGURE 1 :   Helical S_A^* phase with filament texture of III A (n = 18) or 18 See Color Plate IV.

* <u>Series III B</u>

TABLE 1B :   Transition temperatures (°C) and enthalpies in italic (J.g^{-1}) of compounds III B

$$H(CH_2)_nO \underset{F}{-\bigcirc} -COO-\bigcirc-C \equiv C-\bigcirc-COO-\overset{*}{C}H-C_6H_{13} \quad \text{(nF)}$$
$$\underset{CH_3}{|}$$

n	K	S_C^*	S_A	S_A^*	I
8	. 80.5	-	. 119	-	.
	41.5		*8.55*		
9	. 80.2	-	. 115.7	-	.
	44.3		*8.1*		
10	. 93	-	. 115.5	-	.
	48.6		*8.2*		
11	. 96.5	-	. 112.7	-	.
	54.7		*7.9*		
12	. 85.5	-	. 110.7	-	.
	43.8		*6.7*		
14	. 66.5	. 94.9	-	. 104.9$^+$	.
	52	*0.23*		*5.3*	
16	. 61	. 95.6	-	. 101.6^{++}	.
	70.7	*0.42*		*7.1*	
18	. 67	. 93	-	. 97^{++}	.
	67	*0.29*		*5.47*	
20	. 72	. 93	-	. 96.5^{++}	.
	89	*0.23*		*5.2*	

$^+$ helical S_A^* with filament texture
$^{++}$ helical S_A^* with cholesteric texture

This series differs structurally from the III A series by the presence of the fluorine atom in meta position with regard to $-COO-$ group of the core. It is well known that the influence of the fluorine on the mesomorphic properties is more useful and interesting with three benzine ring compounds[11,13]. It displays the same mesomorphic properties (Table 1B) as the series III A but their clarification and $S_A^* - S_C^*$ transition temperatures are lower than those of the former. The tetradecyloxy derivative exhibits the helical S_A^* phase with filament texture but from n = 16 to n = 20, one can observe the S_A^* phase with cholesteric texture (Figure 2a.b) :

a   b
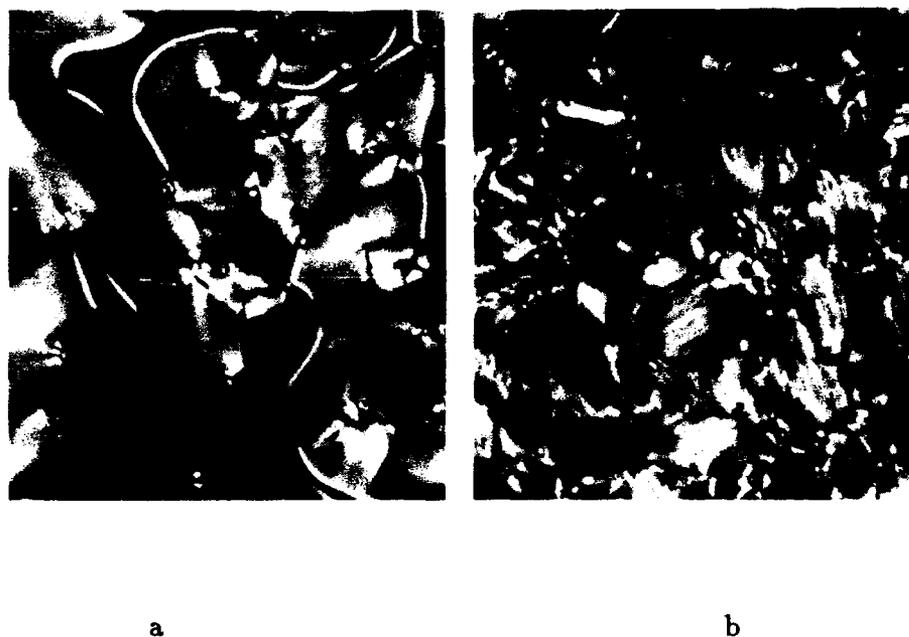
FIGURE 2 :   Cholesteric texture of the S_A^* phase
a) on cooling from the isotropic phase
b) at 94°C for III B (n = 18) or 18F   See Color Plate V.

Despite the cholesteric appearence of the optical texture, we can assess that this phase is not a cholesteric phase : first, the cholesteric phase is not observed in this series with short chains, moreover the lamellar structure of this mesophase has been proved, as discussed in the next paragraph using the racemic compound, the contact method between (R) and (S) enantiomers and X-ray measurements.

* <u>Series III C</u>

TABLE 1C :   Transition temperatures (°C) and enthalpies in italic $(J.g^{-1})$ of compounds III C

$$H(CH_2)_nO-\langle\bigcirc\rangle-COO-\langle\bigcirc\rangle-C \equiv C-\langle\bigcirc\rangle-COO-\overset{*}{C}H-C_6H_{13} \quad (nF_2)$$
$$\underset{F}{} \quad \underset{F}{} \qquad\qquad\qquad \underset{CH_3}{\overset{|}{}}$$

n	K	S_C^*	S_A	S_A^*	I
8	. 74	-	. 124.1	-	.
	48.3		*7*		
9	. 69.2	-	. 121	-	.
	61.4		*6.71*		
10	. 73.9	-	. 121.4	-	.
	50.2		*7*		
11	. 81.1	-	. 11C	-	.
	61.6		*6.81*		
12	. 65.6	-	. 117.3	-	.
	52.7		*6.32*		
14	. 65.5	. 98.5	-	. 112.5[+]	.
	66.2	~ 0		*5.48*	
16	. 65.6	. 102	-	. 109.2[++]	.
	67.1	*0.32*		*5.12*	
18	. 68	. 103	-	. 107[++]	.
	64	*0.27*		*5*	
20	. 65.4	. 98	-	. 103[++]	.
	63.4	*0.19*		*4.9*	

[+] helical S_A^* with filament texture

[++] helical S_A^* with cholesteric texture

This series with two fluorine atoms substituted on the first benzene ring shows the same mesomorphic properties as the IIIA,B series (Table 1C). Their clarification and $S_A^* - S_C^*$ transition temperatures are intermediate between the hydrogen and monofluorine derivatives. We also obtain the helical S_A^* phase with filament texture (n = 14) and from n = 16 with cholesteric texture.

Calorimetric and mixture studies

The transition enthalpies were determined by differential scanning calorimetry (DSC) and are given in Tables IB,C. Generally the enthalpy values for the $S_C^* - S_A^*$ transitions were to small either to be measured or when it is possible comprise between 0.2 to 0.42 cal.g^{-1} These tables show also that the enthalpy values of the $S_A - I$ transitions are higher than those of the $S_A^* - I$ ones. This is due to the fact that the clearing point transition is first order for short alkoxy chains and becomes less first order with very long chains.

DSC shows little difference between the enantiomers and the racemic mixtures for compounds 18F and 18F$_2$.

TABLE 2 : Transition temperatures (°C) and enthalpies (J.g^{-1}) of pure compounds and racemic mixtures

Compound	K	S_C^* or S_C	S_A^* or S_A	I
18F (R) or (S)	. 67	.	93	.	97	.
	67		*0.29*		*5.47*	
Rac.	. 59	.	93.8	.	100.2	.
	68		*0.27*		*6.7*	
18F$_2$ (R) or (S)	. 68	.	103	.	107	.
	64		*0.27*		*5*	
Rac.	. 66	.	103.5	.	112.6	.
	62.6		*0.24*		*5.96*	

We can see in the Table 2 that there is no notable variation of the enthalpies for the melting points and the $S_C - S_A$ or $S_C^* - S_A^*$ transitions but for the clearing points, the enthalpy of the racemic mixtures is higher than that of the enantiomers (only about twenty per cent). Consequently the S_A phase of the racemic mixtures is more stable than the helical S_A^* of the enantiomers (three or five degrees higher). This behaviour is also observed with the contact method.

FIGURE 3 :   Contact preparation between (R) and (S) enantiomers
(18F) See Color Plate VI.

Figure 3 shows an example of such contact between two enan-
tiomers [(R) and (S) 18F]. In the middle of this preparation, the racemic
mixtures exhibit a S_A phase with focal conic or homeotropic textures.
Moving away from the middle we can see at first a helical S_A^* phase
with filament texture and then a S_A^* phase with cholesteric texture cor-
responding to the pure enantiomers. This result confirms that the S_A^*
phase with filament texture has a pitch larger than that of the S_A^* phase
with cholesteric texture and in this case there is apparently a contin-
uous evolution from the classical S_A phase to the helical S_A^* one. But
in other cases, the $S_A - S_A^*$ transition is observed in a mixture[7] or in a
pure compounds[8,9].

Structural studies

X-ray scattering was performed for powder and unaligned sample with
a high temperature Guinier Camera using monochromatic $CoK\alpha_1$, ra-
diation. The seven studied compounds are IIIA (16,18), IIIB (16F,
18F, 20F) and IIIC (16F$_2$, 18F$_2$).
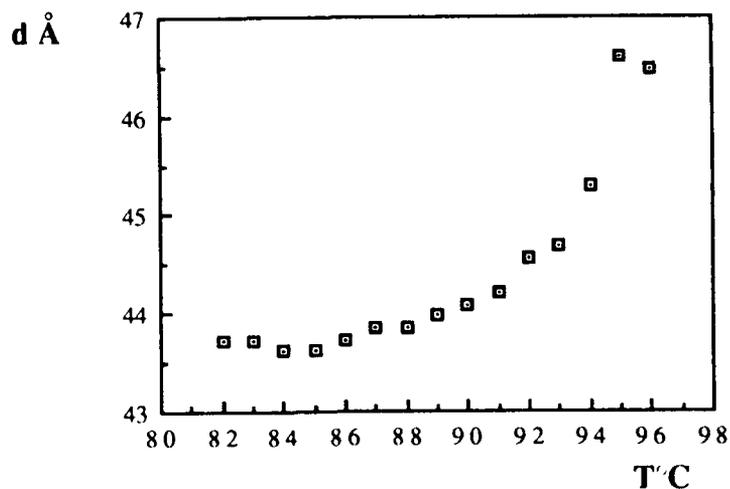
FIGURE 4 : Temperature dependence of the layer spacing for 20F (S)

In Figure 4, we can see that, upon heating the layer spacing of the ferroelectric S_C^* phase is constant and near the $S_C^* - S_A^*$ transition it increases and saturates in the S_A^* phase. The Table 3 gives the fully extended molecular length (ℓ), the layer spacing of S_A^* ($d_{S_A^*}$) S_C^* ($d_{S_C^*}$) phases and the tilt angle θ calculated from the relation :

$$cos\theta = \frac{d_{S_C^*}}{d_{S_A^*}}$$

of these compounds.

TABLE 3 :   Molecular length, layer spacing of S_A^*, S_C^* and tilt angle of compounds IIIA,B,C

Compound	ℓ (Å)	$d_{S_A^*}$ (Å)	$d_{S_C^*}$ (Å)	θ (°)
16	53.6	43.8	40.8	21.3
16	56.2	45.7	42.6	21.2
16F	53.6	43	40.2	20.8
18F	56.2	44.1	41.7	19
20F	58.7	46.5	43.7	20
16F$_2$	53.6	43.3	40.5	20.7
18F$_2$	56.2	43.7	41.3	19

We can see at first that the layer spacings of the S_A^* phase $(d_{S_A^*})$ of the studied compounds are not commensurate with the fully extended molecular lenght (ℓ) of the molecules. The former is largely inferior to the latter (more than 10 Å lower). This behaviour could be explained either by the disorder of the long alkoxy chains leading to the folded shape or by the inclination of the molecules. Actually, it is difficult to clarify this situation and one needs some more X-ray investigation. On the other hand, the three compounds 18, 18F and 18F$_2$ have the same molecular length normally they could have the same S_A^* layer spacing but as we can see in Table 3, the $d_{S_A^*}$ decreases from the hydrogeno (45.7 Å) to the difluorocompound (43.7 Å) and one could expect a small tilt of the molecules in the layer. The highest tilt angle of the S_C^* phase calculated from the ratio between $d_{S_C^*}$ and $d_{S_A^*}$ around 20° is lower than that obtained from the electrooptical measurement. We will give more details in the next paragraph.

Helix pitch measurement

The helical S_A^* phase has the helix axis parallel to the layer planes. Consequently we can use the Grandjean-Cano method to measure their pitch as in the case of the cholesteric phase[14a,b,c]. The Figure 5 shows a temperature dependence of the pitch. It is very short near the $S_A^* - I$ transition and increases quickly with decreasing temperature. Selective reflection of red light occurs for 18F and 20F (S) enantiomers near the $S_A^* - I$ transition. Left rotatory power obtained for visible hight indicates that the helix sense is left. The same behaviour was observed with two fluorine compounds.
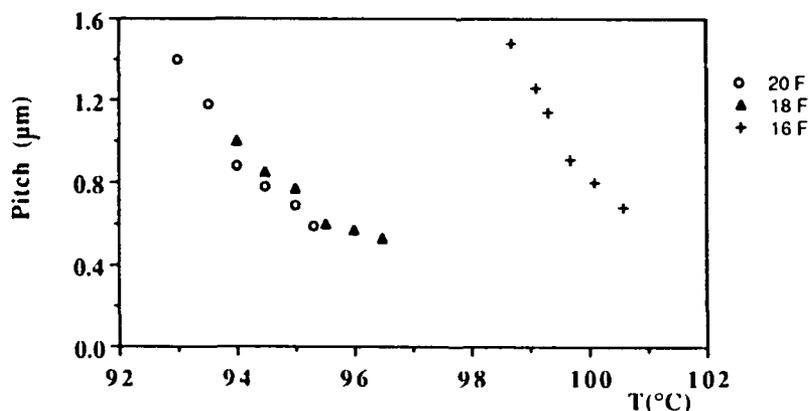
FIGURE 5 :   Helical pitch of the S_A^* phase versus temperature (16F, 18F and 20F)

Electrooptical properties

The spontaneous polarization, response time and tilt angle of compounds IIIB (16F, 18F) and IIIC (16F$_2$, 18F$_2$) were measured as a function of the temperature as described previously[11,15]. Figure 6a,b shows relatively high polarization larger than 60 nC/cm^2 for hexadecyl derivatives and about 45 nC/cm^2 for the longer ones. Using a field around 6V.μm, we have not observed any abnormality in the temperature dependence an the polarization as described by Goodby et al[2].
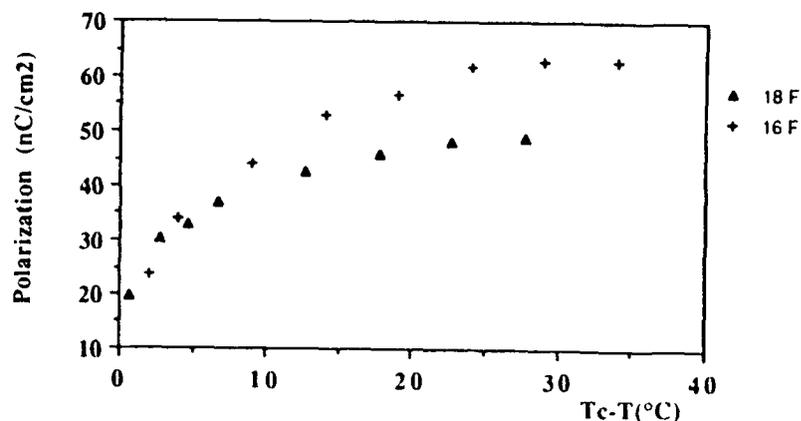
a
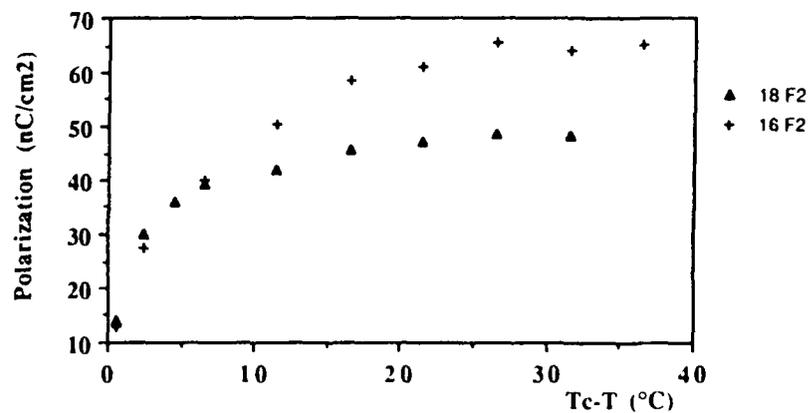
b

FIGURE 6 :   Spontaneous polarization versus $T_c - T$ ($T_c : S_A^* - S_C^*$ transition temperature)
a) for 16F and 18F
b) for 16F$_2$ and 18F$_2$

This behaviour is probably connected to the absence of any additional smectic phase at low temperature in our compounds. The response time of these new materials is fairly fast, below 50 μS at 50°C (Figure 7). The same and consistent behaviour is observed in these two series. For instance, the hexadecyloxy derivatives have a high polarization and a low response time. It is interesting to note that near the transition $S_A^* - S_C^*$ the apparent optical tilt angle is already high more than 10° and in some case near 20° while the saturated angle is about 30° (Figure 8). This angle is larger than that calculated from the layer spacing (see Table 3). This unusual difference could be explained by the influence of electric field or by the existence of a tilt in the high temperature phase :
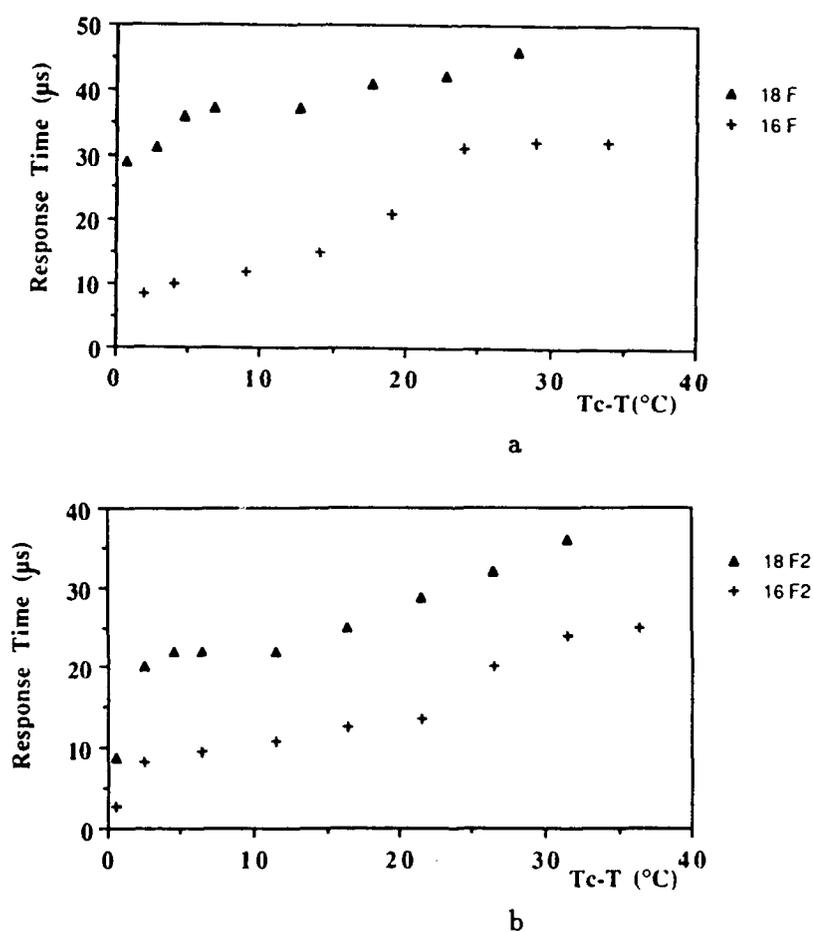
FIGURE 7 :   Response time versus $T - T_c$ (N = 3 KHz, E = 5V.μm^{-1}
a) for 16F and 18F ; b) for 16F$_2$ and 18F$_2$

as a matter of fact in last hypothesis the layer spacing value $d_{S_A^*} = 41.3$ Å(for 18F$_2$) is obviously shorter than the value we should obtain in an orthogonal mesophase of the S_A type ($\ell = 56.2$ Å). Because of this peculiar behaviour the existence of a tilted TGB mesophase is suspected. In order to check this hypothesis several structural investigations are in progress in some new series and will be published elsewhere.
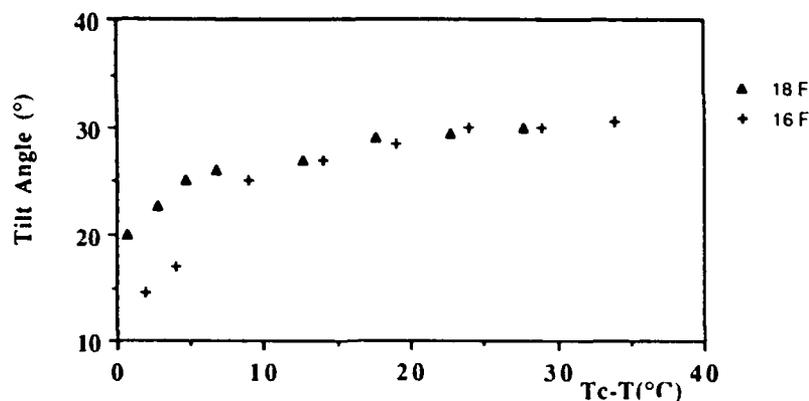
a
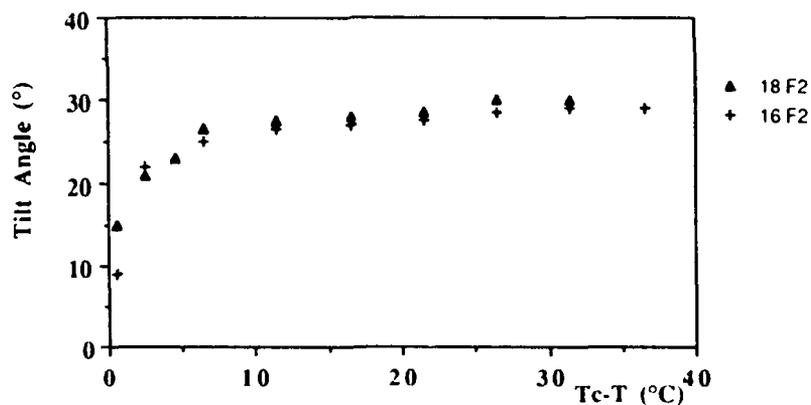
b

FIGURE 8 :   Tilt angle versus $T_c - T$
a) for 16F and 18F
b) for 16F$_2$ and 18F$_2$

Discussion

The helical smectic A^* phase (TGB$_A$) predicted by De Gennes[3] in 1972 was first observed in polymer systems[16] and finally in pure materials[1]. If in the first series reported by Goodby et al and these three series which exhibit a direct $S_A^* - I$ transition one cannot observe a $S_A^* - S_A$ transition (apparently there is an evolution of the helix pitch), in the other series with the sequence $I\ BP\ N^*\ S_A^*\ S_A\ S_C^*$ Slaney et al[8,9] and ourselves[17] give evidence of the $S_A^* - S_A$ transition. This phase S_A^* is called by Renn and Lubensky[4,5] TGB$_A$. Some recent results with their layer spacings suggest that the analogous tilted of TGB$_A$ phase could be obtained as predicted also by these authors[5].

The difference between the IIIA and IIIB,C series is the presence of the fluorine atom in the two latter ones. The Van der Waals radius of the fluorine (1.35 Å) is not much higher than that of the hydrogen (1.1 Å) but it is sufficient to reduce the S_A or S_A^* temperature range when the S_C^* phase appears.

Compound	16	16F	16F$_2$
$\Delta\ S_A^*$ (°C)	10	5	7

In these cases, the shorter this $\Delta\ S_A^*$ temperature range, the higher the existence probability of the S_A^* phase is. Of course, this existence depend mainly on the molecular polarity especially the polarity near the chiral center and the core and also on the chiral chains. As a matter of fact, when we replace the chiral 2-octanol chain by chiral primary alcohol or by chiral alkyl lactate, the cholesteric phase is favoured and one could obtain new sequence with S_A^* phase[18]. On the other hand, when we replace the fluorine by chlorine and bromine (the steric hindrance increases while the polarity decreases), we also obtaine this new S_A^* phase[17]. But if the fluorine is replaced by the cyano group which favours the S_A phase formation, the TGB$_A$ phase is not observed.

CONCLUSION

The new helical smectic $A*$ phase (TGB$_A$) is found in three different series. It is characterized by racemic mixture studies, contact method, layer spacing measurement and helix pitch and sense determination. In these three series the sequence $I\ S_A^*\ S_C^*$ is observed and the S_A^* phase is only obtained with very long alkoxy chains or when the S_A^* temperature range is short and apparently the S_A^* phase and the S_A (obtained with short alkoxy chains) are miscible. The study of the relation between the molecular structure and the existence of the TGB$_A$, TGB$_C$ and $S_A^* - S_A$ transition is in progress.

Acknowledgement

REFERENCES

1. J.W. Goodby, M.A. Waugh, S.M. Stein, E. Chin, R. Pindak, J.S. Patel, Nature (London), 337, 449 (1989)

2. J.W. Goodby, M.A. Waugh, S.M. Stein, E. Chin, R. Pindak, J.S. Patel, J. Am. Chem. Soc., 111, 8119 (1989)

3. P.G. de Gennes, Solid State Commun, 10, 753 (1972)

4. G. Srajer, R. Pindak, M.A. Waugh, J.W. Goodby, J.S. Patel, Phys. Rev. Lett., 64, 13 (1990)

5. S.R. Renn, T.C. Lubensky, Phys. Rev. A,38, 2132 (1988)

6. S.R. Renn, T.C. Lubensky, Mol. Cryst. Liq. Cryst., under press

7. O.D. Lavrentovich, Y.A. Nastishin, V.I. Kulishov, Y.S. Narkevich, A.S. Tolochko, S.V. Shiyanovskii, Europhys. Lett., 13, 313 (1990)

8. A.J. Slaney, J.W. Goodby, J. Mat. Chem., 1, 5 (1991)

9. A.J. Slaney, J.W. Goodby, Liq. Cryst., 9, 849 (1991)

10. W.B. Austin, N. Bilow, W.J. Kelleghan, K.S.Y. Lau, J. Org. Chem., 46, 2280 (1981)

11. M.F. Nabor, H.T. Nguyen, C. Destrade, J.P. Marcerou, R.J. Twieg, Liq. Cryst., under press

12. S.M. Kelly, Helv. Chim. Acta, 72, 594 (1989)

13. K. Furukawa, K. Terashima, M. Ichihaski, S. Saitoh, K. Miyazawa, T. Inukai, Ferroelectrics, 85, 451 (1988)

14. a) F. Grandjean, C.R. Acad. Sci. Paris, 172, 71 (1922)
    b) R. Caz-no, Bull. Soc. Fr. Min. Cryst., 91, 20 (1968)
    c) Y. Bouligand, J. de Phys., 35, 959 (1974)

15. H.T. Nguyen, A. Babeau, C. Léon, J.P. Marcerou, C. Destrade; A. Soldera, D. Guillon, A. Skoulios, Liq. Cryst., 9, 253 (1991)

16. Y.S. Freidzon, Y.G. Tropsha, V.V. Tsukruk, V.V. Shilov, V.P. Shibaev, Y.S. Lipatov, J. Polym. Chem. (USSR), 29, 1371 (1987)

17. A. Bouchta, H.T. Nguyen et al. to be published

18. R.J. Twieg et al. to be published

CHIRAL γ-LACTONES FOR FLC. THE RELATIONSHIP BETWEEN THE MOLECULAR STRUCTURES AND THE PROPERTIES.

KAZUHIKO SAKAGUCHI,[†] YUTAKA SHIOMI,[†] MITSUHIRO KODEN,[††] and TOMOAKI KURATATE[†††]
[†]Research Laboratories, Daiso Co. Ltd., 9, Otakasu, Amagasaki, Hyogo 660, Japan
[††]Cental Research Laboratories, Sharp Corporation, 2613-1, Ichinomoto, Tenri, Nara 632, Japan
[†††]Liquid Crystal Laboratories, Sharp Corporation, 2613-1, Ichinomoto, Tenri, Nara 632, Japan

Abstract   The relationship between the molecular structures of the optically active γ-lactones as chiral dopants and the properties of ferroelectric liquid crystalline (FLC) mixtures containing them are discussed. The design of molecules having a zig-zag shape for superior chiral dopants are suggested.

INTRODUCTION

With increasing interest in the electro-optical devices using FLCs,[1] many materials have been investigated. One of the most important properties for FLCs is the fast response. FLC materials are often prepared by doping chiral compounds having large Ps's to smectic C (S$_C$) liquid crystalline mixtures with low viscosity in order to realize fast response.

We have investigated optically active compounds having chiral γ-lactone ring as chiral dopants because of their large Ps's and fast responses.[2-7] These excellent properties would be based on the unique γ-lactone structures: 1) two asymmetric carbon atoms are fixed in a rigid 5-membered lactone ring, thereby, free rotation of the dipole moiety (an ester group) is considerably restricted, 2) both the carbonyl group and

the ether group are in the same plane and arranged perpendicular to the long axis of the molecule in the same direction. One of the most remarkable points is that the mixtures containing cis-lactones show much larger Ps's and faster responses than those containing trans-lactones in each diastereomer pair of the optically active α,γ-disubstituted-γ-lactones, for example, chiral α-alkyloxybiphenylyl-γ-alkyl-γ-lactones (2).[7] These observations would be explained by the conformational difference between their molecular structures in the chiral smectic C phase (Sc*).[7-9] Since the Sc liquid crystalline molecules have been suggested to be arranged like zig-zag shape as shown in FIGURE 1,[10-12] the chiral dopants would be affected by the zig-zag environment.[4]
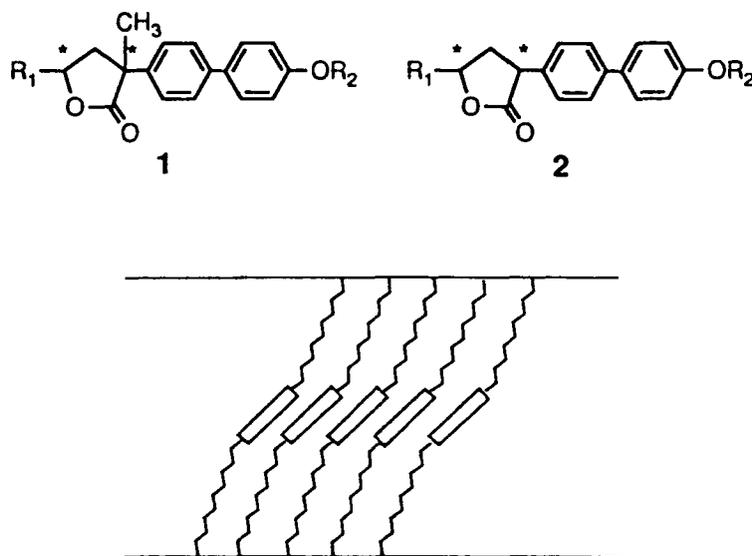
FIGURE 1. The zig-zag conformation of Sc.

Recently, we synthesized new compounds, i.e. optically active α-alkyloxybiphenylyl-α-methyl-γ-alkyl-γ-lactones (1), and found that they showed interesting phenomena; by the introduction of methyl group at α-position of the γ-lactone, the Ps value was lower in the case of the cis-lactone, however, that was higher in the case of the trans-lactone. In this paper, we report the synthesis and some properties of the compounds

(1) and discuss the relationship between their molecular structures presumed by MM2 calculations and the properties in conjunction with the phenomena described above.

EXPERIMENTAL

Preparation of chiral dopants

The γ-lactones **1a** and **1b** were synthesized as shown in SCHEME 1. **2a** (cis) and **2b** (trans) were prepared from (R)-epichlorohydrin in 4 steps.[7-8] The carbanion of the mixture of **2a** and **2b** was treated with methyl iodide in tetrahydrofuran at -78° to afford **1a** (cis, 86%) and **1b** (trans, 3%). Each diastereomer was easily separated by silica gel column chromatography.
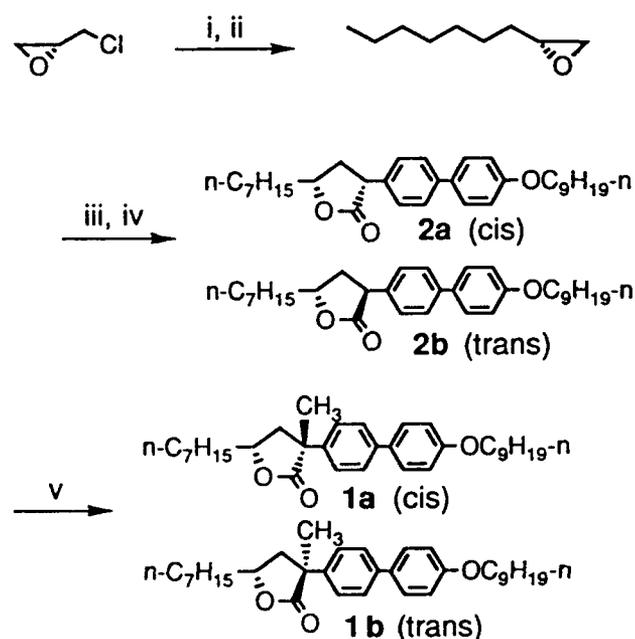
SCHEME 1. i) n-C_6H_{13}MgBr, CuI; ii) NaOH; iii) 2eq. LDA,
HO_2CCH_2⟨◯⟩⟨◯⟩OC_9H_{19}-n ; iv) H_2SO_4; v) LDA, MeI.

Measurements

The FLC mixtures were prepared with 2wt% of the chiral dopants and 98wt% of the achiral S_C liquid crystalline mixture A. The host liquid crystalline mixture A was composed of 2-(4-heptyloxyphenyl)-5-heptylpyrimidine (5wt%), 2-(4-octyloxyphenyl)-5-heptylpyrimidine (10wt%), 2-(4-nonyloxyphenyl)-5-heptylpyrimidine (15wt%), 2-(4-octyloxyphenyl)-5-octylpyrimidine (20wt%), 2-(4-decyloxyphenyl)-5-octylpyrimidine (30wt%), and 2-(4-hexyloxyphenyl)-5-nonylpyrimidine (20wt%). The phase transition temperatures of the host mixture A were Cr <rt S_C 51 S_A 63 N 69 I. (°C) The phase transition temperatures were measured by using a Nikon polarizing microscope fitted with a Mettler FP82 heating stage. FLC cells were constructed using two substrates coated with PVA film, and both of them were rubbed in the same direction. The cell spacing was 2μm. The Ps was measured by the triangular wave method at 25°C. The response was defined as the 0 to 50% change of transmission of light under the voltage of 10 V_{p-p} μm^{-1} at 25°C.

RESULTS AND DISCUSSION

Melting points of the chiral dopants and phase transition temperatures of the FLC mixtures are shown in TABLE I. **1a** and **1b** showed lower melting points than **2a** and **2b** respectively. Almost all the transition temperatures of the mixtures, however, were unaffected by doping of the chiral dopants due to the small amount (2wt%) of doping.

TABLE II shows the electro-optical characteristics of the FLC mixtures comprised of the γ-lactone (2wt%) and the achiral liquid crystalline mixture A (98wt%). **1a** did not show as a large Ps value (+0.7 nC cm^{-2}) and a fast response (258 μs) as **1b** (-0.8 nC cm^{-2}, 191 μs). These observations are obviously different from the cases of **2**. That is, by the introduction of methyl group at α-position of the γ-lactone, the Ps value of the *cis*-lactone was lower, however, that of the *trans*-lactone was higher.

TABLE I. Physical properties of FLC mixtures containing 2wt% of the chiral dopant and 98wt% of the mixture A.

Chiral dopant	mp[a] /°C	Phase transition temp /°C			
		S_C^*	S_A	N^*	I
1a (cis)	72	50	60	67	
1b (trans)	95	48	59	66	
2a (cis)	126	52	62	69	
2b (trans)	—[b]	53	62	69	

a) Melting point of chiral dopant. b) This compound showed mesophases. Cr 96 S_C^* 114 S_A 118 I (°C).

TABLE II. Electro-optical characteristics of FLC mixtures containing 2wt% of the chiral dopant and 98wt% of the mixture A at 25°C.

Chiral dopant	Response[a] /μs	Ps[b] 2wt% /nC cm^{-2}	Tilt angle /deg
1a (cis)	258	+0.7	19
1b (trans)	191	- 0.8	18
2a (cis)	138	+2.9	21
2b (trans)	325	+ —[c]	10

a) Response was defined as the 0 to 50% change of transmission of light under the voltage of 10 V_{p-p}/μm. Cells were coated with polyimide rubbed in the same direction and their thickness was 2 μm. b) Measured by the triangular wave method. c) The absolute value was lower than 0.5.
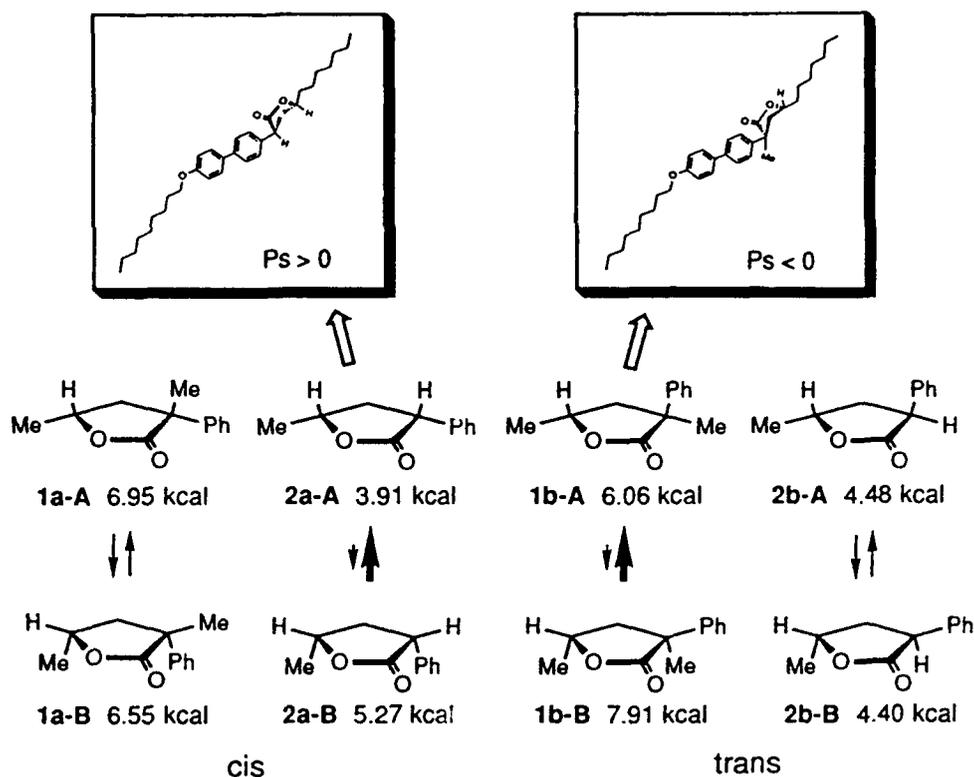
FIGURE 2.   Steric energies of the γ-lactone parts of **1a**, **1b**, **2a** and **2b** calculated by MM2.

FIGURE 2 shows steric energies of the lactones which are the part structures of **1a,1b,2a** and **2b** calculated by molecular mechanics (MM2). In the cases of the cis-lactones, the most stable conformation **2a-A** would fit the zig-zag shape in $S_C{}^*$, and then the dipole moment of **2a** is arranged perpendicular to the axis of the core and alkyl chains, therefore, the sign of Ps is positive and the value is large (+2.9 nC cm^{-2}).[7] **1a-A** which would fit the zig-zag shape, however, is unstable and the contribution of this conformation decreases, therefore, **1a** shows a smaller Ps and a slower response than **2a**. On the contrary, in the cases of the trans-lactones, there would be almost no contributory difference between **2b-A** and **2b-B**, therefore, the Ps value of **2b** is very small (<0.5 nC cm^{-2}) because the direction of the dipole moment would be

flexible in S_C^*.[7] However, **1b-A** is about 1.9 kcal mol^{-1} more stable than **1b-B**, and the contribution of **1b-A** which would comparatively fit the zig-zag shape increases, therefore, **1b** shows a larger Ps and a faster response than **2b**, and the observation of the negative Ps sign of **1b** is reasonable.

In conclusion, the magnitude of the Ps strongly depends on the molecular shape of chiral dopants. The present study demonstrates that it is one of the important factor to design the chiral molecules which smoothly fit the zig-zag shape in S_C^* and have the dipole moment of the appropriate value being arranged perpendicular to the core and alkyl chains in order to get excellent chiral dopants.

REFERENCES

1. N. A. Clark and S. T. Lagerwall, *Appl. Phys. Lett.*, **36**, 899 (1980).
2. M. Koden, T. Kuratate, F. Funada, K. Sakaguchi, Y. Takehira and T. Kitamura, *Proc. of Jpn. Display '89*, 34 (1989).
3. M. Koden, T. Kuratate, F. Funada, K. Awane, K. Sakaguchi, Y. Shiomi and T. Kitamura, *Jpn. J. Appl. Phys.*, **29**, L981 (1990).
4. M. Koden, T. Kuratate, F. Funada, K. Awane, K. Sakaguchi and Y. Shiomi, *Mol. Cryst. Liq. Cryst. Letters.*, **7**, 79 (1990).
5. K. Sakaguchi and T. Kitamura, *Ferroelectrics*, **114**, 265 (1991).
6. K. Sakaguchi, Y. Shiomi, T. Kitamura, M. Koden, T. Kuratate and K. Nakagawa, *Chem. Lett.*, 1109 (1991).
7. K. Sakaguchi, T. Kitamura, Y. Shiomi, M. Koden and T. Kuratate, *Chem. Lett.*, 1383 (1991).
8. Similar discussion: T. Kusumoto, A. Nakayama, K. Sato, K. Nishide, T. Hiyama, S. Takehara, T. Shoji, M. Osawa, T. Kuriyama, K. Nakamura and T. Fujisawa, *J. Chem. Soc., Chem. Commun.*, 311 (1991).
9. Discussion of diastereomeric pairs of fluoroepoxides: D. M. Walba and N. A. Clark, *Ferroelectrics*, **84**, 65 (1988).
10. D. M. Walba, S. C. Slater, W. N. Thurmes, N. A. Clark, M. A. Handschy, J. Xue, D. S. Parmar, S. T. Lagerwall and K. Skarp, *J. Am. Chem. Soc.*, **108**, 5210 (1986).
11. D. M. Walba, R. T. Vohra, N. A. Clark, M. A. Handschy, J. Xue, D. S. Parmar, S. T. Lagerwall and K. Skarp, *J. Am. Chem. Soc.*, **108**, 7424 (1986).
12. E. N. Keller, E. Nachaliel and D. Davidov, *Phys. Rev. A*, **34**, 4363 (1986).

SYNTHESIS, SPECTRA, AND FERROELECTRIC PROPERTIES OF A SERIES OF DIHALOGENATED DOPANTS.

WILLIAM N. THURMES, MICHAEL D. WAND, ROHINI T. VOHRA
Displaytech, Inc., 2200 Central Avenue, Boulder, Colorado 80301

DAVID M. WALBA
Department of Chemistry and Biochemistry, University of Colorado, Boulder, Colorado 80309

Abstract A series of ferroelectric dopants of type $ArOCH_2CHXCHY(CH_2)_2CH_3$, where X and Y are either fluorine or chlorine, were investigated. These compounds were evaluated as a 5% mixture in a phenylpyrimidine host. The compounds with at least one fluorine and with syn halogens all had comparable rise times and switching speeds, although the syn-dichloro compound had a significantly slower rise time. The anti-difluoride was also synthesized by an unambiguous route and its properties were contrasted with the syn-difluoride. This contrasting data helped verify the structures of the two compounds.

INTRODUCTION

Many ferroelectric liquid crystals (FLCs) applications depend on their rapid switching speed. This switching speed can be increased by doping FLCs with high polarization, low viscosity materials. We recently reported[1] a series of high polarization FLC dopants which were based on a difluorohexyloxy chiral tail with the fluorines in a syn configuration. This series of compounds (I) is shown below, where n = 6 through 12. The dipole moments of the difluorinated chiral tail were predicted to be additive, and the compounds were therefore expected to have large spontaneous polarizations. In addition, the combination of a fluorinated tail and a phenylpyrimidine core was expected to impart low orientational viscosity. These predictions were realized, and mixtures containing these compounds were found to have rapid switching times.

I
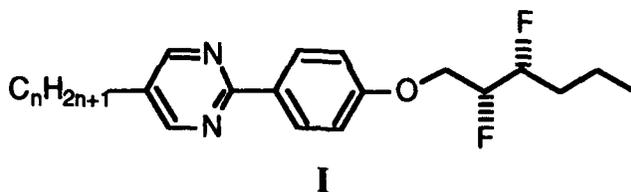
Studies on these compounds led to questions concerning the effect of other halogens on the system. For example, chlorine is bigger than fluorine, which could lead to compounds with greater viscosity. In addition, larger atoms contribute more to steric strain, so the halogens in a chlorinated system have less preference for the gauche

conformation. However, the longer chlorine-carbon bond has a greater charge separation than a fluorine-carbon bond, which should offset its smaller electronegativity difference. The relative influence of these factors on the switching speed was of great interest. In addition, studying the chlorinated systems might lead to new insights about the fluorinated system. A series of syn-dihalogenated compounds of type **II**, where X and Y are either fluorine or chlorine, was accordingly synthesized and studied.

II
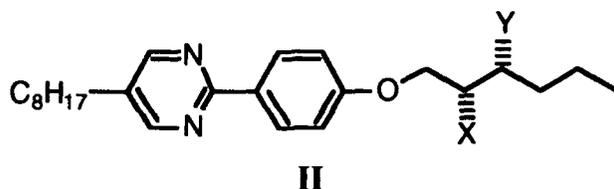
Although several analogs of the type **II** series had been previously synthesized, their achiral tail lengths varied, which can in some cases significantly effect physical properties of the dopants. All dopants used in this study were consequently given a uniform achiral tail length of eight carbons. In addition to the syn-dihalo compounds, the anti-difluoro compound **MDW 389** was also synthesized by an unambiguous route. This compound was made as a contrast to the syn-difluoride, both to elucidate structure-property correlations and to help verify the structure of the syn isomer.

MDW 389
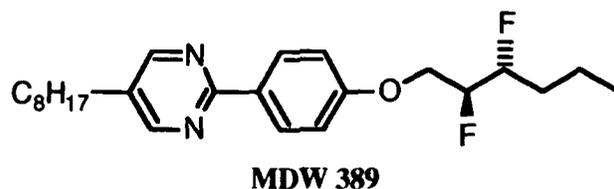
SYNTHESIS OF THE DIHALOALKOXIDES

The synthesis of the dihaloalkoxyphenylpyrimidines is summarized in SCHEME 1. The starting trans-epoxy ether[2] **III** was transformed into the halohydrins in two ways. First, treatment with hydrogen chloride and lithium tetrachlorocuprate gave the chlorohydrin **IV**. Alternatively, its treatment with hydrogen fluoride-pyridine gave the fluorohydrin **V**.

Attaching the second halide to the system was again done using one of two methods. First, a solution of chlorohydrin **IV** was treated with diethylaminosulfur trifluoride (DAST) to give the 2-fluoro-3-chloro compound **MDW 367**. When the chlorohydrin was alternatively treated with thionyl chloride in pyridine, the 2,3-dichloride **MDW 391** resulted. Elucidation of the fluorohydrin into dihalides was done in an analogous manner. Treatment of the fluorohydrin **V** with DAST gave the 2,3-difluoride **MDW 232**, whereas treatment with thionyl chloride gave the 2-chloro-3-fluoro compound **MDW 388**. The DAST and thionyl chloride/pyridine reactions are known to proceed with inversion in most cases.
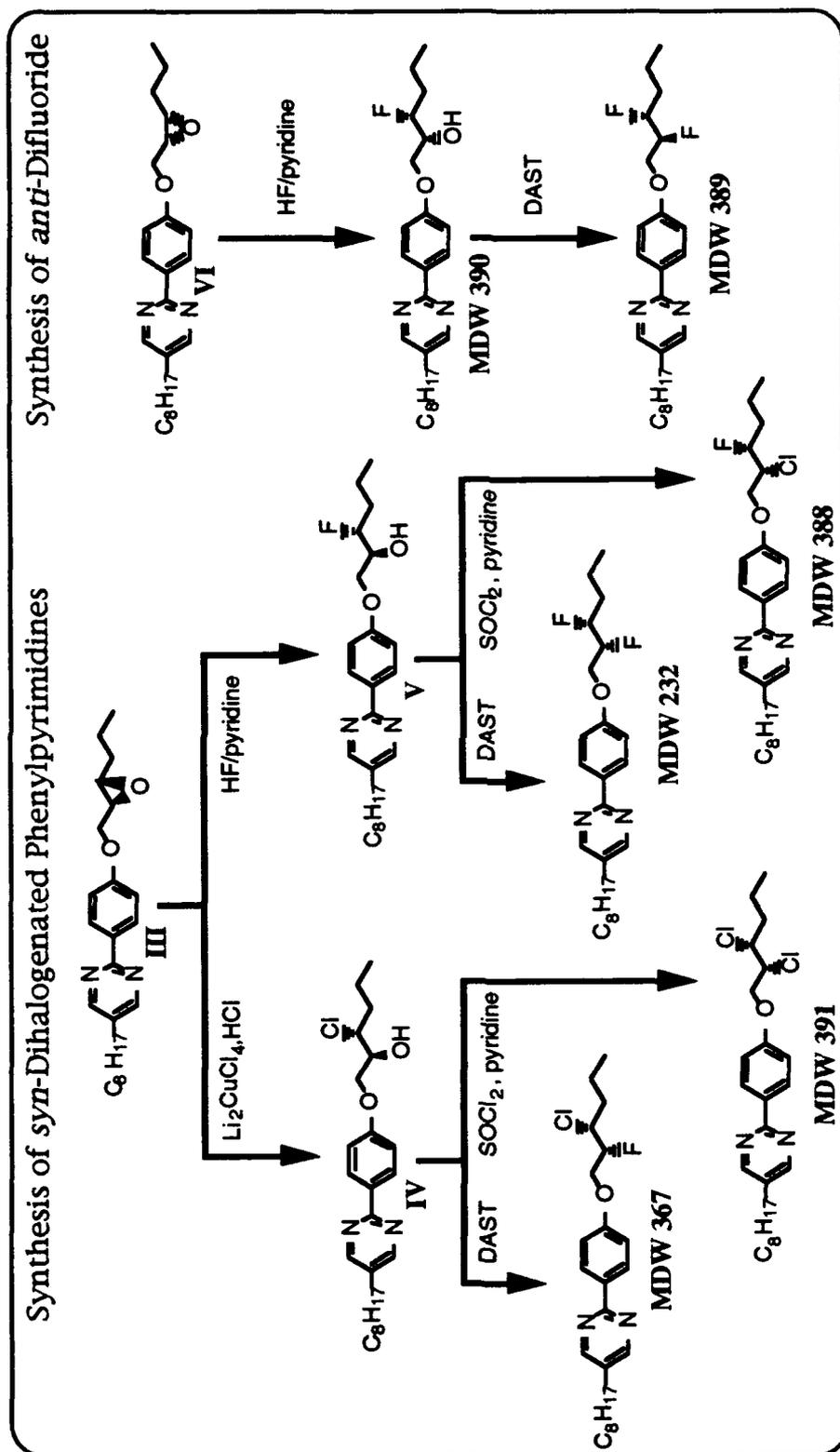
SCHEME 1:   Synthesis of five dihaloalkoxides from epoxides.

Synthesis of the anti-difluoride began with the reaction between cis-epoxide **VI** and hydrogen fluoride-pyridine, which gave the syn-fluorohydrin **MDW 390** as the major product. This compound was interesting in its own right, and was accordingly evaluated. A DAST reaction transformed the fluorohydrin into the difluoride **MDW 389**.

TABLE 1. Evaluation Data on a Series of Dihaloalkoxides[a].

Ar = C_8H_{17}—(pyrimidine ring)—(phenyl ring)—
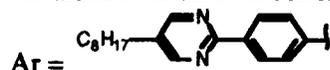
	Structure	θ	P$_s$	P$_0$[b]	τ$^c_{10\text{-}90}$	Phase diagram in host
MDW 232	ArO—(chain with F up, F down)	23	-8.9	-450	42	$I \xrightarrow{87°} N \xrightarrow{80°} A \xrightarrow{62°} C* \xrightarrow{<RT} X$
MDW 389	ArO—(chain with F up, F down)	18.5	+1.5	95	118	$I \xrightarrow{87°} N \xrightarrow{82°} A \xrightarrow{58°} C* \xrightarrow{<RT} X$
MDW 388	ArO—(chain with F up, Cl down)	26.5	-9.5	-425	47	$I \xrightarrow{87°} N \xrightarrow{81°} A \xrightarrow{61°} C* \xrightarrow{<RT} X$
MDW 367	ArO—(chain with Cl up, F down)	21.5	-7.3	-400	50	$I \xrightarrow{86°} N \xrightarrow{80°} A \xrightarrow{58°} C* \xrightarrow{<RT} X$
MDW 391	ArO—(chain with Cl up, Cl down)	26.5	-5.1	-230	66	$I \xrightarrow{87°} N \xrightarrow{81°} A \xrightarrow{59°} C* \xrightarrow{<RT} X$
MDW 390	ArO—(chain with F up, OH down)	22.0	-6.2	-330	64	$I \xrightarrow{89°} N \xrightarrow{82°} A \xrightarrow{58°} C* \xrightarrow{<RT} X$
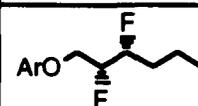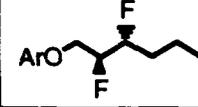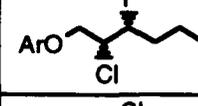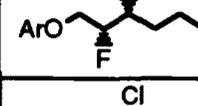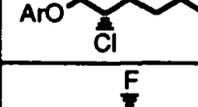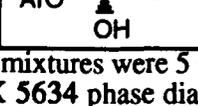
a. All mixtures were 5 wt % in **MX 5634**, a mixture of alkoxyphenylpyrimidines. **MX 5634** phase diagram= I-90→N-83→A-65→C-<RT→X.
b. P$_0$ was obtained by multiplying the measured P$_s$ by 20 to give P$_{ext}$, and dividing by sin θ. It is measured in nC/cm^2.
c. The rise time, given in μs, was measured at 6 V/μm, and extrapolated to 15 V/μm.

EVALUATION OF THE DIHALOALKOXIDES

The series of dihaloalkoxides and the syn-fluorohydrin were doped at 5 wt % concentration into an alkoxyphenylpyrimidine host and the mixtures were evaluated for liquid crystalline properties. The evaluation data for this group of compounds is summarized in TABLE 1.

PHASE DIAGRAMS The syn-3-fluoro compounds slightly depressed the transition points in the phase diagram of the host, but the N* and SmA ranges changed little in width. The other four compounds, however, each increased the width of the SmA phase by four to six degrees.

POLARIZATION The sign of the polarization predicted by the Boulder model[3] is negative for all the syn-substituted compounds, in which the halo or hydroxyl group in the 2 position has an S configuration. For the anti-substituted compound, which has an (R)-2-fluorine, the Boulder model predicts a positive sign of polarization.

In addition, the dipole moments of the halides in the syn-substituted compounds were expected to be additive, leading to a large dipole moment. On the other hand, the dipole moments of the fluorines in the anti-difluoride were expected to counteract each other, leading to a much lower polarization.

In fact, the spontaneous polarizations of these compounds agreed with the Boulder model in both sign and magnitude. As expected, the syn-difluoride **MDW 232** had a large negative polarization, with a P_0 of -450. The two chloro-fluoro compounds had similar, somewhat lower polarizations, with the 2-chloro-3-fluoro compound having the greater polarization. The P_0s of both of these compounds were within 10% of that of the difluoride, showing the compounds to be quite similar. The P_0 of the dichloride was significantly lower, perhaps because the chlorines are too large to favor the gauche configuration. The fluorohydrin had a high polarization and a surprisingly fast switching speed, indicating that the hydroxyl group may be hydrogen bonded with the fluorine. Lastly, the polarization of the anti-difluoride had a positive sign and was quite low, as was expected.

RISE TIME The rise times of the syn-difluoride was the fastest, but both chloro-fluoro compounds were right behind it. This indicates that the viscosity was not significantly changed by the substitution of a chlorine for a fluorine. The dichloride and the fluorohydrin, although they had very different P_0s, had similar rise times, which appears to indicate that the dichloride had low viscosity. The anti-difluoride, with its low P_0, as expected had a long rise time.

STRUCTURAL PROOF OF THE SYN AND ANTI DIFLUORIDES

The anti-fluorohydrin V, precursor to syn-difluoride **MDW 232**, had its regiochemistry unambiguously established by ^{13}C NMR. In ^{13}C NMR, the protons are generally broad-band decoupled, leaving carbon signals as single, uncoupled peaks. The fluorine atom has a spin of $\frac{1}{2}$ but is not decoupled, therefore splitting the carbon signals near it into doublets. The coupling constant's magnitude depends on the bond separation between the carbon and the fluorine. The fluorine in fluorohydrin V was shown to be three carbons away from the aryl ether. The epoxide opening with acid is known to proceed in a stereo-specific fashion, so the stereochemistry of the fluorohydrin was likewise established.

The fluorohydrin was treated with DAST to make the difluoride **MDW 232**. The DAST reaction proceeds with inversion of stereochemistry in all but a few cases in literature. In those instances, a stabilized cationic intermediate could be postulated. However, in this case, no such stabilized intermediate exists. **MDW 232** was therefore assumed to have a syn configuration, but a more rigorous stereochemical proof was required.

Schlosser[4] studied a symmetrical vicinally difluorinated system, which had an alkyl group on both sides of the difluoro entity. He found that the anti-difluoride had a $^3J_{HF}$ of about 14 Hz, whereas the syn-difluoride had a $^3J_{HF}$ of 22 Hz. We have studied a sym-

metrical vicinally difluorinated system[1], believed to possess a syn configuration, and found that it also had a $^3J_{HF}$ of 22 Hz. However, for **MDW 232**, the $^3J_{HF}$ was determined to be 18.2 Hz, halfway between Schlosser's syn- and anti-difluoride values. This discrepancy may be due to the unsymmetrical nature of the difluoroalkoxy system, since the difluoro entity has an alkyl group on one side and an alkoxy group on the other side.

The anti-difluoride **MDW 389** was synthesized, and found to have a $^3J_{HF}$ of 14.3 Hz. This coupling constant agrees with Schlosser's value for the anti system, and is significantly lower than **MDW 232**'s syn coupling constant, thus indicating that in **MDW 389** the fluorines do indeed have an anti configuration. The two compounds, known to have an (R)-fluorine on the third carbon and a fluorine on the second carbon of the chiral tail, had different splitting patterns and different chemical shifts in the ^{19}F NMR. Thus, they were established as enantiomers, and since **MDW 389** was demonstrated to be the anti compound, **MDW 232** must therefore be the syn compound.

Additional proof of **MDW 232**'s stereochemistry was provided by spontaneous polarization evidence. **MDW 232** has an (R)-fluorine on the second carbon, and the sign of its polarization was thus expected to be negative. In addition, when the carbons of the tail line up in the preferred zig-zag, a gauche conformation between the fluorines results, leading to a large additive dipole moment and a large polarization. In contrast, **MDW 389** has an (S)-fluorine on the second carbon, which should give a positive polarization. In a zig-zag tail, its fluorines are anti to one another, so the dipoles cancel out, and a small polarization results. All of these predictions were correct, as **MDW 232** had a large negative polarization and **MDW 389** instead had a small positive polarization.

CONCLUSION

A series of four (R,R)-2,3-dihalohexyloxyphenylpyrimidines, where the halogens were chlorines and/or fluorines, were synthesized. When these compounds had at least one fluorine, they had very high polarizations and fast rise times. When both halogens were chlorine, a moderately high polarization and fast switching speed resulted. The (R,R)-2-hydroxyl-3-fluorohexyloxyphenylpyrimidine and the (S,R)-difluorohexyloxyphenylpyrimidine were also synthesized. The fluorohydrin was found to have a polarization higher than and a rise time comparable to those of the dichloride. The (S,R)-difluoride had both low polarization and slow rise time.

The anti- and syn-difluroides were studied by fluorine and proton NMR to ascertain their stereoconfigurations. Their properties were contrasted to incontrovertibly demonstrate the stereochemistry of each.

[1]   Thurmes, W. N.; Wand, M. D.; Vohra, R. T.; and Walba, D. M. *Mol. Cryst. Liq. Cryst.* **1991**, *204*, 1.

[2]   Walba, D. M.; Vohra, R. T.; Clark, N. A.; Handschy, M. A.; Xue, J.; Parmar, D. S.; Lagerwall, S. T.; Skarp, K. *J. Am. Chem. Soc.* **1986**, *108*, 7424.

[3]   Walba, D.M.; Slater, S.C.; Thurmes, W.N.; Clark, N.A.; Handschy, M.A.; Supon, F. *J. Am. Chem. Soc.* **1986**, *108*, 5210.

[4]   Hamatani, T.; Matsubara, S.; Matsuda, H.; Schlosser, M. *Tetrahedron* **1988**, *44*, 2875.

PROPERTIES OF A SERIES OF PHENYLPYRIMIDINE FERROELECTRIC LIQUID CRYSTALS POSSESSING THE 2,3-DIFLUOROALKOXY TAIL.

MICHAEL D. WAND, WILLIAM N. THURMES, ROHINI T. VOHRA, KUNDALIKA MORE
Displaytech, Inc., 2200 Central Avenue, Boulder, Colorado 80301

DAVID M. WALBA
Department of Chemistry and Biochemistry, University of Colorado, Boulder, Colorado 80309

Abstract   A series of high polarization Ferroelectric liquid crystal (FLC) dopants based on the 2,3-difluorohexyloxyphenylpyrimidine family was modified by 1) fluorination of the core and 2) replacement of the alkyl achiral tail with an alkoxy tail. Their polarization, rise time, N* and C* helical pitch, and effect on smectic A/C* phase transition as a 10% mixture in an achiral phenylpyrimidine host were determined. In all cases, core fluorination and alkoxy substitution results in a decrease in polarization while rise time remained relatively constant. All modifications resulted in a lengthening of the C* pitch relative to the parent structure. In several cases core fluorination resulted in sign reversal of the N* pitch making use of these dopants potentially useful as pitch compensating agents an attractive possibility.

INTRODUCTION

Ferroelectric smectic C* liquid crystals have been used in high speed, multistate electro-optic, display device and opto-electronic computing applications, particularly when incorporated into the surface stabilized ferroelectric liquid crystal (SSFLC)[1] light valve. High polarizations are necessary to achieve the speeds desired in opto-electronic computing, waveguide, and fiber-optic applications while long helical pitch is necessary to afford good alignment in the SSFLC geometry. We recently reported[2] a series of high polarization FLC dopants containing a 2,3-difluorohexyloxy chiral tail with the fluorines in a syn configuration shown below. The dipole moments of the 2,3-difluorinated chiral tail were predicted to be additive, and the compounds were therefore expected to have large spontaneous polarizations. In addition, the combination of a fluorinated tail and a phenylpyrimidine core was expected to impart low orientational viscosity. These predictions were realized, and mixtures containing these compounds were found to have rapid switching times although their rather tight C* pitch limited the use of high concentrations of these dopants in achiral hosts.

I
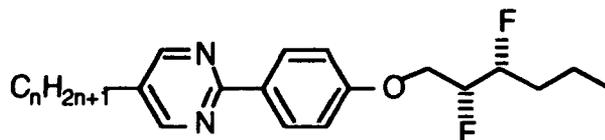
High polarization in an FLC dopant is often accompanyed by tight N* and/or C* helical pitch and typically results in poor FLC alignment when used in the SSFLC mode. In an effort to improve the pitch and polarization of this useful class of compounds, a series of compounds possessing the syn-difluorinated tail, where X and Y, in structure II shown below, are either fluorine or hydrogen, and R is either octyl or octyloxy, were synthesized and evaluated for polarization, switching speed, and helical pitch in both the N* and C* phase.

II
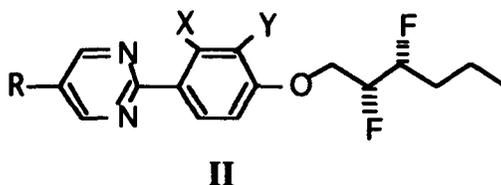
Results from this evaluation showed, in general, a decrease in polarization, while the N* and C* pitch were improved (e.i. lengthened). A detailed discussion of these findings follows.

EVALUATION OF THE DIFLUOROALKOXIDES

The mesomorphic properties of the series of difluoroalkoxides were examined after wh... they were doped at 10 wt % concentration into an achiral phenylpyrimidine host and the mixtures evaluated for ferroelectric properties. Chart 1 shows mesomorphic properties of these compounds whereas Table 1 refers to their respective ferroelectric properties (P$_s$, τ, θ, pitch) in a phenylpyrimidine host.

MESOMORPHIC PROPERTIES. The most striking observation for this series of compounds (as pure compounds) is that the dopants with alkyloxy tails have liquid crystalline phases while the compounds with alkyl tails do not. In fact, the monofluorinated alkoxy compound, MDW427, possesses a 14°C enantiotropic C* phase, the first two-ring compound with a difluoroalkoxy tail showing the desirable tilted smectic phase. It is interesting to note that the presence or absence of a liquid crystalline phase in a particular compound does not seem to be a significant factor in its usefulness as a dopant when used in low concentrations in an achiral host.

PHASE DIAGRAMS OF MIXTURES. In general, this class of dopants shows good solubility with phenylpyrimidine-type hosts. The degree of A/C* transition depression depends upon the degree of ring-fluorine substitution and not on whether the achiral tail is an alkyl or alkoxy moiety. Unsubstituted-core and difluorinated-core dopants MDW232, MDW428, and MDW434 result in a 2 to 3°C suppression of the A/C transition while monofluorinated-core dopants MDW427 and MDW432 show a significantly greater depression of 9°C.

Chart 1. R, R-2,3-Difluoroalkoxy Phenylpyrimidines: Mesomorphic Properties
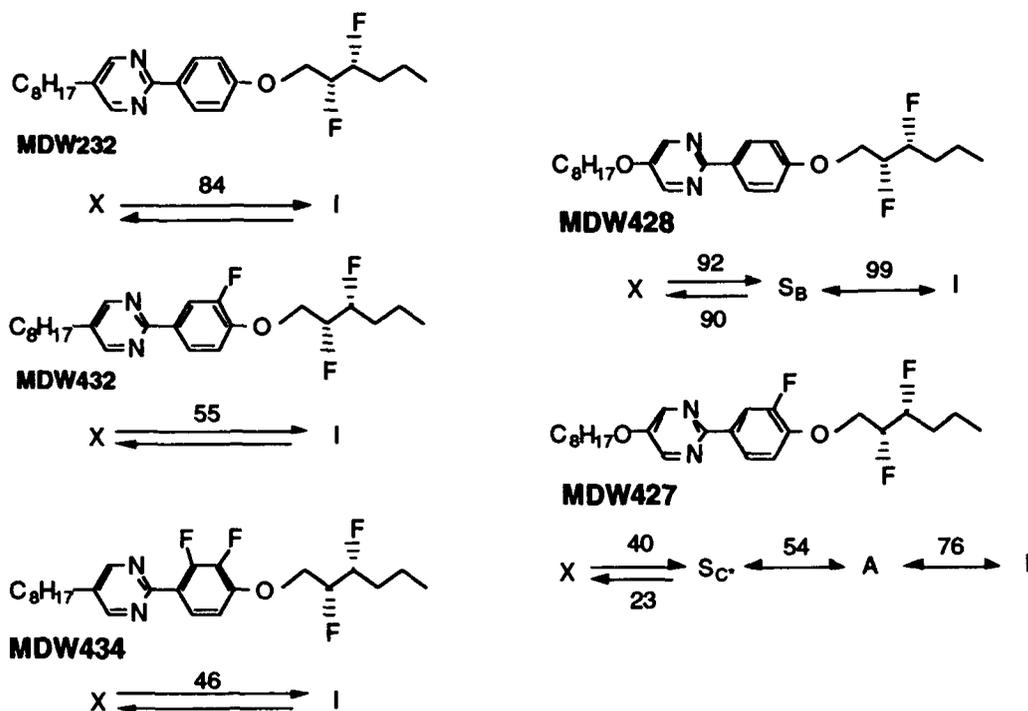
C_8H_{17}—[pyrimidine]—[phenyl]—O—[2,3-difluoroalkyl tail]

MDW232

$$X \underset{}{\overset{84}{\rightleftarrows}} I$$

C_8H_{17}—[pyrimidine]—[fluorophenyl]—O—[2,3-difluoroalkyl tail]

MDW432

$$X \underset{}{\overset{55}{\rightleftarrows}} I$$

C_8H_{17}—[pyrimidine]—[difluorophenyl]—O—[2,3-difluoroalkyl tail]

MDW434

$$X \underset{}{\overset{46}{\rightleftarrows}} I$$

$C_8H_{17}O$—[pyrimidine]—[phenyl]—O—[2,3-difluoroalkyl tail]

MDW428

$$X \underset{90}{\overset{92}{\rightleftarrows}} S_B \overset{99}{\longleftarrow} I$$

$C_8H_{17}O$—[pyrimidine]—[fluorophenyl]—O—[2,3-difluoroalkyl tail]

MDW427

$$X \underset{23}{\overset{40}{\rightleftarrows}} S_{C^*} \overset{54}{\longleftarrow} A \overset{76}{\longleftarrow} I$$

POLARIZATION The sign of the polarization predicted by the Boulder model[3] is negative for the difluoroalkoxy tail in which both fluorines are R in configuration. This is consistent with the values measured for all dopants. The magnitudes of the normalized polarizations ranged from -510 to -230 nC/cm^2. Fluorination of the core in all cases reduced the polarization. Substitution of alkoxy for alkyl achiral tail also decreased the polarization. It is interesting to note that previous research[4] by Displaytech using the 2,3-difluoro tail with the phenylbenzoate core showed a significant increase in polarization upon fluorination of the core, indicating orientation of the ring normal to the smectic C* layer tilt plane and consequent contribution of the ring fluorine dipole to P_S. Although ring orientation in the phenylpyrimidine system is less well understood, we can use fluorination of the ring as a probe to help us gain some insight into the rings probable orientations. Since fluorination of the ring does not increase P_S, we can rationalize that the fluorinated ring resides in the tilt plane, and therefore does not contribute to P_S.. This represents only a glimpse of what we think is happening on a molecular level since we have no easy explanation for the 20% decrease in P_S in both the mono and difluorinated alkyl cases or the further P_S decrease in the alkoxy cases.

Table 1. Difluoroalkoxy dopants at 10% concentration in phenylpyrimidine host.MX6033 [a]

ID#	R	X, Y	SmC — SmA — Ch — I			P_s (nC/cm²)	θ (°)	P_o [b]	$\tau_{10\text{-}90}$ (μs) [c]	N* pitch (μm)	C* pitch (μm)
MDW232	C_8H_{17}—	H, H	60	72	81	-23.5	27.5	-510	37	-7	-2
MDW432	C_8H_{17}—	H, F	54	74	91	-15.0	21.5	-410	35	+16	-6
MDW434	C_8H_{17}—	F, F	61	70	80	-18.3	26.5	-410	37	+3	-3
MDW428	C_8H_{17}O—	H, H	61	73	86	-13.7	25.0	-320	41	-4	-3
MDW427	C_8H_{17}O—	H, F	54	79	85	-8.9	22.5	-230	33	-4	-6

a MX6033 host phase diagram, S_C—63—S_A—77—N—85—I

b P_o was obtained by multiplying P_s by 10 to give Pext and dividing by sin θ

c Rise time measurements performed at 6V/μm and normalized to 15V/μm

All measurements performed at $T_{A/C}$ = -40°C

RISE TIME The rise times of all the dopants measured are remarkably consistent and range from 33 to 41 µsec at 15 v/µm. This is surprising in light of the fact that polarizations vary as much as twofold. Variations in tilt angle can only partly explain the rise times. A decrease in orientational viscosity must account for the remainder. Core fluorination and use of an alkoxy tail both seem to promote a lower viscosity, at least in this system.

C* PITCH. The C* pitch measured in the 10% mixtures ranged from -2 to -6 µm. Monofluorination afforded the longest pitch while, interestingly, addition of a second fluorine caused the pitch to retighten nearly to the original core-unfluorinated value.

N* PITCH. The N* pitch varies to an even greater extent than C* pitch. In the alkylphenylpyrimidines, fluorination of the core actually results in inversion of the sign of the helix, from left-handed (-) to right-handed ( ). Addition of a second fluorine causes further winding of the helix to a more tightly positive value. In the alkoxyphenylpyrimidines, fluorination does not effect the N* helical pitch, measured at -4 µm in both the non-fluorinated and monofluorinated cases.

CONCLUSION

In an effort to enhance the properties of the high polarization FLC dopants (R,R)-2,3-difluorohexyloxyphenylpyrimidines, five analogs were synthesized and evaluated. Polarizations were decreased but did not significantly effect switching speeds. The new compounds exhibit a longer C* pitch affording good alignment in the SSFLC geometry. Several of the analogs showed an inversion of the N* helix upon core fluorination suggesting their use as pitch compensating dopants in FLC mixtures and that core fluorination may be a general technique to modify the helical pitch in other chiral FLC systems. In addition, the data clearly shows that there is not a strong correlation between polarization and helical pitch, or for that matter, between N* and C* pitch.

[1] Clark, N. A.; Handschy, M. A.; Lagerwall, S. T. *Mol. Cryst. Liq. Cryst.* **1983**, *94*, 213-234.
[2] Thurmes, W. N.; Wand, M. D.; Vohra, R. T.; and Walba, D. M. *Mol. Cryst. Liq. Cryst.* **1991**, *204*, 1.
[3] Walba, D.M.; Slater, S.C.; Thurmes, W.N.; Clark, N.A.; Handschy, M.A.; Supon, F. *J. Am. Chem. Soc.* **1986**, *108*, 5210.
[4] Wand, M. D.; Vohra, R. T.; and Walba, D. M. Clark, N.A.; Shao, R. *Mol. Cryst. Liq. Cryst.* **1991**, *202*, 183.

NOVEL FERROELECTRIC LIQUID CRYSTALS HAVING A PLANAR CORE STRUCTURE

AKIHISA YOKOYAMA, ATSUSHI YOSHIZAWA AND TOSHIHIRO HIRAI

Materials Development Research Laboratories,

Nippon Mining Co.,Ltd.

3-17-35, Niizo-Minami Toda-shi Saitama 335, Japan

Abstract   We have designed new core structures, 2-phenylnaphthalene, 2-phenylquinoline and 2-naphthylpyridine, and prepared new ferroelectric liquid crystals having these core structures. One of these compounds, 2, showed a chiral smectic C phase. The SmC* mixtures containing the compound 1 or 3 did not show the zig-zag defects.

1. INTRODUCTION

The surface stabilized ferroelectric liquid crystal display (SSFLCD) is very attractive for a highly multiplexable electrooptical device because of the fast response and the bistability.[1] However, the SSFLCD is still in the development phase owing to the structural complexities in the SSFLC cell, such as the chevron structure[2] and the twisted states.[3]

Much effort has been done to realize the bookshelf or quasi-bookshelf structure, however, only a few studies on the relationship between the chemical structure of the FLC materials and the appearance of the bookshelf structure have been made. Mochizuki et al. showed that

zig-zag defect did not appear in the SmC* phase of the material containing a naphthalene ring.[4] Takanishi et al. investigated the layer structure of a naphthalene-derived SmC* mixture, using XRD in detail.[5]

  In this report, we present ferroelectric liquid crystal compounds 1-5 characterized by a planar and direct-connecting core structure, such as 2-phenyl-naphthalene, 2-phenylquinoline and 2-naphthylpyridine.

The properties of the mixtures containing these compounds are also discussed.

2.EXPERIMENTAL

2.1 Preparation of Compounds

The compounds **1-5** were prepared according to SCHEME 1 by an esterification reaction of (S)-(-)-2-fluoro-2-methyl-heptanoic acid with the corresponding mesogenic phenols **6-10** using dicyclohexylcarbodiimide as a condensation reagent. The compounds were purified by using silica-gel column chromatography followed by recrystallization from ethanol. Their structures were confirmed by I.R. and N.M.R. spectra. Optically active 2-fluoro-2-methyl-heptanoic acid was prepared from corresponding commercially available optically active 2-methyl-1,2-epoxyheptane.[6] The optical purity of 2-Fluoro-2-methyl-heptanoic acid used in this work is 80 % e.e.

$$\overset{\displaystyle O}{\overset{\displaystyle \diagup \diagdown}{H_2C-\underset{\underset{CH_3}{|}}{\overset{*}{C}}-C_5H_{11}}} \quad \xrightarrow[\text{or SiF}_4]{^iPr_2NH \cdot nHF}$$

$$HOCH_2-\underset{\underset{CH_3}{|}}{\overset{*}{CF}}-C_5H_{11} \quad \xrightarrow{\quad KMnO_4 \quad}$$

$$HOOC-\underset{\underset{CH_3}{|}}{\overset{*}{CF}}-C_5H_{11} \quad \xrightarrow[\text{DCC}]{\begin{array}{c} R-\ CORE\ -OH \\ \underline{6 \cdot 10} \end{array}}$$

$$R-\ CORE\ -OCO-\underset{\underset{CH_3}{|}}{\overset{*}{CF}}-C_5H_{11} \quad \underline{1 \cdot 5}$$
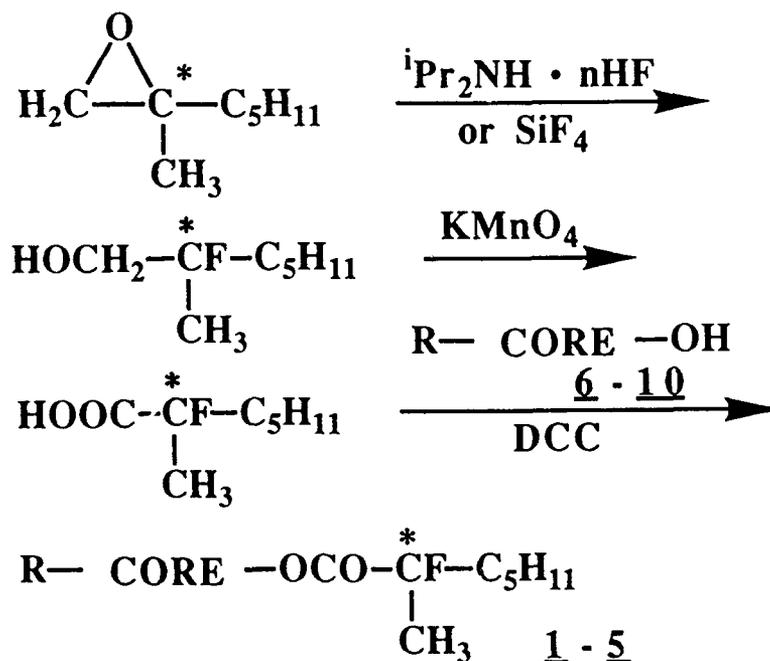
SCHEME 1   The synthetic route of the compounds **1-5**

The phenols 6-10 were obtained according to SCHEME 2. The key step was an aryl-aryl hetero-coupling reaction catalyzed by tetrakis(triphenylphosphine)palladium(0).[7]
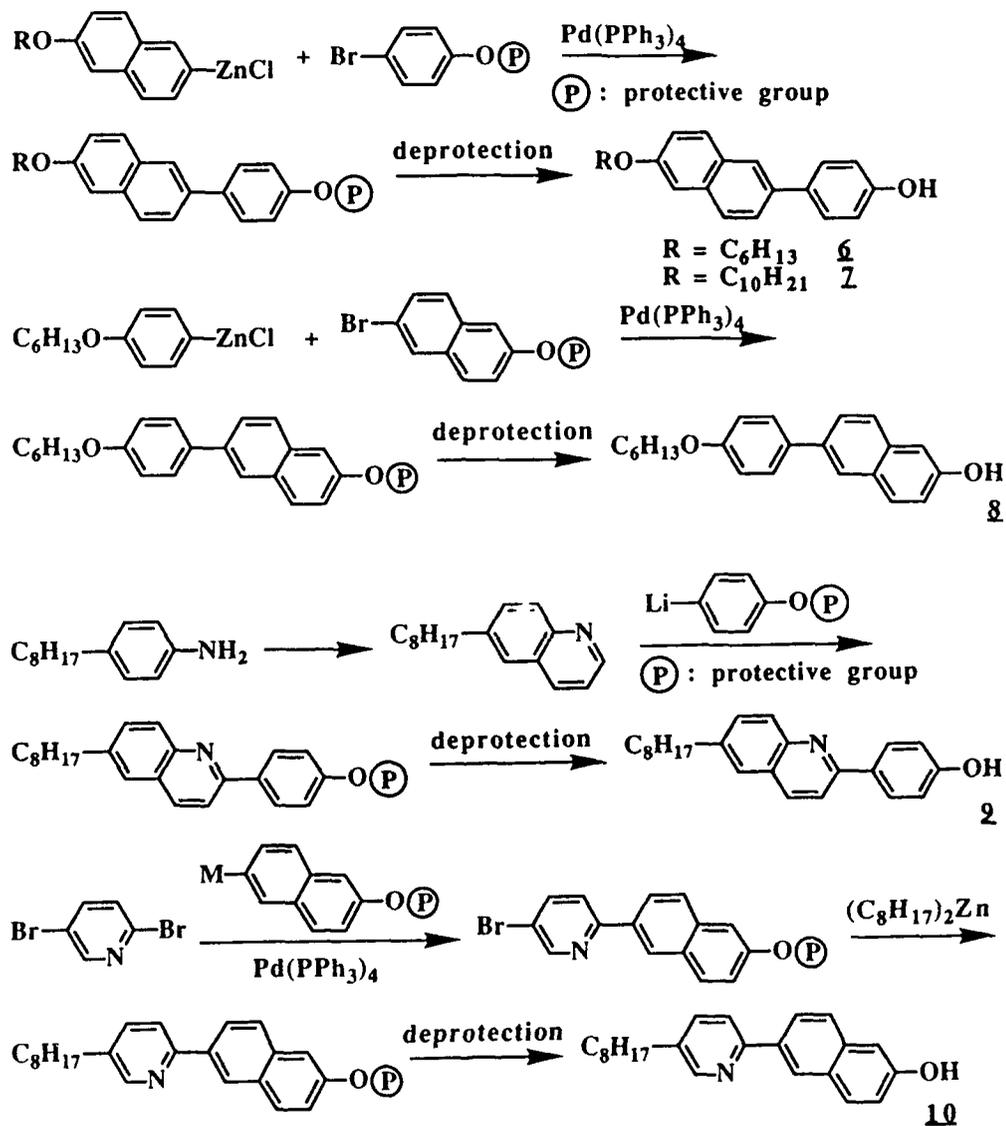
SCHEME 2   The synthetic routes of the phenols 6-10

2.2 Measurement of Physical Properties

The samples were sandwiched between two ITO coated glass plates. The plates were coated with thin polyimide and the surfaces were rubbed unidirectionally. The cell thickness was 3 μm. The transition temperatures of the sample were obtained using a polarizing microscope with a hot stage (Mettler FP-82). Optical micrographs of the texture were taken with the Nikon OPTIPHOT-POL. The spontaneous polarization was measured by the triangular wave method (30Vpp, 100Hz).[8] The sense of spontaneous polarization was determined by the field reversal method by optical observation of the director motion. The definition is the same as that by Lagerwall and Dahl.[9] The tilt angle was directly measured by finding an extinction direction under a DC field (±15V).

3. RESULTS AND DISCUSSION

The phase transition temperatures of the compounds 1-5 are shown in TABLE I. In comparison with 2, the transition temperatures of a compound having an ester linkage in the core, 4-(2-fluoro-2-methylheptanoyloxy)-phenyl 6-decyloxynaphthalene-2-carboxylate (11), are also indicated.

$$C_{10}H_{21}O\text{—}\bigcirc\!\!\bigcirc\text{—COO—}\bigcirc\text{—OCOC}^*FC_5H_{11}$$
$$\underset{CH_3}{|} \quad 11$$
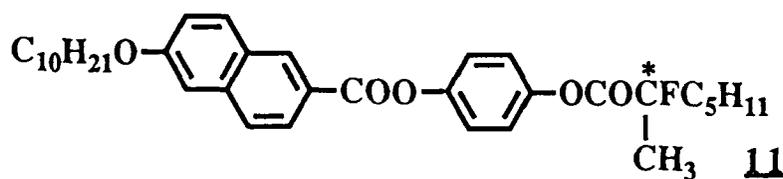
TABLE I   The transition temperatures of the compounds 1-5 and 11

compound	Cr	Sx[1)	Sc*	S$_A$	I
1	• ?[2)	• 80		• 110	•
2	• 81.6		• 85.4	• 96.3	•
3	• 87			• 110	•
4	• 65.3	(• 63.5)[3)			•
5	• 68.5				•
11	• 94.4				•

1) Sx means unidentified smectic phase.

2) Melting point was not clear.

3) Parenthese indicates monotropic phase transition.

Compounds 1-3 exhibited stable smectic phases in comparison with compound 11. This result suggests that the direct-connecting core structure stabilized the mesophase. Only the compound 2 exhibited a SmC* phase. In contrast to 1, it could be explained that the aliphatic interaction of the long alkyl chain of 2 compensated the decrease of the aromatic interaction owing to the bulkiness of the naphthalene ring. In the compound 4 and 5, the thermal stability of the mesophase was extremely lowered.

The chiral structure of the compound 2 contributed to a rather large spontaneous polarization of -175 nC/cm^2 at 77.4 °C. It was already reported that a compound, having the same chiral structure, showed a large spontaneous polarization (max. 400 nC/cm^2).[10] The magnitude of spontaneous polarization and the tilt angle of compound 2 are shown in TABLE II.

TABLE II   The magnitude of spontaneous polarization
and the tilt angle of 2

temperature($°$C)	Ps(nC/cm^2)	tilt angle($°$)
83.4	-105.9	20.6
81.4	-136.6	23.1
79.4	-156.2	26.6
77.4	-175.2	27.3

On purpose to realize the bookshelf structure, the
binary mixtures of chiral dopant (20 mol%) and 5-hexyl-2-
(4'-heptylbiphenylyl)pyrimidine[11] (80 mol%) were prepared.
The transition temperatures and the tilt angle of these
mixtures are shown in TABLE III.

TABLE III   The transition temperatures and the tilt
angle of the mixtures

Chiral dopant	Phase transition temperature					Tilt angle[2]
	Cr[1]	Sc*	S_A	Ch	I	
1	•33.4	•94.0	•110.5	•130.3	•	26.4°
2	•21.6	•92.2	•119.3	•128.0	•	20.9°
3	•27.8	•96.3	•110.1	•128.1	•	29.0°
4	•16.9	•81.9	•110.2	•125.7	•	15.0°
5	•27.5	•80.7	•107.3	•124.2	•	20.1°
11	•21.6		•120.5	•128.8	•	

1) Crystalizing point when it was cooling.
2) Tilt angles were measured at 30 degrees below the
   SmA - SmC* transition temperature.

In the mixture doped with 11, the SmC* phase did not appear. The ester linkage in the core could be considered to hinder the intermolecular interaction to form the SmC* phase. In two mixtures containing 1 or 3, a good alignment was easily obtained and the zig-zag defects did not appear in the SmC* phase. The micrograghs of the mixture including 3 are shown in the FIGURE.

FIGURE   Two views of a twisted cell at zero field placed between crossed polarizers. See Color Plate VII.

The tilt angle at 30 degrees below the SmA – SmC* transition temperatures of the two mixtures was larger than that of the others. The details of the layer structure of the two mixtures are now investigated.

In conclusion, the compounds 1, 2 and 3, having a planar and direct-connecting core, showed stable smectic phases. The mixtures doped with 1, 2, 3, 4 or 5 showed stable SmC* phase in comparison with that doped with 11. In the mixture doped with 11, the ester linkage would be considered to hinder the interaction to exhibit a SmC* phase. Especially in the two mixtures containing 1 or 3,

the zig-zag defects did not appear. Our designed planer
and direct-connecting core structure plays an important
role in the appearance of stable and faborable aligned
SmC* phase.

REFERENCES

1. N.A.Clark and S.T.Lagerwall :
   Appl.Phys.Lett. 36 899 (1980)
2. Y.Ouchi, H.Takano, H.Takezoe and A.Fukuda :
   Jpn.J.Appl.Phys. 27(1) 1 (1988)
3. M.A.Handshy, N.A.Clark and S.T.Lagerwall :
   Phys.Rev.Lett. 51 471 (1983)
4. A.Mochizuki, Y.Yoshihara, M.Iwasaki, M.Nakatsuka,
   Y.Takanishi, Y.Ouchi, H.Takezoe and A.Fukuda : Proc.
   of the 9'th Int. Display Res. Conf., Kyoto 1989 (The
   Society of Information Display, California, 1989) p.30
5. Y.Takanishi, Y.Ouchi, H.Takezoe, A.Fukuda, A.Mochizuki
   and M.Nakatsuka : Jpn.J.Appl.Phys. 29(6) L984 (1990)
6. supplier : Nippon Mining Co.,Ltd.
7. For a review, see : J.K.Stille :
   Angew.Chem.Int.Ed.Engl. 25 508 (1986)
8. K.Miyasato, S.Abe, H.Takezoe, A.Fukuda and E.Kuze :
   Jpn.J.Appl.Phys. 22 L661 (1983)
9. S.T.Lagerwall and I.Dahl :
   Mol.Cryst.Liq.Cryst. 114 151 (1984)
10. N.Shiratori, I.Nishiyama, A.Yoshizawa and T.Hirai :
    Jpn.J.Appl.Phys. 29(11) L2086 (1990)
11. The phase transition of 5-hexyl-2-(4'-heptyl-
    biphenylyl)pyrimidine is Cr 56 Sc 93 N 150 I.

SECTION D
PHASE BEHAVIOR AND MICROSCOPICS

EFFECT OF THE I* PHASE TEMPERATURE RANGE ON THE NATURE OF THE TILTED FLUID TO HEXATIC TRANSITION

V.N. RAJA, S. KRISHNA PRASAD, D.S. SHANKAR RAO
Raman Research Institute, Bangalore 560 080, INDIA
J.W. GOODBY
University of Hull, Hull HU6 7RX, UK
M.E. NEUBERT
Liquid Crystal University, Kent State University
Kent, Ohio 44242, USA

Abstract

High precision layer spacing measurements have been carried out in the C* and I* phases of a number of compounds. The results suggest that the temperature range of the I* phase influences the nature of the tilted fluid to hexatic transition. For smaller ranges of I*, the C* phase evolves continuously to I*. The curves for the temperature variation of the layer spacing indicate that with increasing range of I* one may expect to observe a critical point followed by a line of first-order transitions. The presence of a second hexatic phase, viz., F* below I* also appears to play an important role in determining the nature of the C*-I* transition.
A comparison between this scenario and a similar one proposed by Aharony et.al.,[1] is also presented.

Introduction

Because of the presence of molecular tilt in both the phases, the C to I and equally the C to F transitions are different from the A to hex B transition. The tilt has two important consequences: i) it induces some hexatic order in the C phase, changing it from a tilted fluid to an induced hexatic,[2,3] or in other words

the C phase is simply an I (or F) phase with smaller amplitude of the hexatic order parameter. ii) The symmetry being the same, the transition between C and I (or F) can only be of the first-order type; otherwise there will be just a continuous evolution without any phase transition. Theoretically, the mechanism that drives the fluid - hexatic transition to first-order is the coupling between the bond orientational order(BOO) and another order parameter; the latter can be herringbone order,[4] smectic layer fluctuations,[5] or crystalline order parameter.[1]

On the other hand the symmetry of the order parameter associated with the BOO allows the A - hex B transition to be first order or second order. Experimentally both types have been observed.[6] Despite a number of studies on this transition, the situation regarding the driving mechanism is not quite clear. But one notable conclusion that has been drawn from these studies is that the range of the hexatic phase does not seem to influence the nature of the transition.[7] Only a few measurements dealing with the nature of the tilted version of this transition exist. Very recently Brock et al.,[8] by performing high resolution Xray studies on a single domain 3D film of the racemic version of 8OSI, have shown that C to I transition in this material is of the continuous evolution type.

In this communication, we present the results of high resolution layer spacing measurements across the C to I transition which suggest that the temperature range of the hexatic phase does influence the nature of the fluid-hexatic transition. The effect of having a second hexatic phase at a lower temperature is also discussed.

Experimental

High precision layer spacing measurements have been carried out on the 7th, 10th and 12th homologues of the 4-n-alkoxy biphenyl-4'-(2'-methyl butyl) benzoates (nOBMBB) series.[9] These compounds have the following sequence of phase transitions in the cooling mode

Isotropic - Cholesteric - Smectic C* - Smectic I* - Smectic J*

(The asterisk indicates that the phases are chiral. However in the present discussion we ignore the differences between the chiral and achiral versions). The Xray setup and the experimental procedure have been described in an earlier paper.[10] It will suffice here to mention that the precision in the determination of the wave vector is $2 \times 10^{-4} \text{Å}^{-1}$ and the resolution in the equatorial direction is $1 \times 10^{-3} \text{Å}^{-1}$ half width at half maximum. The constancy of the sample temperature during any measurement is reckoned to be better than 10 mK.

Results

Figure 1 is a plot of the temperature variation of the layer spacing d for the three compounds, which shows an increase on passing from the C to the I phase. For the 7th homologue, although the total variation in d is quite small (0.1Å), a plot on an enlarged scale (inset of Fig.1) shows that the behavior is still the same. Evidently, the total variation and the rate of variation of d with temperature increases with increase in chain length in agreement with measurements on a different series of materials.[11] The absence of any two-phase coexistence confirms that the transition in all the three homologues to be of the continuous evolution type within our experimental resolution. Moreover, the intensity data discussed later also supports

this behavior. Interestingly, there is a progressive increase in the range of the I
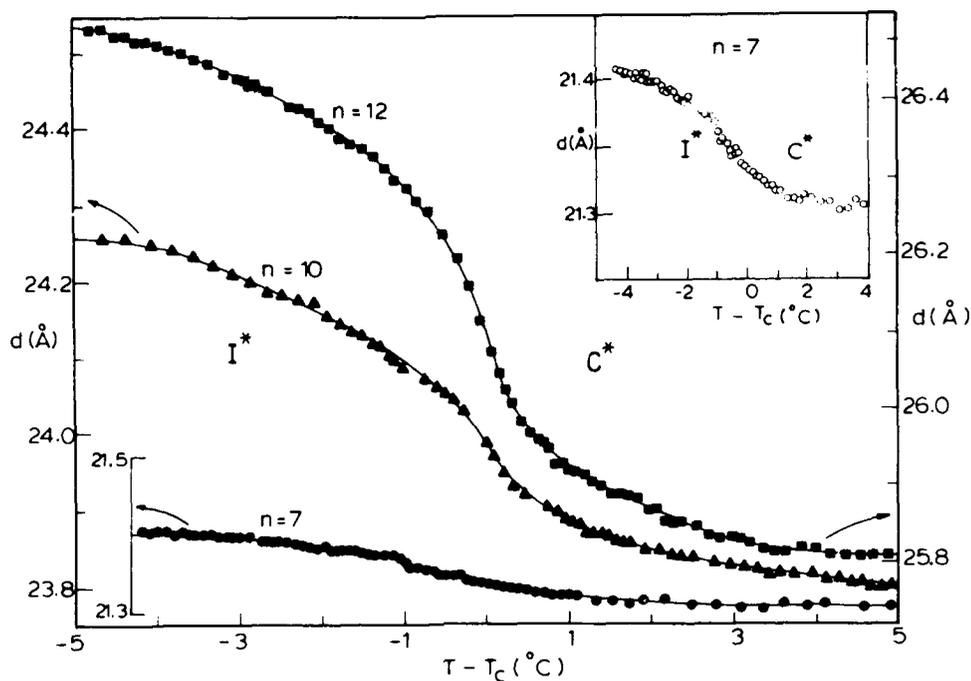
Figure 1: Temperature variation of the layer spacing (d) for the three homologs of nOBMBB series. Solid circles, triangles and squares correspond to the data for the members n=7,10 and 12 respectively. The data for n=7 is also shown in the inset on an enlarged scale.

phase as the chain length increases. (The temperature ranges of the I* phase for

n=7,10 and 12 are 2.1, 8.9 and 16.2°C respectively). A similar trend has been

reported[12] for four different homologs (n=10,13,15 and 19) of the Terepthal-bis

alkyl aniline (TBnA) series[12] which exhibit the C - I transition. In fact, this is true

even for the C - F transition, exhibited by the lower members of the TBnA series.[11]
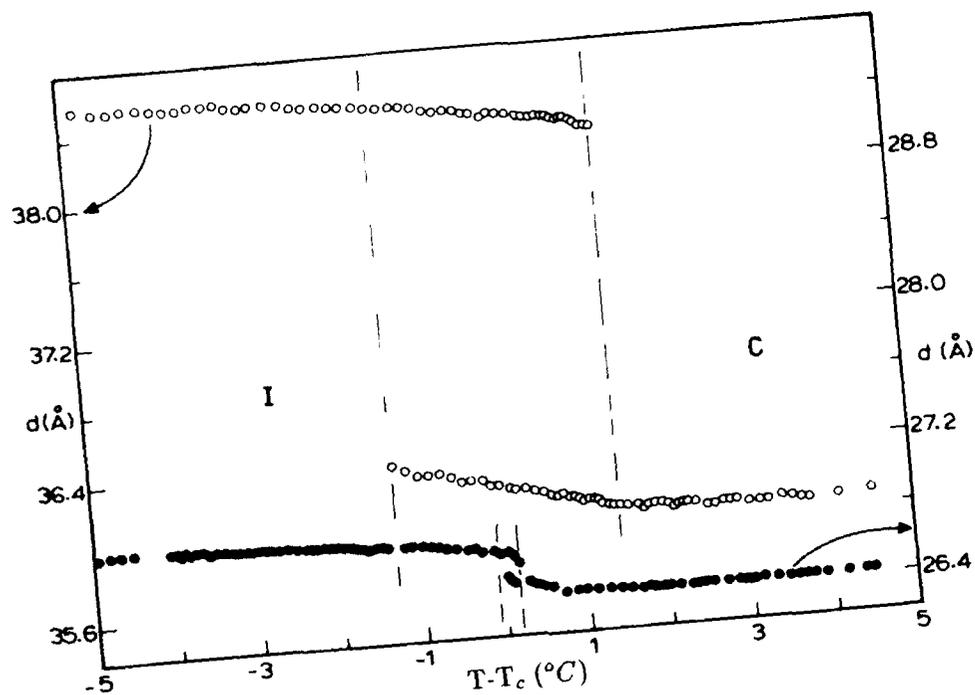
Figure 2: Variation of the smectic layer spacing (d) with temperature in the vicinity of C - I transition for category (i). Solid and open circles correspond to the data for TBHOA and TB10A respectively. The vertical dashed lines indicate the two-phase region.

It may be noted that the compounds of the TBnA series which show a C - I transition also exhibit another hexatic phase, viz., F below the I phase. In order to see whether the presence of the second hexatic phase influences the C - I transition we undertook the following studies. Four compounds divided into two categories were used. Compounds within a category have similar molecular structure and approximately the same range of the I phase; but one of them possesses only the I phase while the other both I and F phases, which together exhibit large hexatic range.

The compounds are

1. bis-(4'-n-heptyloxybenzylidene)-1,4-phenylenediamine(TBHOA) [I]

   Terepthal-bis-decylaniline (TB10A) [I, F]

2. 4-(2'-methylbutyl)phenyl 4'-n-octyloxybiphenyl-4-carboxylate (8OSI*) [I]

   4-(2'-methyl butyl)phenyl 4'-n-octylbiphenyl-4-carboxylate (8SI*) [I, F].
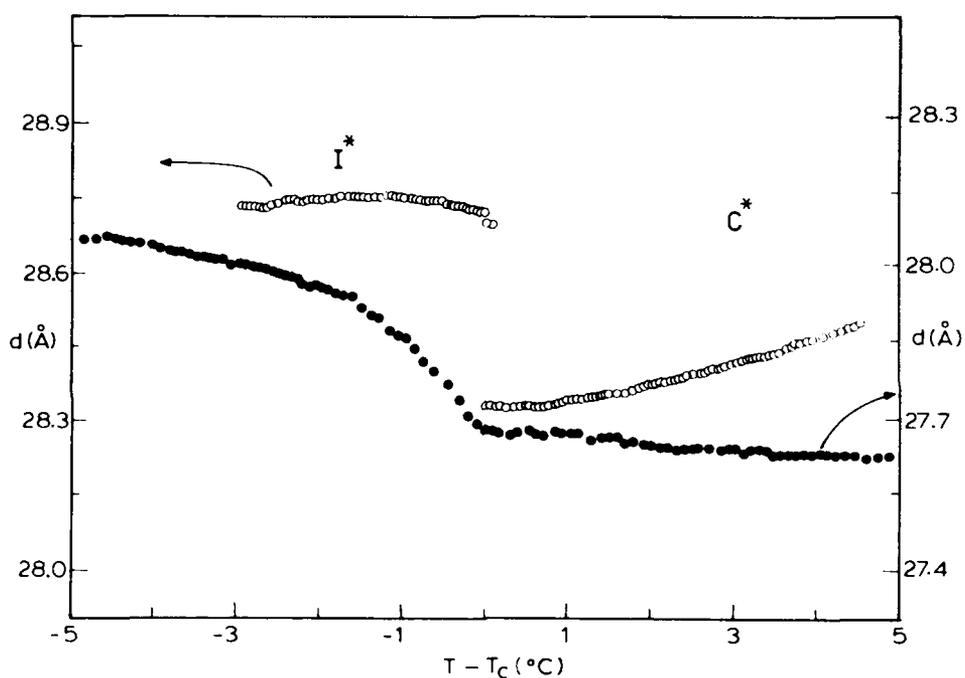
Figure 3: Temperature variation of the smectic layer spacing(d) in the vicinity of C* - I* for category (ii). Solid and open circles correspond to the data for 8OSI* and 8SI* respectively.

The temperature variation of d for category (i) is shown in Fig.2. Both TB10A and TBHOA show the C - I transition characterised by the presence of the coexistence region - a region in which the reflections corresponding to both the phases coexist.

However, the jump in d for TB10A is much larger than that of TBHOA. Results obtained for category (ii) are presented in Fig.3. Here 8SI*, a compound having two hexatic phases, shows a first-order transition while 8OSI* with only one hexatic phase shows a continuous evolution. Thus it appears that the presence of the second hexatic phase makes the C - I transition more strongly first-order.
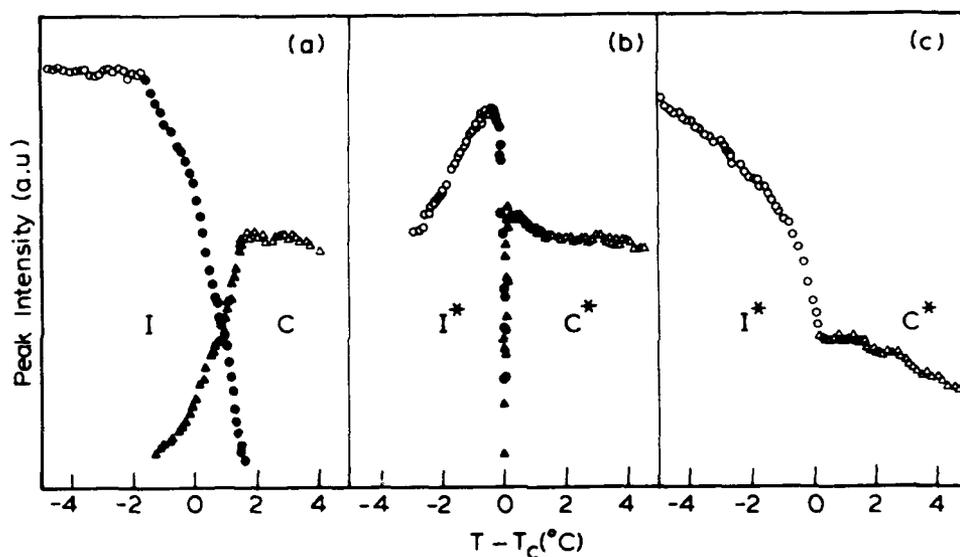
Figure 4: Variation of the intensity of the Xray diffraction maxima as a function of (T-T$_c$) for (a) TB10A, (b) 8SI* and (c) 12OBMBB. Open triangles and circles correspond to the density modulation in the C (or C*) and I (or I*) phases respectively. Solid triangles and circles correspond to the data in the two-phase region. A cross-over in the intensity is seen in the two-phase region.

Plots of the thermal variation of the peak intensity near the C - I transition for the three compounds TB10A, 8SI* and 12OBMBB are given in Fig.4.

As seen in Fig. 2, TB10A shows a strong first-order transition accompanied by a substantial change in the d value. This feature is reflected in the intensity variation(Fig.4a) also as a switchover in the relative intensities of the two peaks in the coexistence region. In fact, the presence of a first-order transition in 8SI* (see Fig.3), albeit quite weak, also gets strikingly manifested (Fig.4b) in the peak intensity variation in the two-phase region. In contrast, the intensity versus temperature plot for 12OBMBB shows a markedly different behavior. The values in the C phase continuously increase into the I phase without any dip in the transition region. Similar behavior of intensity change has been observed for first-order and continuous evolution type of transitions near other smectic-smectic phase transitions.[13]

Discussions

Having observed that the strength of the C - I transition depends on the range of the I phase, it is natural to look for any similar theoretical situations. As mentioned earlier, coupling of the BOO to herringbone order or smectic layer fluctuations or crystalline order parameter has been suggested to change the order of the A - hex B transition. Aharony et al.,[1] who considered the coupling to the crystalline order parameter predicted the phase diagram given in Fig.5a for the A - hex B - Crystal B system. Two notable features seen are a tricritical point (TCP) on the A - hex B line and a triple point where A, hex B and Crystal B phases meet. These authors further argue that a similar phase diagram should exist for the tilted version, i.e., involving C, I and J phases, with some differences. The existence of the induced
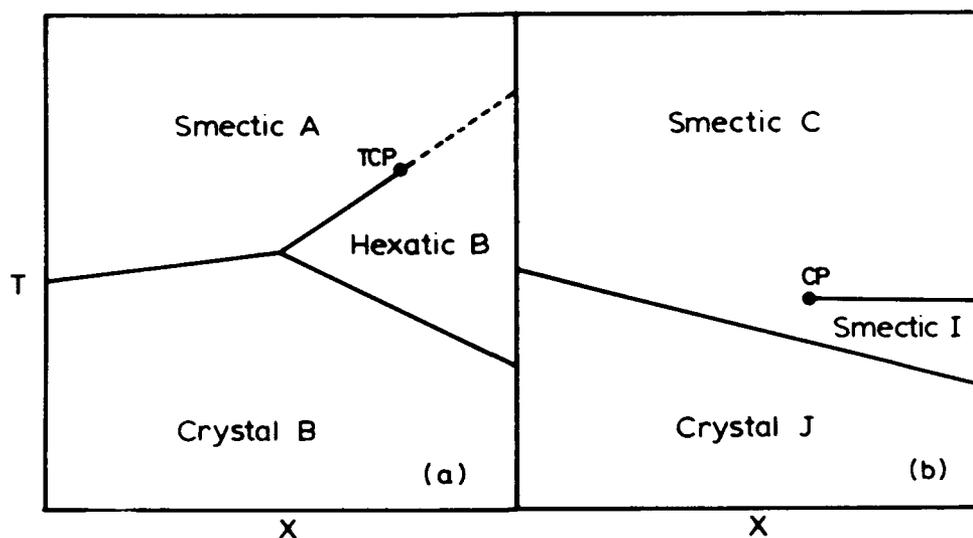
Figure 5: (a) Schematic representation of the temperature-concentration phase diagram near the A - hex B - Crystal B triple point. (reproduced from Ref. 1.) (b) Tentative phase diagram involving C, I and J phases. The broken (full) lines indicate second (first) order transitions.

hexatic order in the C phase and a finite tilt-bond coupling does not permit a second order transition. Consequently, the situation which is similar to the param-agnetic - ferromagnetic transition in the presence of a non-zero applied field, turns the TCP into a critical point (CP). From our Xray studies on nOBMBB it is clear that although d evolves continuously across the C - I transition, the strength of this pseudo transition increases with an increase in the temperature range of the I phase. In other words, as the range of the I phase increases the system approaches the CP and with a further increase in the range one might crossover to a region of first-order transition. Data on compounds belonging to other series also appear

to support this idea. Hence, it seems that the range of the hexatic phase plays a decisive role in controlling the nature of the C - I transition. With this in mind, we propose a tentative phase diagram (Fig.5b) for such systems. To our knowledge, such a phase diagram has not been proposed by any of the theories mentioned above. Obviously, further studies, theoretical as well as experimental, are needed in this direction before this behavior can be generalized.

Acknowledgements

References

[1] A.Aharony, R.J.Birgeneau, J.D.Brock and J.D.Litster, *Phys. Rev. Lett.*,**57**, 1012 (1986).

[2] B.I.Halperin, in *Symmetries and Broken Symmetries*, Ed. N.Boccara (IDSET, Paris, 1980).

[3] D.R.Nelson and B.I.Halperin, *Phys. Rev.* **B21**, 5312 (1980).

[4] R.Bruinsma and G.Aeppli, *Phys. Rev. Lett.*, **48**, 1625 (1982).

[5] J.V.Selinger, *J. Phys. (Paris)*,**49**, 1387 (1988).

[6] C.C.Huang, G.Nounesis, R.Geer, J.W.Goodby and D.Guillon, *Phys. Rev.* **A39**, 3741 (1989).

[7] G.Nounesis, R.Geer, H.Y.Liu, C.C.Huang and J.W.G⋅ ᵗby, *Phys. Rev.* **A40**, 5468 (1989).

[8] J.D.Brock, A.Aharony, R.J.Birgeneau, K.W.Evans-Lutterodt, J.D.Litster, P.M.Horn, G.B.Stephenson, A.R.Tajbakhsh, *Phys. Rev. Lett.*, **57**, 98 (1986).

[9] J.W.Goodby and T.M.Leslie, *Mol. Cryst. Liq. Cryst.*, **110**, 175 (1984).

[10] S.Krishna Prasad, V.N.Raja, D.S.Shankar Rao, G.G.Nair and M.E.Neubert, *Phys. Rev.* **A42**, 2479 (1990).

[11] S.Kumar, *Phys. Rev.* **A23**, 3207 (1981) ; S. Kumar, Ph.D Thesis (Univ. Illinois, 1981).

[12] J.J.Benattar, F.Moussa and M.Lambert, *J. Chim. Phys.* **80**, 99 (1983).

[13] P.S.Pershan, G.Aeppli, J.D.Litster and R.J.Birgeneau, *Mol. Cryst. Liq. Cryst.*, **67**, 205(1981) ; S.Krishna Prasad, R.Shashidhar, B.R.Ratna, B.K.Sadashiva, G.Heppke and S.Pfeiffer,*Liq. Cryst.* **2**, 111(1987).

DESIGN AND SYNTHESIS OF FERROELECTRIC LIQUID CRYSTALS. 15.[1] FLC MATERIALS FOR NONLINEAR OPTICS APPLICATIONS

DAVID M. WALBA,*§‡ M. BLANCA ROS,§ TERESA SIERRA,§ JAMES A. REGO,§ NOEL A. CLARK,†‡ RENFAN SHAO,† MICHAEL D. WAND,‡ ROHINI T. VOHRA,‡ KENNETH E. ARNETT‡ AND STEPHAN P. VELSCO♦

§ Department of Chemistry and Biochemistry and Optoelectronic Computing Systems Center, University of Colorado, Boulder, CO 80309-0215, USA

† Department of Physics and Optoelectronic Computing Systems Center, University of Colorado, Boulder, CO 80309-0390, USA

‡ Displaytech, Inc., 2200 Central Avenue, Boulder, CO 80301, USA

♦ Lawrence Livermore National Laboratory, Livermore, CA 94550, USA

Abstract We have recently reported the first FLCs designed specifically for large second order nonlinear optical (NLO) susceptibility $\chi^{(2)}$; a series of o-nitro-1-methylheptyloxy biphenylbenzoates and phenyl biphenylcarboxylates. Properties of a stable room-temperature C* mixture of two such components (1:1 W316/W317 ≡ MX5679) are presented. The nonlinear susceptibility, as evidenced by the Type 1 eeo d_{eff} for second harmonic generation (SHG) from 1,064 nm light for MX5679 is indeed large relative to other FLCs which have been evaluated for $\chi^{(2)}$ (d_{eff} (ZLI3654) = 0.0016 pm/V, d_{eff} (SCE9) = 0.0037 pm/V, d_{eff} (MX5679) = 0.16 pm/V). The synthesis and some properties of second-generation FLCs designed for NLO applications is also described.

INTRODUCTION

Optical quality thin films possessing large second order nonlinear optical (NLO) susceptibility $\chi^{(2)}$ have many potential uses in photonics. Organic materials are interesting candidates for such applications since organic molecules may possess large, and to a great extent tunable molecular second order susceptibility β.[2] In general, large β is obtained when donor and acceptor groups are coupled by a conjugating spacer unit. In order to be useful, however, the organic molecules must be processed into a supramolecular assembly possessing appropriate structure—typically, though not necessarily,[3] wherein the donor-spacer-acceptor array (β unit) is oriented along a polar axis.

FLCs seem an attractive approach to solution of this problem since the C* phase (the supramolecular assembly when in an aligned thin film on substrates) possesses appropriate symmetry for exhibiting $\chi^{(2)}$, and FLC mesogens may easily possess functional arrays imparting large β to the molecules. Early experiments, however, indicated that FLCs possess very small $\chi^{(2)}$.[4]

We have suggested the reason for the small $\chi^{(2)}$ of FLCs is that, though the molecules may indeed possess large β, the structure of the FLC phase is not correct for producing large $\chi^{(2)}$ when the β units are oriented along the director. Furthermore, the mere presence of large β units normal (or nearly normal) to the director in an FLC phase is ineffective,[5] since these units must also be oriented in a polar fashion along the polar axis.

As outlined in several recent publications,[1a,b,6] we have shown the following: 1) functionalized aromatic rings may be oriented in a controlled and "tunable" way along the polar axis in FLC thin films by steric coupling of the aryl substituents with stereocenters on the chiral tail; 2) the stereocontrol in this "synthesis" can, in some cases, be quite high; and 3) polar orientation of the o-nitroalkoxy β unit along the polar axis in FLCs indeed affords materials with relatively large $\chi^{(2)}$. Thus, the FLC mesogen **W314** (Figure 1) shows d_{eff} = 0.23 at 65°C in a monotropic C* phase at the top of the type 1 eeo angle phase-matched SHG peak from 1,064 nm fundamental light, $d_{22} \cong d_{23} = 0.6$ pm/V, and $\lambda_{max} = 308$ nm in ethanol solvent. This combination of properties is interesting, and proves the basic efficacy of the approach.

W314

X ← 33.6 — C* ← 93.7 — A* ← 119.1 — I
X — 80° → C*

| P/sinθ @ |
| T-Tc = -10° |
| -611 |

W316

X ← 17.5 — C* ← 60.5 — A* ← 89.1 — I

| P/sinθ @ |
| T-Tc = -10° |
| -330 |

W317

X ← 23.5 — A* ← 76.5 — I
X — 41 → A* — 76.5 → I

The LC phase of this material is tentitively identified as a chiral smectic A

MX5679 (1:1 W316:W317)

X ← <rt — C* ← 45 — A* ← 79 — I
X — <rt → C*

Pobs@ T-Tc=-23° = -222

| Pext/sinθ @ |
| T-Tc = -23° |
| -545 |
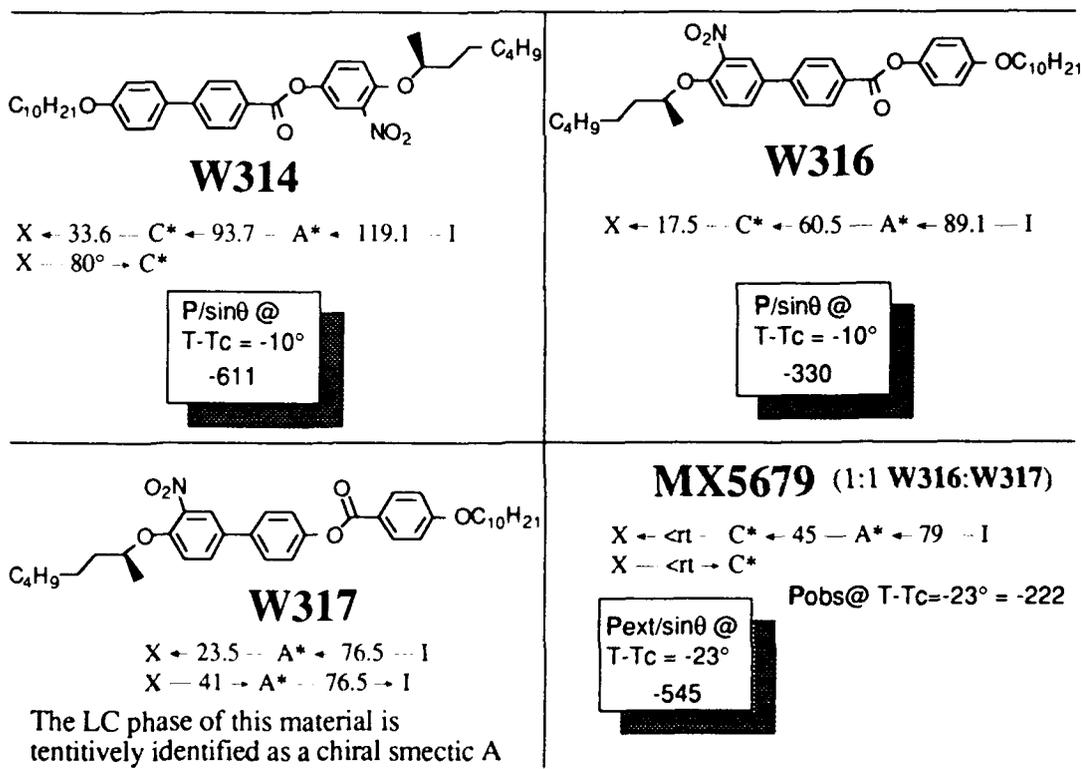
FIGURE 1   The chemical structure and some FLC properties of first generation FLC mesogens designed for large $\chi^{(2)}$.

In this paper we report some FLC and NLO properties of an enantiotropic room temperature mixture of first generation FLC/NLO components, and the synthesis and some FLC properties of second generation FLCs for NLO.

FIRST GENERATION FLC MATERIALS FOR NLO

The goal of the first generation design effort was polar orientation of the o-nitroalkoxy β unit with good stereocontrol along the polar axis of FLCs. While the ortho-disubstituted benzene unit is a good conjugating spacer, as indicated below, the o-nitroalkoxy array is not expected to possess a large β (the molecular β increases very roughly with the square of the separation between the donor and acceptor). Even so, with the nitro acceptor and alkoxy donor, this unit is expected to show β values larger than typical functional arrays oriented along the polar axis in FLCs (e.g. C—X, C—CN, and C=O units).

W314; P_{obs} = -2.1 D/molecule

o-nitroanisole; μ = 4.8D
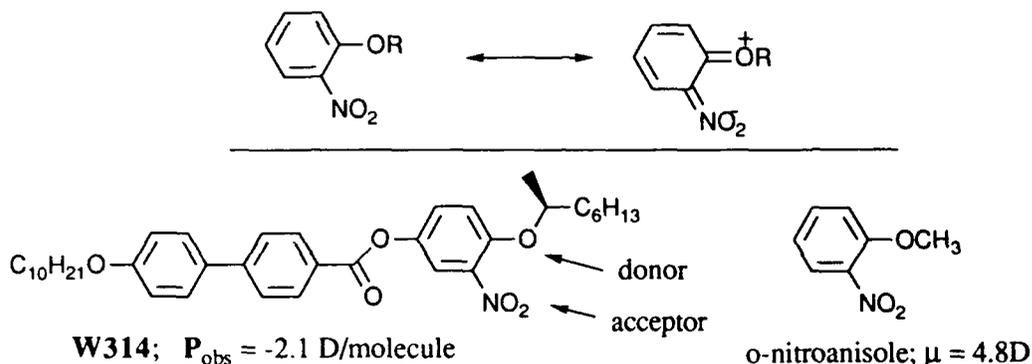
Indeed, in **W314** at 34°C, polarization measurements suggest that about 40% of the nitroalkoxy dipole is oriented along the polar axis—a degree of stereocontrol for this system unachievable using electrical poling techniques. In addition, the measured NLO susceptibility of this material seems consistent with the proposed structure of the phase. Unfortunately, the enantiotropic C* phase of **W314** is narrow, occurring only between about 80°C and 94°C.

Mixing experiments using the first generation FLC/NLO components revealed a two-component mixture possessing an enantiotropic C* phase at room temperature. The phase sequence and polarization of this mixture (**MX5679**) are given in Figure 1, along with the structure and properties of the component. f the mixture (**W316** and **W317**). Note that **W317** possesses no observable C* phase, but shows a broad enantiotropic phase tentatively identified as a chiral smectic A which exhibits a very large electroclinic effect.[7]

D.M. WALBA, ET AL

The material **MX5679**, as well as the commercial FLCs **ZLI3654** and **SCE9**, were evaluated for $\chi^{(2)}$ in homeotropically aligned FLC cells at room temperature with a field applied along **P** to unwind the helix. For all three materials, the intensity of the SHG signal from a 1,064 nm fundamental along the type 1 eeo angle phase-matching locus was measured relative to quartz as standard.[8] The results of this investigation are given in Table 1. The d_{eff} values in the table derive from measurements of SHG intensity at the top of the phase-matching peak. To our knowledge, these experiments represent the first time the phase-matching loci of an FLC sample have been mapped and characterized.

TABLE I Values of the ferroelectric polarization, SHG efficiency, and $\chi^{(2)}$ (d_{eff}), for representative FLCs and for the FLC phase of **MX5679**. Values for some inorganic crystals are included for comparison.

Entry number	compound	P (nC/cm^2)	|P| relative to ZLI3654	d_{eff} (pm/V)	d_{eff} relative to ZLI3654	SHG arb units
1	ZLI3654	-29	1	0.0015	1	1
2	SCE9	+33.6	1.16	0.0037	2.5	6.1
3	MX5679	-222	7.66	0.16	110	1.1 x 10^4
4	KH$_2$PO$_4$ (KDP)[9]			$d_{36} = 0.39$		
5	KTiOPO$_4$ (KTP)[10]			$d_{31} = 5.9$		

Several aspects of the data shown in the Table deserve special comment. First, it should be noted that the d_{eff} values <u>are not</u> proportional to **P**. This is expected, since μ (the dipole moment) and β (the second order susceptibility) derive from different aspects of the molecular structure. Thus, the chiral components of **ZLI3654** are α-chloroesters (doped to about 20% of the mixture).[11] Since the polarization induced by these mesogens presumably derives from orientation along the polar axis of aliphatic carbon-halogen and/or ester units, and such units possess small β, even the extrapolated d_{eff} (assuming a linear relationship between concentration of the polar component and d_{eff}) of about 0.0075 pm/V is quite small, though the extrapolated polarization of about 150 nC/cm^2 is respectably large. While the composition of SCE9 is not published, this material presumably possesses chiral cyano mesogens. A similar argument for the small magnitude of d_{eff} for SCE9 also holds, though without knowing the concentration of the chiral components, even a qualitative argument is difficult to make.

In any event, as expected by our model, where the polarization of **MX5679** derives from orientation of the o-nitroalkoxy unit along the polar axis, the observed second order susceptibility of the mixture is dramatically enhanced relative to the commercial mixtures even when normalizing for polarization (a direct comparison of the values obtained for **MX5679** and for **W314** is not possible without further experiments, which are in progress). Given that the actual d coefficients must be larger than d_{eff}, the NLO susceptibility observed for **MX5679** is comparable to that for inorganic crystals such as KDP. The enhanced properties of the first generation FLCs for NLO are more dramatic when comparing SHG efficiency, which goes as d_{eff}^2. In this figure of merit, **MX5679** is improved over **ZLI3654** by a factor of 10,000.

ORIENTATION OF THE P-NITROANILINE UNIT ALONG THE POLAR AXIS

Given the results with first generation materials, we feel the prospects for achieving FLC thin films with larger $\chi^{(2)}$ are excellent. Many approaches toward this end may be envisioned, the most immediate being improvement of the β of the mesogens by incorporation of a good donor group para to the acceptor in the β functional array. Thus, one may argue that p-nitroaniline (the prototypical NLO unit) should possess a β value about 7 times that of o-nitroanisole. By incorporating an amino grouping para to the nitro group in compounds of the same class as **W314**, **W316** and **W317**, the susceptibility of the resulting FLCs should be enhanced substantially according to our model, since the geometry is such that a large resultant of a large component of the β tensor should be oriented along **P** in these second generation materials.

Initial experiments in synthesis of the "p-nitroaniline" FLCs focussed upon the p-nitroaniline derivative **W341**, prepared by hydrolysis of the acetamide **W340**, as indicated in Figure 2. While discussion of the entire synthesis route is outside the scope of this paper, the acetamide **W340** is selectively hydrolyzed under quite mild acidic conditions to give the desired amine **W341** in the presence of the aromatic ester unit.

We felt the **W341** structure was especially interesting for two reasons. First, as shown in Figure 2, the nitroaniline unit should be well oriented along the polar axis of the phase according to our model. Second, as indicated in the drawing above, two donor/acceptor pairs are coupled by resonance across the ring (two ortho and one para) in this system. It thus seems reasonable that this system may possess even larger β than p-nitroaniline, though we know of no experimental results addressing this question.

While unfortunately **W341** is not mesogenic, preliminary evaluation of the FLC properties of the material was accomplished using the 5% and 10% by weight mixtures with racemic host **MDW158** (the racemate of Keller's phenylbenzoate host, 4-[(4-Methyl-
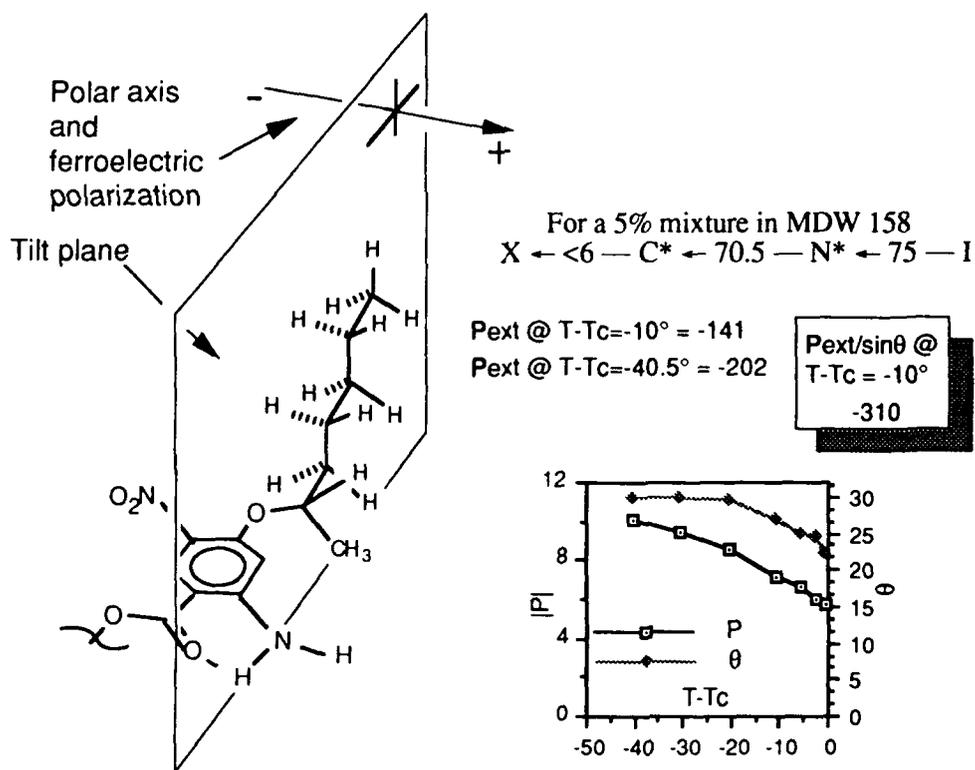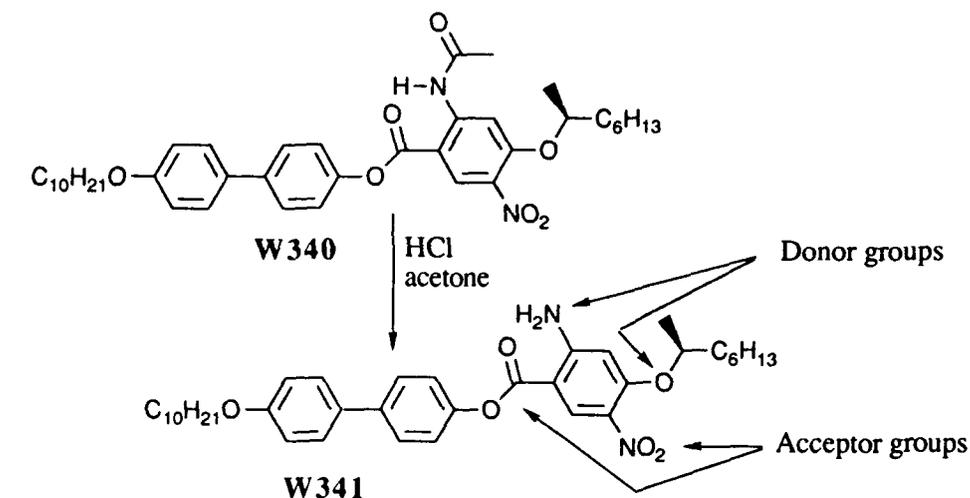
FIGURE 2 Last step in the synthesis of **W341**, the proposed preferred
          conformational and rotational orientation of **W341** relative to the tilt
          plane, and FLC properties of **W341** in a mixture with host
          MDW158.

hexyl)oxy]phenyl 4-(decyloxy)benzoate[12]). As expected based upon the model illustrated in Figure 2, compound **W341** induces a large negative polarization in the mixture, implying some orientation of the nitroaniline unit along **P** (the 10% mixture showed P_{obs} = -19.4 nC/cm^2 @ T-T$_c$ = -45°C, θ = 28°, in good agreement with the data shown in the Figure).

While more experiments are needed to fully explore the structure of FLC films of **W341**, including of course NLO measurements, we speculate that the polarization is actually reduced relative to first order expectation by orientation of the carbonyl group in the core, which is expected to form an intramolecular hydrogen bond with the amino grouping as indicated. In this case, the dipole from the carbonyl is opposed to that from the nitroaniline and nitroalkoxy units. Importantly, this lessening of the spontaneous polarization from the carbonyl, if it occurs, is not expected to reduce the hyperpolarizability by an equivalent amount.

Further evidence for the model of the FLC structure in compounds of this series derives from interesting observations made during the synthesis. Thus, for all of the acetamido intermediates leading to **W340** in the synthesis, and possessing a carbonyl grouping ortho to the amide unit, the resonant λ_{max} is apparently significantly blue shifted relative to expectation (the compounds are white instead of light yellow). A priori one may expect that the lone pair on nitrogen in the amides such as *W340 should be in resonance* with the nitro grouping across the ring, affording a UV absorption tailing into the visible. We propose, however, that when a carbonyl group is located ortho to the amide (aldehyde, acid, or ester), the resulting intramolecular hydrogen bond causes adoption of a conformation where the lone pair is orthogonal to the ring, and instead is delocalized onto the carbonyl of the acetyl group in amide resonance. Thus, the p-nitroacetanilide unit possesses two acceptors (the nitro group, and a nitrogen atom with positive charge density), and a blue-shifted λ_{max}. Hydrolysis of the amide, giving **W341**, restores the resonance across the ring. Thus as expected, **W341** is light yellow.

This argument suggested the synthesis of the amino-acetamide **W342** (Figure 3) easily obtained by catalytic hydrogenation of **W340**. Importantly, this material is mesogenic, exhibiting a monotropic A* phase. This proves that incorporation of functionality at four positions on an aryl ring in molecules of this type does not preclude the formation of LC phases. Also, preliminary measurements indicate that the polarization of **W342** is in fact positive, in good agreement with the model. Thus, the ortho amino grouping is now the donor, while the acetamido grouping is an inductive acceptor, giving a ground-state dipole moment for the array opposed to the dipole associated with the alkoxy grouping, parallel to that of the carbonyl group. This argument gets some additional support by the observation that **W342** is indeed very light yellow, suggesting a red-shifted

λ_{max} relative to **W340**. Experiments aimed at further exploration of these effects are in progress.

10% (wt) in **MDW158**

X $\leftarrow$ 20.7 — C* $\leftarrow$ 66.5 — A* $\leftarrow$ 72.5 — I

Pext @ T-Tc=-10° = +33 nC/cm^2

Pext @ T-Tc = -26.5° = +43 nC/cm^2

W342

X —82 → I

X $\leftarrow$ 50 — A* $\leftarrow$ 63.1 — I

Pext/sinθ @
T-Tc = -10°

+50
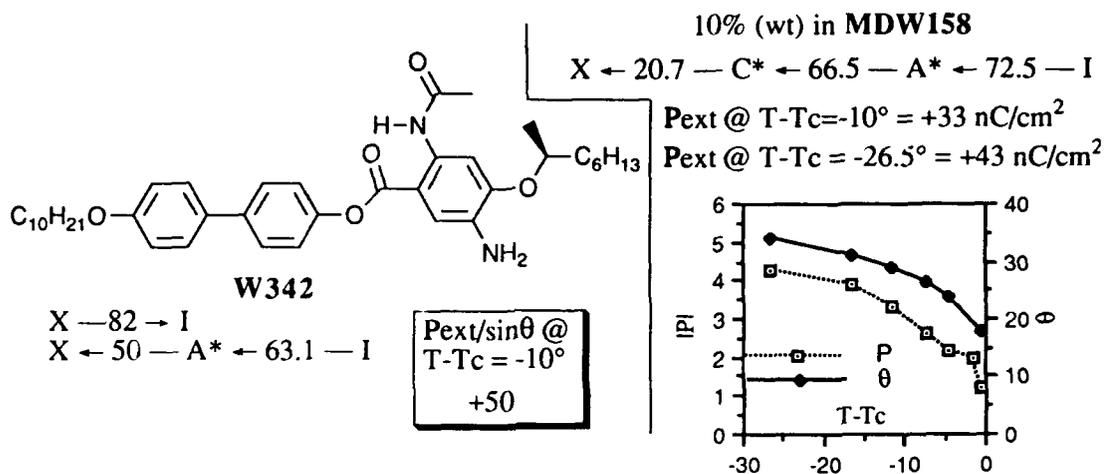
FIGURE 3   Structure and some data on **W342**.

FLC/NLO MATERIALS WITH HIGH INDEX CORES

A problem with this approach to the creation of NLO thin films is that much of the volume of the material is NLO "inactive". Referring to the structure of **W342**, the biphenyl unit, the achiral alkoxy tail, and the alkyl part of the chiral tail are, by our way of thinking, essentially "solvent" for the NLO active part of the molecule, thus diluting the $\chi^{(2)}$ of the film.

While this type of effect is seemingly unavoidable in FLCs, it can of course be minimized by incorporating two chiral tails into the molecular structure, and making all of the rings NLO active—an approach under active investigation in these laboratories. A related, and perhaps more interesting partial solution to this dilution problem involves the use of a core structure possessing high linear polarizability α (i.e. a high refractive index along the director). While the argument suggesting that large α along the director may increase the magnitude of some of the β components is outside the scope of this paper, we present here exemplary structures designed to test the idea.

Specifically, LCs possessing the tolane core[13] are well known to possess a large index along n̂, suggesting FLC/NLO structures possessing o-nitroalkoxy units coupled with tolane cores. Figure 4 gives the structures and FLC properties of some mixtures of the tolane lactate ester compounds **W334** and **W336**. Here, the chiral tail is the well-known lactate ester unit.[14] Due to lack of good understanding of the conformational

C$_{10}$H$_{21}$O—〈=〉—=—〈=〉—O

W336

C$_{10}$H$_{21}$O—〈=〉—=—〈=〉—O

W334 NO$_2$

MX512

10% mixture of W336 in MDW158

X ← 20 — C* ← 56.6 — A* ← 64.3 — N* ← 66.8 — I

Pext @ T-Tc=-10° = +63

Pext @ T-Tc=-31.6° = +100

Pext/sinθ @
T-Tc = -10°
+164

MX510

10% mixture of W334 in MDW158

X ← 23 — C* ← 60.5 — A ← 67.5 —

Pext @ T-Tc=-10° = +79.4

Pext @ T-Tc=-35.5° = +199

Pext/sinθ @
T-Tc = -10°
+238

MX518

10% mixture of W334 in ZLI3234B

X ← <10   C* ← 53.7 — A* ← 68.8 — N* ← 85 — I

Pext @ T-Tc=-10° = +112

Pext @ T-Tc=-43.7° = +203

Pext/sinθ @
T-Tc = -10°
+362
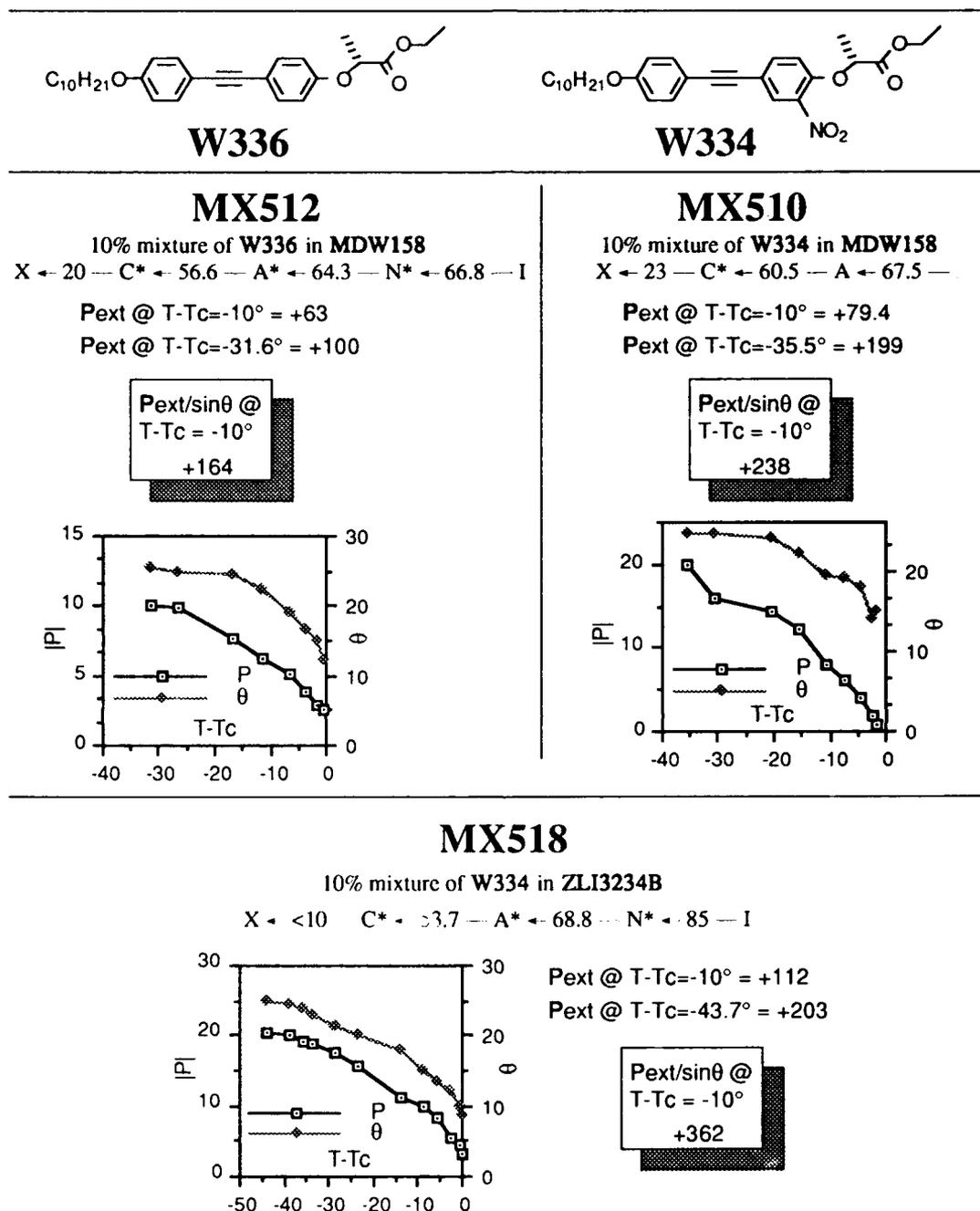
FIGURE 4 Structures and evaluation of the FLC properties of the tolanes **W334** and **W336** as dopants. Neither neat material possessed any LC phases.

properties of this chiral tail, it was difficult to predict a priori whether orientation of an ortho nitro substituent would occur in this system. The data presented in Figure 4 tend to

suggest that the nitroalkoxy unit is in fact oriented in a polar fashion in the nitro compound **W334**. Thus, the unsubstituted analogue **W336** shows a significantly smaller polarization in a mixture with **MDW158** than the o-nitro substituted compound **W334**, which was evaluated in both **MDW158** and **ZLI3234B**.[15]

It should be noted, however, that in this system the degree of orientation of the nitroalkoxy unit is apparently not as great as occurs in the 1-methylheptyloxy compounds described above, where the polarization increases almost an order of magnitude upon incorporation of the nitro group. In any event, evaluation of FLC components of this type for second order susceptibility should prove interesting from the NLO viewpoint, and may also shed some light on the origins of the large polarization observed for the lactate esters.

CONCLUSION

First generation FLCs designed for large $\chi^{(2)}$ in aligned films indeed show a large enhancement in $\chi^{(2)}$ of the films. As expected, the $\chi^{(2)}$ is not proportional to **P**, and may increase much faster than **P** with appropriately designed FLCs. These results suggest that very large increases in $\chi^{(2)}$ of FLC films should be possible.

Synthesis of several second generation FLCs for NLO applications has been achieved, and FLC properties of some of the new materials, including an FLC component possessing the prototypical organic NLO moiety (the p-nitroaniline unit) oriented along **P**, are reported.

ACKNOWLEDGEMENT

REFERENCES

[1]   Previous papers in the series include: a) D. M. Walba, M. B. Ros, N. A. Clark, R. Shao, M. G. Robinson, J.-Y. Liu, K. M. Johnson and D. Doroski, J. Am. Chem. Soc., (in press). b) D. M. Walba, M. B. Ros, N. A. Clark, R. Shao, K. M. Johnson, M. G. Robinson, J. Y. Liu and D. Doroski, Mol. Cryst. Liq. Cryst., 51-60 (1991), and references therein. For a recent review, see: D. M. Walba, in Advances in the Synthesis and Reactivity of Solids, edited by T. E. Mallouk (JAI Press Ltd, Greenwich, Connecticut, 1991), pp. 173-235.

[2]   For a leading reference on the molecular origins of β, see: S. R. Marder, D. N. Beratan and L.-T. Cheng, Science, 252, 103-106 (1991).

3   J. A. Giordmaine, Phys. Rev., 138, A1599-A1606 (1965).

4   a) A. N. Vtyurin, V. P. Ermakov, B. I. Ostrovskii and V. F. Shabanov, Phys. Status Solidi B, 107, 397-402 (1981). b) N. M. Shtykov, M. I. Barnik, L. A. Beresnev and L. M. Blinov, Mol. Cryst. Liq. Cryst., 124, 379-390 (1985). c) A. Taguchi, Y. Ouchi, H. Takezoe and A. Fukuda, Jpn. J. Appl. Phys., 28, L 997-L 999 (1989). d) J. Y. Liu, M. G. Robinson, K. M. Johnson and D. Doroski, Optics Letters, 15, 267-269 (1990).

5   H. Kapitza, R. Zentel, R. J. Twieg, C. Nguyen, S. U. Vallerien, F. Kremer and C. G. Willson, Adv. Mater., 2, 539-543 (1990).

6   D. M. Walba, M. B. Ros, N. A. Clark, R. Shao, K. M. Johnson, M. G. Robinson, J. Y. Liu and D. Doroski, in Materials for Nonlinear Optics: Chemical Perspectives, edited by G. D. Stucky (American Chemical Society, Washington, DC, 1991), pp. 484-496.

7   P. A. Williams, M. B. Ros, N. A. Clark, R. Vohra, D. M. Walba and M. D. Wand, Ferroelectrics, this issue.

8   Details of the characterization of these materials will be reported elsewhere.

9   D. Eimerl, Ferroelectrics , 72, 95 (1987).

10   Eaton, D.F. "Nonlinear Optical Materials: The Great and Near Great," in Materials for Nonlinear Optics: Chemical Perspectives, Stucky, G. D. (Ed.); American Chemical Society, Washington, DC, 1991; Vol. 455, pp 128-156.

11   Data from E. Merk, Darmstadt, commercial FLC data sheet.

12   P. Keller, Ferroelectrics, 58, 3 (1984).

13   For a report of tolane FLCs, see: K. Seto, H. Shimojitosyo, H. Imazaki, H. Matsubara and S. Takahashi, Mol. Cryst. Liq. Cryst. Letters, 7, 1-5 (1990).

14   M. F. Bone, M. J. Bradshaw, L. K. M. Chan, D. Coates, J. Constant, P. A. Gemmell, G. W. Gray, D. Lacey and K. J. Toyne, Mol. Cryst. Liq. Cryst., 164, 117-134 (1988).

15   C. Escher, T. Geelhaar and E. Böhm, Liquid Crystals, 3, 469-484 (1988). We thank T. Geelhaar (E. Merk, Darmstadt) for providing the excellent achiral host ZLI3234B.

STATIC AND DYNAMIC PROPERTIES OF OPTICAL SECOND HARMONIC GENERATION IN FERROELECTRIC LIQUID CRYSTAL

MASANORI OZAKI, MANABU UTSUMI, TATSUYA GOTOU,
YOSHIAKI MORITA, KAZUHIRO DAIDO, YUTAKA SADOHARA
AND KATSUMI YOSHINO
Department of Electronic Engineering, Faculty of Engineering, Osaka University
2-1 Yamada-Oka, Suita, Osaka 565 JAPAN

ABSTRACT   The second harmonic generation (SHG) in the ferroelectric liquid crystal (FLC) has been studied as functions of electric field strength, sample thickness, rotating angle, temperature and molecular structure. A sharp angular phase-matching curve of the SHG controlled by an electric field is observed even in the liquid crystal. The temperature dependences of the phase-matched SHG and Maker fringe in the ferroelectric phase have also been studied and nonlinear optical coefficients are obtained as a function of temperature. The SHG in several kinds of FLCs is measured in the Sm C* and crystalline phase. Anomalous temperature dependence of the SHG is also observed in DOBA-1-MPC.

INTRODUCTION

The second harmonic generation (SHG) in organic material has attracted considerable attention from both fundamental and practical points of view.[1,2] In liquid crystals, mainly in nematic liquid crystals which have been widely used in display devices, only the third harmonic generation has been studied,[3] because in these compounds the center of inversion symmetry still remains except for some special cases such as thin film in which the existence of the surface lowers the symmetry.[4]

On the other hand, recently, the ferroelectric liquid crystal (FLC) has been developed as the material for high speed display devices.[5] In these compounds, to realize the ferroelectricity, the optical chiral carbon has been introduced in their molecular structures by which the center of inversion symmetry has been lost. Therefore, FLC is expected to be the active material for SHG.

The tilt direction of the FLC molecules can be switched by the reversal of the polarity of the applied field and the response time of this switching is very short. Therefore, the high speed modulation of SHG can be expected in the FLC device.

Some studies on SHG in the FLCs have been carried out[6-8] and the angularly phase matched SHG has also been reported.[9-12] However, the SHG signal was very weak and the profile of the angular dependence of SHG was broad. Recently, the attempt to design

the optimum molecular structure for SHG has been made.[13] In this paper, we report a detailed study on SHG in FLC as functions of electric field strength, rotating angle, temperature, cell thickness, molecular structure and so on.
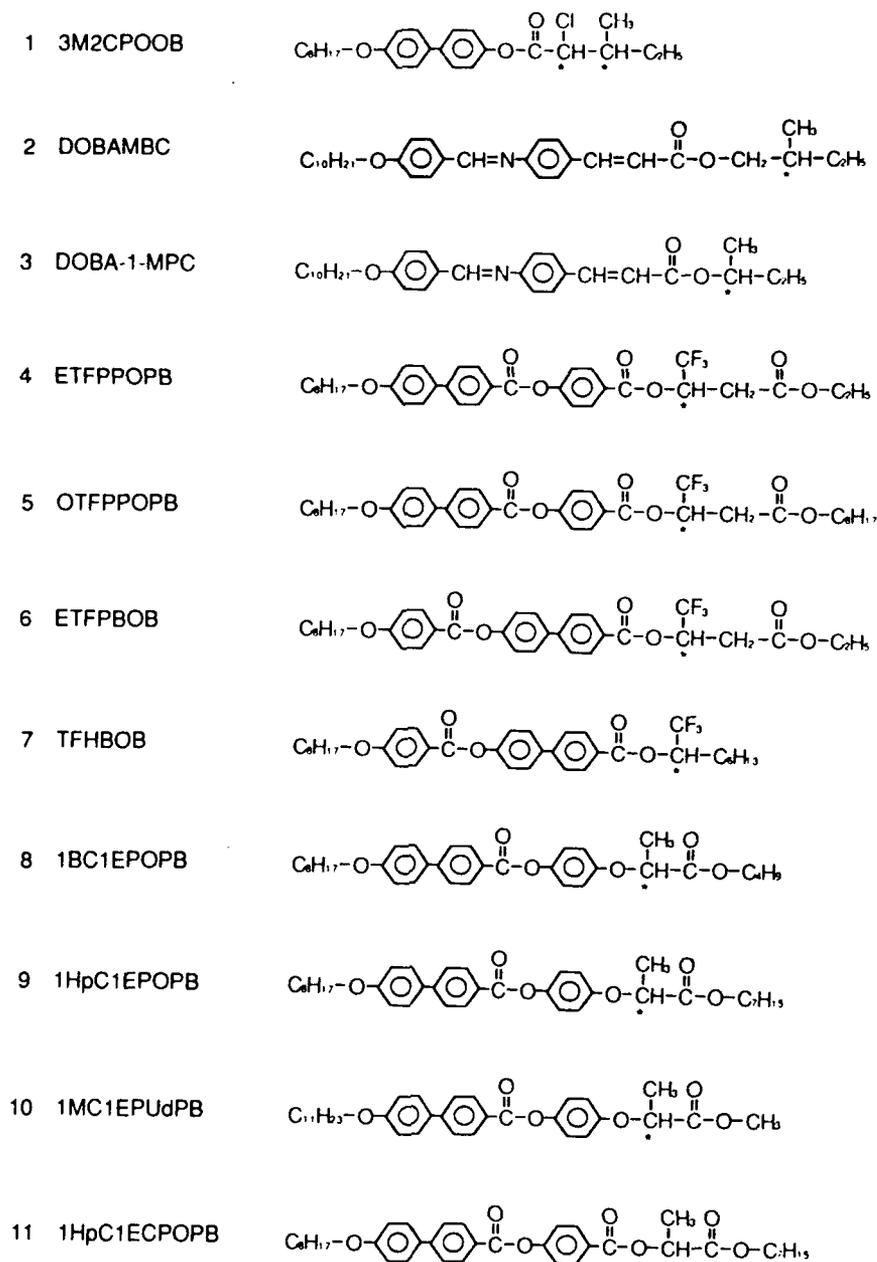
FIG.1   Molecular structures of ferroelectric liquid crystals used in this study.

EXPERIMENTAL

The molecular structures of the FLCs used in this study are shown in Figure 1. The preparation method and the fundamental electric and optical properties of this compound have previously been reported.[14-19] The compound mainly used for a detailed study was (2S,3S)-3-methyl-2-chloropentanoic acid 4',4"-octyloxybiphenyl ester (3M2CPOOB).[14,15]

The sample was sandwiched between two glass plates whose surfaces were treated by a silane coupler (AY43-021, Toray Dow Corning Silicone) to obtain the homeotropic alignment for SHG measurement. Aluminum or stainless sheets of 10 - 260 μm in thickness were used as electrodes and spacers. The separation between electrodes was typically 1 mm.

Figure 2 shows the transmission spectrum of a homeotropic aligned cell of 50 μm in thickness under an electric field. The optical transmission range extends to near 300 nm in the short wavelength side. This indicates that the compound can be used in the wide visible and even ultraviolet region.
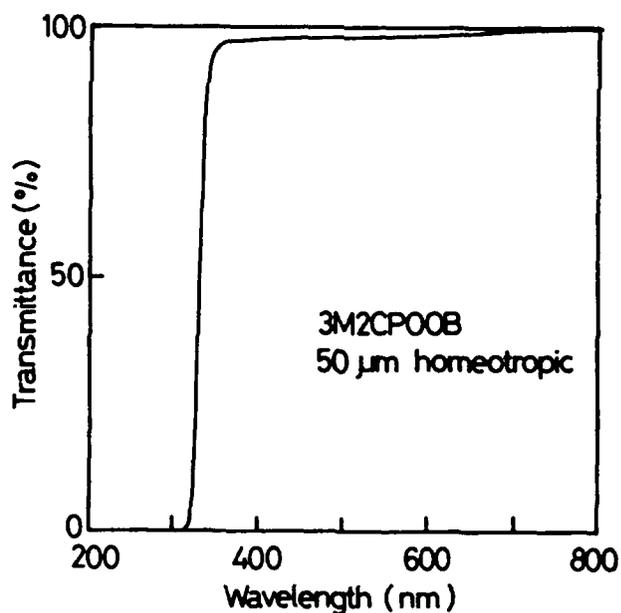
FIG.2   Transmission spectrum of a homeotropic aligned 3M2CPOOB cell. Cell thickness is 50 μm.

For the measurement of the angularly phase-matched SHG, the sample cell was rotated around the y axis parallel to an electric field E, as shown in Figure 3. The fundamental light impinged on the cell perpendicular to the rotating axis (y) and propagated in the x-z plane. The rotating angle θ was defined as the angle between the glass plate normal (z) and the propagation direction of the fundamental light in the liquid crystal. The angle θ was corrected using the equation, $\theta = Sin^{-1}(\theta_{in}/n_g)$, where θ_{in} is the angle between the glass plate normal and the direction of the incident light in air, n_g is the refractive index of the glass (n_g=1.51 for 1064 nm). The refraction at the glass-liquid crystal interface was neglected.

A Q-switched Nd-YAG pulsed laser (wavelength: 1.064 µm, pulse width : 10 ns) was used for the fundamental light source after passing through a visible cut filter, polarizer and λ/2 plate. The fundamental beam was weakly focused by a lens (f=300 mm). The generated harmonic light (532 nm) was monitored from the rear of the sample cell with a photomultiplier after passing through the analyzer. To eliminate the fundamental light, infrared cut filters and an interference filter at wavelength 532 nm were installed in front of the photomultiplier. The detected signal was sent to a boxcar integrator which was operated with a personal computer.

(a)   (b)
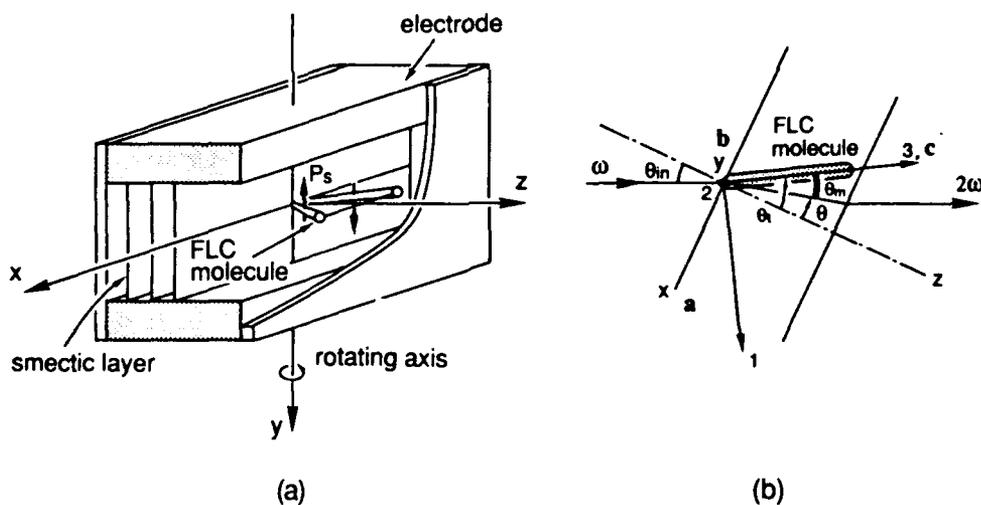
FIG.3   Cell configuration for the measurement of the SHG.

RESULTS AND DISCUSSION

TEMPERATURE DEPENDENCE OF SHG

Temperature dependence of the SHG intensity in 3M2CPOOB under no bias field is shown in Figure 4 for a homeotropic alignment. The fundamental light was penetrated

perpendicularly into the glass plate (θ=0). In the isotropic and smectic A phases no SHG was observed. These phases are non-ferroelectric phase and there is a center of inversion symmetry. In the cooling stage the SHG was not observed also in the chiral smectic C phase in which the center of the inversion symmetry was absent.
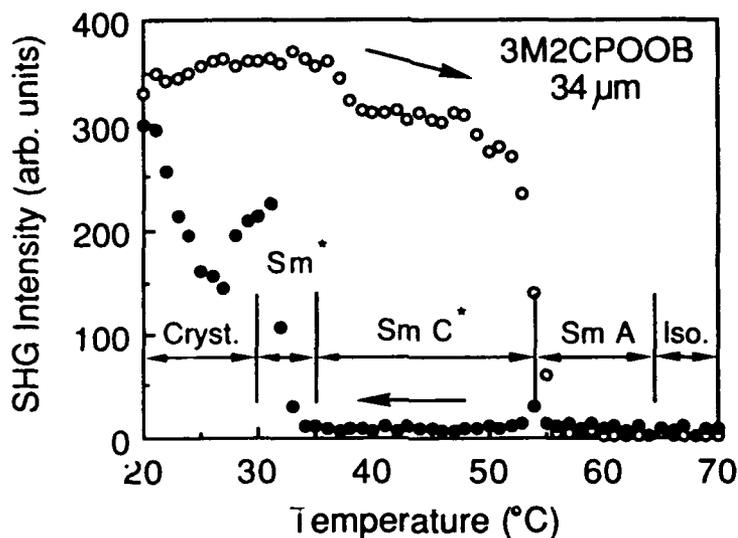
FIG.4   Temperature dependence of the SHG intensity in 3M2CPOOB.

The long molecular axes of FLC tilt at an angle θ_t from the layer normal (z axis), and the tilt direction under no bias field rotates around the layer normal from one layer to the next, resulting in the construction of a helical structure. In this structure the cancellation of the SHG in each smectic layers results in the disappearance of the macroscopic SHG.

However, in the heating stage the SHG was effective in the chiral smectic and crystalline phases. This may correspond to the SHG observed by means of the powder technique in the nonlinear optical material.[20]

ELECTRIC FIELD DEPENDENCE OF SHG

Under a dc bias field above a certain threshold, the spontaneous polarization orients along the field (y axis), and the molecules lie in the x-z plane as shown in Figure 3. In other words, the helical structure of the FLC turns into the unwound structure by the electric field. In this state, the FLC has a C2 symmetry, and dipole moments are oriented in the direction of the two-fold axis normal to the molecular long axis and parallel to the smectic layer. Therefore, the SHG can be observed above the critical field enough to unwind the helical structure.

M.OZAKI et al.
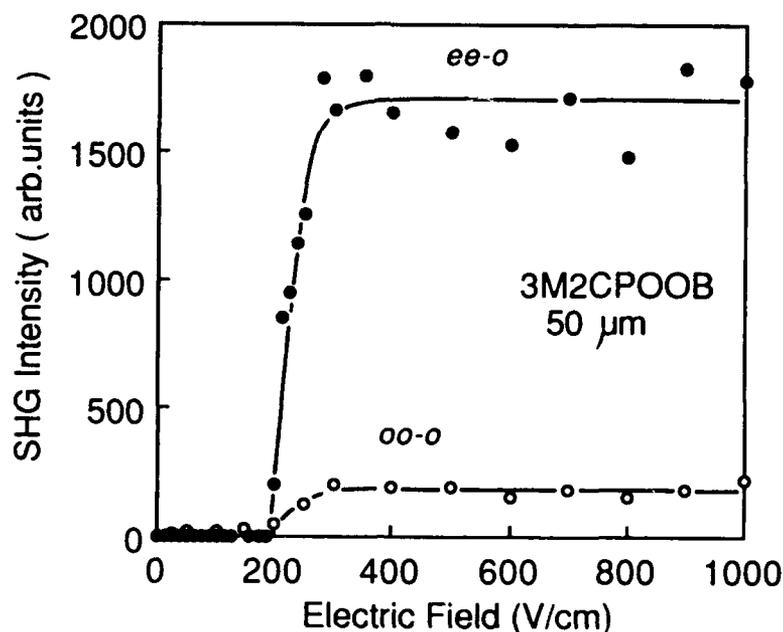
FIG.5 Electric field dependences of the SHG intensity in 3M2CPOOB.

Figure 5 shows the electric field dependence of the SHG intensity in the Sm C*
phase for the rotating angle θ of about -2.5°. As is evident from this figure, the
enhancement of the SHG intensity is confirmed above around 200 V/cm, which
corresponds to the critical field enough to unwind the helical structure.

Figure 5 also shows the dependence of the SHG intensity on the polarizations of
the fundamental and second harmonic lights. In this figure, ee-o means that two waves of
the extraordinary type result in the ordinary wave of the second harmonic (the
extraordinary and ordinary waves lie in the x-z and y-z planes, respectively). It should be
noted that only the ordinary wave of the harmonic light is observed and the extraordinary
wave of that can't be observed. For the point group C_2, the second harmonic
polarizations P_1, P_2 and P_3 along the axes 1, 2 and 3 shown in Figure 3 are given by

$$P_1 = 2\varepsilon_0 d_{14}E_2E_3 + 2\varepsilon_0 d_{16}E_1E_2$$

$$P_2 = \varepsilon_0 d_{21}E_1{}^2 + \varepsilon_0 d_{22}E_2{}^2 + \varepsilon_0 d_{23}E_3{}^2 + 2\varepsilon_0 d_{25}E_3E_1 \tag{1}$$

$$P_3 = 2\varepsilon_0 d_{34}E_2E_3 + 2\varepsilon_0 d_{36}E_1E_2,$$

where d_{ij} are the elements of the second-order nonlinear susceptibility tensor and E_1, E_2
and E_3 the electric field components of the fundamental wave along dielectric axes.

For this point group only the component of the SHG parallel to the two fold axis is
permitted. Therefore, the ordinary wave (parallel to axis y) of harmonic light is the
permitted component and the extraordinary wave is forbidden in consistent with the result
shown in Figure 5.

The dynamic change of the SHG intensity by the application of a stepwise electric field is shown in Figure 6(a). The fundamental light was irradiated perpendicularly into the cell surface. The radiation of a pulsed fundamental light was delayed for a certain time after the application of the stepwise field. As is evident from this figure, the response can be divided into two components, that is, very fast (several hundred µs) and relatively slow (several hundred ms) responses. Figure 6(b) shows the static field dependence of the SHG intensity at $\theta=0$ corresponding to the dynamic response shown in Figure 6(a). The slight increase of the SHG before the main enhancement due to the unwinding of the helical structure was observed. Therefore, the fast component of the SHG shown in Figure 6(a) may be attributed to the slight deformation of the helical structure before the complete unwinding.
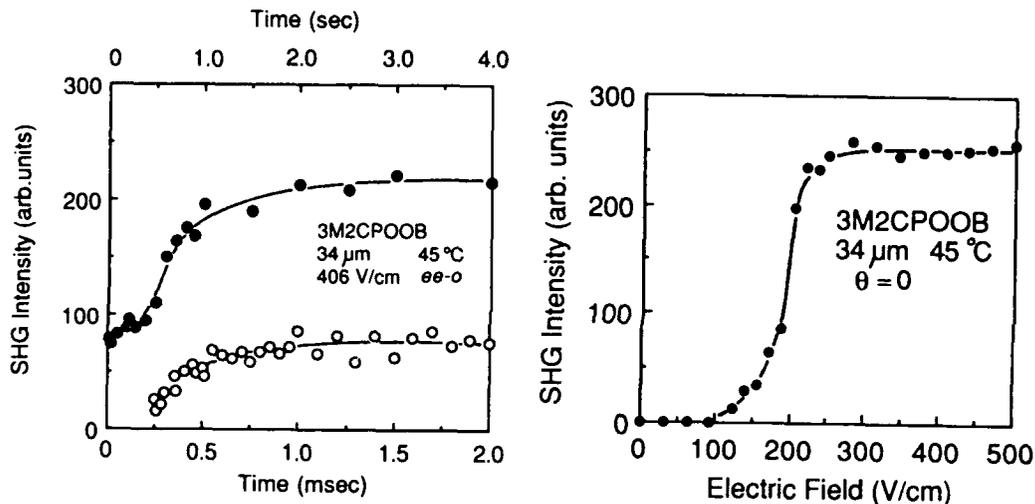
FIG.6   (a) Dynamic change of the SHG intensity by the application of the stepwise voltage. $\theta=0$.

(b) Electric field dependence of the SHG intensity for a normal incident.

ANGULAR PHASE-MATCHING OF SHG AND CELL THICKNESS DEPENDENCE

Figure 7 shows angular dependences of the SHG intensity under the electric field. Two extraordinary waves result in the ordinary wave of the second harmonic(ee-o). Type I phase-matching of SHG was observed at $\theta\sim$-2.5°. As is evident from Figure 3, the phase-matching angle between the optical axis of the liquid crystal and the direction of the fundamental light, θ_m, can be estimated using the relation $\theta_m=\theta_t$-θ, where θ_t is the tilt angle of FLC molecules from the smectic layer normal. At this temperature, θ_t is 28° in 3M2CPOOB, and the phase-matching angle is obtained as $\theta_m=25.5°$ from the phase-matching curve shown in Figure 7.
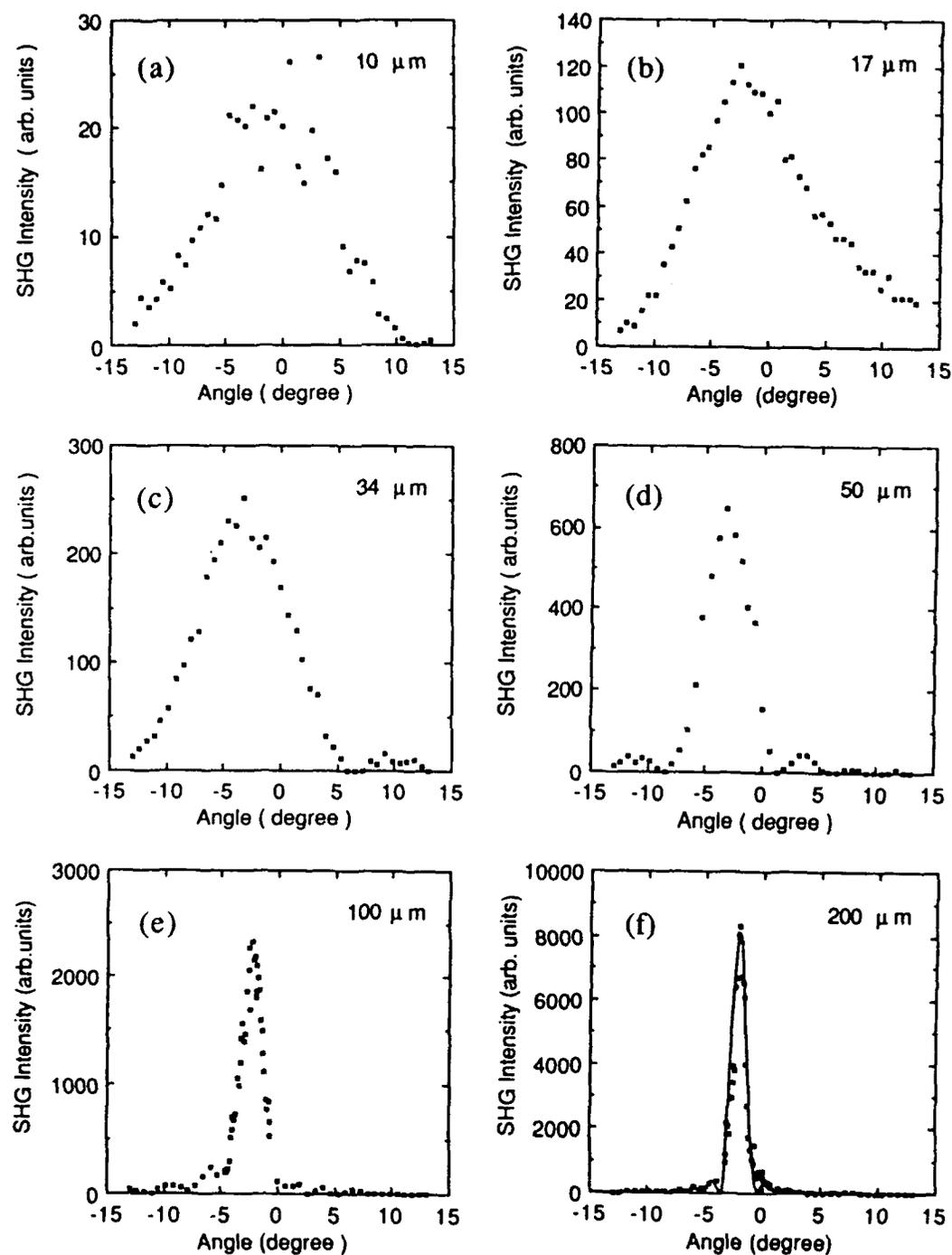
FIG.7 Angular dependences of the SHG intensity under a bias field (500V/cm).
Calculated phase-matching curve is also shown in (f). Tc-T=6.5°C.

For a positive uniaxial crystal with normal dispersion of the refractive indices the phase-matching angle is evaluated as follows,

$$\theta_m = \tan^{-1}\left(\frac{n_e^\omega}{n_0^\omega} \sqrt{\frac{(n_0^{2\omega})^2 - (n_0^\omega)^2}{(n_e^\omega)^2 - (n_0^{2\omega})^2}} \right), \qquad (2)$$

where n_e^ω and n_0^ω are refractive indices of extraordinary and ordinary waves for the fundamental light, respectively, and $n_0^{2\omega}$ is that of the ordinary wave of the harmonic light.

Although refractive indices in the Sm C^* phase can't be easily measured, those in the Sm A phase can be obtained using a wedge cell. For light sources several lines of Ar ion, He-Ne and AlGaAs lasers were used. The experimental results were fitted with Sellmeir's dispersion formula,[20] and $n_e^\omega = 1.589 \pm 0.003$, $n_e^{2\omega} = 1.614 \pm 0.003$, $n_0^\omega = 1.477 \pm 0.003$ and $n_0^{2\omega} = 1.500 \pm 0.003$ for 1064 and 532 nm were obtained. The phase-matching angle calculated from measured refractive indices using Eq.(2) was $\theta_m = 27.6 \pm 3.5°$. The result almost agrees with the value obtained from the phase-matching curve within the experimental errors because θ_m strongly depend on the refractive indices.

It should be noted that the profile of the phase-matching curve of the SHG depends on the cell thickness and a sharp profile of the phase-matched SHG is observed in a thick cell. Although some studies on the angularly phase-matched SHG have previously been reported, in those studies the width of the phase-matching curve was broad and the full angular width at one-half the intensity maximum of the phase-matching curve $\Delta\theta$ was about several or tens degrees. On the other hand, neglecting beam walk-off due to the birefringence, in solid materials the phase-matching curve of the SHG depends on the sample thickness and the sharp peak is obtained in a thick sample. It is very interesting whether the sharp phase matching curve can be observed in the liquid crystal or not because the liquid crystal molecules are almost freely rotating around their long axis and orientationaly fluctuating.

As is evident from Figure 7, in a thick cell (200μm) a very sharp phase-matched SHG is observed and $\Delta\theta$ is about one degree. This indicates that the phase-matching behavior is hardly influenced by the free rotation and orientational fluctuation of the liquid crystal molecules even in the thick cell.

The tilt direction of the FLC molecules in a homeotropic aligned cell can be easily switched by the polarity reversal of the applied field and the response time of this switching is very short. This switching of the tilt direction causes the change of the matching position in the angular dependence of the SHG. In other words, an intense phase-matched SHG is controlled by the polarity of the applied voltage. Therefore, the

high speed modulation of the SHG can be realized in the FLC device. Especially, the faster operation may be expected by using the sharp profile of the angularly phase-matched SHG reported in this paper.

Neglecting the depletion of the fundamental light, the SHG intensity is given by

$$P_{2\omega} = \frac{2\,\mu_0^{3/2}}{\varepsilon_0^{3/2}}\;\frac{P_\omega^2\,d_{eff}^2\,\omega^2\,l^2}{A\,n^3}\;\frac{\sin^2(\Delta kl/2)}{(\Delta kl/2)^2}\,, \qquad (3)$$

where l is the interaction length, A is the beam area, d_{eff} is the effective nonlinear optical coefficient, ε_0 and μ_0 are free space permittivity and permeability, and $\Delta\kappa = k_{2\omega} - k_\omega$ is the phase mismatch between the fundamental and SH waves with wave vector k_ω and $k_{2\omega}$, respectively. The theoretical fitting curve using Eq.(4) is also shown in Figure 7(f), which is in good agreement with the experimental data. This also supports that the thick sample used in this study is of high optical quality and there is no effect of the dynamic motion and fluctuation of the molecules.

The walk-off angle ρ is also of interest. Using the measured refractive indices, the walk-off angle at critical phase-matching angle θ_m was estimated to be $\rho = 3.2°$. This is a rather small value and is consistent with the sharp phase-matching curve shown in Figure 7.

Figure 8 shows dependences of the peak intensity of the phase-matched SHG, I_{max}, on the fundamental light intensity and cell thickness. Both plots fit well to the straight line of slope 2. These results satisfy the theoretical relation among $P_{2\omega}$, P_ω and l described in Eq.(4).
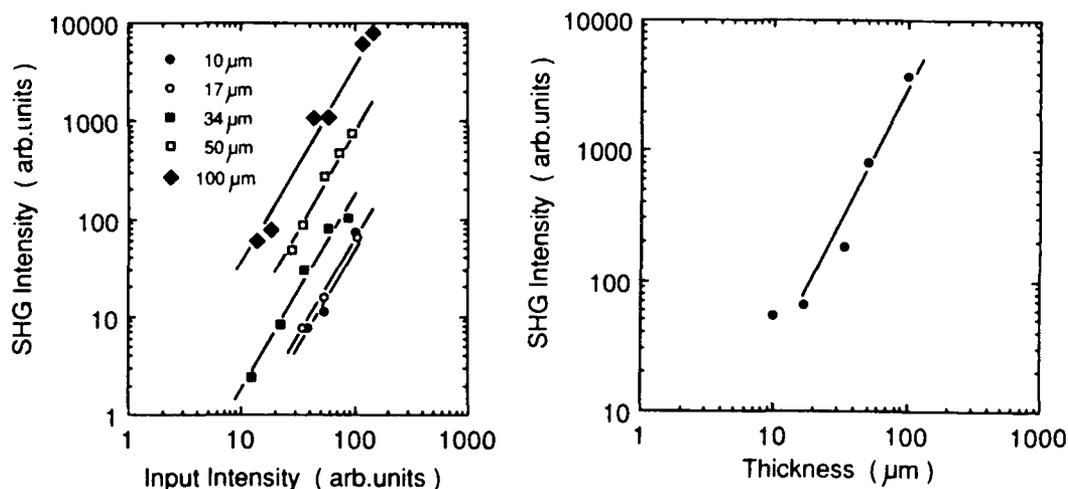
FIG.8   (a) Dependence of the SHG intensity on the fundamental light intensity.

(b) Dependence of the SHG intensity on the cell thickness.

The effective nonlinear coefficient d_{eff} in the present cell configuration is given by the next equation.

$$d_{eff} = \varepsilon_0 d_{21}\cos^2\theta + \varepsilon_0 d_{23}\sin^2\theta + 2\varepsilon_0 d_{25}\cos\theta\sin\theta. \tag{4}$$

At the condition of the phase-matching ($\theta=\theta_m$), $d_{eff}= 0.80d_{21} + 0.20d_{23} + 0.80d_{25}$. In order to determine the value of d_{eff}, a relative measurement with respect to $LiNbO_3$ was performed. The relative intensity and refractive indices gave $d_{eff}=0.01$ pm/V. This value is small in comparison with the other organic nonlinear material. However, the nonlinear coefficient depends on the material of the liquid crystal. Particularly, the liquid crystal with large spontaneous polarization P_s does not always show the large nonlinear coefficients. It is necessary to design the optimum molecular structure of the liquid crystal for SHG.

TEMPERATURE DEPENDENCE OF PHASE-MATCHED SHG

Figure 9 shows the temperature dependence of the profile of the phase-matched SHG in 100 μm cell. As is evident from Figure 9, the angle θ shifts with temperature. Figure 10(a) shows temperature dependences of θ_m and $\Delta\theta$. Though $\Delta\theta$ is independent of the temperature, θ_m at each temperature slightly depends on the temperature. As mentioned previously, θ_m is sensitive to any small change in the refractive indices of the molecules. Therefore, the temperature dependence of θ_m may correspond to that of the refractive indices.
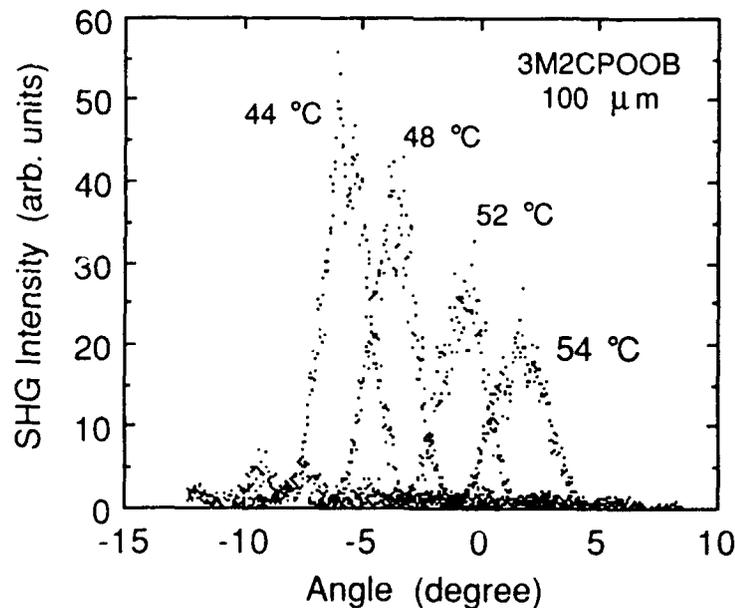
FIG.9 Angularly phase-matching curves at various temperatures.
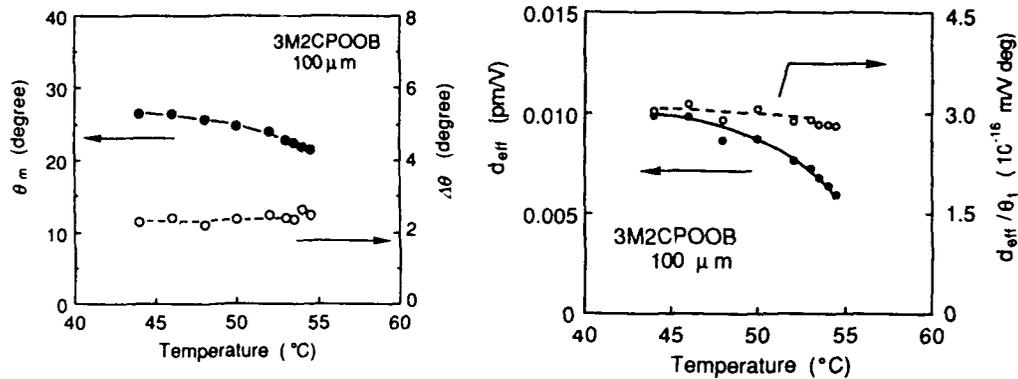
FIG.10   (a) Temperature dependences of   (b) Temperature dependences of
          θm and $\Delta\theta$ of phase-matching d_{eff} and d_{eff}/θ_t in 3M2CPOOB.
          curve in 3M2CPOOB 100 μm cell.

The phase-matched SHG intensity, I_{max}, increases with decreasing temperature. Figure 10(b) shows the temperature dependence of d_{eff}. d_{eff} increases with decreasing temperature. This result could be explained as follows. The molecular long axis of FLC tilts with respect to the smectic layer normal with decreasing temperature, and the magnitude of the tilt angle increases monotonously. As the tilt angle increases, the free rotation around the long molecular axis is reduced, resulting in the increase in P_s.

Figure 10(b) also shows temperature dependence of d_{eff}/θ_t. It is found that d_{eff} is in proportion to θ_t. This may indicate that the hinderance of the free rotation of the molecules due to the tilt causes the enhancement of d_{eff}.

MAKEr FRINGE IN FLC

Figure 11(a) shows the Maker fringe for d_{22} in 3M2CPOOB. Both fundamental and harmonic lights are ordinary wave. In addition to the Maker fringe, a sharp peak is observed. The position of this peak coincides with the center of the phase-matching curve at corresponding temperature and is reversed with respect to the origin by the polarity reversal of the applied field. Therefore, the sharp peak in the Maker fringe as shown in Figure 11(a) is seemed to be attributed to the phase-matched component of the SHG due to the imperfection of the alignment of the molecules or smectic layers. The coherence length l_c was determined using the positions of the fringe minima. $l_c = 12.3$ μm. The value of d_{22} can be determined using the amplitude of the fringe maxima. Figure 11(b) shows temperature dependence of d_{22}. d_{22} slightly increases with decreasing temperature. However, the change in d_{22} is gentler than that in d_{eff} shown in Figure 10(b).
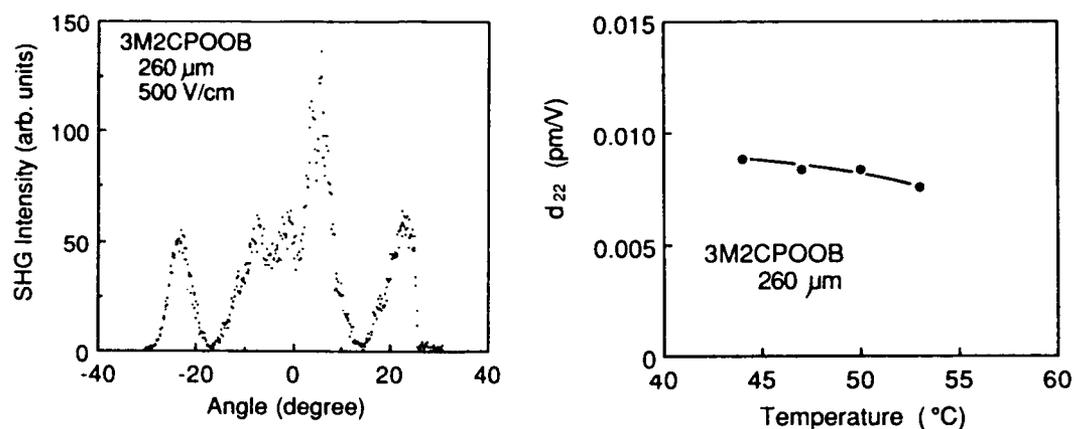
FIG.11   (a) Maker fringe for d_{22} of 3M2CPOOB

(b) Temperature dependece of the value of d_{22} obtained from Maker fringe in 3M2CPOOB.

TABLE   I   Spontaneous polaization, SHG intensities in the Sm C* and crystalline phases in FLCs used in this study.

		Ps(nC/cm²)	SHG(Sm C*)	SHG(cryst.)
1.	3M2CPOOB	-200	100	56
2.	DOBAMBC	-5	1.2	1
3.	DOBA-1-MPC	-20	0.3	1
4.	ETFPPOPB	150	21	84
5.	OTFPPOPB	-90	6	425
6.	ETFPBOB	110	-	133
7.	TFHBOB	-45	-	26
8.	1BC1EPOPB	240	11	4
9.	1HpC1EPOPB	130	3	1
10.	1MC1EPUdPB	100	6	0
11.	1HpC1ECPOPB	-55	3	1

* The SHG intensity is expressed in values relative to the phase-matched SHG intensity in 3M2CPOOB.

DEPENDENCE OF THE SHG ON MOLECULAR STRUCTURE

Dependence of the SHG intensity on the molecular structure of FLC was studied. Table I shows the molecular structure, spontaneous polarization and the SHG intensity in the Sm C* and crystalline phases. The SHG intensity is expressed in values relative to the phase-matched SHG intensity of 3M2CPOOB in the Sm C* phase. The obvious relationship between the molecular structure and the SHG intensity has not been observed in compounds used in this study. However, it should be noted that the SHG intensity in the crystalline phase depends on the molecular structure. That is, compounds 1, 4, 5, 6, 7 which include the halogens in their molecular structure indicate the intense SHG compared with compounds 2, 3, 8, 9, 10 and 11.

It should be noted that the compounds with large Ps such as 8, 9, 10 and 11 does not always show the intense SHG. In other words, there is no obvious relation between the SHG efficiency and the magnitude of Ps. Let us take another example. In DOBA-1-MPC, a large Ps compared with that in DOBAMBC can be obtained by decreasing the distance between chiral center and the dipole moment, and the core and dipole moment parts are the same as that in DOBAMBC. However, the SHG intensity in DOBA-1-MPC is less than that in DOBAMBC. This result indicates that relation between the core and dipole parts may contribute to the SHG efficiency.
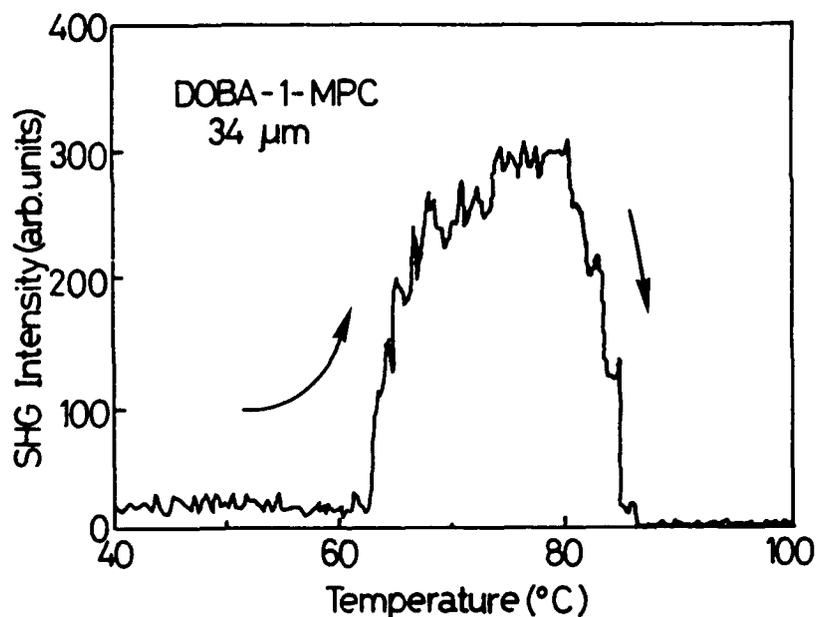
FIG.12   Temperature dependence of the SHG intensity of DOBA-1-MPC in the heating stage from the crystalline phase.

ANOMALOUS TEMPERATURE DEPENDENCE OF SHG IN DOBA-1-MPC

Figure 12 shows the temperature dependence of the SHG intensity of DOBA-1-MPC in the heating stage from the crystalline phase. Though the SHG intensity in the crystalline phase was weak, in the Sm C* phase the intense SHG was observed under no bias field, which is comparable to the intensity of the phase-matched SHG in 3M2CPOOB. The appearance of the SHG in this temperature range was not influenced by the application of the electric field and the angular dependence of the SHG intensity was not observed.

In 3M2CPOOB, the intense phase-matched SHG can be observed in the Sm C* phase in which a good alignment has been established by cooling from the isotropic phase. However, in DOBA-1-MPC, the intense phase-matched SHG was not observed even in the Sm C* phase with an excellent alignment at the cooling stage as shown in Table I. Therefore, there is no relation between the appearance of the SHG in the heating stage and the intense phase-matched SHG in the cooling stage.

SUMMARY

The detailed study on the angularly phase-matched SHG in the ferroelectric phase of FLC was reported. It was found that the width of the phase-matching angle depended strongly on the cell thickness, and the sharp type I phase-matching with the full angular width at one-half maximum of ~1° was realized even in the liquid crystal in thick cell. The temperature dependences of the phase-matching behavior and Maker fringe were also studied and nonlinear optical coefficients were obtained. The SHG intensity in several kinds of FLCs were measured in the Sm C* and crystalline phases. Anomalous temperature dependence of the SHG in DOBA-1-MPC was also observed.

REFERENCES

1) B.F.Levine, C.G.Bethea, C.D.Thurmond, R.T.Lynch and J.L. Bernstein, J.Appl.Phys, **50**, 2523(1979).
2) J.Zyss, J.F.Nicoud and M.Coquillay, J.Chem.Phys., **81**, 4160(1984).
3) K.Y.Wong and A.F.Garito, Phys.Rev.A, **34**, 5051(1986).
4) W.Chen, M.B.Feller and Y.R.Shen, Phys.Rev.Lett., **63**, 2665(1989).
5) N.A.Clark and S.T.Lagerwall, Appl.Phys.Lett., **36**, 899(1980).
6) A.N.Vtyurin, V.P.Ermakov, B.I.Ostrovskii and V.F.Shabanov, Phys.Stat.Sol.(B), **107**, 397(1981).
7) N.M.Shtykov, M.I.Barnik, L.A.Beresnev and L.M.Blinov, Mol.Cryst.Liq.Cryst., **124**, 379(1985).
8) K.Yoshino, S.Kishio, M.Ozaki, A.Yokotani, T.Sasaki and C.Yamanaka, Technol.Rept.Osaka Univ., **37**, 283(1987).
9) M.Ozaki and K.Yoshino, Technol.Rept.Osaka Univ., **39**, 217(1989).
10) A.Taguchi, Y.Ouchi, H.Takezoe and A.Fukuda, Jpn.J.Appl.Phys., **28**, L997(1989).
11) M.Ozaki and K.Yoshino, Jpn.J.Appl.Phys., **28**, L1830(1989).

12) J.Y.Liu, M.G.Robinson, K.M.Johnson and D.Doroski, Opt.Lett., **15**, 267(1990).

13) D.M.Walba, M.B.Ros, N.A.Clark, R.Shao, K.M.Johnson, M.G.Robinson, J.Y.Liu and D.Doroski, Mol.Cryst.Liq.Cryst., **198**, 51(1991).

14) T.Sakurai, N.Mikami, R.Higuchi, M.Honma, M.Ozaki and K.Yoshino, J.Chem.Soc.Chem.Commun., 978(1986).

15) M.Ozaki, K.Yoshino, T.Sakurai, N.Mikami and R.Higuchi, J.Chem.Phys., **86**, 3648(1987).

16) K.Yoshino, M.Ozaki, T.Sakurai, K.Sakamoto and M.Honma, Jpn.J.Appl.Phys., **23**,L175(1987).

17) K.Yoshino, M.Ozaki, H.Taniguchi, M.Ito, K.Satoh, N.Yamasaki and T.Kitazume, Jpn.J.Appl.Phys., **26**, L77(1987).

18) H.Taniguchi, M.Ozaki, K.Yoshino, K.Satoh, N.Yamasaki, Ferroelectrics, **77**, 137(1988).

19) K.Yoshino, M.Ozaki, K.Nakao, H.Taniguchi, N.Yamasaki and K.Satoh, Liq.Cryst., **5**, 1203(1989).

20) S.K.Kurtg and T.T.Perry:J.Appl.Phys., **39**, 3798(1968).

21) M.Born and E.Wolf, Principles of Optics, (Pergamon, Oxford, 1974).

CHIRAL ESTERS AND THEIR MIXTURES WITH STABLE S_C^* PHASE AT AMBIENT TEMPERATURE

JÁNOS SZABON, LAJOS BATA, KATALIN FODOR-CSORBA, NÁNDOR ÉBER, ANIKÓ VAJDA
Central Research Institute for Physics of the Hungarian Academy of Sciences, H-1525 Budapest 114, P.O.B. 49. Hungary

Abstract   Calculated and experimental phase diagrams of binary mixtures of the homologous series of (S)(+)-4-(2'-methylbutyl)-benzoate esters of the 4-n-alkoxybenzoic acids were compared. Eutectics occured if the length ratio of the components were smaller than r=0.9. If r≥0.9, co-crystallizations were detected. In mixtures of neighbouring homologues even the rule of additivity was valid for the melting curve (r=0.93-0.96, isomorphous systems). Eutectic mixtures of the **n=8** and **n=7** homologues (exhibited stable chiral smectic C phase around room temperature) were proved in spite of their length ratio of 0.96. Spontaneous polarization and helical pitch were measured both in the single compounds as well as in their mixture.

1. INTRODUCTION

The S(+)-4-(2'-methylbutyl)benzoate esters of the 4-n-alkoxybenzoic acids
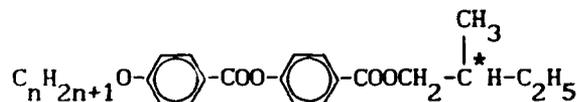
were synthesized via the reaction of the 4-n-alkoxybenzoic acid chlorides and S(+)-4-(2'-methylbutyl) 4-hydroxybenzoate. The alkoxy chain varied from **n=7** to **n=16**, thus the lengths of the molecules were in the range of 3.025 nm to 4.150 nm. The purity of these compounds was checked by IR and NMR spectroscopy as well as by chromatographic and DSC methods.[1] Their phase transition temperatures and other properties were studied and compared with data in the literature.[2-5]

All the homologues studied have monotropic chiral smectic C*, $S_{C'}^*$ phases, i.e. their melting temperatures are above the temperatures of the S_C^* - S_A^* phase transition. By measuring the thermodynamic

properties of the single compounds one can calculate the isobaric binary phase diagram to predict the range of existence of the S_C^* phase in the mixture.[6-8]

The spontaneous polarization and the helical pitch of the single compounds as well as of a binary mixture were measured.

2. EXPERIMENTAL

The thermodynamic data of the single compounds and their binary mixtures were studied by means of a Perkin Elmer-DSC2 differential scanning calorimeter, equipped with a subambient accessory and a PC based data acquisition system. Sample weights were 1-3 mg. Heating and cooling rates were varied between $1.25-10^{\circ}$C/min.

To measure the temperatures of second order phase transitions depolarized light intensity measurements, DLI, were made using a hot-stage microscope with crossed polarizers, equipped with a selenium light detector connected to a two-channel potentiometric recorder. Heating and cooling rates were varied between $1.25-5^{\circ}$C/min.

Diagrams of state of the binary mixtures were established by the Kofler-contact method[6] using a polarizing microscope with a Peltier heating-cooling stage as well as by determining the transition temperatures of samples of different concentrations by DSC and DLI.

The eutectic temperatures of the mixtures could be calculated from the measured enthalpies and melting temperatures of the single compounds[7] by applying the relations of Le Chatelier, Schröder and van Laar.[8]

The estimation of the molecular length was based on an improved Corey-Pauling spacefilling model[9] using the all-trans stretched molecular conformers of the alkoxy chains.

Spontaneous polarization for substances **n=7,8,9** as well as the mixture of **n=8** with 36 mol% **n=7** was measured by a Diamant-bridge technique.

The helical pitch of the S_C^* phase was obtained by measuring the distance between the lines corresponding to the full pitch, using 10μm thick nearly homogeneous planar aligned cells under an Amplival pol-u polarizing microscope.

3. RESULTS

The thermodynamic data as well as the molecular lengths of the compounds are given in Table I. As all the S_C^* phases of the pure homologues are monotropic, enantiotropic mesophases could only be obtained by the eutectic depression of melting in mixtures.

TABLE I   Molecular length, phase transition temperatures and enthalpies for the homologues of the S(+)-4-(2-methylbutyl)-benzoate esters of 4-n-alkoxybenzoic acids. () denotes monotropic phase transition.

n	L	Crystal - S_A^*		$(S_C^* - S_A^*)$		$S_A^* - I$	
	nm	$°C$	$kJmol^{-1}$	$°C$	$kJmol^{-1}$	$°C$	$kJmol^{-1}$
7	3.025	42.2	-21.0	(23.5)	≤0	52.0	-4.03
8	3.150	34.0	-23.7	(31.0)	≤0	57.0	-4.30
9	3.275	57.0	-30.7	(36.0)	≤0	57.5	-4.65
10	3.400	51.1	-27.7	(39.0)	≤0	59.0	-5.11
11	3.525	56.7	-26.5	(38.0)	≤0	60.0	-5.24
12	3.650	58.1	-32.3	(40.5)	≤0	60.5	-5.60
16	4.150	47.8	-50.2	(34.5)	≤0	61.0	-6.90

3.1. Isobaric phase diagrams

The calculation of the phase diagrams[7] was based on   the following assumptions:

- the two components are immiscible in solid phase, i.e. do not form mixed crystals,
- the liquid phase is an ideal mixed one, i.e. the activity coefficients of the components in the liquid phase equal one,
- the melting enthalpies are temperature-independent.[7,8]

The calculated eutectic temperatures with the corresponding concentrations are given in Table II. The A-B components are denoted by their alkoxy carbon number n=7-12,16.

TABLE II   Calculated eutectic temperatures and concentrations (in mol% of B) for the A-B binary mixtures.

A B	n=7 ($^{\circ}C$ at x_B)	n=8 ($^{\circ}C$ at x_B)	n=9 ($^{\circ}C$ at x_B)	n=10 ($^{\circ}C$ at x_B)	n=11 ($^{\circ}C$ at x_B)	n=12 ($^{\circ}C$ at x_B)
n= 7	– –	12.7 46.6%	25.5 67.9%	22.2 61.8%	24.1 65.4%	26.9 70.8%
n= 8	12.7 53.4%	– –	21.7 72.6%	19.0 66.2%	20.5 69.7%	22.9 75.5%
n= 9	25.5 32.1%	21.7 27.4%	– –	32.9 43.3%	35.7 48.3%	38.3 53.4%
n=10	22.2 38.2%	19.0 33.8%	32.9 56.7%	– –	31.8 54.6%	34.5 60.0%
n=11	24.1 34.6%	20.5 30.3%	35.7 51.7%	31.8 45.4%	– –	37.5 54.9%
n=12	26.9 29.2%	22.9 24.5%	38.3 46.6%	34.5 40.0%	37.5 45.1%	– –
n=16	27.5 28.1%	23.9 22.5%	36.5 50.3%	33.6 41.9%	35.8 48.1%	37.7 54.4%

Isobaric phase diagrams of the binary mixtures were measured. Eutectic systems were detected in most cases except mixtures of neighbouring homologues, which proved to be more or less isomorphous systems. As examples, diagrams of state are presented in Figure 1 for the n=8 and n=12 compounds as component A. The other component of the mixtures, B, were homologues with small differences in the number of the carbon atoms in their alkoxy chains. In other words, the ratios of their molecular lengths,

$$ r = \begin{cases} L_A/L_B & \text{if} \quad L_A < L_B \ , \\ L_B/L_A & \text{if} \quad L_B < L_A \ , \end{cases} $$

were close to 1. Here L_A and L_B mean the molecular lengths of the A and B components of the mixture, respectively. Dotted lines mark S_C^*-S_A^* phase transitions in the supercooled state.
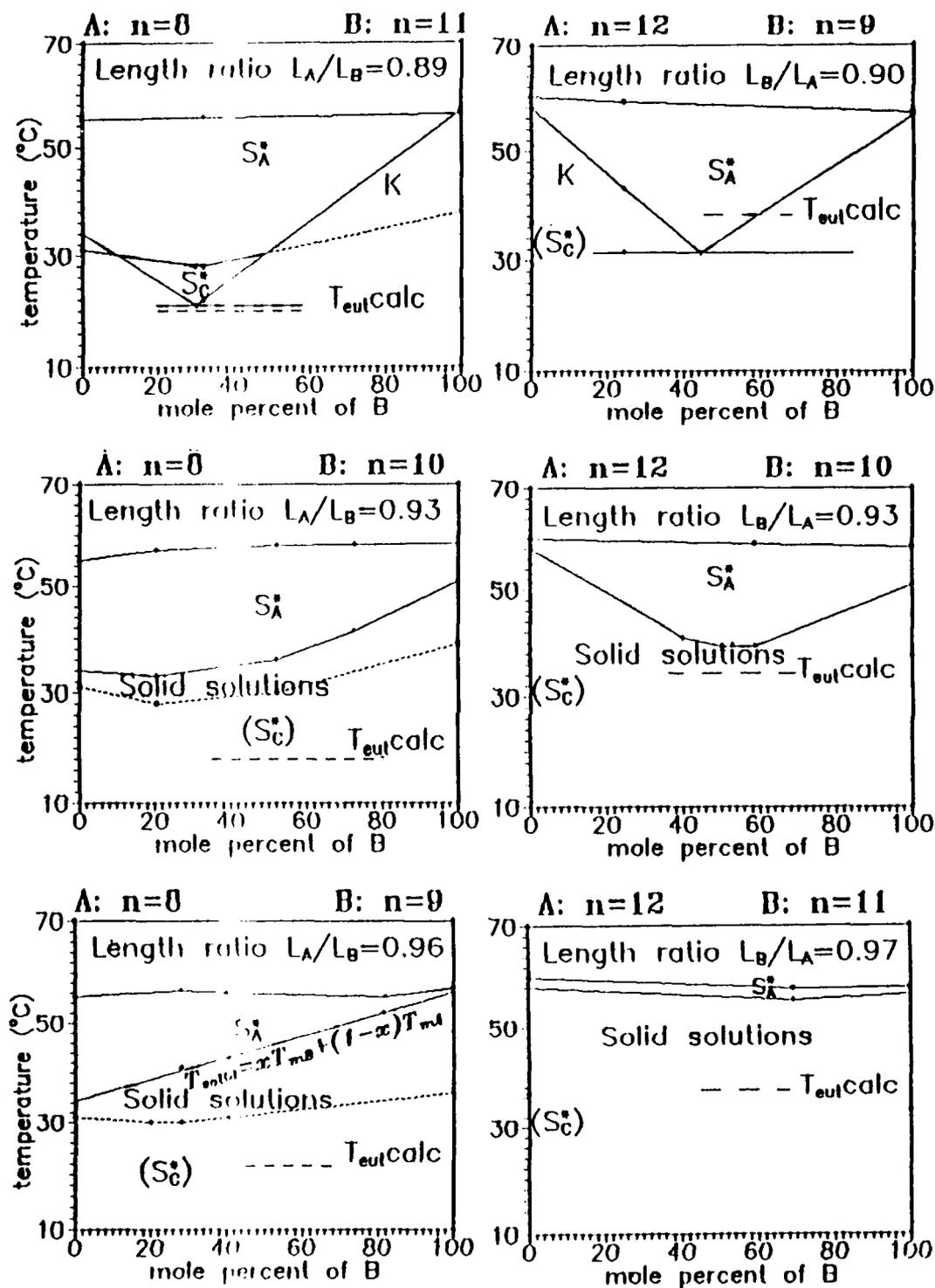
FIGURE 1   Isobaric binary phase diagrams, at different length ratio values. Dotted lines monotropic transitions, dashed lines calculated values.

3.2. Spontaneous polarization and helical pitch

We measured the spontaneous polarization and helical pitch of the homologues. Results are shown in Table III. The temperature dependence of the spontaneous polarization for some compounds and a binary mixture are given in Figure 2. The spontaneous polarization of the mixture n=8 and n=7 containing 36 mol% n=7 fell in between the values of the components.

TABLE III   Results of spontaneous polarization and helical pitch measurements.

Compounds	P_S (nC/cm^2)	Pitch (μm)
n= 7	1.42 (22.5^{o}C)	---
n= 8	4.90 (26.5^{o}C)	1.3
n= 9	3.33 (34.5^{o}C)	2.7
n=10	5.00*	---
n=12	---	2.0
n=16	---	2.0
n=7/n=8	3.12 (21.0^{o}C)	2.6

*from Reference 11.
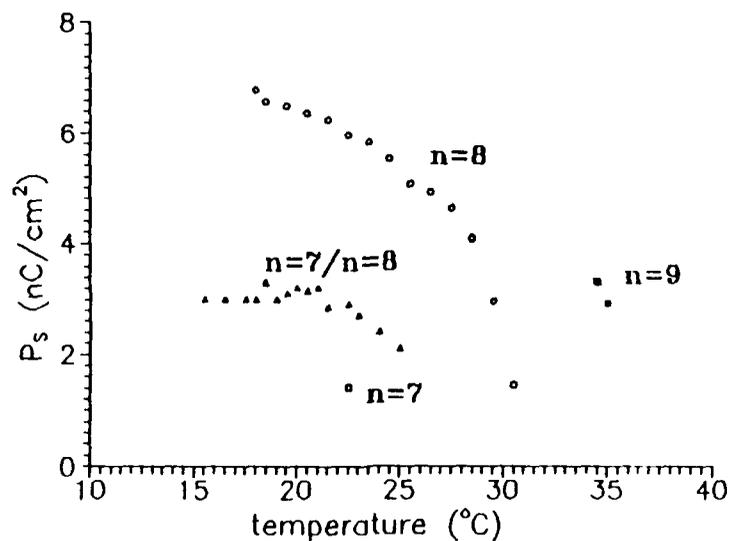
FIGURE 2   Temperature dependence of the spontaneous polarization for compounds n=7, n=8, n=9 and a mixture n=7/n=8.

4. DISCUSSION

The calculated and the experimental isobaric phase diagrams can be compared. The differences, D, of the observed melting temperatures, T_{exp}, and the calculated eutectic ones, T_{calc},

$$D = T_{exp} - T_{calc}$$

taken at the calculated eutectic compositions, are demonstrated in Table IV as a function of the difference in the alkoxy carbon numbers of the components. denoted by **d**, as well as a function of the ratio of their molecular lengths **r**.

TABLE IV   The differences D between the calculated and the experimental melting temperatures at the calculated eutectic composition for two series of binary mixtures of homologues n=12, and n=8, compared to earlier studies of nematogens[7] with the same differences, d, of the alkoxy carbon numbers.

d	r	A: n=12		A: n=8		Ref. 7
		B:	D (^{o}C)	B:	D (^{o}C)	D (^{o}C)
8	0.76			n=16	-4	+1 -1
5	0.83	n= 7	-4			
4	0.86	n= 8	-6	n=12	-6	-2
4	0.88	n=16	-12			+8
3	0.90	n= 9	-6	n=11	+1	
2	0.93	n=10	+5	n=10	+14	+10 (0)
1	0.96			n= 9	+26	
1	0.96			n= 7	0	
1	0.97	n=11	+22			

In all systems presented in Table IV the calculated and the measured melting temperatures do not coincide (D ≠ 0), except the anomalous case of n=8/n=7:

-if r≤0.83, i.e. d≥5, eutectics occured and D seems to decrease

as the difference of the molecular lengths grows,

-at $0.86 \leq r \leq 0.88$, i.e. d=4, the *negative* differences were the greatest,
-if $r \geq 0.93$, i.e. $d < 2$, great *positive* differences could be observed.
In the system of n=8/n=7, r=0.96, d=1, there is no difference: $D = 0$.

Compared to the binary mixtures of other homologous systems[7,8] studied earlier similarities as well as differences can be observed.

In the majority of our binary systems eutectics occured if $r \leq 0.83$, d≥5, similarly to nematogens[7]. This is also in aggreement with the earlier results on n-paraffins[10] as eutectics were found in binary systems if the molecular lengths of the components were sufficiently different.

Contrary to nematogens[7], if $0.86 \leq r \leq 0.88$, i.e. with 4 carbons as difference in lengths, greater *negative* extrema were demonstrated (Table IV). The greater depression of melting points are probably due to the hindered packing arising from chirality.

As a result of co-crystallization, solid solutions (i.e. mixed solid crystals) occured in binary mixtures of neighbouring members of the homologous series of 4-n-alkoxy azoxybenzenes[7] (d=2, their length ratios were $r \geq 0.80$). Similarly, great *positive* differences were found in our chiral mixtures between measured and calculated melting temperatures due to co-crystallization. (However, the ratios of the molecular lengths of the components were $r \geq 0.93$, which were greater values than r=0.80 above.) As can be seen in Figure 1., for the system of **n=8/n=9**, the melting temperatures are additive according to the equation of

$$T^x_{solid} = T^B_{melting} + (1-x)T^A_{melting} \qquad (x=\text{mole fraction of } B)$$

indicating complete solid solubility.

The binary mixture of the **n=8/n=7** system is rather different from the others (Table IV). At the length ratio of r=0.96, d=1, at which in the other systems solid solutions occured, a pronounced eutectic behaviour catches the eye (see Figure 3). At the first instance this reminds us of the PAA-PAP system in which deep eutectic appeared in spite of the smallest value of d (d=2, dialkoxy compounds), due to the methoxy and ethoxy side groups[7] which differ frequently from the normal trend of clearing and melting point behaviour.

In the n=8/n=7 system the side chains are rather longer. Their

diagram of state shows ideal melted as well as solid phases with no solid solution in spite of one methylene group as the only difference between the structure of the components. The additivity rule for the temperatures of the S_C^*- S_A^* phase transition, T_{CA}.

$$T_{CA}^x = xT_{CA}^B + (1-x)T_{CA}^A \qquad \text{where } x=x_B \text{ ,}$$

was strictly valid in this system.
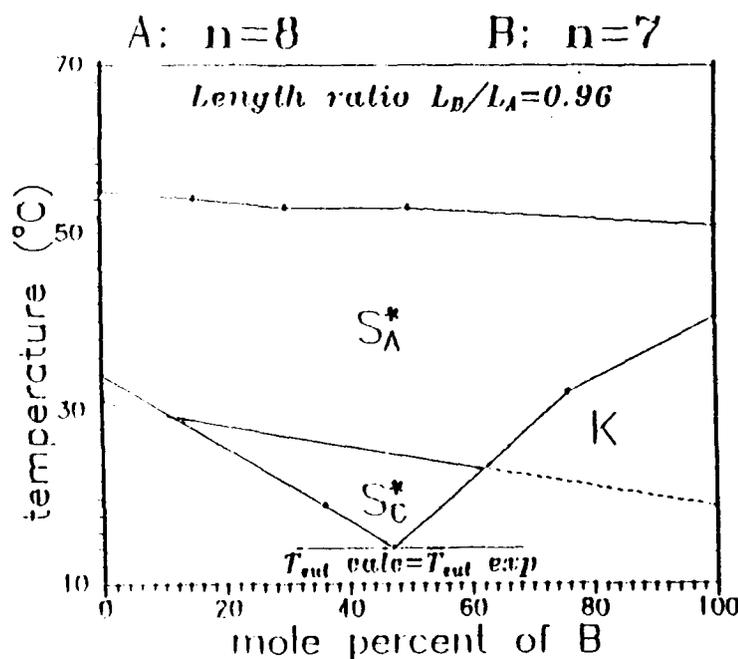
FIGURE 3   Diagram of state for the binary mixture of n=8/n=7.

SUMMARY

Eutectics were found in binary mixtures of homologues of the S(+)-4(2'-methylbutyl)benzoate esters of the 4-n-alkoxybenzoic acids up to the length ratio of r=0.9. Stable S_C^* phases were detected in most cases as the experimental solidus lines showed steep depressions in the diagrams of state while the S_C^*-S_A^* transition lines were more or less additive.

On the other hand mixed solid crystals could be detected in mixtures consisting neighbouring homologues ($r \geq 0.93$) which melted above the temperature of the calculated eutectic as well as the S_C^* phase. Even the rule of additivity was found to be valid concerning melting points in a few mixtures indicating isomorphous systems.

An anomalous behaviour was detected in case of the binary system **n=8/n=7**. The rule of additivity was valid only for the temperature curve of the $S_C^*-S_A^*$ phase transition, and eutectics occured, with $T_{exp}-T_{calc} = 0$ in spite of the similarity of the components. The values of the spontaneous polarization fell in between those of the components.

REFERENCES

1. L. Bata et al.   To be published.
2. J. W. Goodby and T. M. Leslie, in Liquid Crystals and Ordered Fluids Vol. 4. Eds. A. C. Griffin and J. F. Johnson, (Plenum Press, New York, London, 1984) pp. 1.
3. S. Hattori, K. Kondo, T. Kitamura and Y. Hanawa, Eur. Pat. 163,229 A2 (1985) CA. 104. 160062r (1986).
4. K. Furukawa and K. Terashima, Eur. Pat. 192,267 (1986) CA. 106. 59031w. (1987).
5. S. Kajiyama, A. Takahara and H. Kikuchi, Jpn. Kokai Tokkyo Koho JP 62,260,859 (1987) CA. 108. 168789m (1988).
6. L. Kofler and A. Kofler, Thermomikromethoden zur Kennzeichung organischer Stoffe und Stoffgemische (Verlag Chemie, Weinheim, 1954)
7. D. Demus, C. Fietkau, R. Schubert and H. Kehlen, Mol. Cryst. Liq. Cryst. 25. 215 (1974).
8. M. Domon and J. Billard, Pramana, Suppl. 1. 131 (1975)
9. S. Diele, personal commun.
10. G. J. Asbach and H. G. Kilian, Ber. Bunsenges. 74, 814 (1970)
11. J. S. Patel and J. W. Goodby, Opt. Eng. 26. 373-84 (1987).

ELECTROCLINIC AND DIELECTRIC PROPERTIES OF CHIRAL SmC INFLUENCED BY THE SUBSTANCE CHIRALITY

M. Glogarová, Ch. Destrade[§], J.P. Marcerou[§], J.J. Bonvent[§], H.T. Nguyen[§]

Institute of Physics, Czechoslovak Acad. Sci.,
Na Slovance 2, 18040 Prague 8, Czechoslovakia

[§] Centre de Recherches Paul Pascal,
Chateau Brivazac, 33600 Pessac, France

Abstract The left and right handed versions of a chiral SmC* material have been mixed to change the substance chirality. The dielectric and electroclinic properties measured in the temperature range $T_c \div T_c + 2K$ and the frequency range 120 Hz $\div$ 1.6 MHz allow to determine the relaxation frequency f_r, dielectric susceptibility χ_{ec} and electroclinic coefficient e of the soft mode for the studied mixtures. The dependences $1/\chi_{ec}(T)$, $1/e(T)$, $f_r(T)$ obey the Curie-Weiss law. From these dependences the first three coefficients of the free energy and the viscosity of the soft mode have been determined. The C coefficient driving the linear interaction $CP\Theta$ is the only one influenced by the chirality. It depends linearly on the mixture concentration n. This dependence results in the shift of the phase transition temperature $\Delta T_c \sim n^2$.

INTRODUCTION

The molecular chirality is a necessary condition for the occurence of the ferroelectric smectic C* (Sm C*) phase in a mesogenic substance[1]. The effect of chirality on ferroelectric properties has been studied by mixing a non-chiral substance exhibiting a Sm C phase together with a chiral substance, either non-mesogenic[2], or exhibiting a cholesteric phase[3], or a Sm C* phase[4,5]. In all cases the increase in chiral substance concentration results in an increase in the spontaneous polarization[3-5] and decrease in the pitch of the Sm C* structure space modulation[3]. Moreover, when mixing two different Sm C and Sm C* substances, the tilt angle can depend on concentration[4]. It has been also found that when mixing a non-chiral and chiral substance which exhibit a second order phase transition Sm A → Sm C and a first order phase transition Sm A → Sm C* resp., the character of the phase transition Sm A → Sm C* of the mixture can be changed with the concentration[5].

All described results have been obtained by mixing two different

substances. Then the effect of chirality could not be studied in a pure form being complicated by other differences between molecules of both substituents. In this respect we intend to study properties of one substance the chirality of which is changed by mixing its left handed (L) and right handed (D) varieties. One may expect that as a result of the chirality change, in the main, the linear coupling between the phase transition parameter (tilt angle θ) and polarization (P), which is the source of ferroelectricity in Sm C^* phase, is changed, becoming zero for the non-ferroelectric racemic mixture.

In the present contribution we study the influence of the variation of the linear coupling between P and θ on the soft mode, which is reflected in electroclinic and dielectric properties[6] and in the shift of the phase transition Sm A $\rightarrow$ Sm C^* temperature T_c. The latter has been experimentally found as reported in Ref.[7].

THEORETICAL BACKGROUND

Macroscopic properties of ferroelectric liquid crystals near their phase transition can be derived from the free energy density of the Landau type[8]

$$F = \frac{1}{2}\alpha(T-T_o)\theta^2 + \frac{1}{2\varepsilon_o\chi_\perp} P^2 - C\theta P - PE.$$ (1)

This simplest expansion can describe linear electroclinic and dielectric response to the applied electric field in the paraelectric Sm A phase:

$$\theta = eE,$$

$$P = \varepsilon_o\chi E,$$

where the electroclinic coefficient

$$e = \frac{\varepsilon_o\chi_\perp C}{\alpha(T-T_c)},$$ (2a)

the increase of susceptibility due to the softening of the polarization mode near above the phase transition[6] compared with its high temperature value $\chi_\perp$ is

$$\varepsilon_o\chi = \frac{\varepsilon_o^2\chi_\perp^2 C^2}{\alpha(T-T_c)},$$ (2b)

and the increase of the phase transition temperature (T_c) against its

value T_o for the non-chiral (racemic) mixture is

$$T_c - T_o = \frac{\epsilon_o X_\perp C^2}{\alpha} .$$ (2c)

In the free energy (1) the first two terms are non-chiral, the other two are of a chiral character.

The relaxation frequency of the mode in Sm A phase is calculated from the dynamic equations

$$- \frac{\partial F}{\partial \Theta} = \gamma \frac{\partial \Theta}{\partial t}$$

$$- \frac{\partial F}{\partial P} = 0 ,$$ (3)

where γ is a viscosity connected with the soft mode, which is supposed to be temperature independent. From (3) one obtains a frequency dependence of Θ on the a.c. electric field $E = E_o e^{i\omega t}$

$$\Theta = \frac{\epsilon_o X_\perp C E_o}{\alpha (T - T_c)(1 + i\omega/\omega_r)} ,$$ (4)

where

$$f_r = \frac{\omega_r}{2\pi} = \frac{\alpha (T - T_c)}{2\pi\gamma}$$ (5)

is a relaxation frequency of the soft mode.

EXPERIMENT

The L and D varieties of

$$C_7H_{15}O - \langle O \rangle - \langle O \rangle - O_2C - \overset{*}{C}H - CH(CH_3)_2$$
$$|$$
$$Cl$$
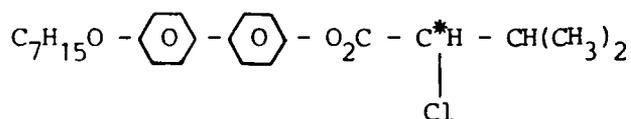
exhibit the equal phase sequence

Sm G[*] 70.3 Sm C[*] 73.1   Sm A 81.1 Isotropic

with monotropic Sm G[*] and Sm C[*] phases. Mixtures of L and D varieties have been prepared: M1: 89 %, M2: 74 %, M3: 65 %, R: 50 % of L.

The samples confined between two glass electroded plates 12 μ m spaced have got the "book shelf" geometry. The alignment has been achieved by rubbing a polymer layer on the glass plates, by shearing the upper glass plate after the sample has been filled and simultaneous application of an electric field $\sim$ 20 Hz, 30 $\div$ 40 V. This combined procedure results in a homogeneous planar structure in Sm A phase. In Sm C[*] phase no dechiralization lines are observed with the samples of the above mentioned

thickness, so that the samples are unwound by the boundary interactions. Nevertheless, a very fine, dim stripe texture exists in both Sm A and Sm C[*] phases which is interpreted as long focal conics[9].

The electroclinic response has been detected as an electric signal on PIN photodiode which measures changes of the polarized light intensity going through the sample. The sample has been placed between crossed polarizers the optical axis making $\pi/8$ angle with one of them. Then, at small deviation angles, the transmitted light intensity is proportional to the deviation of the optical axis, i.e. to the tilt angle and is modulated at the same frequency as the applied field. The electroclinic effect has been measured by a lock-in detector in the frequency range 120 Hz $\div$ 1.6 MHz in order to determine its relaxation frequency. Before the a.c. measurement the electroclinic signal has been calibrated for the deviation of the optical axis by rotating the sample from the $\pi/8$ position by a definite angle.

Unfortunately, the calibration has changed within 10 % when checked before the measurement and after finishing a thermal run, probably owing to a movement and additional creation of defects during the temperature change and also due to non-perfect long term stability of the electro-optical equipment.

The permittivity has been determined by measuring a voltage U_m on the constant capacitor Co which is in series with the sample

$$\epsilon_{tot} = \frac{d}{S} \, Co \, \frac{U_m}{U_a} \, ,$$

where d and S are the sample thickness and surface, U_a is the voltage applied on the sample. Measured total relative permittivity is a sum of several contributions

$$\epsilon_{tot} = 1 + \chi_\infty + \chi_\perp + \chi_{ec} \tag{6}$$

where χ_∞ contains high frequency molecular librations and electron polarization contributions, $\chi_\perp$ is a contribution of the high temperature hard mode and χ_{ec} is the increase of permittivity due to the soft mode.

At low frequency the permittivity has been measured simultaneously with the electroclinic coefficient at the same temperature and field conditions (for the apparatus see Ref. 10).

It has been tested for each experiment that both electroclinic and dielectric responses are measured at linear regime, i.e. the induced tilt

angle and the induced polarization are proportional to the applied field. This condition has been fulfiled under the applied field intensity lower than 4×10^5 V/m at the temperature of about T_c + 2K and 8×10^4 V/m close above T_c.

The heating oven with a double shielding has allowed to stabilize the sample temperature within 0.03 K.

For each studied concentration of L handness (namely 100 %, 89 %, 74 %, 65 % and 50 %) T_c has been determined by microscopic observation at cooling at a constant rate 0.1 deg/min. For this purpose a non--aligned fresh sample has been used without any thermal treatment.

EXPERIMENTAL RESULTS

The shift of T_c with the concentration (n) is shown in Figure 1.
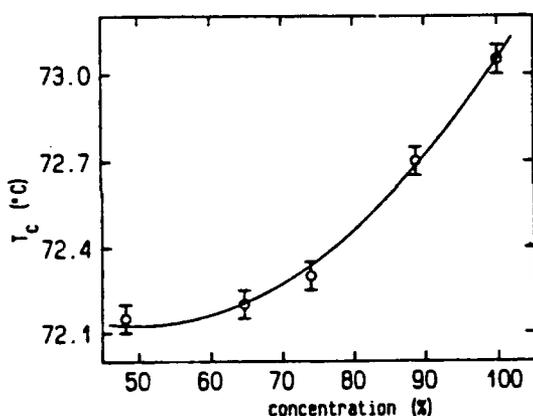
FIGURE 1

The shift of the Sm A → Sm C* phase transition temperature with the concentration of L handness. The solid line is a quadratic dependence fitted to the experimental points.

The solid line represents a fitted quadratic T_c (n) dependence, which is valid within the experimental errors.

The relaxation frequency (f_r) of the soft mode has been obtained by fitting the measured θ (f) dependence which has the Lorentzian shape, to the formula (4). In accordance with the formula (5), the f_r (T) dependences for all concentrations obey the Curie-Weiss law (see Figure 2). The f_r (T) lines have nearly the same slope $\frac{\alpha}{2\pi\gamma}$ showing α and γ are concentration independent.

The temperature dependences of the reciprocal value of the low frequency electroclinic coefficient 1/e (T) are in Figure 3. The higher concentration of L the lower slope which is determined from the formula (2a) as $\frac{\alpha}{\epsilon_0 \chi_\perp C}$.
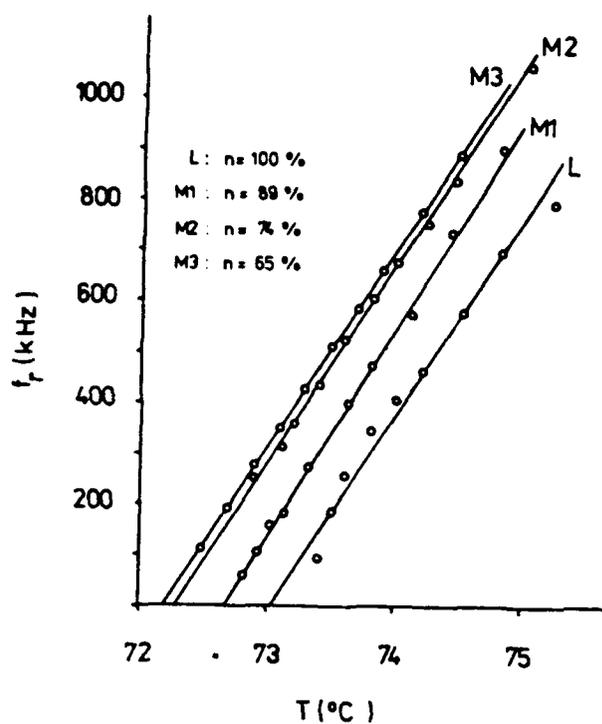
FIGURE 2

Temperature dependences
of relaxation frequencies
of the soft mode for de-
noted concentration of L
handness.
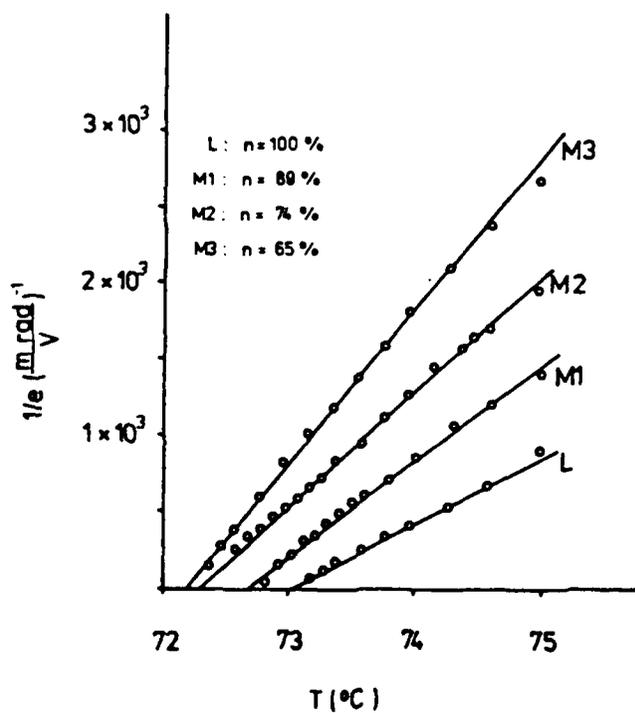
FIGURE 3

Temperature dependences
of reciprocal values of
electroclinic coeffi-
cients.

In Figure 4 the permittivity ε_{tot} is plotted versus e. The points
correspond to different temperatures. The slopes of the lines represent
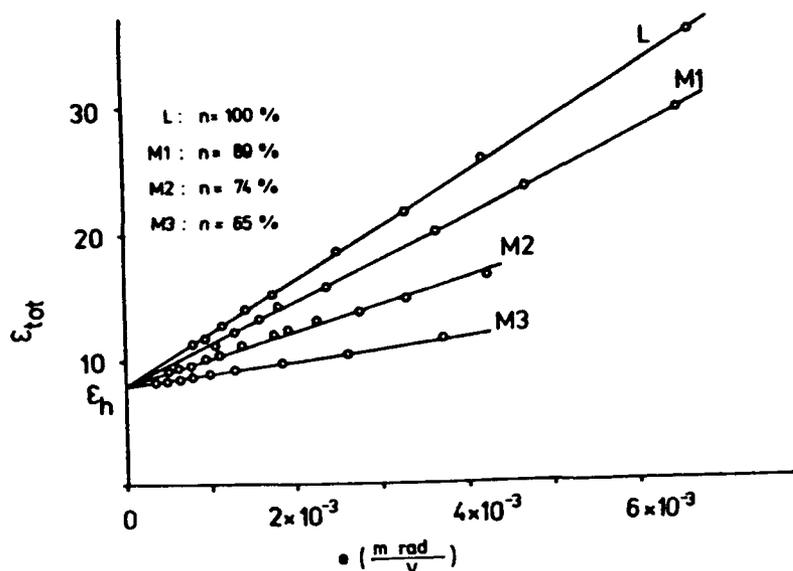
FIGURE 4   The measured permittivity versus electroclinic
coefficient. The temperature is increasing from
the right to the left, $\varepsilon_h = 1 + \chi_\infty + \chi_\perp$.

$\varepsilon_o \chi_\perp C$ values for respective mixture (cf. relations 2a, b). The extrapola-
ted non-zero value of ε_{tot} at e = 0 represents (see eq. 6)

$$\varepsilon_h = 1 + \chi_\infty + \chi_\perp.$$

The soft mode dielectric susceptibility is $\chi_{ec} = \varepsilon_{tot} - \varepsilon_h$. The temperature
dependence of $1/\chi_{ec}$, for different concentrations, is shown in Figure 5.
For all mixtures the dependences have the form of the Curie-Weiss law as
expected from the free energy (see eq. 2b).

QUANTITATIVE RESULTS AND CONCLUSIONS

In the studied temperature interval (2K) above T_c the temperature depen-
dence of quantities characterizing the soft mode; $1/\chi_{ec}(T)$, $1/e(T)$, $f_r(T)$
obey the Curie-Weiss law. It confirms for the studied system, the simple
linear description given by the expressions (2a, b) and (5). From slopes
of those dependences and from $\varepsilon(e)$ the coefficients in the free energy
(1), α, $\chi_\perp$, C and the viscosity of the soft mode γ are calculated. The
results are gathered in Table 1 for all studied mixtures.

The value $\chi_\perp$ has been determined from the measured value $\varepsilon_h =$
$1 + \chi_\infty + \chi_\perp = 8$ (see Figure 4) taking $\chi_\infty = 2$, which contains high fre-
quency molecular librations and electron polarization. The quantities

L   n = 100 %
M1 n = 89 %
M2 n = 74 %
M3 n = 65 %

1.0

0.8

0.6

$1/x_{ec}$

0.4

0.2

M3

M2

M1

L

72   73   74   75

T (°C)
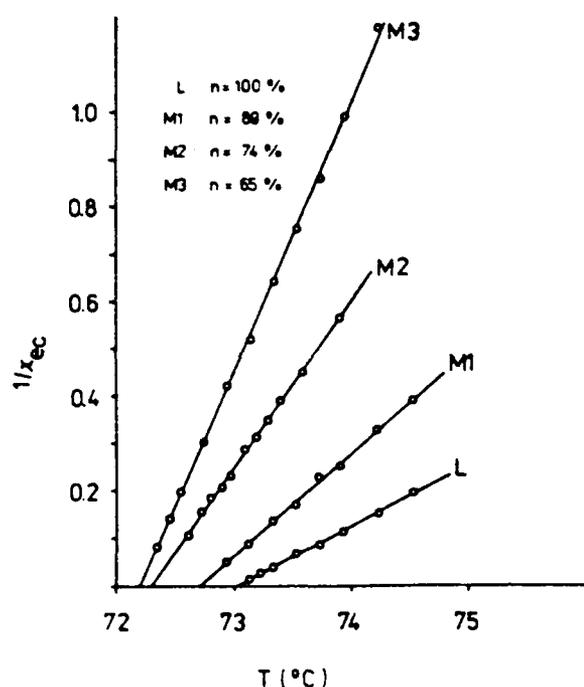
FIGURE 5

Temperature dependences of reciprocal values of dielectric susceptibility

TABLE I   First coefficients in the free energy for the studied system: L: n = 100 %, M1: n = 89 %, M2: n = 74 %, M3: n = 65 % of L variety. For any mixture the shown values are an average of values obtained from measurements on two different samples, $\bar{\alpha}$ is an average from all mixtures

mixture	L	M1	M2	M3
$\varepsilon_0 X_\perp C$ $(C\ m^{-2}rad^{-1})$	3.1×10^{-3}	2.5×10^{-3}	1.7×10^{-3}	1.1×10^{-3}
C $(V\ m^{-1}\ rad^{-1})$	7.1×10^{7}	5.7×10^{7}	3.8×10^{7}	2.3×10^{7}
α $(N\ m^{-2}K\ rad^{-2})$	1.8×10^{5}	1.4×10^{5}	1.1×10^{5}	1.0×10^{5}
$\bar{\alpha}$		1.3×10^{5}		
$X_\perp$		8		
γ (poiseuille)		5.3×10^{-2}		

$\varepsilon_0 X_\perp C$ allow to determine the part of the spontaneous polarization in the Sm C* phase which arises from the linear interaction $CP\Theta$, $P_s(lin) = \varepsilon_0 X_\perp C\Theta_s$, where Θ_s is the spontaneous tilt angle. An experimental study (which will be published in details elsewhere) shows that calculated $P_s(lin)$ is comparable to the measured spontaneous polarization for all

studied concentrations.

The values α/γ determined from $f_r(T)$ are found independent on chirality within the precision of ± 4 %. From this result one can infere both α and γ are chirality independent. On the other hand α caluclated from $1/e(T)$ exhibits a scatter of ± 30 % when comparing measurements with all mixtures (see Table 1). It is due to the rather high scatter of e measurements on different samples. Using the mean value of $\bar{\alpha} = 1.34 \times 10^{c}$, the viscosity of the soft mode is determined (see Table 1).

In Figure 6 the concentration dependence of C coefficient is shown.
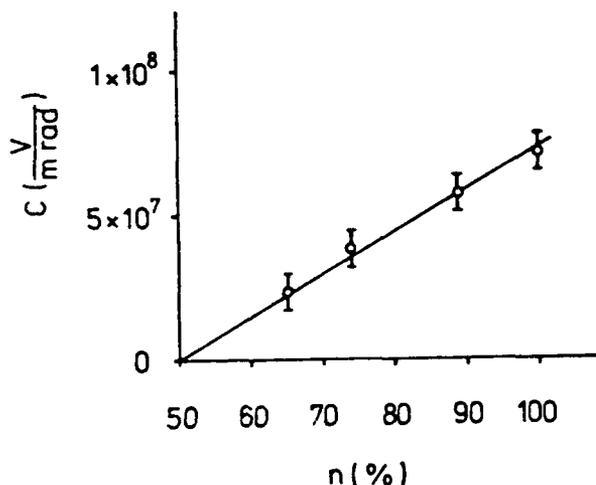
FIGURE 6

Concentration dependence of coupling constant between polarization and tilt angle.

Within the range of experimental errors, it can be approximated by a line which starts at the point $C = 0$, $n = 50$ % (racemic mixture), $C = 14.6 \times 10^{5}(n-50)$. This result, namely $C \sim n$, is in a qualitative accordance with the experimentally found shift of T_c with concentration $\Delta T_c \sim n^2$ (see Fig. 1 and eq. 2c). Using the experimental values for L substance the difference in T_c between L and racemic substances is calculated $T_c(L) = \frac{\varepsilon_o \chi_\perp C^2}{\alpha} = 1.3$ K. This value is higher compared to the measured shift $\Delta T_c(L) = 0.9$ K (see Fig. 1), but it is still within the precision limits when taking into account the accuracy of $\varepsilon_o \chi_\perp C$ and α.

It can be concluded that the induced effects above the Sm A → Sm C* phase transition of the studied system can be described by a simple free energy taking into account only the second order terms in P and Θ and the bilinear interaction CPΘ. The respective coefficients in the free energy are determined. It was found that the chirality influences only the C coefficient of the interaction. The dielectric susceptibility, electroclinic coefficient and T_c decrease when the chirality is lowered.

The shift of T_c calculated from the free energy is in a quantitative agreement (within the precision limits) with the measured ΔT_c.

REFERENCES

1. R. B. Meyer, L. Liébert, L. Strzelecki, and P. Keller, J. de Phys., Lett., 36, 69 (1975).
2. W. Kuczyński and H. Stegemeyer, Chem. Phys. Letters, 70, 123 (1980).
3. J. Pavel, M. Glogarová, D. Demus, A. Mädicke, and G. Pelzl, Cryst. Res. and Technol., 18, 915 (1983).
4. M. Glogarová, J. Pavel, S.S. Bawa, D. Demus, S. Diele, and G. Pelzl, Liquid Crystals, 3, 353 (1988).
5. Ch. Bahr and G. Hepke, Phys. Rev.Lett., 65, 3297 (1990).
6. M. Glogarová, Mol. Cryst. Liq. Cryst., 191, 71 (1990).
7. Ch. Bahr, Glenn Brown award lecture, 13th I.L.C.C. Vancouver (1990).
8. S. A. Pikin and V. L. Indenbom, Uspekhi Fiz. Nauk, 125, 251 (1978).
9. J. Pavel and M. Glogarová, Liquid Crystals, 9, 87 (1991).
10. L. Dupont, M. Glogarová, J. P. Marcerou, H. T. Nguyen, C. Destrade, and L. Lejček, J. de Physique, in press.

TILT ANGLE BEHAVIOR OF SMECTIC C PHASE

MITSUHIRO KODEN and TOHKO ANABUKI[1]
Central Research Laboratories, Sharp Corporation,
2613-1, Ichinomoto, Tenri, Nara 632, Japan

Abstract   The tilt angle behavior of the smectic C phase of single compounds and binary mixtures which were doped with 1wt% of a chiral dopant was investigated by using surface-stabilized ferroelectric liquid crystal cells.   The effect of the molecular structure of single compounds on the tilt angle was investigated. The effect of the mixing of two compounds with different molecular structures on the tilt angle was investigated.   It was found that the tilt angles correlated to the ratio of the S_c-S_A transition temperature to the S_A-N(or I) transition temperature.

INTRODUCTION

Recently, much effort has been devoted to investigations of ferroelectric liquid crystal (FLC), which was originally predicted and demonstrated by Meyer,[2] due to their scientific interest and their great possibility of application in electro-optic devices.[3]   While all tilted chiral smectic phases show ferroelectricity, the chiral smectic C phase has been studied mainly because of their low viscosity and fast response time.   The important properties of FLC materials determining device characteristics are phase sequence, phase transition temperatures, spontaneous polarization, tilt angle, viscosity, helical sense, helical pitch, dielectric anisotropy, etc. Since the spontaneous polarization influences the response time which is closely related to the scanning line of XY-matrix FLC devices, many studies on the spontaneous polarization have been reported.   On the other hand, there has been rather few studies investigating the tilt angle behavior, though the tilt angle is also important parameter describing the molecular orientations of the smectic C phase and influencing the characteristics of FLC devices.

Some rules are known about the tilt angle behavior.   First, the temperature dependence of the tilt angle is said to be represented by

$\theta = \theta_0 (T_{C \cdot A} - T)^\beta$, where $T_{C \cdot A}$ is the S_C-S_A transition temperature.[4] Second, the tilt angle is known to influence the spontaneous polarization and the response time.[5]   Third, the tilt angle of the smectic C phase is said to be related to the phase sequence of a material; the tilt angle tends to be small when a material shows INAC (Isotropic - Nematic - Smectic A - Smectic C) or IAC phase sequence, but it tends to be large when a material shows INC phase sequence.[6]

In this study, we measured the tilt angle behavior of single compounds and binary mixtures by using surface-stabilized FLC cells. The effect of the molecular structure on the tilt angle and the effect of the mixing of two compounds on the tilt angle were investigated. In addition, we were interested in the quantitative relationship between the tilt angle and the ratio of the S_C-S_A transition temperature to the S_A-N or S_A-I transition temperature $(T_{C \cdot A} / T_{A \cdot N, I})$.

EXPERIMENTAL

The molecular structures of compounds in this study were summarized in Tables I ~ VII.   Binary mixtures in this study were prepared by mixing

TABLE I . Molecular structures of compounds 1.

R—⟨=N⟩—⟨⟩—OR'
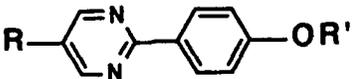
No.	R	R'
1a	$C_7H_{15}-$	$-C_9H_{19}$
1b	$C_8H_{17}-$	$-C_6H_{13}$
1c	$C_8H_{17}-$	$-C_8H_{17}$
1d	$C_8H_{17}-$	$-C_{10}H_{21}$
1e	$C_9H_{19}-$	$-C_6H_{13}$
1f	$C_9H_{19}-$	$-C_7H_{15}$
1g	$C_9H_{19}-$	$-C_8H_{17}$
1h	$C_9H_{19}-$	$-C_9H_{19}$

TABLE II . Molecular structures of compounds 2.

C_8H_{17}—⟨⟩—⟨=N⟩—⟨⟩—OR
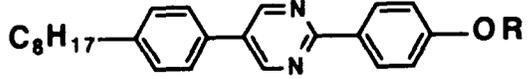
No.	R	Absolute configuration
2a	$-C_5H_{11}$	–
2b	$-CH_2-CH(CH_3)-C_2H_5$	S
2c	$-CO-CH(CH_3)-C_2H_5$	S

TABLE III. Molecular structures of compounds 3.

$$RO-\!\!\bigcirc\!\!-COO-\!\!\bigcirc\!\!-OR'$$

No.	R	R'	Absolute configuration
3a	$C_8H_{17}-$	$-C_6H_{13}$	–
3b	$C_8H_{17}-$	$-C_7H_{15}$	–
3c	$C_8H_{17}-$	$-C_8H_{17}$	–
3d	$C_8H_{17}-$	$-CH_2-CH(CH_3)-C_2H_5$	racemic mixture

TABLE IV. Molecular structures of compounds 4.

$$R-\!\!\bigcirc\!\!-COO-\!\!\bigcirc\!\!-\!\!\bigcirc\!\!-OR'$$

No.	R	R'
4a	$C_9H_{19}-$	$-C_8H_{17}$
4b	$C_6H_{13}O-$	$-C_8H_{17}$
4c	$C_8H_{17}O-$	$-C_8H_{17}$

TABLE V. Molecular structures of compounds 5.

$$RO-\!\!\bigcirc\!\!-\!\!\bigcirc\!\!-COO-\!\!\bigcirc\!\!-OR'$$

No.	R	R'	Absolute configuration
5a	$C_7H_{15}-$	$-CH_2-CH(CH_3)-C_2H_5$	S
5b	$C_8H_{17}-$	$-C_4H_9$	–
5c	$C_8H_{17}-$	$-C_6H_{13}$	–
5d	$C_8H_{17}-$	$-C_8H_{17}$	–
5e	$C_8H_{17}-$	$-CH_2-CH(CH_3)-C_2H_5$	S
5f	$C_{10}H_{21}-$	$-CH_2-CH(CH_3)-C_2H_5$	racemic mixture
5g	$C_{10}H_{21}-$	$-CH(CH_3)-C_6H_{13}$	racemic mixture
5h	$C_2H_5-CH(CH_3)-(CH_2)_5-$	$-C_{12}H_{25}$	S

TABLE VI. Molecular structures of compounds 6.

No.	R	R'	Absolute configuration
6a	$C_7H_{15}-$	$-CH_2-CH(CH_3)-C_2H_5$	S
6b	$C_8H_{17}-$	$-CH_2-CH(CH_3)-C_2H_5$	S
6c	$C_8H_{17}-$	$-CH_2-CH(C_2H_5)-C_4H_9$	racemic mixture

TABLE VII. Molecular structures of compounds 7.
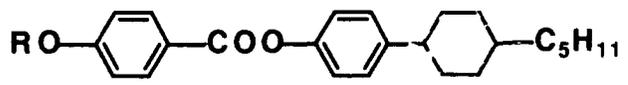
No.	R
7a	$C_8H_{17}-$
7b	$C_{10}H_{21}-$

TABLE VIII. Molecular structures of compounds 8 and 9.

No.	Structure
8	
9	(2S,4S)
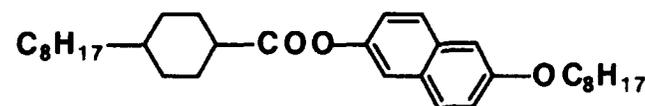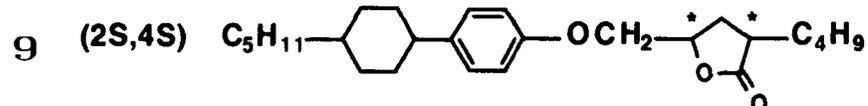
these compounds.   All the compounds and binary mixtures were rendered ferroelectric by doping of 1wt% of a chiral compound 9.[7]

The FLC cells were constructed with two glass plates coated with an indium-tin-oxide (ITO) electrode and a rubbed polyimide film.   The two glass plates were separated by 2µm.   The rubbing direction on the two glass surfaces was parallel.   After the cell was filled with the

mixture, it was thermostatted on a Mettler hot stage and set under an Olympus polarizing microscope.   The cell was heated to the isotropic phase and then cooled at a rate of about 5K/min.

Square wave voltage was applied to the cell at each temperature. Rotating the stage of the polarizing microscope, two extinction positions were determined in both sides of the layer normal.   The angles between the two extinction positions were measured, changing the magnitude of voltage (V=±10~50V).   Half the maximum value of the measured angles was defined to be the tilt angle at each temperature.

RESULTS AND DISCUSSION

The transition temperatures and the tilt angles at $T_{c-A}-20K$ for compounds 1~8, which were doped with 1wt% of chiral compound 9, are summarized in Table IX.   The compositions, transition temperatures
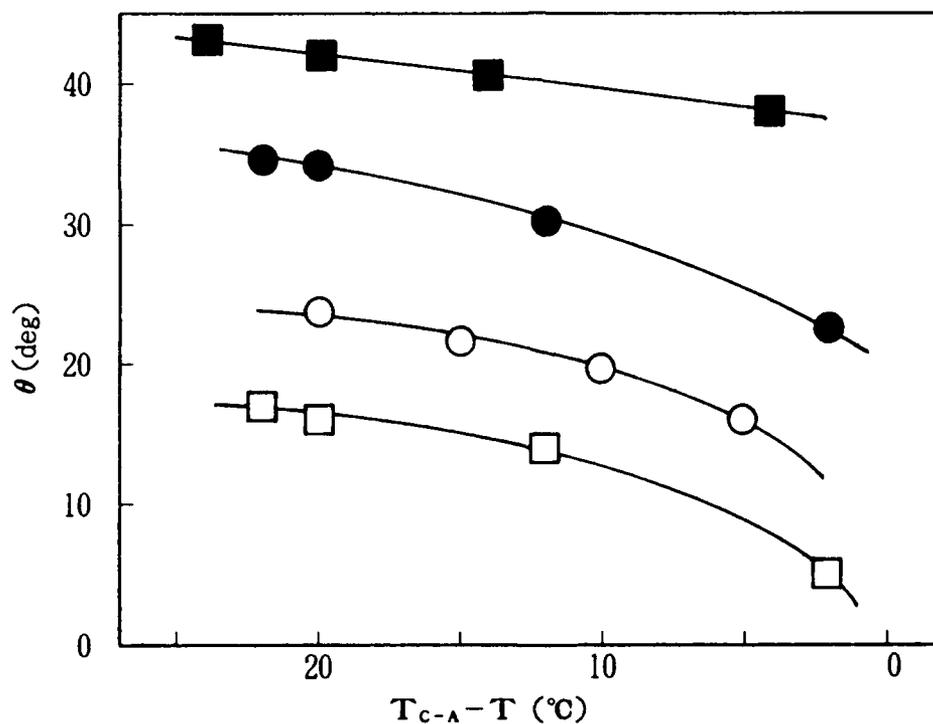
FIGURE 1. Temperature dependence of the tilt angles of Compounds 3c(●), 3d(○), 4c(■), and 5d(□).

TABLE IX. The transition temperatures and the tilt angle at T_{C-A}-20K for compounds $1 \sim 8$ doped with 1wt% of compound 9.

Compound	Transition temperature (°C)				θ at T_{C-A}-20K
	S_C	S_A	N	I	(deg)
1a	• 51	• 58	• 70	•	21.5
1b	• 40	• 60	• 64	•	17.0
1c	• 57	• 65	• 70	•	22.0
1d	• 61	• 67	• 71	•	23.0
1e	• 48	• 71	• 72	•	13.5
1f	• 50	• 74	–	•	13.0
1g	• 60	• 75	–	•	17.5
1h	• 59	• 74	–	•	18.0
2a	• 156	• 185	–	•	22.0
2b	• 139	• 168	–	•	26.5
2c	• 157	• 174	–	•	28.0
3a	• 65	–	• 89	•	31.0
3b	• 69	–	• 87	•	29.5
3c	• 72	–	• 90	•	34.0
3d	• 45	• 61	–	•	23.5
4a	• 151	–	• 170	•	44.5
4b	• 147	• 148	• 197	•	44.5
4c	• 159	–	• 189	•	42.0
5a	• 136	• 189	–	•	13.0
5b	• 145	• 205	• 214	•	11.5
5c	• 162	• 201	• 204	•	16.5
5d	• 162	• 199	–	•	16.0
5e	• 145	• 186	–	•	22.0
5f	• 139	• 182	–	•	20.5
5g	• 116	• 142	–	•	22.5
5h	• 164	• 172	–	•	32.5
6a	• 130	• 189	–	•	19.5
6b	• 138	• 187	–	•	21.5
6c	• 120	• 148	–	•	24.0
7a	• 94	–	• 176	•	33.0
7b	• 115	• 116	• 167	•	24.5
8	• 46	• 108	–	•	16.0

TABLE X. The transition temperatures and the tilt angle at $T_{C-A}-20K$ for binary mixtures doped with 1wt% of compound 9.

Component		Mole%	Transition temperature (°C)							θ at $T_{C-A}-20K$
A	B	of B	S_C		S_A		N		I	(deg)
1c	6c	74	•	96	•	129	–		•	19.5
2a	5a	50	•	128	•	178	–		•	14.5
2a	6a	50	•	106	•	186	–		•	11.0
2a	6c	8	•	138	•	185	–		•	16.0
2a	6c	16	–		•	180	–		•	
2a	6c	34	–		•	174	–		•	
2a	6c	54	•	88	•	165	–		•	5.0
2a	6c	64	•	110	•	165	–		•	15.0
2a	6c	76	•	112	•	158	–		•	16.5
5a	5e	49	•	141	•	187	–		•	22.5
5a	6a	50	•	120	•	192	–		•	17.0
5a	6c	49	•	112	•	174	–		•	16.5
5a	7b	50	•	93	•	158	•	172	•	12.5
5e	6b	10	•	138	•	189	–		•	20.0
5e	6b	19	•	129	•	189	–		•	18.0
5e	6b	39	•	126	•	190	–		•	17.0
5e	6b	59	•	129	•	189	–		•	18.0
5e	6b	79	•	132	•	188	–		•	19.0
5e	6b	90	•	137	•	188	–		•	20.5
5e	6c	18	•	128	•	185	–		•	16.5
5e	6c	36	•	121	•	179	–		•	13.0
5e	6c	57	•	121	•	171	–		•	16.5
5e	6c	67	•	119	•	167	–		•	19.0
5e	6c	77	•	117	•	164	–		•	22.5
5e	6c	89	•	119	•	155	–		•	23.0
5e	7b	19	•	116	•	180	–		•	14.5
5e	7b	39	•	97	•	168	•	169	•	13.0
5e	7b	59	•	99	•	155	•	170	•	10.5
5e	7b	79	•	111	•	143	•	168	•	20.5
6a	6c	19	•	125	•	182	–		•	18.5
6a	6c	37	•	124	•	174	–		•	17.5
6a	6c	57	•	121	•	165	–		•	20.5
6a	6c	77	•	120	•	157	–		•	22.0
6c	7b	21	•	99	•	154	–		•	17.5
6c	7b	43	–		•	155	–		•	
6c	7b	62	–		•	156	•	158	•	
6c	7b	81	–		•	149	•	162	•	

and the tilt angles at $T_{C A}$-20K for the binary mixtures, which were also doped with 1wt% of chiral compound **9**, are summarized in Table **X** .   The tilt angle of some binary mixtures could not be measured because of disappearance of the smectic C phase.

All the compounds and the binary mixtures showed normal temperature dependence of the tilt angle.   Some examples are shown in Figure 1.   Compounds **3c** and **4c**, which showed a INC phase sequence showed the large tilt angle and the gentle temperature dependence. On the other hand, compounds **3d** and **5d**, which showed a IAC phase
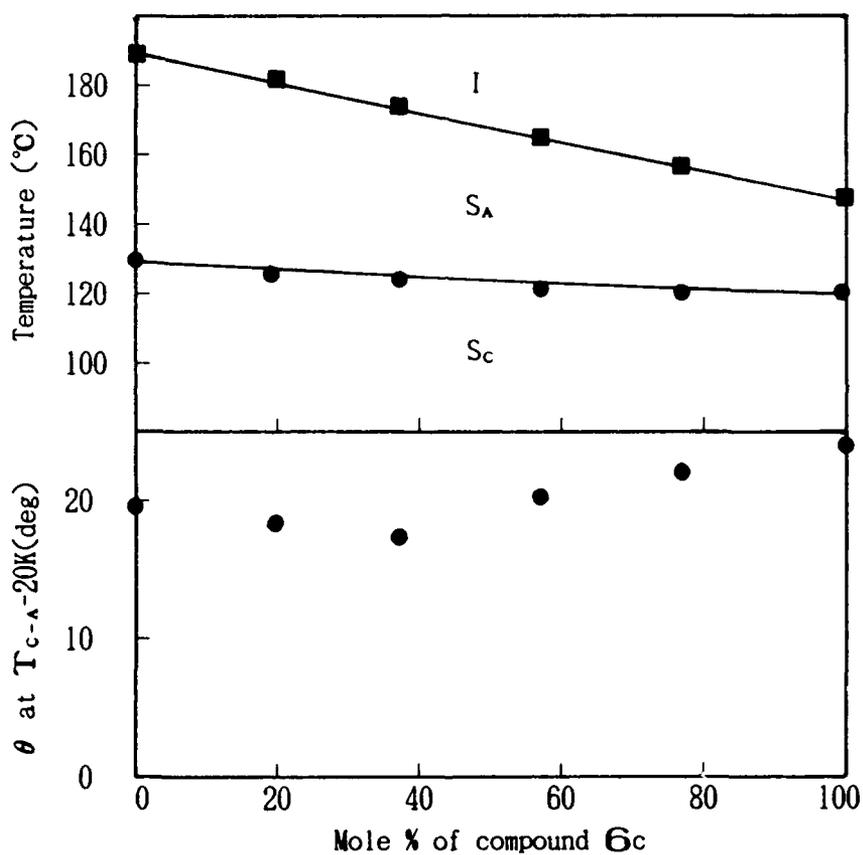
FIGURE 2. Plots of the tilt angle at $T_{C A}$-20K and the transition temperatures versus the composition of the binary mixture of compounds **6**a and **6**c.   ● ;$T_{C A}$, ■ ;$T_{A I}$

sequence, showed the small tilt angle and the rapid temperature
dependence (Figure 1).   The relationship between the phase sequence
and the tilt angle is also confirmed in a comparison between compounds
7a and 7b.

The data in Table IX indicate some information about the
relationship between the tilt angle and the molecular structure.   For
example, comparing compounds 3c, 4c, and 5d, all of which are
phenyl benzoate derivatives, the order of the tilt angles is
4c > 3c > 5d.   This implies that the location of the ester group
plays an important role to the value of the tilt angle.

Some examples of the phase diagrams and the tilt angle behavior
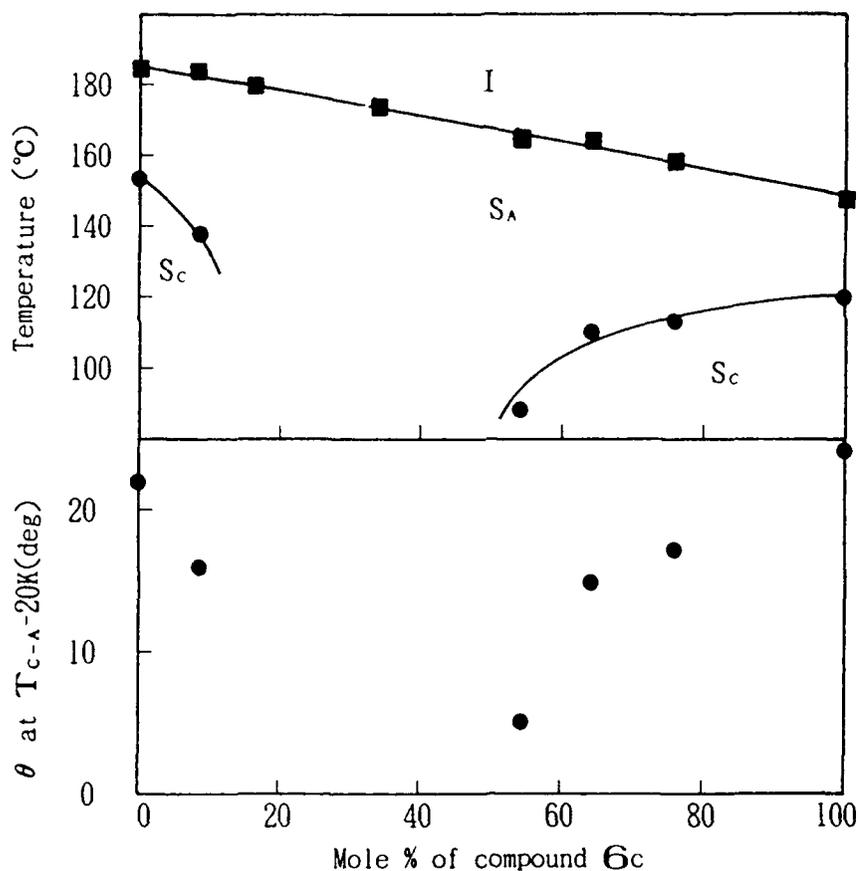
FIGURE 3. Plots of the tilt angle at $T_{C-A}-20K$ and the
transition temperatures versus the composition of the binary
mixture of compounds 2a and 6c.   ● ;T_{C-A}, ■ ;T_{A-I}

for the binary mixtures are shown in Figures 2 and 3. For the
mixtures shown in Figure 2, the S_C-S_A and S_A-I transition temperatures
showed almost ideal linear lines and the tilt angle showed a slightly
deviated line. This is attributed to the small difference in the
molecular structure between the two components (6a and 6c). In
contrast, Figure 3 showed the rapid depression of the S_C-S_A transition
temperatures and the tilt angles and the disappearance of the smectic
C phase. This is attributed to the large difference in the molecular
structure between the two components (2a and 6c).

Figure 4 shows the plots of the tilt angles versus the ratio of
the S_C-S_A transition temperature to the S_A-N or S_A-I transition
temperature ($T_{C-A}/T_{A-N,I}$) for all the single compounds and the
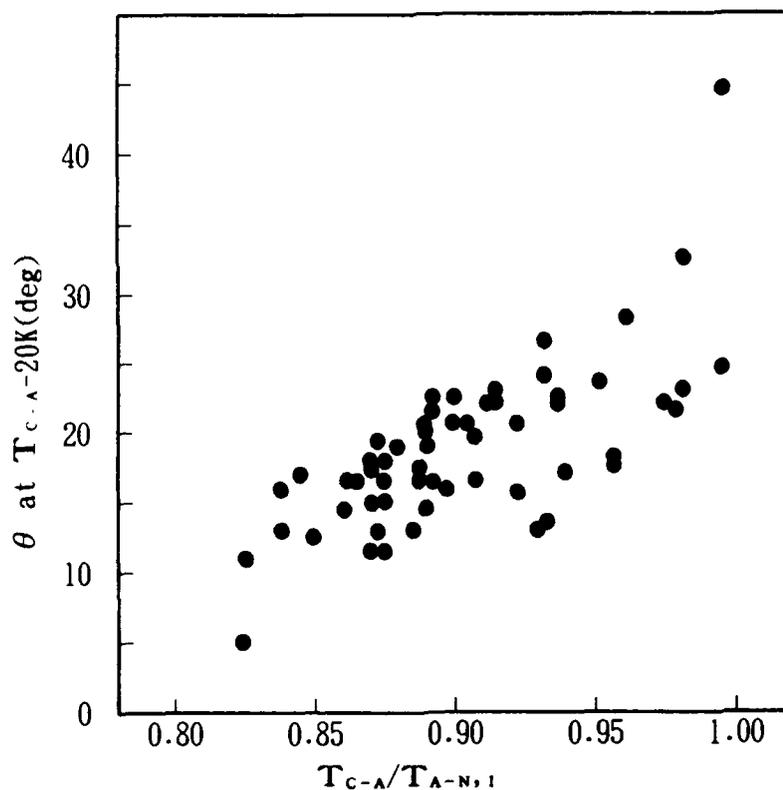
FIGURE 4. Plots of the tilt angle at T_{C-A}-20K versus
$T_{C-A}/T_{A-N,I}$ for single compounds and binary mixtures in this
study.

binary mixtures in this study.   It is interesting that the tilt angles and the phase transition temperatures of several kinds of compounds and several kinds of binary mixtures are represented by one relationship.

Figure 5 shows the plots of the tilt angles versus $T_{C-A}/T_{A-N,I}$ for compounds 1, 5, and 6.   For each compound, the tilt angles showed a good correlation with the $T_{C-A}/T_{A-N,I}$ due to their same core structure.   The slope for compounds 5 is similar to that for compounds 1.   However, the slope for compounds 6 is smaller than those for compounds 1 and 5.   This might be attributed to the effect of the alkoxycarbonyl group joined to the phenyl ring of compounds 6.

The smectic C phase appears when the molecules in the smectic A phase are forced to tilt with respect to the layers.   The experimental results suggest that the intermolecular interaction forcing the tilting of molecules influences the tilt angle and the relative thermal stability of smectic C phase to the smectic A phase.
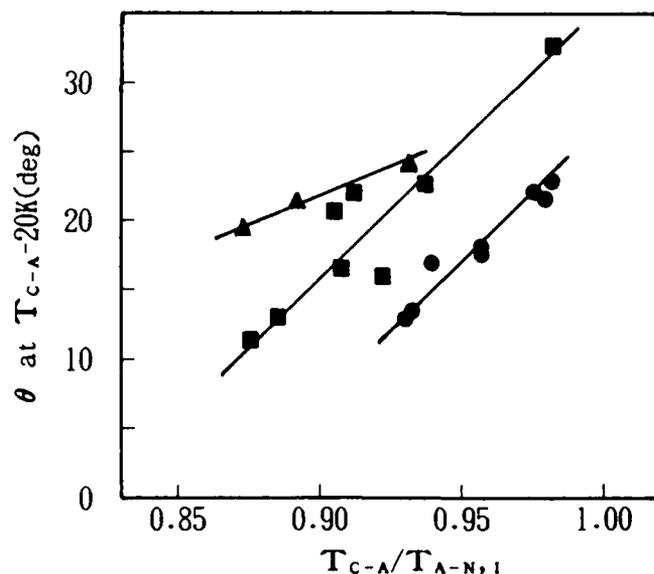
FIGURE 5. Plots of the tilt angle at $T_{C-A}-20K$ versus $T_{C-A}/T_{A-N,I}$ for single compounds 1 (●), 5 (■), and 6 (▲).

CONCLUSION

In this study, the tilt angle of smectic C phase was determined by using FLC cells filled with single compounds and binary mixtures doped with 1wt% of a chiral dopant. It was found that the tilt angles correlated to the ratio of the S_C-S_A transition temperature to the S_A-N or S_A-I transition temperature ($T_{C-A}/T_{A-N,I}$). In particular, the good correlation was obtained for series of compounds which possess the same core structure.

ACKNOWLEDGMENT

REFERENCES

1. On leave from Nagaoka University of Technology, Nagaoka, Niigata 940-21.
2. R. B. Meyer, L. Liebert, L. Strzelecki, and P. Keller, J. Phys. Lett. (Paris), 36, 69 (1975).
3. N. A. Clark and S. T. Lagerwall, Appl. Phys. Lett., 36, 899 (1980).
4. Ph. Martinot-Lagarde, R. Duke, and G. Durand, Mol. Cryst. Liq. Cryst., 75, 249 (1981).
5. G. Durand and Ph. Martinot-Lagarde, Ferroelectrics, 24, 89 (1980).
6. J. S. Patel and J. W. Goodby, Opt. Eng., 26, 37 (1987).
7. K. Sakaguchi and T. Kitamura, Ferroelectrics, 114, 265 (1991); M. Koden, T. Kuratate, F. Funada, K. Awane, K. Sakaguchi, and Y. Shiomi, Mol. Cryst. Liq. Cryst. Lett., 7, 79 (1990).

HIGH PRESSURE STUDIES ON FERROELECTRIC LIQUID CRYSTALS

S.M.KHENED, S.KRISHNA PRASAD, V.N.RAJA
S.CHANDRASEKHAR and B.SHIVKUMAR

Raman Research Institute, Bangalore 560 080, INDIA

Abstract

In contrast to the wealth of data available on ferroelectric liquid crystals at atmospheric pressure, only a few reports of studies at high. pressure exist. We have undertaken systematic high pressure studies of the properties of these materials. In this paper the results of detailed measurements of spontaneous polarisation and transverse static dielectric constant as functions of pressure for two different compounds exhibiting low and high values of polarisation are presented.

Introduction

The promising aspects of ferroelectric liquid crystals as materials for high speed electro-optic devices have initiated a lot of work on the experimental as well as theoretical front. Although the physical properties of these materials have been extensively studied at atmospheric pressure [1] there have been only a few detailed high pressure studies[2-4], and even these have been confined to materials exhibiting very low values of spontaneous polarisation. We report here the effect of pressure on spontaneous polarisation and static transverse dielectric constant in materials exhibiting low as well as high values of spontaneous polarisation.

Experimental

The structural formulas and phase transition temperatures (in $^\circ C$) of the compounds used[5] are given below.

$$C_7H_{15}O-\langle O \rangle-CH=CHCOO-\langle O \rangle-OOCCHCH_2CHCH_3 \quad c7$$

with substituents Cl and CH_3 on the chain, and $*$ marking the chiral centre

Iso 90.5^o A 67.0^o C*

$$C_{11}H_{23}O-\langle O \rangle-CH=CH-COO-\langle O \rangle-COO-CH_2-CH-CH_2-CH-CH_3 \quad I11$$

with substituents Cl and CH_3 on the chain, and $*$ marking the chiral centre
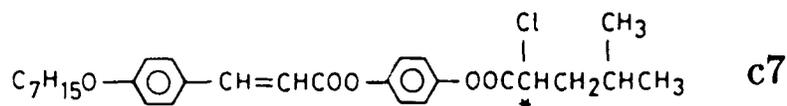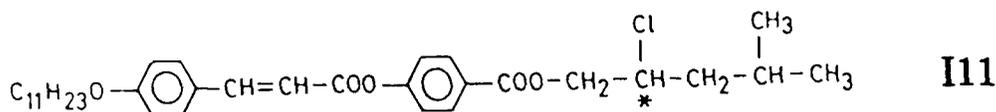
Iso 80.0^o A 64.5^o C*

Phase diagrams

For mapping the phase boundaries, we used the laser optical transmission technique. An optical high pressure cell[6] equipped with sapphire windows was used for these experiments. The liquid crystalline sample was sandwiched between two optically polished sapphire cylinders and enclosed in an elastomer (Fluran) tube. The transmitted light intensity was used to identify the transition.

Spontaneous polarisation and dielectric constant

For these measurements the sapphire rods were replaced by steel cylinders which acted as electrodes. Care was taken to see that the sample assembly was elec-

trically isolated from the rest of the high pressure set up. The surface of the steel cylinders coming into contact with the sample were coated with a polymer solution and rubbed unidirectionally to get planar orientation of the molecules. The data presented here were obtained from three independent sets of measurement, a fresh sample being loaded in the high pressure cell each time. The good reproducibility of the data showed that the alignment of the sample was very good. Screws threaded into the steel rods established the contact between sample and the measuring set up. The sample temperature was monitored using a chromel- alumel thermocouple mounted in the cell body. The precision in the measurement of temperature is reckoned to be $\pm 10 mK$, while that of pressure is ± 3 bar. The setup used for P_s measurements, which is based on the Dia- mant bridge technique, is described elsewhere[7]. The capacitance measurements were done using a versatile variable frequency Impedance Analyser (HP4192A). The magnitude and frequency of the applied voltage 5V,105Hz) were very low compared to the unwinding field and Goldstone mode relaxation frequency values.[8] The experiments were always conducted isobars i.e.,the measurements were made by keeping the pressure constant and varying the temperature at a uniform rate of $10^{\circ}C/h$.

Results and Discussion

Fig.1 and 2 show the pressure-temperature (P-T) phase diagram for C7 and I11 respectively. It is observed that in both the compounds the temperature range of the smectic A phase increases with increasing pressure although the extent of increase is different for the two compounds(4.8 $^{\circ}C/kbar$ for C7 and 1.7$^{\circ}C/kbar$ for I11). This behavior is in agreement with earlier reports [4] on phase diagrams
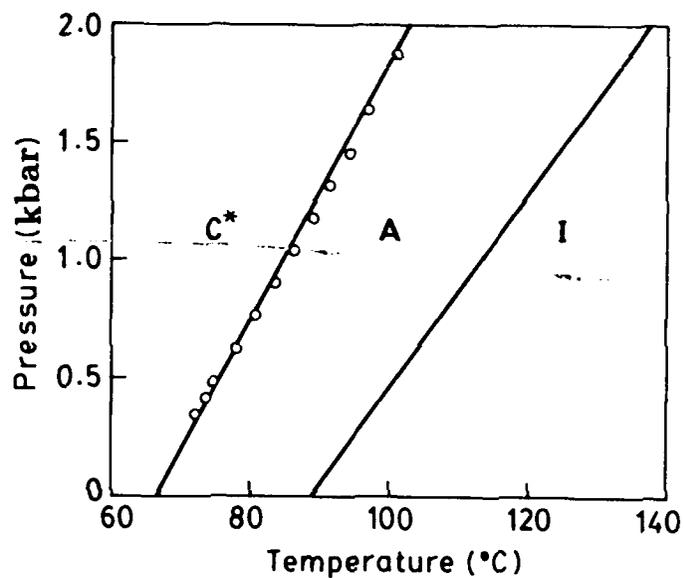
Figure 1: P - T diagram for C7. Solid lines are the fits to the optical transmission data and the circles, the values from polarisation measurements.
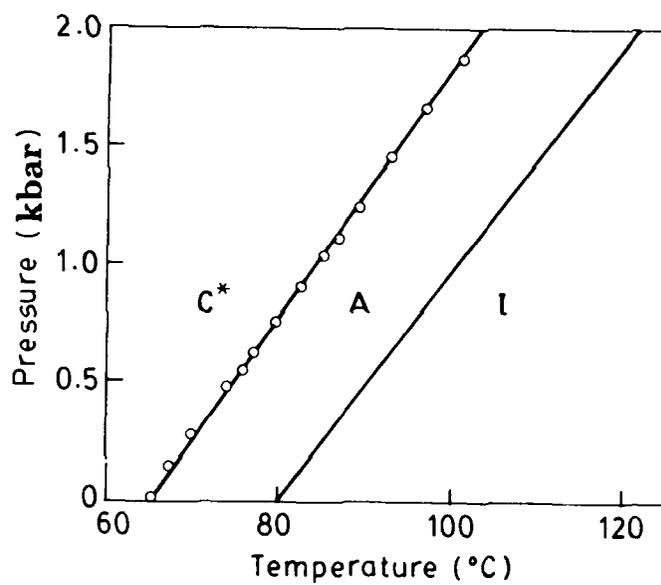
Figure 2: P - T diagram for I11. (See legend of Fig.1.)

of ferroelectric compounds at high pressure. Fig.3 is a plot of D-E hysteresis loops obtained using the Diamant bridge method for C7 at .001 (room pressure), 1 and 2kbar. The following salient features are seen: with increasing pressure,
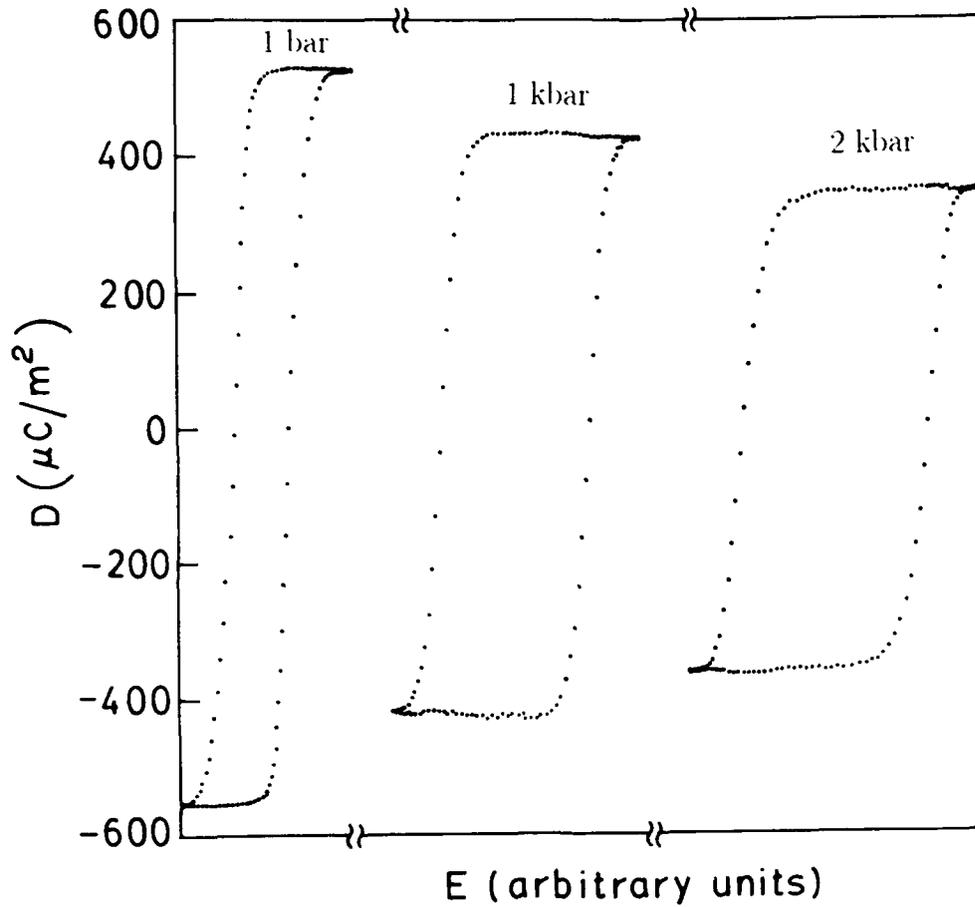
Figure 3: Hysteresis loops obtained for C7 at   a) .001 kbar, b) 1 kbar and c) 2 kbar

(1) the electrical displacement D decreases; (2) the coercive field E_c (obtained from the value of the applied field at the instant D=0) increases; (3) the critical helix unwinding field E_h also increases.
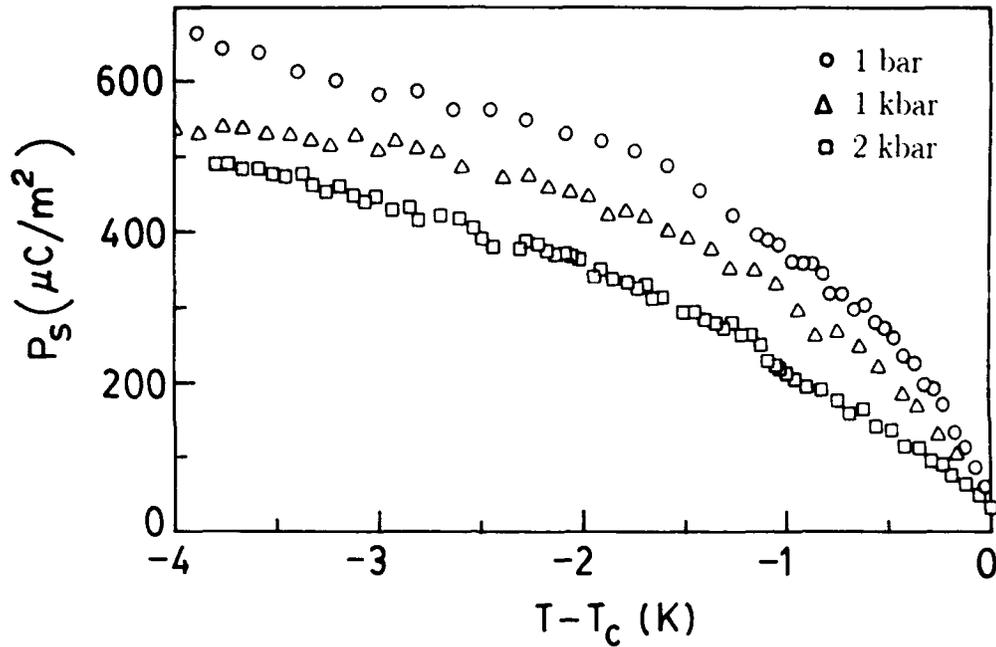
Figure 4: Thermal variation of P_s obtained for C7 at a).001 , b) 1 and c) 2 kbar

Fig.4 shows the temperature variation of P_s at three different pressures for C7 while Figs. 5 and 6 show the pressure varition of P_s at a given relative temperature (T_c-2°C) for C7 and I11 respectively (Here T_c is the A-C* transition temperature at any given pressure). From these three figures it is clear that with increasing pressure 1) the magnitude of P_s decreases and 2) dP_s/dT decreases close to the transition. To quantify this we have fitted the P_s versus temperature data at each pressure to a simple power law expression $P_s = P_o(T_c - T)^\beta$. The β value thus obtained shows a marked increase with increasing pressure; the value is 0.44 for room pressure data and 0.68 for the data obtained at 2kbar.

It is well known that the coupling between P_s and the tilt angle (which is
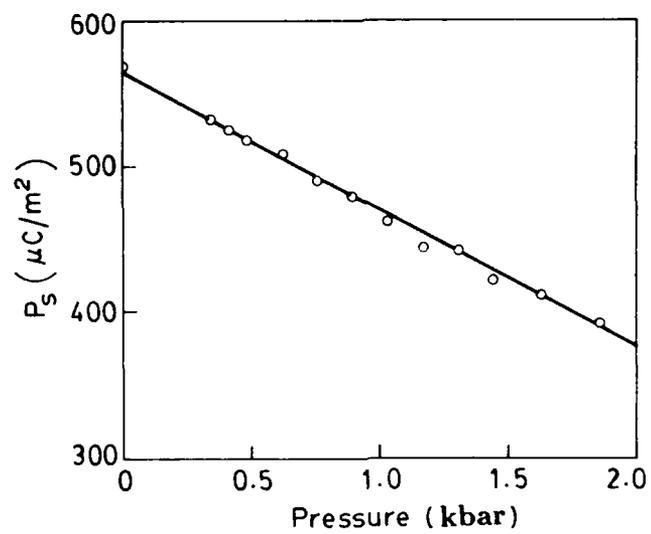
Figure 5: Effect of pressure on P_s for C7
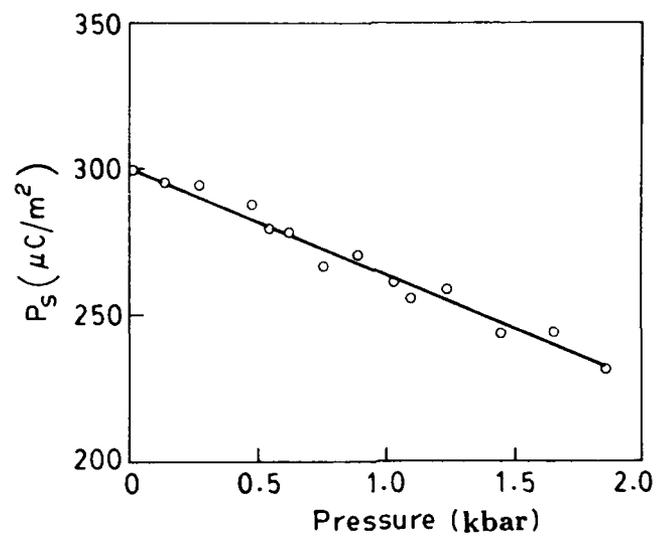
Figure 6: Effect of pressure on P_s for I11

the primary order parameter for this transition) is not purely linear and that bi-quadratic coupling terms play a significant role. If the coupling is purely linear then the value of β should not exceed 0.5, the mean field value for the order parameter exponent.[9] Thus, the present results are indicative of appreciable influence by non-linear coupling terms also. Indeed, it appears that with increasing pressure the relative contribution of the linear term decreases. This is a surprising result since the coefficients of the coupling terms are generally assumed to be characteristic of the material. Another factor which could have brought about a change in β is the mean field - tricritical point (MF-TCP) crossover phenomenon observed generally in compounds exhibiting the A-C transition.[10] All the experiments conducted at room pressure indicate that the nature of such a crossover is governed by the strength of the transverse dipole moment of the constituent molecule[11] and/or the temperature range of the smectic A phase[12]. As Fig.1 shows the temperature range of A phase does increase with increasing pressure. In order to see whether the first factor mentioned above could also be playing a significant role we measured the transverse dielectric constant across the A-C* transition as function of the applied pressure.

Dielectric Constant

Even though the structure and hence the true dipole moment of the molecule remain invariant, the effective dipole moment may vary with increasing pressure. In a first approximation the static dielectric constant can be taken as a measure of this effective dipole moment. Since the P_s data appears to indicate a possible decrease in the effective dipole moment, we have measured the sample capacitance C corresponding to the transverse dielectric constant $\epsilon_\perp$.
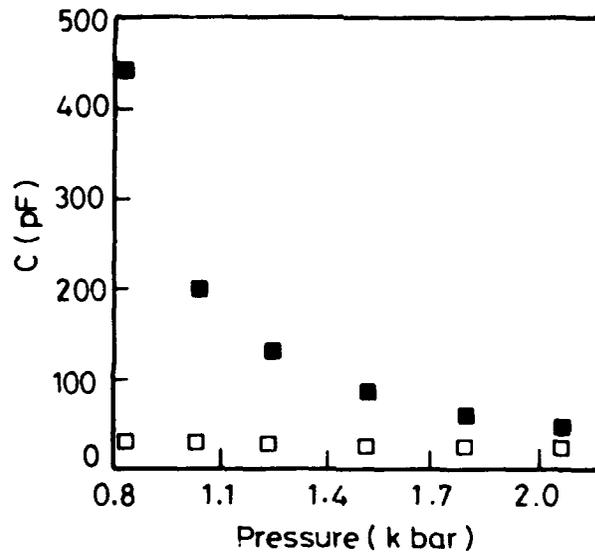
Figure 7: Effect of pressure on the measured sample capacitance of C7 at ■ $(T_c-2)^\circ C$ (C* phase) and □ $(T_c+7)^\circ C$ (A phase)

Fig.7 shows the measured capacitance (C) as a function of pressure in the C* phase at the relative temperature of $(T_c-2)^\circ C$ and in the A phase at $(T_c+7)^\circ C$. It is evident that C in the C* phase is very much more sensitive to pressure than that in the A phase. This is brought out in a more striking fashion in Fig.8, which shows purely ferroelectric part of C in the C* phase. Here the plots represent the measured capacitance in the C* phase after eliminating the non-ferroelectric contribution as well as any other experimental artefacts by subtracting the value in the A phase at $(T_c+7)^\circ C$ where the capacitance is
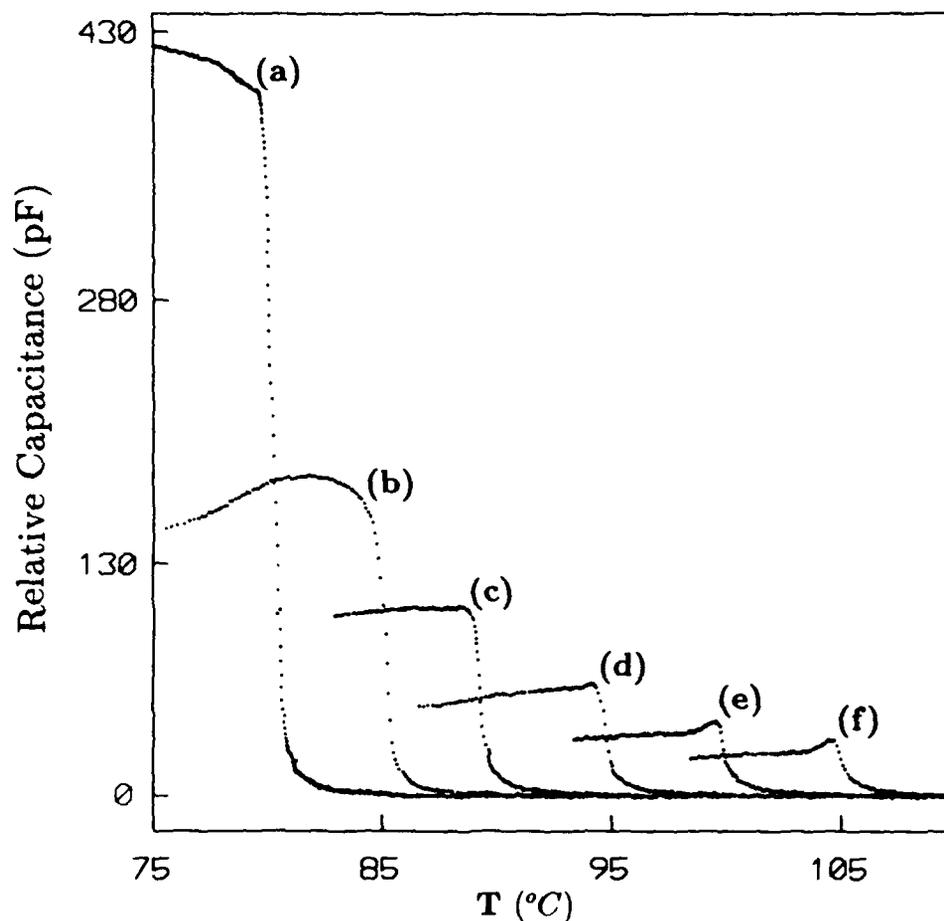
Figure 8: Influence of pressure on the relative sample capacitance of C7 at a) 0.8, b)1.1, c)1.3, d)1.6, e)1.8 and f)2.1 kbar

practically independent of temperature. This figure demonstrates the drastic decrease in C in the C* phase with increasing pressure. Similar features were observed by Yasuda et.al.,[3] in DOBAMBC. One factor that could contribute to this behavior is that the Goldstone mode relaxation frequency f_G decreases with increasing pressure and consequently the response of the system at the measur-

ing frequency can not be considered as static. Preliminary data on rotational viscosity variation with pressure corroborate this view.

Conclusions

We have studied the effect of pressure on spontaneous polarisation and transverse dielectric constant near the A-C* transition. Our results show that

1. the magnitude of P_s as well as its rate of variation with temperature decreases with increasing pressure.

2. the transverse static dielectric constant $\epsilon_\perp$ in the C*phase decreases drastically with increasing pressure.

References

[1] For a recent review see, L.A.Beresnev, L.M.Blinov, M.A.Osipov and S.A.Pikin, *Mol.Cryst.Liq.Cryst.*, **158A**, 1(1988).

[2] D.Guillon, P.E.Cladis, J.Stamatoff, D.Aadsen and W.B.Daniels, *J.Physique Lett.*, **40**, L-459(1979).

[3] N.Yasuda, S.Fujimoto and S.Funado, *J.Phys.* **D18**, 531(1985).

[4] S.Krishna Prasad, B.R.Ratna, R.Shashidhar and V.Surendranath, *Ferroelectrics*, **58**, 101(1984).

[5] B.Shivkumar, B.K.Sadashiva, S.Krishna Prasad and S.M.Khened, *Ferroelectrics*, **114**, 761(1991).

[6] A detailed description of the original setup and its modifications are given in A.N.Kalkura, R.Shashidhar and M.S.Urs, *J.Physique*, **44**, 51(1983); R.Shashidhar, S.Krishna Prasad and S.Chandrasekhar, *Mol.Cryst.Liq.Cryst.*, **103**, 137(1983) ; S.Krishna Prasad, Ph. D Thesis, Univ. of Mysore **1985**.

[7] S.Krishna Prasad, S.M.Khened, S.Chandrasekhar, B.Shivkumar and B.K.Sadashiva, *Mol.Cryst.Liq.Cryst.*, **182B**, 313(1990).

[8] S.Krishna Prasad, S.M.Khened, V.N.Raja and S.Chandrasekhar, Paper presented at the 3rd International Conference on Ferroelectric Liquid Crystals, Boulder 1991.

[9] C.C.Huang, *Mol.Cryst.Liq.Cryst*, **144**, 1(1987).

[10] R.Shashidhar, B.R.Ratna, Geetha G. Nair, S.Krishna Prasad, Ch.Bahr and G.Heppke, *Phys.Rev.Lett.*, **61**, 547(1988).

[11] H.Y.Liu, C.C Huang, T.Min, M.D.Wand, D.M.Walba, N.A.Clark, Ch.Bahr and G.Heppke, *Phys.Rev.***A40**, 6759(1989).

[12] S.Krishna Prasad, V.N.Raja, D.S.Shankar Rao, Geetha G. Nair and M.E.Neubert, *Phys.Rev.***A42**, 2479(1990).

MEASUREMENT OF ROTATIONAL VISCOSITY IN THE *SMECTIC C** PHASE

S.KRISHNA PRASAD, S.M.KHENED, V.N.RAJA and B.SHIVKUMAR

Raman Research Institute, Bangalore 560 080, INDIA

Abstract

Several methods have been employed to determine the rotational viscosity γ_ϕ in the smectic C* phase associated with the molecular motion around the cone about the layer normal. We have measured this parameter using four different techniques and show that the values are in good agreement with each other. We have also studied the effect of chain length on γ_ϕ in the C* phase and γ_s the viscosity associated with tilt angle fluctuations, in the A phase. The results suggest that the activation energy associated with these motions is basically controlled by the rigid core and not by the chain length of the molecule.

Introduction

The rotational viscosity in the Smectic $C^*(C^*)$ phase is an important parameter for understanding the dynamics of ferroelectric electro-optic switching. It is the viscosity associated with the motion of the tilted molecule along the cone of azimuthal angles. Several methods have been developed to measure this parameter[1], but a detailed comparison of the values obtained by the different techniques does not seem to have been made. Moreover, there are hardly any systematic studies of this viscosity as a function of the chain length of the molecule. We present here the measurements of the rotational viscosity for a

homologues series of compounds using various techniques. We also present the results of γ_s, the rotational viscosity associated with tilt angle fluctuations.

Experimental

Experiments have been conducted on six homologs ($n=7$ to 12) of [2S,3S]-4-(2-chloro-4-methylpentanoyloxy)phenyl *trans* -4"-n-alkoxy cinnamate.[2] The structural formula and transition temperatures(C^o) for these compounds (short form Dn) are given below.

$$H_{2n+1}C_nO-\langle O \rangle-\overset{\overset{H}{|}}{C}=\overset{\overset{}{|}}{\underset{\underset{H}{|}}{C}}-\overset{\overset{O}{||}}{C}-O-\langle O \rangle-O-\overset{\overset{O}{||}}{C}-\overset{\overset{*}{\underset{\underset{Cl}{|}}{CH}}}-\overset{\overset{*}{\underset{\underset{CH_3}{|}}{CH}}}-CH_2-CH_3$$
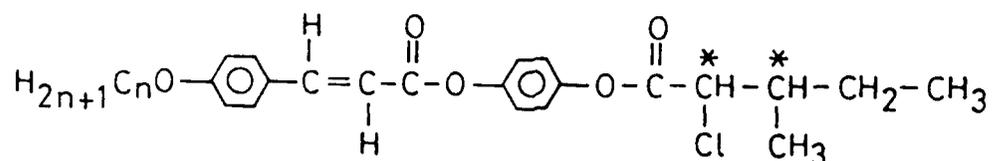
n	K		C^*		A		Ch		I
7	.	61.5	.	68.5	.	88.0	.	95.0	.
8	.	61.0	.	73.0	.	93.0	.	96.5	.
9	.	69.0	.	78.0	.	95.0	.	97.0	.
10	.	56.0	.	80.0	.	98.5	.	99.0	.
11	.	50.0	.	83.5	.	99.5	.	—	.
12	.	56.5	.	84.5	.	100.0	.	—	.

In all the experiments the samples were filled between two ITO coated glass plates treated with a polymer solution for homogeneous alignment. The sample thickness was $\sim 5\mu$m. It is known that pinning of the domain walls prevent complete bulk switching at low field values and consequently introduces an error in the determination of γ_ϕ. With this in mind, in all the experiments we took care to see that the fields employed were always high enough to practically eliminate the pinning effect. At each temperature γ_ϕ values obtained for different fields were fitted to a straight line, the zero intercept of which was taken as the final value for γ_ϕ . (The value of γ_ϕ did not vary by more than 5% over the entire range indicating that in this regime γ_ϕ is almost field independent). We now briefly describe the principles underlying the different methods employed to determine γ_ϕ.

a) Optical response method

A He-Ne laser (Spectra Physics 120S) and a fast response (rise time $\sim$ 10ns) photodiode (Centronics OSI5) were used to get the transient optical response of the sample. Fig. 1 shows a typical response curve for an applied square wave field.

The optical switching time τ is defined here as the measured response time for a full reorientation of the optic axis. (Since we are interested in comparing optical and non-optical methods of obtaining γ_ϕ, we prefer this definition to the usually used rise time definition of τ_{10-90}). γ_ϕ is computed using the simple relation[1]

$$\gamma_\phi = P_s E\tau$$
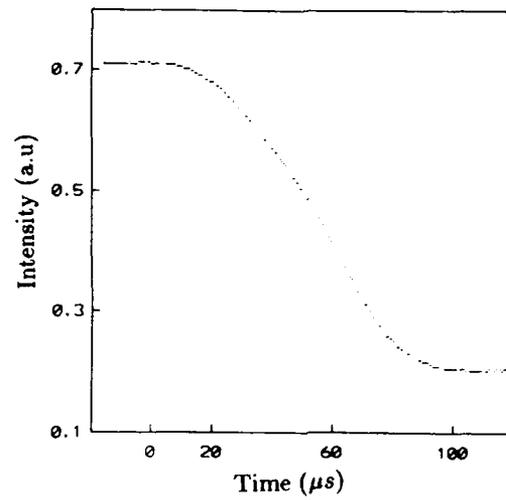
Figure 1: *Optical response to an applied square wave field - experimental curve for D8*
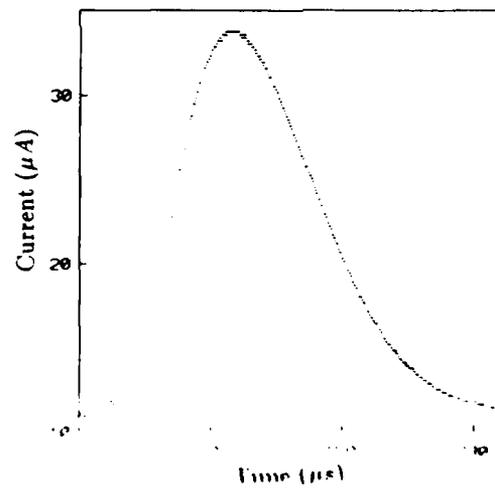
Figure 2: Current response to an applied square wave field - experimental curve for D8

b) Transient current response to an applied square wave field

In this method the transient current generated in the sample due to the application of a square wave field is measured using a current sensor resistor. The value of this resistor was chosen to be small so that it makes a negligible contribution to the RC constant of the sample. Fig. 2 shows a typical response curve.

γ_ϕ is obtained using the expression[3]

$$\gamma_\phi = \frac{P_s E}{k cos \phi}$$

where E is the applied electric field.

The angle ϕ between the P_s vector and the electric field direction is given by

$$\phi = 2 sin^{-1}[(\beta - (\beta^2 - 2\beta + 2)^{1/2})/(2(\beta - 1)]$$

$$k = \frac{1.76275}{\tau}$$

$$\beta = exp(k\tau_s)$$

τ_s is the position of the polarisation current peak with respect to the applied pulse in the time domain and τ its FWHM.

c) Transient current response to an applied triangular wave field

A typical current response curve to an applied triangular wave field is shown in Fig.3.
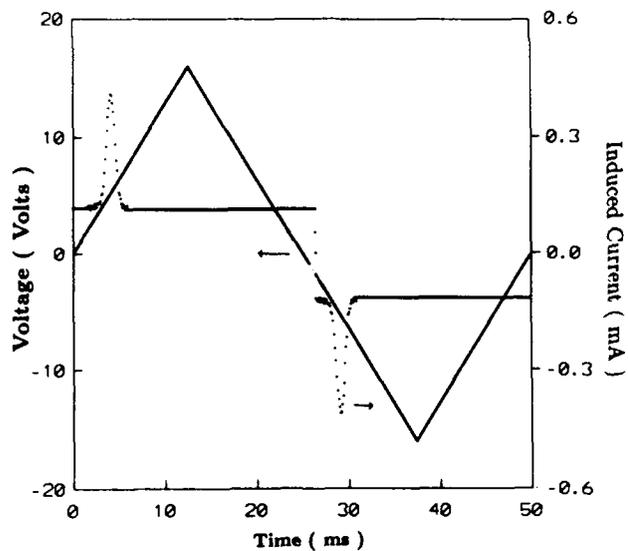
Figure 3: *Current response to an applied triangular wave field - experimental curve for D8*
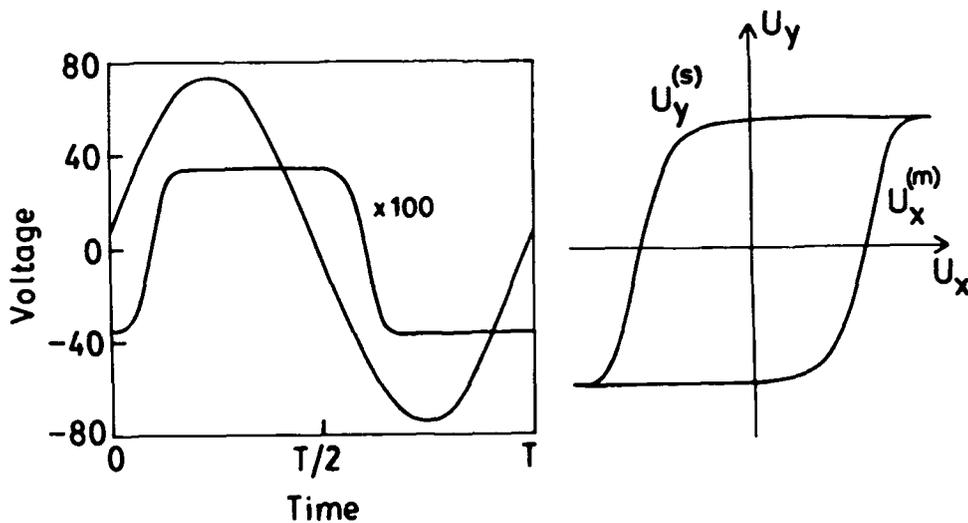
Figure 4: *Current response to an applied sine wave field and the hysteresis loop - experimental curve for D8*

In this method γ_ϕ is calculated using the expression[4]

$$\gamma_\phi = \frac{A P_s^2 E_m}{I_m}$$

d) Transient current response to an applied sine wave field

The convenience of this method[5] lies in the fact that the information is extracted from the usual D-E hysteresis loop. Fig. 4 shows the sample response to an applied sine wave field and also the hysteresis loop.

γ_ϕ is given by the expression

$$\gamma_\phi = \frac{C\, U_y^2\, U_x(m)}{A\, d\, \omega\, (dU_y/dU_x)\, (U_o^2 - U_x^2(m))^{1/2}}$$

C: Capacitance used in the fixed arms of the bridge.

U_y: Output voltage of the sample extrapolated to zero applied field.

$U_x(m)$: Coercive field.

U_o, ω: Amplitude and frequency of the applied field.

A, d: Area and thickness of the sample.

Results and Discussion

Comparison between different techniques

Fig. 5 is an Arrhenius plot of ln γ_ϕ versus 1/T for n=8 homolog using the four methods described above.
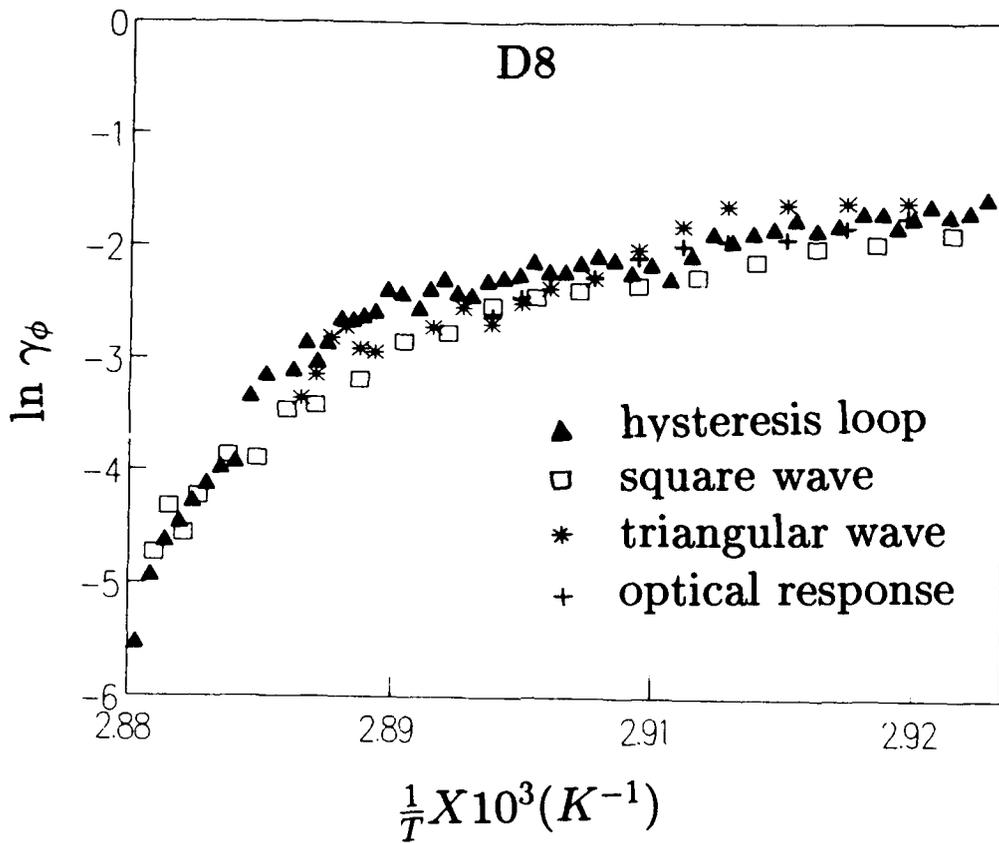
Figure 5: *Comparative plot of ln γ_ϕ versus 1/T for D8 obtained by four techniques discussed in the text*

The salient features seen are

1. There is excellent agreement between the values obtained from the different methods throughout the range of the measurement.

2. Away from the transition the behaviour is arrhenius type but on approaching Tc it is non-arrhenius. A power law type of expression describes the data better than the arrhenius law. However a single exponent does not

seem to describe the data over a wide range of temperature. This is probably due to the mean-field to tricritical cross-over behavior generally observed near the A-C* transition.[6]

Effect of chain length

Fig. 6 is a plot of ln γ_ϕ as a function of $1/T$ for six homologs of this series i.e., n=7 to 12.
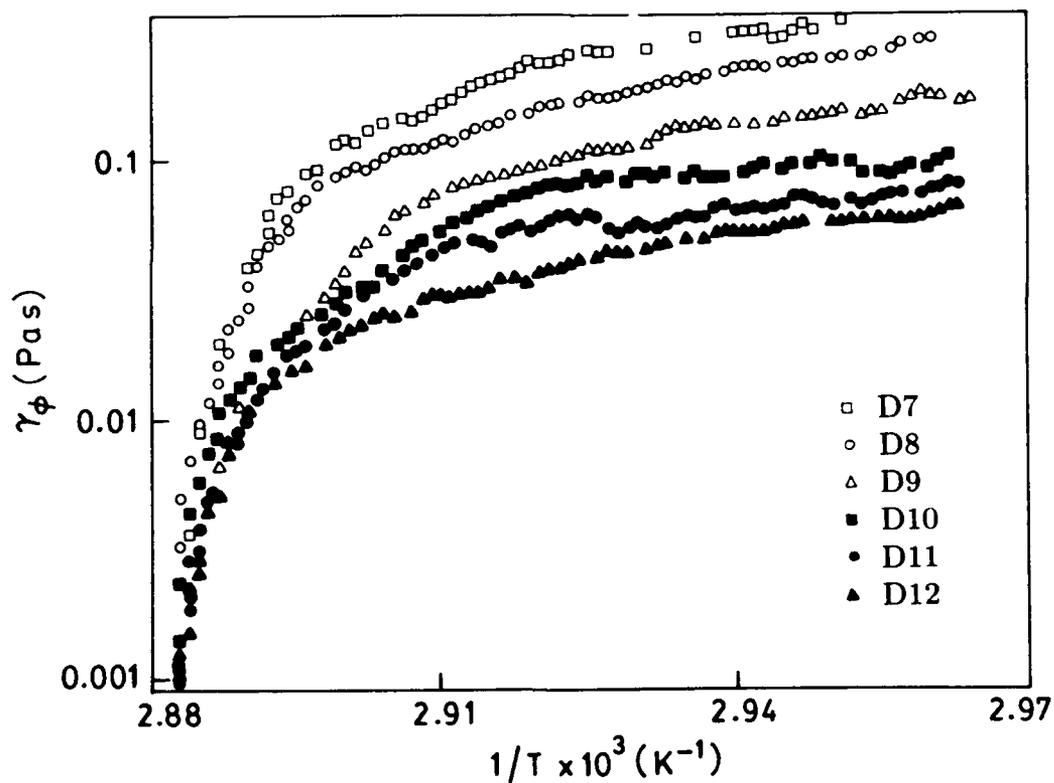
Figure 6: *Plot of ln γ_ϕ versus $1/T$ for the six homologs D7 to D12*

We present only the results obtained using the hysteresis loop method (which, as we showed earlier, agree very well with values determined by the other methods). To facilitate comparison we have normalized the plots by assuming a single Tc. The notable features are

1. There is a systematic variation in the magnitude of γ_ϕ with chain length.

2. Away from the transition, the slope of the plots and thus the activation energy is approximately the same for all the homologs.

These results suggest that although the absolute value of γ_ϕ is influenced by the alkyl chain length the temperature variation is essentially controlled by the rigid core. To see whether these features are useful in selecting suitable materials for device switching let us consider the well known empirical relation.

$$\tau = \frac{\gamma_\phi}{P_s E}$$
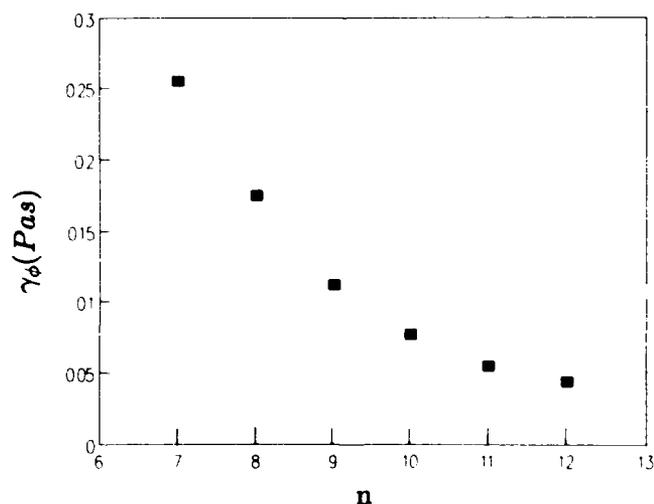
Figure 7: *Dependence of γ_ϕ on chain length at $T_c - 5^\circ C$*
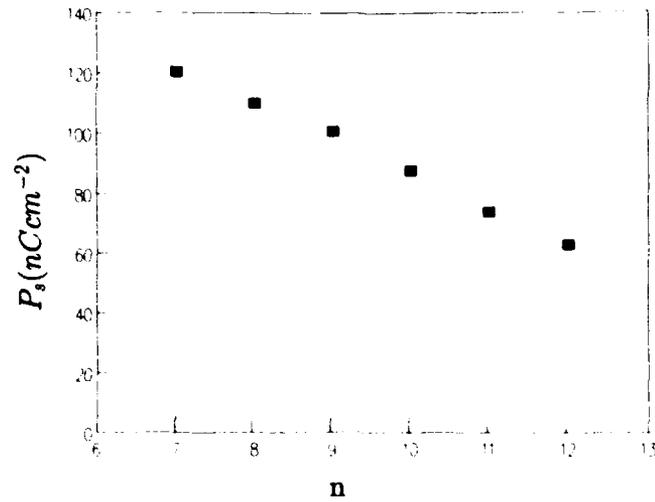
Figure 8: *Dependence of P_s on chain length at $T_c - 5°C$*
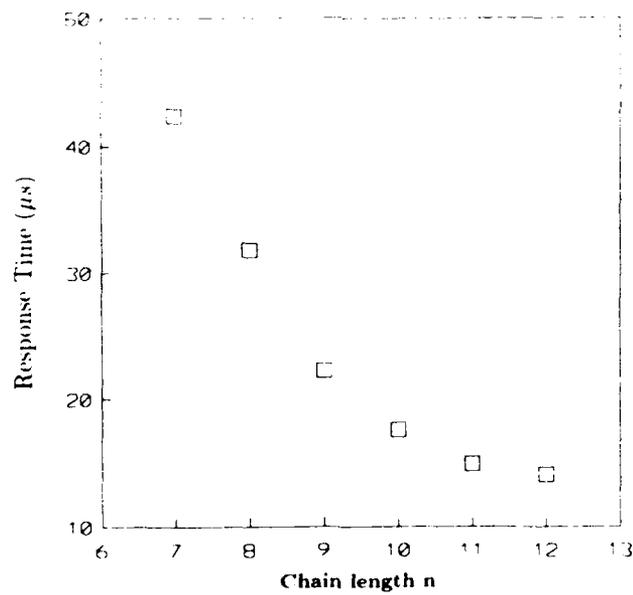
Figure 9: *Dependence of response time τ on chain length at $T_c - 5°C$*

Fig. 7 and Fig. 8 are ¡   of γ_ϕ and P_s obtained at $T_c - 5°C$ as a function of chain length. It is observed that P_s varies linearly for higher homologs, but γ_ϕ appears to reach a lower limit for longer chain lengths. Fig.9 shows τ values obtained for an applied field of E=50 kV/cm, plotted against chain length. The figure shows that although τ can be decreased substantially by increasing n for the lower members of the homologous series, it reaches a limiting value perhaps imposed by the rigid core of the molecule. This suggests that while selecting materials for fast response the limitation imposed by the rigid core should also be kept in mind.

Soft mode viscosity

Unlike γ_ϕ there are only a few studies[7,8] of γ_s, the viscosity associated with tilt amplitude fluctations. We have determined γ_s using the dielectric dispersion method. The method is based on the predictions of the generalized mean field model.[9] According to this model the expression for γ_s is given by the product of the dielectric strength $\Delta\epsilon_s$ and the relaxation frequency f_s of the soft mode (tilt amplitude fluctuation mode)

$$\gamma_s = \frac{(\epsilon C)^2}{2\pi\Delta\epsilon_s f_s}$$

where C is the piezoelectric P_s-θ coupling coefficient and ϵ is the high temperature dielectric constant

Since the coupling coefficient C is not known we define a quantity η as

$$\gamma_s \propto \eta = \frac{\epsilon^2}{2\pi \Delta \epsilon_s f_s}$$

The values of $f_s, \Delta\epsilon_s$ and ϵ have been obtained from dielectric measurements for the 7th and 12th homologs. η values computed using this data are plotted in Fig. 10. Its value increases by about 40%(at $T_c + 2^\circ C$) from D7 to D12, but there is no significant change in the rate of variation with temperature as n is increased.
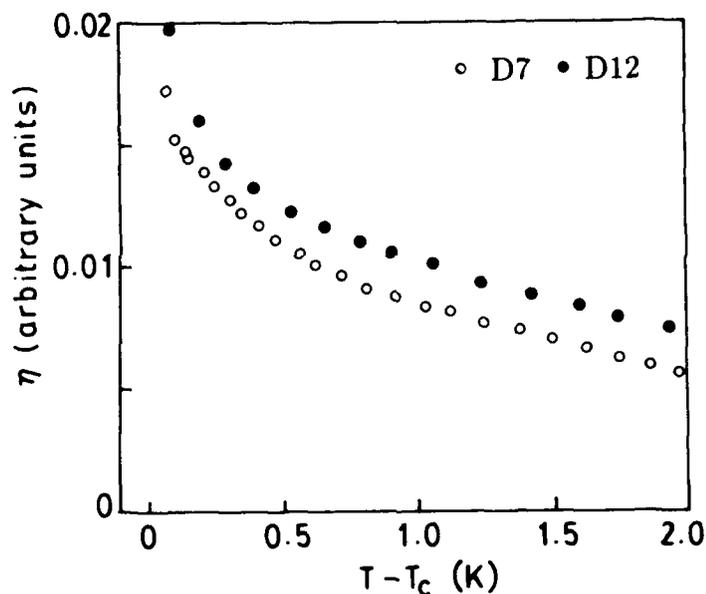
Figure 10: *Temperature dependence of η for D7 and D12*

As shown in Fig. 11 and Fig. 12, η also behaves in a non-arrhenius fashion close to the transition. The slope of this line is a measure of the activation energy. Again it is seen that the slope and thus the activation energy associated with tilt fluctuations does not change much on increasing the chain length.
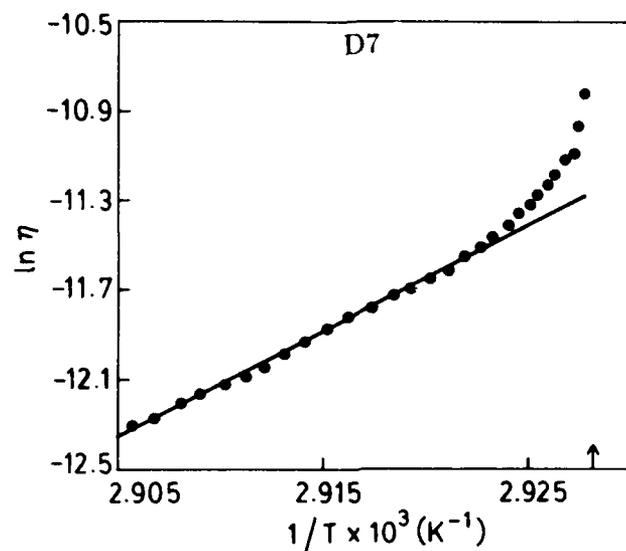
Figure 11: *Arrhenius plot of η for D7*
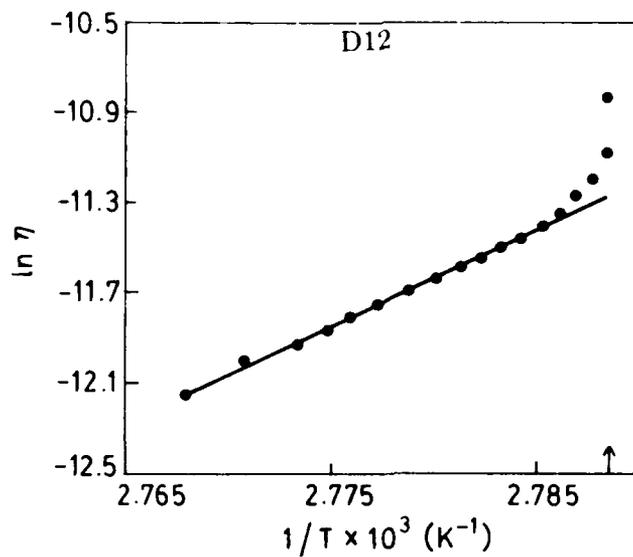
Figure 12: *Arrhenius plot of η for D12*

Conclusions

1. γ_ϕ values obtained from four different methods are in good agreement with each other.

2. With increase in chain length γ_ϕ decreases in a systematic but non-linear fashion.

3. The activation energy associated with both γ_ϕ and γ_s appears to be independent of the chain length of the molecule.

Acknowledgements

References

[1] For a review see K.Skarp, *Ferroelectrics*, **84**, 119 (1988).

[2] B.Shivkumar,B.K.Sadashiva,S.Krishna Prasad and S.M.Khened, *Ferroelectrics*, **114**, 761(1991).

[3] I.Dahl,S.T.Lagerwall and K.Skarp, *Phys.Rev.* **A36**, 4380(1987).

[4] C.Escher,T.Geelhaar and E.Bohm, *Liquid Crystals*, **3**, 469(1988).

[5] C.Escher,H.R.Dubal,W.Hemmerling,I.Muller,D.Ohlendorf and R.Wingen, *Ferroelectrics*, **84**, 89 (1988)

[6] C.C.Huang, *Mol.Cryst.Liq.Cryst.* **144**, 1 (1987).

[7] E.P.Pozhidaev,M.A.Osipov,V.G.Chigrinov,V.A.Baikalov,L.M.Blinov   and

     L.A.Beresnev, *JETP*, **67**, 283(1988).

[8] F.Gouda,K.Skarp and S.T.Lagerwall, *Ferroelectrics*, **113**, 165(1991).

[9] T.Carlsson,B.Zeks,C.Filipic and A.Levstik, *Phys.Rev.* **A42**,877(1990).

THE EFFECTIVE USE OF THE PRECISE SOLUTION
OF THE VAN LAAR EQUATION FOR THE CALCULATION
OF THE BINARY PHASE DIAGRAM WITH A SMECTIC C PHASE

ARNOLD RABINOVICH * and ANNA GANELINA
*Department of Chemistry, Polytechnic University, Brooklyn New York, 11201, U.S.A.

Abstract The paper presents the calculation method of phase diagrams of binary liquid crystal systems based on the original van Laar equation. Phase transition lines are obtained using the differential scanning calorimeter data with the accounting for an interaction in system components, even for weak first-order transitions. Minimum set of experimental data is necessary. The method was applied for the calculation of phase diagrams of different systems containing smectic C - nematic transitions. Surprisingly good results had been obtained.

(phase diagram; binary system; smectic C phase; van Laar equation)

INTRODUCTION

The problem of understanding of the formation of liquid crystal systems is of the key importance because of its wide applications. As a rule, the knowledge of the phase diagrams (PD) is necessary for the development and exploration of systems. The experimental study of the PD is very laborious and is often unsuccessful. On the other hand, the complete information about binary systems is very useful (or even necessary) for the study of the multicomponent system, and, therefore, every attempt to estimate the binary PD might be a step forward in its scientific and practical applications. Simple models were used for PD calculations. These models are based very often on the reduced van Laar equation[1] in the form of the Schroeder - le Schautelier equation[2,3]. However, the results obtained are sometimes unsatisfactory, because of simplifications about interactions in the systems[2]. In order to find a reliable way of phase diagram calculations, we return now to the original van Laar theory, reported in 1908[1].

THEORY

In his fundamental work van Laar developed the equations (1) below for the lines of the phase transitions, based on the van der Waals theory. The full mathematical analysis had been made, and all possible forms of solutions and extremums had been discussed, and dependences of solutions upon interaction parameters had been considered. Van Laar equations are presented as follows:

$$\frac{\Delta H_1^0 - A'\, S^2 + A\, L^2}{T} = \frac{\Delta H_1^0}{T_1^0} - R \ln\left(\frac{1-L}{1-S}\right); \tag{1a}$$

$$\frac{\Delta H_2^0 - A'\,(1-S)^2 + A\,(1-L)^2}{T} = \frac{\Delta H_2^0}{T_2^0} - R \ln\left(\frac{L}{S}\right), \tag{1b}$$

where ΔH_1^0, ΔH_2^0, and T_1^0, T_2^0 are the enthalpy changes and temperatures of phase transitions of components, respectively; T is a current temperature of the system. Parameters A and A' characterize the interaction between the components in the neighboring phases (liquid and solid, or nematic and smectic and etc.). L and S are fractions of the first component in the high ("liquid") and low ("solid") phases, respectively. Terms $A'\, S^2$ and $A\, L^2$ are the enthalpies of mixing. All notations mentioned above were used in van Laar's original work. Many line shapes of the first-order phase transitions with variable ratios and values of the parameters A and A' were obtained by the eqs.(1). One can us_ the original van Laar equations for calculations of mesogenic PD without using very strong assumptions such as "zero interaction in both phases"[2, 3], i.e. A=A'=0, or "complete immiscibility in low temperature phase"[2, 4, 5], i.e. A=0.

Recently, instead of traditional ideal solution approach, the regular solution theory has been successfully applied to calculations of the binary mesogenic phase diagrams[6, 7].

Nevertheless, if parameters A and A' are used, they are considered to be independent of the composition and of temperature within the phases.

In other words, we can substitute very strong assumptions[2-5] by the less restrictive ones. These parameters might be calculated with the values of the enthalpy changes for several compositions in the binary system in the following way: according to the van Laar theory, numerators in the left sides of the equations (1) are the enthalpies of a transition per mole of the first and the second components, respectively. The experimentally measured enthalpy change of the transition is related to A, A' and L, S as follows:

$$\Delta H = \left(\Delta H_1^0 - A \cdot S^2 + A L^2 \right) x +$$
$$\div \left[\Delta H_2^0 - A' (1-S)^2 + A (1-L)^2 \right] (1-x), \qquad (2)$$

where x is the mole fraction of the first component in the system. Thus, one can solve the set of equations (2) in order to obtain parameters A and A'. When parameters are known from the solution of eqs.(2), the numerical solution of eqs.(1) can be performed. Thus, we can obtain the dependences of L and S upon temperature, i.e. to construct the phase diagram. We were able to develop the algorithm for the calculation of the phase transition lines L(T) and S(T) on the basis of these two sets of equations.

RESULTS

Differential scanning calorimetry is appropriate as a source of the experimental data for the calculations, mentioned above. All experimental results represented below had been obtained on the differential scanning calorimeter DSC-111 (SETARAM, France).

Transition temperatures T_1^0 and T_2^0, enthalpy changes of the components ΔH_1^0 and ΔH_2^0, and values of enthalpy changes for several (sometimes even one) mixtures is the minimum set of the experimental data necessary for the calculation of the PD. Our program was used for the calculation of PD of systems.

Both experimental data for the calculations and systems are collected in the Table 1. Our experiments on phase transitions were carried out with the resolution accuracy of enthalpy changes not less than 10^{-3} Kcal/mole. In order to verify our calculation we used only some of the experimental points (for example, two points out of five) for each phase transition in the system.

Table 1. The experimental data of the liquid crystalline systems used for the computer calculation

Substances/Systems		Change of enthalpy (Kcal/mol) Temperature of transition (°C)				
		Melting	SmC-SmA	SmC-N	SmA-N	Iso
1	$C_8H_{17}O$-⬡-COO-⬡-OC_6H_{13}	8.4 / 55	{0.04} / {65}	0.04 / 65		0.2 / 89
2	$C_9H_{19}O$-⬡-⬡(N,N)-C_8H_{17}	10.65 / 34	0.001 / 55		0.1 / 67	1.2 / 71
3	C_9H_{19}-⬡-COO-⬡-OC_6H_{13}	6.3 / 44		0.02 / (23)		0.8 / 64
4	C_7H_{15}-⬡(N)-⬡(F)-OC_8H_{17}	9.3 / 28	0.006 / 49		{0.001} / {55}	1.1 / 53
5	$C_5H_{11}O$-⬡-CH=N(OH)-⬡-C_5H_{11}	7.25 / 41		0.19 / 63		0.15 / 91
6	$C_8H_{17}O$-⬡-CH=N-⬡-NO_2	10.5 / 92				0.36 / (90)
7	$C_{12}H_{25}O$-⬡-CH=N-⬡-$COOC_2H_5$	10.7 / 72				1.5 / 98
1 - 2	x= 0.4 x= 0.6 x= 0.8	8.93 8.79	 0.01		0.041 0.09	0.6 0.81
1 - 3	x= 0.2 x= 0.4 x= 0.52 x= 0.8	6.93 6.9		 0.044 0.040		0.47 0.59 0.52
1 - 4	x= 0.25 x= 0.54 x= 0.75	5.44	 0.002 0.007		 0.062	0.6 0.8
5 - 1	x= 0.2 x= 0.345 x= 0.4 x= 0.8	 7.63 9.2		0.07		 0.35 0.45

Substances: 1 - 5[9], 6,7[2]; { } - virtual, ( ) - monotropic

The results of simulation and analysis of calculations of real systems proved, that the reliable calculation of the weak transition (ΔH < 0.1 Kcal/mole) can be carried out using only two or three experimental points.

COMPUTED PHASE DIAGRAMS OF THE BINARY SYSTEMS

A and A' are the only parameters used and they have been calculated from the experimental data. For all diagrams below:

⊚ — for these points the experimental values of both T^0 and ΔH were used for the calculation;

o — the ΔH value only was used for the calculation;

• — we did not use these experimental points for calculations.
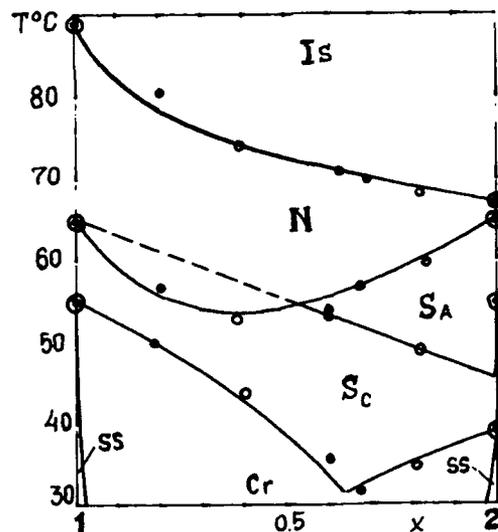
FIGURE 1   System 1 - 2 (ss) are the solid solution regions. N - Sm C transition of the first component is considered as a combination of the virtual N - Sm A and Sm A - Sm C transitions [8]. It allowed us to obtain good results in the region where Sm A - Sm C transitions appeared evident. The same system has been obtained by DTA (See Fig. 8 in [9]).

A. Z. RABINOVICH and A. V. GANELINA
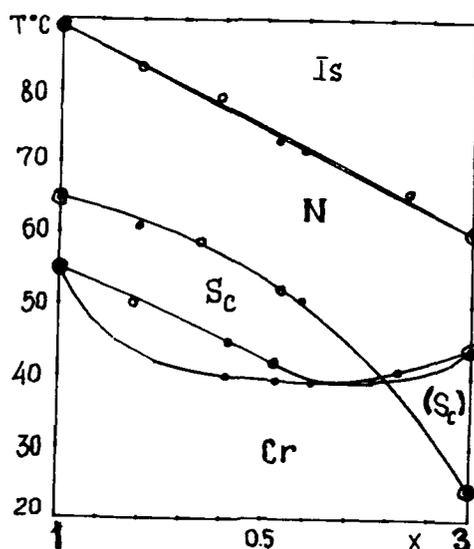
FIGURE 2   System **1 - 3**. The calculation procedure allows to determine the boundaries of the continuous solutions. Experimentally one cannot decide what the "solidus" is. Is it a nonvariant equilibrium or continuous solution boundary. (See DTA results for this system in the Fig.3 in [9]).
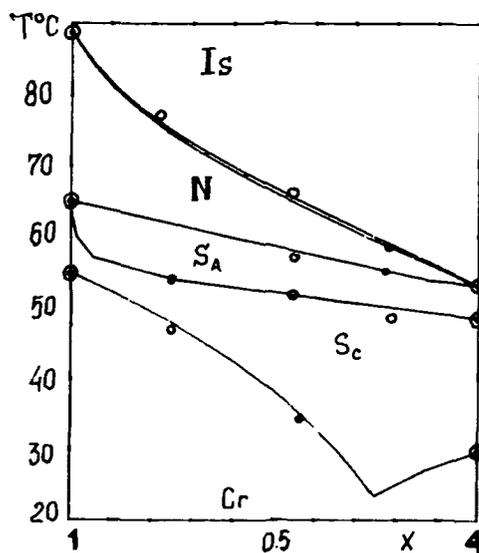
FIGURE 3   System **1 - 4**. N - SmA and N - SmC transitions of the component **1** were calculated similarly to those in Fig.1. Isotropic - SmA transition of the component **4** was considered as a combination of the virtual isotropic - N and N - SmA transitions. The solid solution regions have width of about 10^{-8} mol.%, so they are invisible. (See Fig.10 in [9]).
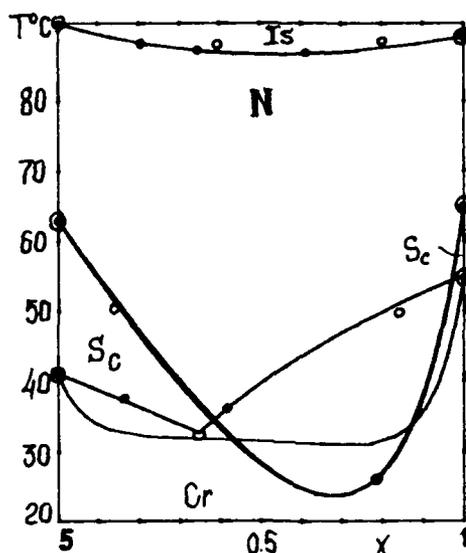
FIGURE 4 System 5 - 1. An immiscibility of the SmC phases was observed experimentally (Fig. 11 in [9]). However, it is evident from the calculation that these are the continuous SmC-solutions with the minimum, lying below the equilibrium solid phase. After the calculation was made we carried out the experiment for the x=0.8 and indeed, we succeeded to find the predicted supercooled SmC phase.
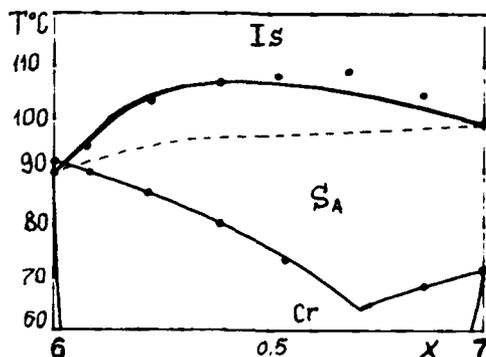
FIGURE 5 Phase diagram of the system 6-7 calculated on the basis of the experimental data from reference[2]. It can be easily seen that our procedure results lie closer to the experimental points (solid lines) than the results of the calculations in accordance to Schroeder - le Schautelier equation (dashed lines). Just the same can be noted about the Crystal - Sm A transition where our calculation predicts the solid solutions and leads to a better fit with the experimental results.

CONCLUSIONS

1. The direct use of the original van Laar theory with the constant parameters of interaction and with possibilities of the DSC allows to estimate the kind of phase diagram even for the the weak first-order transitions.

2. The calculation procedure allows construction of a phase diagram without extensive experimental work.

3. The calculation of phase diagram sometimes leads to prediction of the behavior in a metastable region.

REFERENCES

1. J.J. van Laar, Z.Phys.Chem., 1908, 63, 216, 64, 257.
2. R.J. Cox et al., Mol.Cryst.Liq.Cryst., 1981, 69, 293.
3. D. Demus et al., Mol.Cryst.Liq.Cryst., 1974, 25, 215.
4. A.V. Ivaschenko et.al., Mol.Cryst.Liq.Cryst., 1976, 33, 195.
5. W. Kuszynski et.al., Mol.Cryst.Liq.Cryst., 1988, 146, 237.
6. G.R. van Hecke, J.Phys. Chem., 1979, 83, 2344.
7. G.R. van Hecke et al., J.Phys. Chem., 1980, 84, 263.
8. M. Dommon and J. Billard, Pramana Suppl., 1975, 1, 131.
9. J.Narkevich, A.Z.Rabinovich et al., Ferroelectrics, 1991, 114, 385

EXPERIMENTAL STUDIES IN THE VICINITY OF THE C*-I* TRANSITION

V.N.RAJA, S.KRISHNA PRASAD, S.M.KHENED and D.S.SHANKAR RAO

Raman Research Institute, Bangalore 560 080, INDIA

Abstract

Precise layer spacing, polarisation and dielectric measurements have been performed on two compounds CE8 and 8OSI* both of which exhibit the C* and I* phases. High resolution X-ray studies confirm that the C*-I* transition is first-order in CE8, whereas the I* phase evolves continuously from the C* phase in 8OSI*. The thermal variation of the tilt order is reflected in the temperature dependence of polarisation and dielectric constants.

Introduction

It is now very well established[1] that the coupling between tilt angle (θ) and polarisation (P_s) is an essential feature of ferroelectricity in liquid crystals. While these two parameters have been studied extensively in the C* phase, comparatively few measurements have been made for the I* phase and other higher order smectics. In this paper we present measurements of the θ, P_s and the static dielectric constant ($\epsilon_\perp$) of two compounds (CE8 and 8OSI* of BDH), which exhibit both the C* and I* phases.

Experimental

The molecular structure and the phase sequence exhibited by these two compounds are given below.

C_8H_{17}—⟨O⟩—⟨O⟩—CO—⟨O⟩—$CH_2\overset{*}{C}H$—C_2H_5 **CE8**
  ‖
  O
  |
  CH_3

Iso⟷Ch⟷A⟷$\overset{*}{C}$⟷$\overset{*}{I}$⟷$\overset{*}{F}$⟷$\overset{*}{J}$⟷$\overset{*}{G}$→Crystal

$C_8H_{17}O$—⟨O⟩—⟨O⟩—CO—⟨O⟩—$CH_2\overset{*}{C}H$—C_2H_5 **8OSI***
  ‖
  O
  |
  CH_3

Iso⟷Ch⟷A⟷$\overset{*}{C}$⟷$\overset{*}{I}$⟷$\overset{*}{J}$⟷$\overset{*}{K}$→Crystal

Structurally both are esters with a phenyl 4-biphenyl-4'-carboxylate central core. The only difference in the structure is that CE8 has an alkyl group while 8OSI* has an alkoxy group. Both these materials exhibit C* to I* phase sequence but CE8 has in addition an F* phase below the I* phase. All these phases were identified optically by observing the textural changes with a polarising microscope.

For tilt angle measurements, an X-ray setup was used. The details of the setup and the experimental procedure have been described elsewhere[2]. The resolution in the equatorial direction was $1 \times 10^{-3} Å^{-1}$ HWHM and the precision in the determination of the wavevector is $2 \times 10^{-4} Å^{-1}$. The temperature was maintained constant during any measurement to a value better than 10mK.

Measurement of the P_s was carried out using a calibrated Diamant bridge. The sample was taken in between two ITO coated glass plates which had the electrodes etched on them. Mylar spacers defined the thickness of the cell. Typical cell thickness was about 5μm. The details of the cell structure and measurement techniques have been described earlier[3]. A very low frequency (20Hz) sinusoidal wave was used to obtain the hysteresis curve. The sample cell was placed in a Mettler FP80 hot stage and the temperature of the sample was monitored using a bead thermistor YSI 44011. Measurements of P_s in the C* phase of CE8 were in good agreement with the values reported earlier[4].

For static dielectric constant measurements the capacitance of the sample was measured using an Impedance Analyzer (HP4192A). The cell was similar to the one used for the P_s measurements. ITO treated glass plates were coated with polymer solution and rubbed unidirectionally for planar orientation of the molecules. Samples were cooled from the isotropic phase slowly at the rate of 1°C/h to get good alignment. For the data acquisition and also for storing and analysing the data, a microcomputer was used in all the cases. The details of the technique are published in an earlier paper[5].

Results and Discussion

The plots of tilt angle versus temperature for CE8 and 8OSI* are shown in figures 1 and 2 respectively. The tilt angle jumps abruptly across the transition in CE8 accompanied by a two phase region, clearly indicating that the transition is first order. On the other hand in 8OSI* the tilt angle decreases continuously across C* to I* phase transformation.
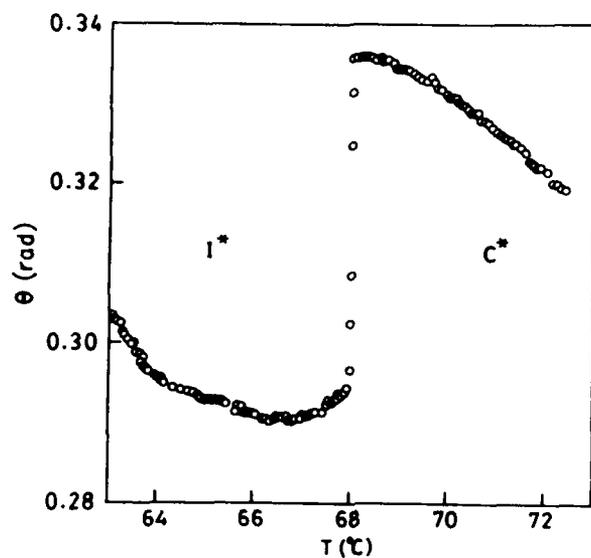
Figure 1: Temperature variation of the tilt angle for CE8
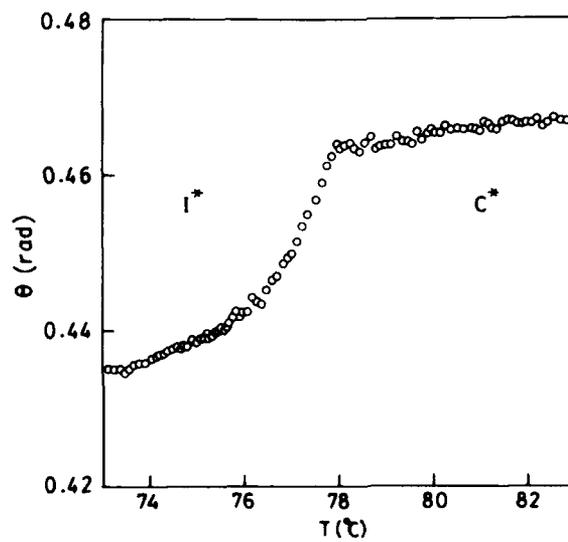
Figure 2: Temperature dependence of the tilt angle for 8OSI*

Theoretically it has been argued[6] that there is no symmetry change between C* and I* phases and as a consequence the transition can only be first order in nature. The absence of a two phase coexistence region and equally the absence of a jump in the tilt angle in 8OSI*, within experimental limits, confirms that it is not a first order transition. One may therefore conclude that the I* phase evolves continuously from the C* phase. This result is in agreement with the high resolution Xray studies of Brock et.al.,[7] on the racemic form of 8OSI* using thin films. They showed that a finite degree of bond orientational order persists well into the C phase indicating that the two phases are not thermodynamically distinct.

Experiments were then conducted to see whether these features get reflected in P_s and the dielectric constant as well. The uniformity of the sample alignment was checked by optical observation. Hysteresis loops were observed in the C* and I* phases by applying fields upto 300 kV/cm.

The plot of P_s versus temperature for CE8 is shown in Fig.3. In the C* phase P_s shows a slow rise with decrease in temperature, attaining a value of $40\mu C/m^2$. On cooling it further into the I* phase there is an abrupt increase in the value of P_s accompanied by an increase in the coercive field. Over a temperature range of 0.5° to 1.0°C in the vicinity of transition the hysteresis loop looks quite different from that in the C* phase. In this region the loop clearly shows the coexistence of two domains with different relaxation times. On further cooling one of the domain gradually shrinks resulting in a single domain just as in the C* phase. These features are in close agreement with earlier observations[8,9]. The plot of P_s versus temperature for 8OSI* is shown in Fig.4. In the C* phase P_s is more or less saturated near the transition which is to be expected because the tilt angle is saturated. In the transition region , P_s starts rapidly decreasing and the hysteresis
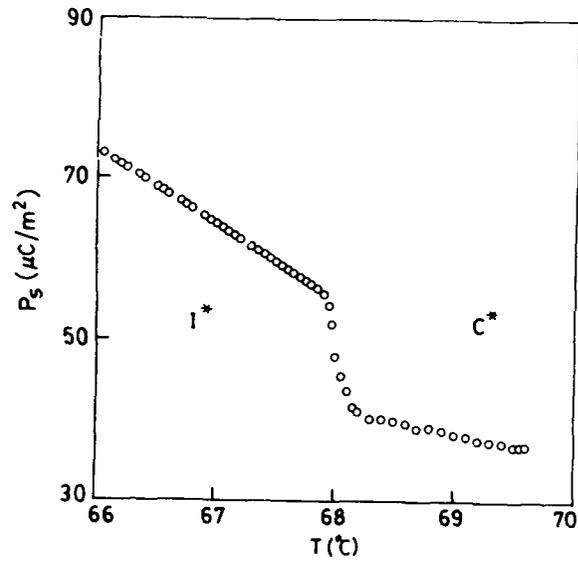
Figure 3: Temperature variation of P_s for CE8
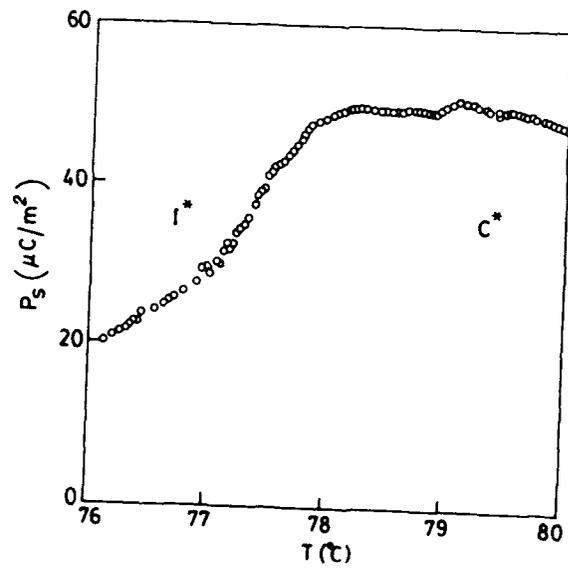
Figure 4: Temperature variation of P_s for 8OSI*
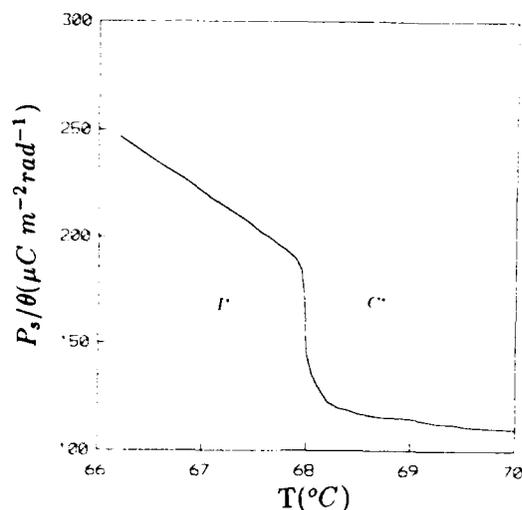
Figure 5: P_s/θ verses temperature for CE8

loop does not show any coexistence of two domains. On further cooling P_s decreases but the coercive field increases. The decrease in P_s clearly indicates that P_s is proportional to θ not only in the C* phase but also in the I* phase. In fact, it has been reported earlier[9,10] that in the vast majority of compounds this linear relationship between P_s and θ is maintained not only in the C* phase but also in the more highly ordered ferroelectric smectic phases (I*, F*, J*......). In this respect the behavior of CE8 is surprisingly different from that of 8OSI*.

Theoretically, because of the bilinear P_s-θ coupling the polarisation is expected to be proportional to tilt,[1,11,12] and measurements [13] have shown that P_s/θ is weakly dependent on temperature in the C* phase away from the C* - A transition. However,this does not appear to be true in the I* phase of the two compounds studied here. The plots of P_s/θ for CE8 and 8OSI* are shown in Figs. 5 and 6 respectively. In both the cases P_s/θ exhibits a strong temperature dependence in the I* phase. The behavior is similar to that of the P_s variation with temperature,
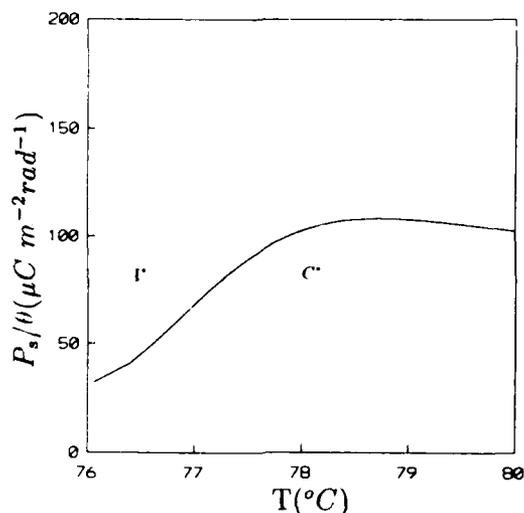
Figure 6: Temperature variation of the P_s/θ for 8OSI*

suggesting that the P_s variation is more than the tilt angle variation especially near the transition for both the materials.

Static dielectric constant measurements were also made for the two compounds. The plots of the perpendicular component of the dielectric constant($\epsilon_\perp$) against temperature are shown in figures 7 and 8. These measurements were performed at low frequency (500Hz). This low-frequency dielectric constant, characterising the dielectric strength of the ferroelectric relaxation, shows dramatic changes in the vicinity of the C*-I* transition. In both the cases the dielectric constant decreases at the transition, and on further cooling it remains practically constant. It is interesting to note that the drop in the $\epsilon_\perp$ value is seen to be more for 8OSI* than for CE8. From the mean-field model[13], one should expect the P_s/θ variation to be reflected in the temperature dependence of $\epsilon_\perp$ also, if other parameters like pitch, elastic constant etc., remain unaltered. However, as mentioned earlier the P_s/θ ratio increases in CE8 but decreases in 8OSI*. Thus, although the 8OSI* data can
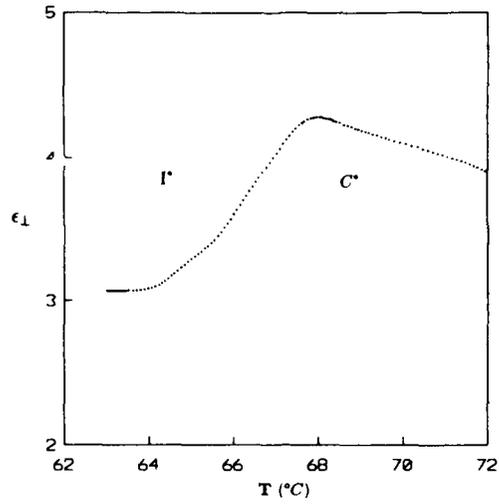
Figure 7: Temperature variation of $\epsilon_\perp$ for CE8
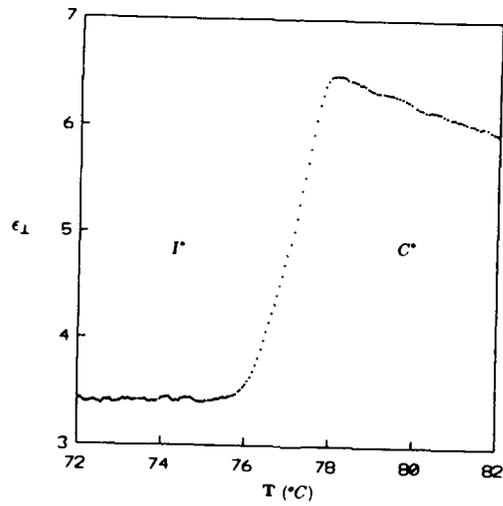
Figure 8: Temperature variation of $\epsilon_\perp$ for 8OSI*

be explained by the P_s/θ ratio, the CE8 data suggests that other parameters may also be playing a significant role. It may be mentioned here that in the C* phase, both the Goldstone mode and the soft mode contribute to the low frequency dielectric constant. Earlier studies [14,15] have shown that the Goldstone mode frequency increases across C* to I* transition but no detailed temperature variation of the relaxation frequency and its strength are available in the I* phase. Experiments in this direction are in progress.

In conclusion the nature of the C* to I* phase transition is clearly revealed by the tilt angle measurements. The results indicate that the linear relationship between P_s and θ is not generally valid. Clearly further experiments in other compounds are needed to understand this problem.

Acknowledgements

References

[1] B.Zeks, T.Carlsson, C.Filipic and B.Urbenc, Ferroelectrics, **84**, 3(1988).

[2] S.Krishna Prasad, V.N.Raja, D.S.Shankar Rao, G.G.Nair and M.E.Neubert, Phys.Rev. **A42**, 2479 (1990).

[3] S.K.Prasad, S.M.Khened, S.Chandrasekhar, B.Shivkumar and B.K.Sadashiva, Mol.Cryst.Liq.Cryst., 182B, 313 (1990).

[4] G.Spruce and R.D.Pringle, Liquid Crystals, **3**, 507 (1988).

[5] S.M.Khened, S.Krishna Prasad, B.Shivkumar and B.K.Sadashiva, J.Phys.(paris) II, **1**, 171(1991).

[6] D.R.Nelson and B.I.Halperin, Phys.Rev. **B21**, 5312(1980).

[7] J.D.Brock, A.Aharony, R.J.Birgeneau, K.W.Evans-Lutterodt, J.D.Litster, P.M.Horn, G.B.Stephenson and A.R.Tajbakhsh, Phys.Rev.Lett., **57**, 98 (1986).

[8] M.F.Bone, D.Coates and A.B.Davey, Mol.Cryst.Liq.Cryst., **102**, 331 (1984).

[9] J.Wahl and S.C.Jain, Ferroelectrics, **58**, 481 (1984).

[10] R.Eidenschink, T.Geelhaar, G.Andersson, A.Dahlgren, K.Flatischler, F.Gouda, S.T.Lagerwall and K.Skarp, Ferroelectrics, **84**, 167 (1988).

[11] R.Blinc and B.Zeks, Phys.Rev. **A18**, 740(1978).

[12] L.G.Benguigi, Ferroelectrics, **58**, 269(1984).

[13] S.Dumrograttana and C.C.Huang, Phys.Rev.Lett., **56**, 464(1986).

[14] R.J.Cava, J.S.Patel and E.A.Rietman, J.Appl.Phys., **60**, 3093(1986).

[15] M.Pfeiffer, S.Wrobel, L.A.Beresnev and W.Haase, Mol. Cryst. Liq. Cryst., **202**, 193(1991).

AUTHOR INDEX

Proceedings of The Third International Symposium on Ferroelectric Liquid Crystals

Volumes 121–122

Special Issue on Piezoelectric and Electrostrictive Actuators

A special issue of the international journal *Ferroelectrics* is scheduled for the middle of 1992 on the subject "Piezoelectric and Electrostrictive Actuators."

Recent developments in piezoelectric and electrostrictive ceramics are remarkable, especially in the field of optics and precision machinery. Camera shutters, dot-matrix printers, and air valves have been widely commercialized. Ultrasonic motors will partially replace conventional electromagnetic motors in the future.

This special issue will cover the fundamental studies of ceramic actuators and applications:

1. Ceramic actuator materials — piezoelectrics, electrostrictors, phase transition — related ceramics
2. Fabrication processes — powders, tape casting
3. Micro/macrostructure — grain size dependence, monomorph, electrode configuration
4. Control technique — polarization control, pulse drive method
5. Applications — deformable mirrors, positioners, pulse drive motors
6. Ultrasonic motors

Invited and contributed papers are welcome. All manuscripts will be reviewed. Manuscripts should be prepared according to the instructions on the inside back cover of "Ferroelectrics."

Authors are cordially invited to submit their papers not later than December 31, 1991 to the Guest Editors below:

Professor Kenji Uchino
Department of Physics
Sophia University
Kioi-cho 7-1, Chiyoda-ku
Tokyo 102, Japan
        or
Materials Research Laboratory
The Pennsylvania State University
University Park, PA 16802, USA
(July 1-September 30)

Professor L. Eric Cross
Materials Research Laboratory
The Pennsylvania State University
University Park, PA 16802

For further information, please feel free to contact the Guest Editors.

The Eighth
INTERNATIONAL MEETING OF FERROELECTRICITY

8–13 August 1993
National Institute of Standards and Technology
Gaithersburg, Maryland USA

The scope of the conference will be similar to that of the preceding IMFs. Both invited and contributed papers will be presented on fundamental and applied research on ferroelectrics, including but not limited to:

Phase transitions and critical phenomena
Electronic structure, quantum effects
Lattice dynamics, lattice instabilities, and soft modes
First principles calculations
Low-temperature properties
Superconductivity in oxides
Charge density waves, polarization fluctuations
Structure and crystal growth
X-ray and neutron scattering
Acoustic and ferroelastic properties
Dielectric, piezoelectric, and pyroelectric properties
Optical properties and phase conjugation
Modulated and incommensurate systems

Disordered and glassy systems
Domains, domain boundaries, and imperfections
Raman, Brillouin, IR, and submillimeter
  spectroscopy
NMR, ESR, PAC, and other types of spectroscopy
Electron microscopy
High-pressure effects
Polymers and liquid crystals
Ceramics and composite materials
Sensors, actuators, and transducers
Thin films and surfaces
Ferroelectric/semiconductor integration

Wallace A. Smith	L. Eric Cross	George W. Taylor
Office of Naval Research	Pennsylvania State University	Princeton Resources
IMF8 Chairman	IMF8 Vice Chairman	IMF8 Vice Chairman

To receive future announcements, send your name and address to:

Ms. Kathy Kilmer, IMF8 Conference Manager
National Institute of Standards and Technology
Administration Building, Room A917
Gaithersburg, MD 20899
TEL (301) 975-2776; FAX (301) 926-1630

Title and Name _____

Institution _____

Department _____

Street _____

City/State/Zip _____

Country _____

Phone _____

FAX _____

❏ I will present a paper entitled: _____

❏ I will be accompanied by _____ guests.

❏ I will attend, but will not present a paper.

❏ I will not attend, but would like to be kept informed.

"Arthur von Hippel Special Issue" on Dielectric properties of Ferroelectrics

A special issue of *Ferroelectrics* is planned in honor of Professor Arthur von Hippel's 93rd birthday. Because Professor von Hippel founded the Massachusetts Institute of Technology Laboratory for Insulation Research in 1940 and supervised it until his retirement, we thought a fitting topic for this special issue would be "Dielectric Properties of Ferroelectrics." This is only one of his many areas of interest, and papers on other topics of particular interest to him are welcome.

Papers reporting original research on this topic not published elsewhere are requested. They should be sent to one of the Guest Editors named below, who will arrange for refereeing and publication. Also, we invite submission of review papers, but to avoid duplication, the topic of the review should be discussed with one of the Guest Editors beforehand.

To facilitate correspondence, it is suggested that you work with the Guest Editor in your geographical area as listed below.

Europe (including USSR) and Africa:
Professor Bozena Hilczer
Institute of Molecular Physics
Polish Academy of Sciences
Smoluchowskiego 17/19
60-179 Poznan, Poland

Asia and Australia:
Professor Toshio Mitsui
Department of Physics
School of Science and Technology
Meiji University
1-1-1 Higashimita, Tama-ku
Kawasaki 214, Japan

North and South America:
Professor V. Hugo Schmidt
Department of Physics
Montana State University
Bozeman, MT 59717 USA

We ask that you submit your manuscript by December 31, 1991 to one of the above Guest Editors.

Second USSR/USA Seminar on Ferroelectricity

22-26 June 1992
A.F. Ioffe Physical Technical Institute
194021 St Petersburg, USSR

Organizing Committee
A.M. Prokhorov, Honorary President

USSR	USA
Chairman: K.S. Aleksandrov	Chairman: G.W. Taylor
Vice-Chairman: L.A. Shuvalov	Vice-Chairman: S.K. Kurtz
V.V. Lemanov	Secretary: J.F. Scott
O.O. Vendik	Members: L.E. Cross
Secretary: V.M. Fridkin	A. Bhalla
N.K. Yushin	A. Glass
Program Chairman: A.K. Tagantsev	V.H. Schmidt
Local Arrangements: A.I. Nikkonen	N. Clark
	G. Samara
	K. Lyons
	F. Ullman

For information please contact:
V.V. Lemanov
A.F. Ioffe Physical Technical Institute
194021 St Petersburg, USSR
Tel. No 007812 515 6660
Telex 121 1453 FTIANSU
Fax No 007812 515 6747

or

G.W. Taylor
Princeton Resources
P.O. Box 211
Princeton, NJ 08540 USA
Tel. No. (609) 921-3192
Fax No. (609) 924-9020

The seminar will be devoted to the physics of
ferroelectrics and related materials:

1. Optics and Spectroscopy
2. Films and Composites
3. Liquid Crystals and Glasses
4. Superconducting Oxides
5. Structure and Properties of New Crystals and Ceramics
6. Disordered Ferroelectrics

"Nakamura Special Issue" on Structural Phase Transitions in Ferroelectrics and Related Materials

A special issue of the international journal *Ferroelectrics* is scheduled for late 1991 on the subject "Structural Phase Transitions in Ferroelectrics and Related Materials."

This special issue will be dedicated to Professor Torutaro Nakamura on the occasion of his sixty-eighth birthday. Professor Nakamura's work is well known internationally. During his eminent scientific carer, his seminal contributions are responsible for several milestones in the history of ferroelectricity research.

This special issue will cover the full scope of ferroelectric phenomena discussed in the light of the physics of the structural phase transition.

Invited papers and tributes will make up the bulk of the issue, but contributed papers are welcome as well.

Authors are cordially invited to submit their papers not later than June 30, 1991, to one of the guest editors listed here:

Professor L. Godefroy
Laboratoire de Physique du Solide
Université de Bourgogne
BP 138, F-21004
Dijon Cédex, France

Professor W. Kinase
Department of Physics, School of Science and Engineering
Waseda University
3-4-1 Okubo, Shinjuku-ku
Tokyo 169, Japan

Professor A.P. Levanyuk
Institute of Crystallography
USSR Academy of Sciences
59 Leninsky Prospekt
117333 Moscow, USSR

Professor F.G. Ullman
Electric Engineering Department
University of Nebraska
Lincoln, NE 68588-0511 USA

Manuscripts should be prepared according to the instructions on the inside back cover of *Ferroelectrics*. All manuscripts will be refereed.

The following Japanese associate guest will assist Professor Kinase: Professor K. Ohi, Professor A. Sawada, Professor M. Takashige, and Dr. S. Kojima.

For further information, please contact any of the guest editors listed above.

Special Issue on
Ferroelectricity, Structural Instability,
and High-Temperature Superconductivity

A special issue of the international journal *Ferroelectrics* is scheduled for 1991 on the subject "Ferroelectricity, Structural Instability, and High-Temperature Superconductivity." The aim of this issue is to present a review of the present state of the art (experimental as well as theoretical), on possible interrelations, common features, and outstanding differences of ferroelectric and superconducting oxides. Emphasis is put on their structural instability, which is common to both ferroelectricity and superconductivity. Authors are invited to submit their contributions to one of the Guest Editors, listed below.

A. Bussmann-Holder
Max-Planck Institut für
Festkörperforschung
Heisenbergstraße 1
D-7000 Stuttgart 80
Federal Republic of Germany

S. K. Kurtz
Materials Research Laboratory
Pennsylvania State University
University Park, PA 16802 USA

Eiko Matsushita
Maritime Safety Academy
Kure 737, Japan

N. M. Plakida
Joint Institute for Nuclear Research
141980 Dubna, USSR

J. F. Scott
Physics Department
University of Colorado
Boulder, CO 80309 USA

Manuscript should be prepared according to the instructions on the inside back cover of *Ferroelectrics*. All manuscripts will be refereed. For further information, please contact any of the Guest Editors listed above.

ISAF '92

IEEE International Symposium on the Application of Ferroelectrics

August 31 - September 2, 1992
Hyatt Regency, Greenville, South Carolina

Sponsored by the Ultrasonics, Ferroelectrics and Frequency Control Society of the IEEE
in Cooperation with the Electronics Division of the American Ceramic Society

---

First Call for Papers
Abstract Deadline: February 1, 1992

Meeting Chair:
Prof. Gene Haertling
206 Olin Hall
Clemson University
Clemson, SC 29634-0907
Tel. (803) 656-0180
Fax (803) 656-2698

The next International Symposium on the Application of Ferroelectrics will be held August 31 - September 2, 1992, in Greenville, South Carolina.

This biannual meeting emphasizes the application of ferroelectric materials in the form of single crystals, bulk ceramics, and thick and thin films. Papers are solicited describing original work in the following categories. These categories reflect those properties of the materials which primarily determine their application. **Within each category, papers are requested covering processing; properties; theory and modelling; performance (reliability and failure); and particularly new applications and new materials.**

Technical Program Chair:
Prof. Angus I. Kingon
Materials Research Ctr.
N.C. State University
Centennial Campus
Box 7919
Raleigh, NC 27695-7919
Tel. (919) 737-2867
Fax (919) 737-3419

• **Ferroelectric**

Materials and applications in which the primary property utilized is polarization reversal (ferroelectric switching) Topics include thin film processing, integrated memories, integration, performance, fatigue, ageing, modelling and new applications.

• **Dielectric**

Materials and applications in which the primary property utilized is the high permittivity of the ferroelectric materials. Topics include multilayer capacitors; thick film capacitors; thin film integrated static capacitors; packaging; dielectric breakdown and reliability; high frequency dielectrics; PTC materials; boundary layer capacitors; and processing. A new topic will be electrorheological fluids.

• **Piezoelectric and Electrostrictive**

Materials and applications in which the primary property utilized is piezoelectricity (and the related electrostriction). Applications to include actuators; transducers; micromotors and microactuators; resonators; and sensors. Topics to include processing and modelling, and material categories to include ceramics, ceramic/polymer composites, and polymers.

• **Electrooptic, Pyroelectric, etc.**

Materials and applications in which the primary properties utilized are the electrooptic effect, pyroelectricity, photorefraction, and related optical properties. This category will include ferroelectric liquid crystals. Applications to include phase modulators, second harmonic generators, displays, optical NDRO devices, optical comparators, digital and analogue image storage, thermal sensors and imagers, detectors, etc.

Accommodations

Accommodations will be available at the Hyatt Regency in downtown Greenville, South Carolina or at several other hotels and motels in the local area. The Hyatt will serve as the conference headquarters. More detailed information will be supplied at a later date.

Location

Greenville, South Carolina is located approximately 150 miles northeast of Atlanta, Georgia along Interstate I-85 connecting Atlanta and Charlotte, North Carolina. International flights are available into Atlanta, GA and Charlotte and Raleigh, NC. Domestic flights are also available into the Greenville-Spartanburg airport located 10 miles from downtown Greenville.

During the symposium, the group will be traveling to Clemson, SC, abouth 30 miles west of Greenville, for a brief visit to the campus of Clemson University and an evening outdoor social function at Lake Hartwell on the University grounds.

Abstracts

Abstracts are to be submitted according to the accompanying abstract format. The deadline is February 1, 1992. Abstracts to be submitted to the Technical Program Chair, Prof. Angus I. Kingon, at the address given. Abstracts will receive careful evaluation. Evaluation criteria will include; scientific contribution, originality; overall interest to the ferroelectrics (including user) community; and clarity.

Notice of acceptance of abstracts will be mailed in April 1992. Complete manuscripts must be received by August 1, 1992, to ensure timely review. The symposium proceedings will be published shortly after the symposium.

A second call for papers will be issued in September 1991. That announcement will include a list of invited speakers. Program details and lodging information will be mailed in April 1992.

ISAF '92
Preparation of Abstracts

TITLE UPPER CASE ADJUSTED LEFT.
(Space)
A.A. Author One and B.B. Author Two[1]
Affiliation and Address
[1]Second Affiliation and Address if required.
(Space)

    Abstract to fill the remaining space. No references or figures to be included. The complete abstract to fit into this space measuring 13.5 by 18 centimeters. Presenting author underlined, if known. Single spacing (12 pt. Times). This abstract will be printed in this camera-ready form to be available at the symposium.

*Include funding agency acknowledgement if desired.

Please mark the category into which you feel your paper best fits:
- ❑ Ferroelectric
- ❑ Piezoelectric and electrostrictive
- ❑ Dielectric
- ❑ Electrooptic, pyroelectric, optical, etc.

Name and address of author to whom correspondence should be sent:

Name _____

Address _____ _____

_____

Telephone _____ FAX _____

Check box:
- ❑ I prefer oral presentation
- ❑ I prefer poster
- ❑ I do not have a preference

- ❑ I plan to bring my spouse/guest

Submit your abstract (by February 1, 1992) to: **Prof. Angus I. Kingon/Ms. Jan Jackson
Materials Research Center
North Carolina State University, Centennial Campus
Box 7919, Raleigh, NC 27695-7919.**

ISAF '92

In order for the organizers to ensure appropriate facilities and lodging, please indicate your interest in the symposium:

❏ I intend to attend and submit a paper by February 1, 1992. A tentative title is _____
_____(optional).

❏ A second paper will be entitled: _____
_____(optional).

Category: ❏ Ferroelectric   ❏ Dielectric
              ❏ Piezoelectric and electrostrictive   ❏ Electrooptic, pyroelectric, optical, etc.

❏ I will attend, but not present a paper.
❏ I will not be attending. Please remove my name from your mailing list.

Name _____

Address _____
_____

Telephone _____ FAX _____

Return as soon as possible to: **Prof. Gene Haertling**
                                   206 Olin Hall
                                   Clemson University
                                   Clemson, SC 29634-0907

ISAF '92

ECAPD2/ISIF4
The Second European Conference on
The Applications of Polar Dielectrics
and
The Fourth International Symposium on
Integrated Ferroelectrics

Imperial College of Science, Technology, and Medicine
South Kensington, London, UK

12–15 April 1992

The program will include the following topics:

- FERROELECTRICS: fundamental properties, new materials
- THIN FILMS: memory devices thin film capacitors, piezoelectric devices
- PROCESSING: single crystals, fibers, ceramics, thin films
- DIELECTRICS: multilayer capacitors, relaxors, microwave dielectrics
- PIEZOELECTRICS: sensors, actuators, motors, polymers, composites
- PYROELECTRICS: detectors, imaging

- INTEGRATED CERAMICS: smart materials, multi-component structures
- ELECTROOPTICS: nonlinear optics, organic materials, devices

To receive further details on ECAPD2/ISIF4, please contact the Conference Secretary:

Ms. K. J. Humphrey
ECAPD2
Alcan International Ltd.
Southam Road
Banbury, Oxfordshire
OX16 7SP, United Kingdom
TEL: +44–295–274348
FAX: +44–295–274210

FERROELECTRICS
and related materials

NOTES FOR CONTRIBUTORS

Manuscripts should be typewritten with double-spacing and submitted in triplicate. Authors are requested to forward their manuscripts to either the Editor:

G. W. Taylor
Princeton Resources,
P.O. Box 211,
Princeton, NJ 08540, USA

or one of the Associate Editors:

Peter Günter	Sidney B. Lang	Koichi Toyoda
Institut für	Department of Chemical	Research Institute of
Quantenelektronik	Engineering	Electronics
ETH	Ben Gurion University of	Shizuoka University
CH 8093 Zürich	the Negev	Hamamatsu 432
Switzerland	Beer Sheva 84120, Israel	Japan

Submission of a paper to *Ferroelectrics* will be taken to imply that it represents original work not previously published, that it is not being considered for publication elsewhere, and that if accepted it will not be published elsewhere in the same form, in any language, without the consent of the editors.

It is a condition of the acceptance by the editor of a typescript for publication that the publishers acquire automatically the copyright in the typescript throughout the world.

Manuscript length: The maximum length preferred is 35 units, where a unit is a double-spaced typewritten page or one figure. Longer papers, or papers not following the prescribed editorial format, cannot be guaranteed prompt publication.

Abstracts and Key Words: Each manuscript should contain a leading abstract of approximately 100–150 words and be accompanied by up to six key words which characterize the contents of the paper.

Figures should be given numbers and captions, and should be referred to in the text. Captions should be collected on a separate sheet. Please label each figure with the figure number and the name of the author. Line drawings of high enough quality for reproduction should be prepared in India ink on white paper or on tracing cloth; coordinate lettering should be included. Figures should be planned so that they reduce to a 6½ cm column width. The *preferred* width of submitted figures is 12 to 15 cm, with lettering 4 mm high, for reduction by one-half. Photographs intended for halftone reproduction should be good, original glossy prints, at roughly twice the desired size. Redrawing, and author's alterations in excess of 10%, will be charged.

Color Plates: Whenever the use of color is an integral part of the research, or where the work is generated in color, the journal will publish the color illustrations without charge to authors. Reprints in color will carry a surcharge. Please write to the Editor for details.

Equations should be typewritten wherever possible, with subscripts and superscripts clearly indicated. It is helpful to identify unusual symbols in the margin.

Units: Acceptable abbreviations will be found in the *Style Manual* of the American Institute of Physics and similar manuals. Metric units are preferred.

References and Notes are indicated in the text by superior numbers; the full list should be collected and types on a separate page at the end of the paper. Listed references are arranged as follows:

1. J. C. Slater, *J. Chem. Phys.* **9**, 16 (1941).
2. F. Jona and G. Shirane, *Ferroelectric Crystals* (Pergamon Press, Oxford, 1962), pp. 186–7.

Proofs: Page proofs, including figures, will be forwarded by air mail to authors for checking.

Reprints: Reprints may be purchased; a reprint order form will be sent with page proofs.

There are no page charges to authors or to institutions.

Rubbing direction

(A)

Rubbing direction

(B)

Rubbing direction

(C)

$300\mu m$

0

COLOR PLATE I.
See Kimura et al., Figures 3a, b and c.
FERROELECTRICS, Volume 121(1–4).

COLOR PLATE II.
See Shao *et al.*, Figure 1.
FERROELECTRICS, Volume 121(1-4).

COLOR PLATE III.
See Shao *et al.*, Figure 2a.
FERROELECTRICS, Volume 121(1-4).
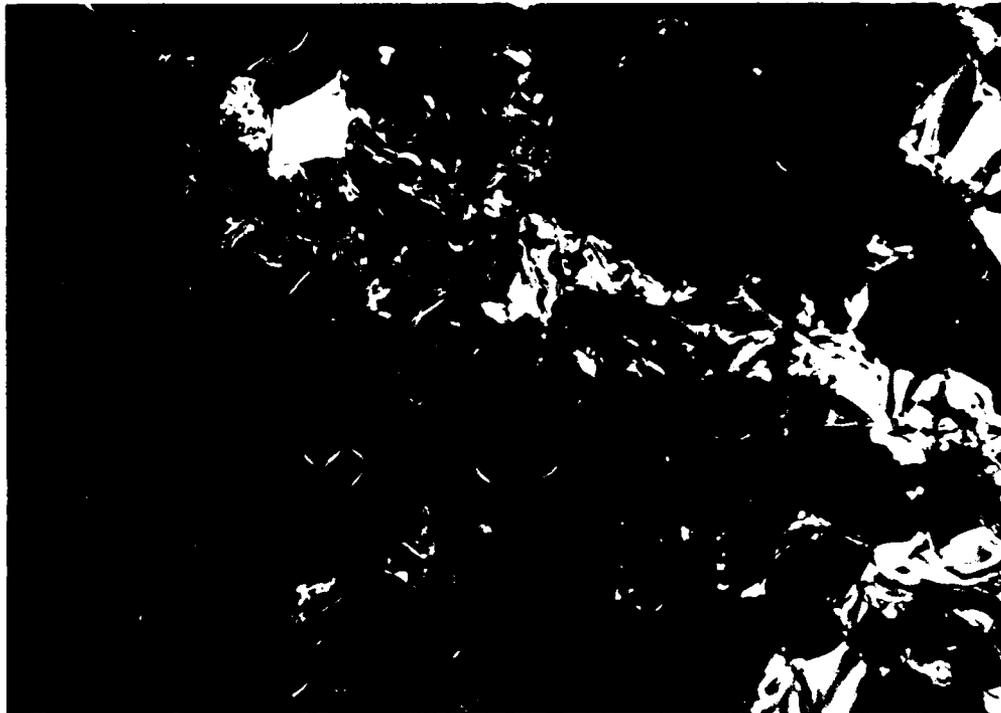
COLOR PLATE IV.
See Nguyen et al., Figure 1.
FERROELECTRICS, Volume 121(1–4).

COLOR PLATE V.
See Nguyen et al., Figure 2a and b.
FERROELECTRICS, Volume 121(1–4).

COLOR PLATE VI.
See Nguyen *et al.*, Figure 3.
FERROELECTRICS, Volume 121(1–4).

COLOR PLATE VII.
See Yokoyama *et al.*, Figure.
FERROELECTRICS, Volume 121(1–4).

(continued from inside front cover)

Ordering Information